Universitat Autònoma de Barcelona

Neutrophilic asthma modelling and translational markers

CRISTINA UJALDÓN MIRÓ

ADVERTIMENT. L'accés als continguts d'aquesta tesi doctoral i la seva utilització ha de respectar els drets de la persona autora. Pot ser utilitzada per a consulta o estudi personal, així com en activitats o materials d'investigació i docència en els termes establerts a l'art. 32 del Text Refós de la Llei de Propietat Intel·lectual (RDL 1/1996). Per altres utilitzacions es requereix l'autorització prèvia i expressa de la persona autora. En qualsevol cas, en la utilització dels seus continguts caldrà indicar de forma clara el nom i cognoms de la persona autora i el títol de la tesi doctoral. No s'autoritza la seva reproducció o altres formes d'explotació efectuades amb finalitats de lucre ni la seva comunicació pública des d'un lloc aliè al servei TDX. Tampoc s'autoritza la presentació del seu contingut en una finestra o marc aliè a TDX (framing). Aquesta reserva de drets afecta tant als continguts de la tesi com als seus resums i índexs.

ADVERTENCIA. El acceso a los contenidos de esta tesis doctoral y su utilización debe respetar los derechos de la persona autora. Puede ser utilizada para consulta o estudio personal, así como en actividades o materiales de investigación y docencia en los términos establecidos en el art. 32 del Texto Refundido de la Ley de Propiedad Intelectual (RDL 1/1996). Para otros usos se requiere la autorización previa y expresa de la persona autora. En cualquier caso, en la utilización de sus contenidos se deberá indicar de forma clara el nombre y apellidos de la persona autora y el título de la tesis doctoral. No se autoriza su reproducción u otras formas de explotación efectuadas con fines lucrativos ni su comunicación pública desde un sitio ajeno al servicio TDR. Tampoco se autoriza la presentación de su contenido en una ventana o marco ajeno a TDR (framing). Esta reserva de derechos afecta tanto al contenido de la tesis como a sus resúmenes e índices.

WARNING. The access to the contents of this doctoral thesis and its use must respect the rights of the author. It can be used for reference or private study, as well as research and learning activities or materials in the terms established by the 32nd article of the Spanish Consolidated Copyright Act (RDL 1/1996). Express and previous authorization of the author is required for any other uses. In any case, when using its content, full name of the author and title of the thesis must be clearly indicated. Reproduction or other forms of for profit use or public communication from outside TDX service is not allowed. Presentation of its content in a window or frame external to TDX (framing) is not authorized either. These rights affect both the content of the thesis and its abstracts and indexes.

TESIS DOCTORAL

Neutrophilic asthma modelling and translational markers

DOCTORANDA

CRISTINA UJALDÓN MIRÓ

DIRECTOR

David Ramos Barbón

TUTOR

Cándido Juárez Rubio

CODIRECTOR

Eder Mateus Medina

Programa de Doctorado en Inmunología Avanzada, Departamento de Biología Celular, Fisiología e Inmunología IIB Instituto de Investigación Hospital de la Santa Creu i Sant Pau, Universidad Autónoma de Barcelona, 2020

DEPARTAMENTO DE BIOLOGÍA CELULAR, FISIOLOGÍA E INMUNOLOGÍA

FACULTAD DE BIOCIENCIAS, UNIVERSIDAD AUTÓNOMA DE BARCELONA

MEMORIA PRESENTADA POR:

CRISTINA UJALDÓN MIRÓ

PARA OPTAR AL GRADO DE:

DOCTORA EN INMUNOLOGÍA

Tesis realizada en el laboratorio de Neumología del *Institut del Hospital de la Santa Creu i Sant Pau* de Barcelona bajo la dirección y codirección del Dr. David Ramos y el Dr. Eder Mateus.

La doctoranda	El director	El codirector
CRISTINA UJALDÓN MIRÓ	**DR.DAVID RAMOS BARBÓN**	**DR.EDER MATEUS MEDINA**

Barcelona, Septiembre del 2020

THESIS COMMITEE MEMBERS

PRESIDENT	**Dra. Victoria del Pozo Abejón**
VOCAL	**Dr. Pascual Martínez Peinado**
SECRETARY	**Dra. Nuria Climent Rodríguez**

INDEX

SUMMARY

Animal models of allergic airway inflammation are helpful tools to study the pathogenesis of asthma and potential therapeutic interventions. Despite the long use of experimental asthma models, the nature of allergen-driven experimental asthma and allergen delivery route with the use of adjuvants may be distant from human allergic sensitization and the physiopathology of actual asthma. The aim of this work has been to establish a murine asthma model through close-to-real pathogenic procedures that allow representing different airway inflammatory profiles as seen in clinical practice, with their associated cardinal disease traits, providing an extended set of tools for the comparative investigation of disease mechanisms and, eventually, identifying novel diagnostic or therapeutic targets. We chose for this purpose the C57BL/6J mouse, a non-Th2-biased inbred strain, house dust mite (HDM) as a relevant aeroallergen in human asthma, and intranasal (*i.n.*) instillations for an inhalational delivery route.

We started with dose-finding experiments combined with allergen exposure length testing. We found evidence of a T-cell driven adaptive immune response in a High-dose, 4-week (4W) setup as reflected by increased $CD3^+$ $CD4^+$ T cells and the production of HDM-specific IgE, along with a mixed eosinophilic and neutrophilic inflammatory infiltrate, and airway hyperresponsiveness. Longer exposures (6 weeks) led to a declined T-cell response and abrogation of airway hyperresponsiveness and the eosinophilic infiltrates, suggesting immunoregulation on the Th2 arm. From the data of these experiments, we chose the High-dose 4W protocol for further development, although this model still failed to generate airway remodeling. Aiming at representing airway remodeling, we tested delivering HDM in combination with *Staphylococcus aureus* enterotoxin-B (SEB) or α-galactosylceramide (α-Galcer). The addition of SEB elicited airway remodeling but inhibited airway hyperresponsiveness and $CD4^+$ T-cell infiltration, and α-Galcer failed to reproduce all cardinal asthma traits. Thus, both strategies failed to generate competent asthma models encompassing airway remodeling.

By Western blot analysis, we found that the DerP1 and DerP2 antigens undergo degradation in standardized, reconstituted HDM extract. Aeroallergen antigens may, therefore, undergo spontaneous degradation in environmental conditions leading to conformational changes that modify the immune response. By controlling the HDM preservation status, the use of partially degraded allergens (hereinafter termed H4 model) induced dominant neutrophilic inflammation, whereas preserved antigens (H20 model) elicited dominant eosinophilic inflammation. Both models showed evidence of a $CD4^+$ T cell-driven adaptive immune response with Th2 functionality leading to HDM-specific IgE production and successfully developed airway inflammation and remodeling.

The latter differed in its patterns, *i.e.*, mucoid with increased airway contractile tissue mass in the H20 eosinophilic model versus fibrotic remodeling in the neutrophilic model. Upon kinetics analyses of immune response outcomes, these diverging models showed complex patterns that varied through time and were concordant with the eosinophilic versus neutrophilic profiles. This H20-eosinophilic versus H4-neutrophilic model diversion encompasses a broad representation of inflammometric profiles seen in real-world clinical practice.

Employing these models, kinetic phenotyping of the infiltrating eosinophils and neutrophils by cell surface markers related to maturation, migration, and proinflammatory versus immunomodulatory activity (Ly6, CD11b, SiglecF) allowed us to identify subpopulations that varied between the models and fluctuated across time. These changing subpopulations likely involve functional implications not yet identified.

Finally, we performed proteomics in murine BAL and induced sputum from asthmatics. Overall, the proteomics data support that the H4 and H20 models are driven by close-to-human's immune responses. We identify immune response-related gene expression patterns with some differences from proteins previously linked to atopic asthma and some proteins differing between eosinophilic and neutrophilic asthma. Further study of gene expression differing between the inflammatory profiles may point towards targets of potential diagnostic or therapeutic value.

ABBREVIATIONS

α-GalCer: α-Galactosylceramide

α-SMA: Alpha-smooth muscle actin

ACN: acetonitrile

ADAM: A disintegrin and metalloproteinase domain

AHR: airway hyperreactivity

ANOVA: analysis of variance

APC: antigen presenting cell

ASM: airway smooth muscle

BAL: bronchoalveolar lavage

BPIFB1: BPI fold-containing family B member 1

BSA: Bovine serum albumin

C5/C6: complement component 5/6

CCR: C-C chemokine receptor

CD: cluster differentiation

CHIL3L1: chitinase-3-like

CRP: C-reactive protein

CTSD: Cathepsin D

CTSG: Cathepsin G

CXCL: C-X-C motif chemokine ligand

Cys-LTR: cys leukotriene receptors

Cys-LTs: cysteinyl leukotrienes

DC: dendritic cell

Derp: *Derpatophagoides pteronyssinus*

DPBS: Dulbecco's buffer saline

DTT: Dithiothreitol

EEF1A1: Elongation factor 1-alpha 1

EGF: epidermal growth factor

ELANE: Neutrophil elastase

EPX: Eosinophil peroxidase

Fc: immunoglobulin crystallizable fragment

FCN1: Ficolin-1

FcεRI: high-affinity IgE receptor

FcεRII: low affinity IgE receptor

FEV_1: forced expiratory volume in 1 second

FGA: fibrinogen alpha chain

FGB: Fibrinogen beta chain

FGG: fibrinogen gamma chain

FN1: Fibronectin type II domain containing
GINA: Global Initiative for Asthma
GM-CSF: granulocyte-macrophage colony-stimulating factor
GPI: glucose-6-phosphate isomerase
GRB2: Growth factor receptor-bound protein 2
H&E: Haematoxylin-eosin
HDM: House Dust Mite
HRG: histidine-rich glycoprotein
HRP: horseradish peroxidase streptavidin
HRV: human rhinoviruses
IFN-γ: interferon gamma
IFN: interferons
Ig: immunoglobulin
IL: interleukin
ILCs: innate lymphoid cells
IO: Ionomycin
IP3: inositol-1,4,5-trifosphate
ITGAM: Integrin alpha-M
ITIH4: inter-alpha-trypsin inhibitor heavy chain H4
KNG: kininogen-1
LGALS3: Galectin-3
LPS: lipopolysaccharide
LTA4H: Leukotriene A-4 hydrolase
LTs: Leukotriene
MBP: major basic protein
MCh: methacholine
MLC: myosin light chain
MLCK: myosin light chain kinase
MMP: Matrix Metalloproteinase
MPO: Myeloperoxidase
MT: Masson's Trichrome
NETs: neutrophil extracellular traps
(NF)-κβ: nuclear factor κβ
NK: natural killer
NKT: natural killer T
ON: overnight
ORM1: aplha-1-acid glycoprotein

OVA: ovalbumin

p-MLC: phosphorylated-MLC

PAMPs: pathogen-associated molecular patterns

PAS: Periodic acid-Schiff

PBS: Phosphate buffer saline

PGD2: prostaglandin D2

PGLYRP1: peptidoglycan recognition protein 1

PMA: Phorbol Myristate Acetate

PRG2: Bone marrow proteoglycan

PRG3: Proteoglycan 3

PRRs: pattern recognition receptors

PYCARD: Apoptosis-as asociated speck-like protein containing a CARD

RBC: Red blod cell

RHOA: Transforming protein RhoA

ROS: reactive oxygen species

RSV: respiratory syncytial virus

RT: room temperature

S100AB: protein S100-AB

SCID: severe combined immunodeficiency

SEB: Staphylococcal Enterotoxin B

SERPING1: plasma protease C1 inhibitor

SMC: Smooth muscle cell

TAGLN2: Transgelin-2

TCR: T-cell receptor

TF: tissue factor

TGF-β: transforming growth factor beta

Th1/2: Type 1/2helper T lymphocyte

TIMP-1: tissue inhibitor of matrix metalloproteinase-1

TLR: toll like receptor

TMB: 3,3',5,5'-Tetramethylbenzidine

TNF: tumor necrosis factor

TSLP: thymic stromal lymphopoietin

TTN: Titin

VTN: Vitronectin

WG: Wright-Giemsa

µm: micrometer

INTRODUCTION

1. Asthma

Asthma is classically described as reversible airflow obstruction in association with non-specific bronchial hyperreactivity and chronic airway inflammation (1, 2). Asthma has evolved as a global problem, impacting 300 million people worldwide (3), with 250.000 annual deaths (4, 5), and is associated with a significant health and economic burden (6, 7). Asthma presents the highest incidence in developed countries. This trend may perhaps be partly explained by the hygiene hypothesis since industrialization and urbanization are associated with an increased incidence of allergic diseases (8).

Asthma has long been associated with excessive T-helper cell type 2 (Th2) responses with specific IgE production and eosinophilic inflammation. These key features only encompass allergic asthma, leaving aside a diagnostic umbrella for the heterogeneous term of asthma as per the Global Initiative for Asthma (GINA) guidelines (9). Rather than a single disease, asthma is a collection of different “endotypes” (disease mechanisms) and varying “phenotypes” (clinical variants) that commonly manifest wheezing, shortness of breath, cough, chest tightness, and variable airflow obstruction (10, 11).

Although the two main asthma phenotypes consist of allergic and non-allergic, a broad spectrum of factors based on the level of severity, the frequency of exacerbations, the presence or absence of chronic airflow obstruction, the age of disease onset, and even the response to particular therapies are all factors determining further clinical diversity. As a result, the asthma phenotypes are based on clinical criteria and physiological characteristics that result from a combination of hereditary and environmental influences (like allergens) that can affect the disease, and it seems unattainable to establish fixed categorical phenotypes. It is noteworthy to highlight this complexity together with the severe asthma segment, which encompasses 5 to 10% of the asthmatics, who manifest symptoms refractory to therapy (10, 12) and account for the majority of asthma morbidity and mortality (10). The variability within severe asthma makes it necessary to improve the identification of molecular and immunological traits that can be transferred to decision-making in asthma management (10, 12).

1.1. Epidemiology

Epidemiological studies have shown a consistent association between atopy and asthma. Diet, food intolerance and sensitivity, and intake levels of specific micronutrients, are potential risk factors for asthma over two decades (13).

Among adults with non-atopic severe asthma, nearly 60% are obese (14, 15). The prevalence of obesity increased dramatically in many countries in the latter decades of the twentieth century, particularly in Western developed countries. Several other factors are associated with asthma, like a higher frequency of gastroesophageal reflux, the upregulation of immunologic and inflammatory responses, and a shared genetic basis for both conditions (15, 16).

In Western Europe, independently of body mass index or age, atopic asthma relates to a higher prevalence of specific IgE to house dust mites (HDM) such as *Dermatophagoides pteronyssinus*, cats, grass (Timothy grass), or *Cladosporium (17)*. Among young adults between 20 and 44 years, the prevalence of specific IgE was higher in Australia, New Zealand, the United States, the United Kingdom, and the Netherlands than in Spain, Iceland, or Italy. Another study in children between 8 and 12 years old showed that the prevalence was higher in Almería (Spain) and Rome but lower in India, Mumbai, Estonia, and Tallinn (18). Interestingly, variation between countries, regions and even individual test centers is significant, although the prevalence of HDM allergy is constantly found in Western nations (19), affecting between 65 to 130 million persons, which is equivalent from 1% to 2% of the world's population (20). Unlike what occurs in Western countries, in areas such as Africa, the discrepancy between the methods used to assess sensitization to certain mites (skin prick test results and the levels of allergen-specific IgE) makes it difficult to assess the sensitization prevalence. For this reason, the relative prevalence of responses to a standardized panel of allergens is more informative than an absolute prevalence (13).

1.1.1. Genetic factors

Asthma tends to cluster in families, proven by familial aggregation and prevalence in twins, supporting the hypothesis that there is a genetic link within asthma. Moreover, it has been shown that gender is also a risk factor for asthma. Among young children, the male gender is more frequent, whereas adolescents and adults show females to be at greater risk, a genetic predisposition that renders some patients more vulnerable to sensitization than others (13, 21).

Genetic studies have identified single nucleotide polymorphisms in ADAM33 (22), transforming growth factor (TGF)-β1 (23), IL4R, and IL4 (24) that are associated with lower lung function and also have been associated with near-fatal exacerbations of asthma. Other genetic factors are abnormalities in histone deacetylation pathways,

overexpression of the alternative non-functional glucocorticoid receptor β, or transcription-factor interference with the functional glucocorticoid receptor α. All of these factors influence the response to corticosteroid therapy and triggers persistent inflammation (12).

Epigenetic effects associated with HDM allergen sensitization are involved in airway remodeling and airway hyperresponsiveness (25). Moreover, a single nucleotide polymorphism in the thymic stromal lymphopoietin is associated with aberrant innate immunity in this asthmatic response (26).

1.1.2. Environmental factors

In the first years of life, lower respiratory tract infections are caused by human rhinoviruses (HRVs), respiratory syncytial virus (RSV), parainfluenza viruses, and other pathogens, which may cause wheezing in children with or without asthma. Although the primary focus of childhood wheeze and asthma has been on viral respiratory tract infection, bacterial airway colonization has also been associated. Among them, *Streptococcus pneumoniae*, *Haemophilus influenzae*, *Moraxella catarrhalis* (13), and *Staphylococcus aureus* (27) are the most frequent.

Another environmental factor is inhaled aeroallergens that can penetrate the airway epithelium and stimulate inflammatory responses in the airways (28). The probability of inhalation and how the allergen penetrates into the lung vary depending on the molecule size of different mite-related products. Smaller particles (1.1-4.7 μm) are more difficult to inhale but can penetrate deeper into the lung (29), while larger particles (>4.7 μm) are more frequently inhaled and induce a more substantial early-phase response than the smaller ones provoking fewer symptoms (30-32).

Allergic effects to HDM, one of the most frequent indoor allergens, are orchestrated by the innate and adaptive immune system (33, 34), a combined effect that makes HDM allergens so powerful (35). Proteases are essential components in this response, but other immunogenic epitopes like structural polysaccharide chitin from the exoskeleton, microbial adjuvant, and ligands from mite-associated compounds can also activate the immune system (34, 35). The chronicity of this immune response is critical and known to be increased in patients with HDM allergy (36).

HDM allergens cause different effects depending on their molecular structure and activity. The most significant allergens present in HMD are represented by Derp1 and Derp2 and have very different effects. The Derp1 molecule, highlighted by its protease activity, potentially destroys the epithelial tight junctions causing direct damage to the respiratory epithelial cells. In addition to its powerful direct effects, Derp1 can also activate the innate immune response and is recognized by protease-activated receptors and Toll-like receptors (TLR) that mimic the molecular pattern activation associated with pathogens, facilitating an allergic reaction to non-enzymatic allergens (33, 34). Derp2 might induce mimicry of the TLR-4 coreceptor MD-2 (34). The dominant causative allergen in a population might differ regionally and could also vary among patients (37). Moreover, climatic variables such as humidity are critical factors for HDM species by affecting their prevalence both inside and outside homes (38).

1.2. Allergen effects on asthma

About two-thirds of asthma cases are allergen-induced diseases. Intermittent allergen exposure, such as for seasonal allergens like ragweed, produces recurrent episodes of airway inflammation, whereas persistent airway inflammation upon continuous allergen exposure, such as for perennial allergens like HDM, mediates the chronicity of the response. Chronic allergen exposure triggers a distinct array of immunobiological and biochemical responses that impact the airway structure and contribute to clinical symptoms (39, 40). In humans, the resulting airway remodeling includes changes such as airway wall thickening due to goblet cell and airway smooth muscle (ASM) hyperplasia, epithelial cell hypertrophy, subepithelial fibrosis, and collagen deposition (41, 42).

Prevalence data from HDM allergen sensitization in the general worldwide population have shown 50% of adults and 90% of children being affected among asthmatic patients (5, 28, 33). A standardization in epidemiologic research is needed due to the heterogeneity of populations, terminology, and endpoints in the literature. Improved understanding of HDMs, their allergens, and their microhabitats will enable the development of more effective outcomes for patients with HDM allergies (28).

2. The immune system

The immune system is a complex network of organs, cells, and proteins that defends the body against infection. The innate immune system can identify pathogen-associated molecular patterns (PAMPs) to detect potentially infectious microbes and damage-associated molecular patterns (DAMPs) that are released from injured or dying cells. Immune system alterations can lead to allergic diseases such as allergic asthma.

2.1. Inflammatory infiltrates and response in asthma

The infiltration of inflammatory cells into the airway (predominantly granulocytes and lymphocytes) and the sequential interaction with resident cells (mast cells, epithelial cells, macrophages) generates positive feedback that contributes to the chronic inflammation and clinical manifestations associated with asthma.

2.1.1. Role of Innate immune pathways

The **innate immune response** induced in the airway epithelium is a dynamic orchestrator of immune responses in asthma. Most asthmatics present tight junction damage in the epithelial barrier reducing its integrity, facilitating the access of allergens and microbes to the stromal tissue. Moreover, protease-containing allergens such as HDM are able to directly cleave epithelial tight junctions and disrupt barrier structures. Furthermore, the airway epithelial cells recognize these allergens or microbes by pattern recognition receptors (PRRs) and respond rapidly with the release of alarmins such as thymic stromal lymphopoietin (TSLP), IL-25, and IL-33. While TSLP, IL-25, and IL-33 can activate Group-2 innate lymphoid cells (ILC2s), TSLP also primes a specialized population of antigen-presenting cells, the dendritic cells (DCs) to promote adaptive immunity by activating T and B cells (10).

Recent studies have shown that innate immunity has a leading role in the pathophysiology of asthma, mediating the interconnection of innate and adaptive immunity (**Figure 1**).

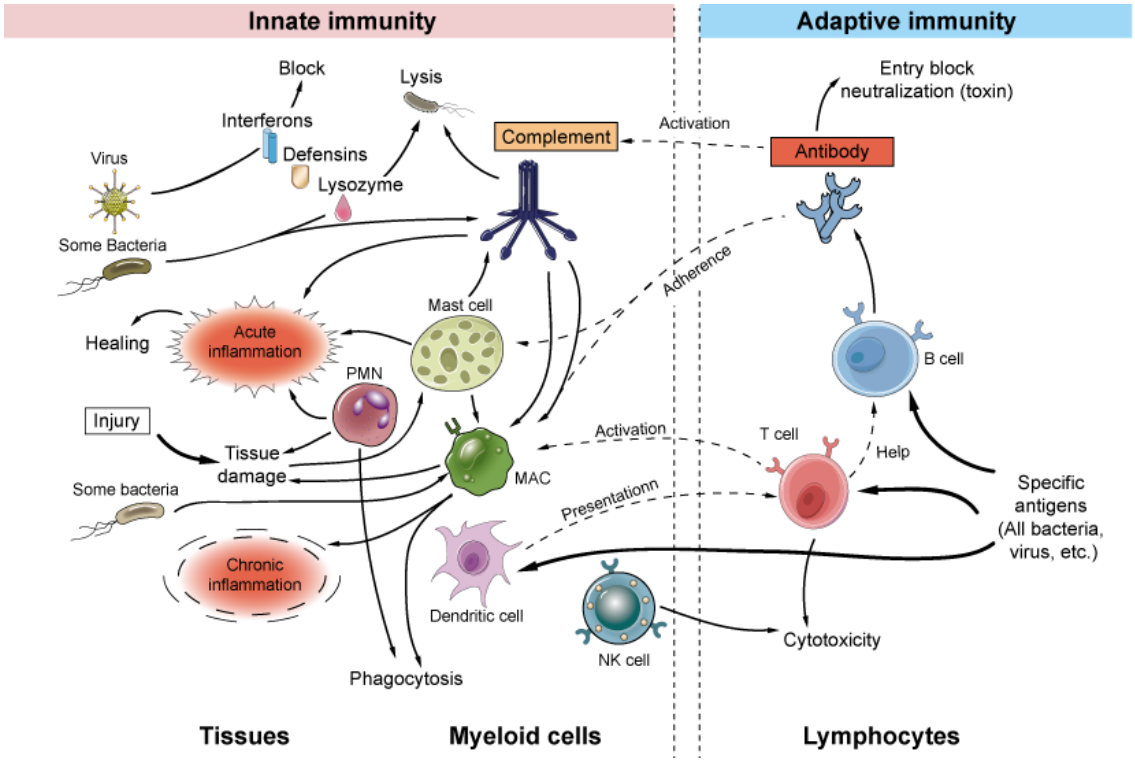

Figure 1. The innate and adaptive immune system. The immune system is formed by the first line of defense or the innate system, which provides a rapid non-specific response, involving NK cells, macrophages, dendritic cells, mast cells, basophils, neutrophils and eosinophils. The second line of defense or the adaptive system is a long-term specific antigen response since it generates memory, involving both T and B lymphocytes. (Reproduced from **creative-diagnostics.com**).

- Dendritic cells (DCs)

The underlying mucosa associated with the airway epithelium hosts a specialized population of antigen-presenting cells called DCs (43). DCs express innate immune receptors that lead them to uptake and process antigens (such as allergens) into small peptides and present them through the class-II major histocompatibility (MHC-II) complex for T-cell receptor (TCR) recognition.

DCs are subdivided into two types, conventional DCs (cDCs) and plasmacytoid DCs (pDCs) (5). Sputum and peripheral blood from asthmatic patients contain increased numbers of both DCs, which increase even further upon allergen challenge. Inflammatory DCs are sufficient for the development of Th2 immunity to HDM allergen when the first exposure occurs by inhalation. For inhaled allergens, DCs amplify the Th2 response through basophils and TLR4 signaling on epithelial cells (44). TLR activation on epithelial cells stimulates the production of Th2 chemokines and cytokines (IL-25, IL-33, and granulocyte-monocyte colony stimulation factor (GM-CSF)) that enhance DC motility and antigen sampling (45).

- Innate Lymphoid Cells (ILCs)

ILCs are a family of lineage-negative innate lymphocytes that, unlike T and B cells, do not present surface markers nor antigen-specific receptors and do not participate in classical allergen-specific activation (5). ILCs are underrepresented in lymphoid tissues but, in contrast, are enriched in parenchymal tissues, especially mucosal surfaces. At the mucosa of the lungs, ILCs seem to be important regulators of epithelial barriers due to their strategic localization, and can respond rapidly to pathogens, promoting the adaptive immune response (46). Based on the cytokine profile and transcription factor expression, three groups of ILCs were classified in parallel to the different effector T-helper cell subsets (262). Th1 cells and their innate counterparts, ILC1s, express T-bet and produce IFN-γ to fight against intracellular pathogens. Th2-like ILC2s express GATA-3^{HIGH} and can secrete IL-5, IL-13 and epidermal growth factor (EGF). The third subtype, that is the more heterogeneous group, is the ILC3s that correspond with the Th17 response and is characterized by the expression of RORγt+ together with IL-17, GM-CSF and IFN-γ (5).

ILCs indirectly react to pathogens through cytokine activation produced by myeloid or epithelial cells, such as IL-12 for ILC1s; IL-33, IL-25, IL-4 and Alarmins as TSLP for ILC2s; and IL-23 or IL-1α/β for ILC3s (46).

- Natural Killer (NK) cells

NK cells are a relevant link between the innate and adaptive immunity. Infectious agents can activate not only macrophages and epithelial cells but also NK cells, which stimulate the secretion of cytokines such as GM-CSF (47) and enhance the acute inflammatory response. Moreover, NK cells can activate the production of growth factors in fibroblasts, contributing to the persistence of the inflammatory response (47). Referred to as innate immunity, NK cells are now considered ILCs, first classified into Group 1 and now as a separate group. Moreover, they represent the innate immunity analogue of cytotoxic $CD8^+$ T cells in the adaptive immune response.

- Neutrophils

Due to their ability to target and kill pathogens by different mechanisms, neutrophils are the first line of defense during pulmonary infection (48). One of these mechanisms is the capacity to release chemotactic factors and preformed granule proteins that attract

monocytes and macrophages to the site of infection and promote the immune infiltrates (49). Moreover, neutrophils have direct antimicrobial activity by the generation of reactive oxygen species (ROS), activation of granular proteases, and release of neutrophil extracellular traps (NETs) (50). Neutrophils can contribute to airway remodeling, airway narrowing, mucus hypersecretion (51), increased ASM responses (52), and a rapid decline in lung function (53, 54). Their role in airway remodeling is due to the release of proteases like MMP-9 (54, 55), and neutrophil elastase (56), which augments IL-8 production from airway epithelial cells, inducing feedback of neutrophil recruitment to the airways. Elastase also inactivates tissue inhibitors of MMP-1 (TIMP-1), which inhibits MMP-9, causing an increase in levels of MMP-9 and Elastase (57). An imbalance in MMP-9/TIMP-1 has also been associated with persisting wheezing in preschool children (58). The epithelial barrier function can also be affected by an increased neutrophil burden in the airways of patients with severe asthma (59).

- Eosinophils

Eosinophils are granulocytes with characteristic acidophilic granules, also known as secondary granules, that differentiate them from neutrophils and basophils. The secondary granules contain a large number of mediators that can be released upon stimulation, as basic proteins, cytokines (IL-13 and IL-5), chemokines (such as eotaxins), as well as cysteinyl leukotrienes (Cys-LTs) such as LTC4, LTD4, and LTE4, capable of inducing inflammation and tissue damage. The primary mediators are proteins contained in the eosinophilic granules (*i.e.*, major basic protein (MBP), eosinophil peroxidase, eosinophil cationic protein, and eosinophil-derived neurotoxin) that have direct effects on the host tissues and can promote inflammation (60, 61). Eosinophils also express receptors that recognize cytokines, patterns, Siglec-8, the immunoglobulin crystallizable fragment (F_C) region, lipids, and can also express MHC-II receptors (62, 63).

Eosinophil development in the bone marrow is stimulated by IL-3, IL-5, and GM-CSF. The IL-5 also induces eosinophil tissue recruitment together with upregulation of chemokines like eotaxins, which respond via CCR3 receptors expressed on the eosinophils (63). Additionally, activated eosinophils can produce profibrotic factors that can increase bronchial fibroblast deposition of extracellular matrix. These factors are associated with features of remodeling, mainly related to subepithelial fibrosis (64). Their inflammatory factors promote ASM contractility and inhibit its relaxation (65). Cys-LTs are potent bronchoconstrictors that stimulate ILC2 production of type-2 cytokines, acting in synergy with IL-33 and driving a self-amplifying loop of Th2 inflammation (10).

2.1.2. Adaptive immune response (T and B cells)

The **adaptive immune response** provides specific antigen recognition and memory. This memory is essential to respond faster and effectively after a rechallenge by the same antigen. This response follows the innate immune response and is much more complex; however, it requires the cooperation of the T and B lymphocytes with innate myeloid cells to proceed with a complete response (**Figure 1**).

2.1.3. T-Cell Plasticity and Heterogeneity in Asthma

In asthma, the T helper cell subpopulations do not show finally differentiated static conditions. Instead, they show a degree of plasticity that leads them to transdifferentiate into other effector $CD4^+$ subtypes by the influence of environmental factors. Due to this plasticity, effector $CD4^+$ T cells may concomitantly pertain to Th1 and Th2 responses in asthma (66) and have crosstalk between cytokines related to each subtype with simultaneous involvement of additional innate and adaptive immune pathways. The Th1/IFN-γ axis is thought to modulate Th2 inflammation through a balance between its suppressive effect on Th2 activation and its impact on Th2 cell recruitment into the airways. However, it is not clear if the Th1 response is able to potentiate Th2 inflammation. Th2 and Th17 overlap has also been evidenced in severe asthma. The presence of both Th2 and Th17 cells in bronchoalveolar lavage (BAL) is an indicator of severe asthma as compared with the presence of Th2 or Th17 cells alone. A possible mechanism because IL-17 and Th2 cytokines are highly pathogenic, is their capacity to act synergically and enhance airway leukocyte recruitment by airway epithelial cells stimulation (67).

Environmental signals can support heterogeneity and plasticity in ILCs (68) Together, both the plasticity of T cells and ILCs are added to the complexity of inflammation in severe asthma. These facts raise the consideration that, contrary to highly polarized and unambiguous endotypes, severe asthma might represent a spectrum of overlapping inflammatory states.

2.1.4. T-helper asthma endotypes (Th2, Th1/Th17)

$CD4^+$ T cell responses in asthma are very heterogeneous and comprise multiple subsets. For this reason, the basis of asthma endotypes is the understanding of the dominant $CD4^+$ T cell response. Since the discovery of the classical $CD4^+$ T cell subsets (the Th1 and Th2 subpopulations), it was established that the Th2 cell is the main driver of eosinophilic airway inflammation (69). Wenzel et al. proposed two groups of asthma, namely Th2 and non-Th2 subtypes, based on the presence of airway eosinophilic inflammation observed in the clinical phenotypes (**Figure 2**) (66). This led to polarization into two major asthma endotypes: Th2-high (eosinophilic) and Th2-low (non-eosinophilic), being Th2-low considered the most relevant to severe asthma (69).

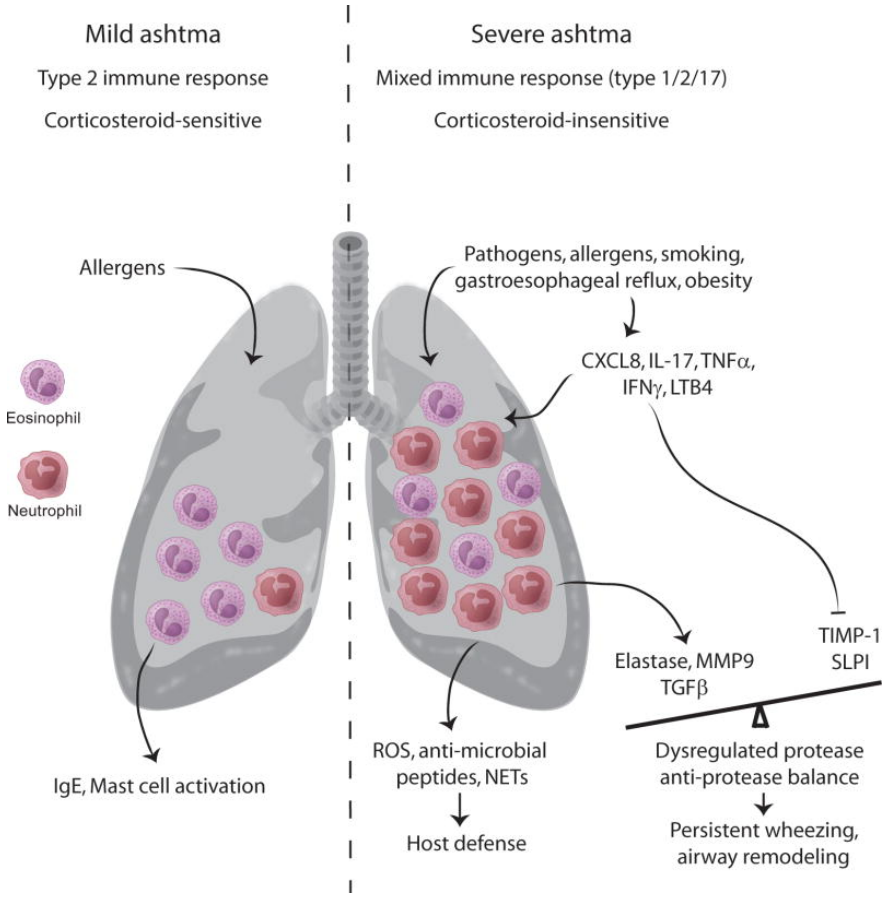

Figure 2. Endotype features of mild and severe asthma. Mild asthma is characterized by type 2 inflammation in combination with eosinophilia in the airways, accompanied by elevated IgE levels with good response to Corticosteroids. By contrast, Severe asthma is characterized by a mixed response of Th1/2/17 inflammation together with mainly neutrophils and are related with poor response to Corticosteroids. (Reproduced from Carr, T. F., Zeki, A. A., & Kraft, M. (2018)).

- Th2 Low (Th1/IFN-γ and Th17/IL-17)

Recent studies in both mice and humans have highlighted increased Th1/IFN-γ and Th17/IL-17 responses in asthma, particularly in corticosteroid-resistant severe asthma, which is often associated with airway infiltration by neutrophils (70, 71).

Th1 cells are a subset of $CD4^+$ T lymphocytes that have an essential role in the elimination of intracellular pathogens, which survive inside the phagocytic cells, and contribute to abrogating chronic infections (72). The Th1 cells secrete IFN-γ, promote macrophage and cytotoxic $CD8^+$ T cell activation, and stimulate B cells to secrete IgG, which opsonizes pathogens (73). In contrast, Th2 cells promote the elimination of extracellular pathogens and are implicated in allergic diseases (74). In addition, when dendritic cells interact with particular pathogens, they promote the secretion of IL-6 and TGF-β, which induce Th17 differentiation (75, 76). These T cells produce the IL-17 cytokine family, which promotes the secretion of the granulocyte colony-stimulating factor (G-CSF) and IL-8, and induces neutrophilic infiltration of the airways (77, 78).

High transcripts of IL17A were found in the sputum of patients with asthma and correlated with CXCL8 (IL-8) transcripts, sputum neutrophils, and asthma severity (79). CXCL8 is the most potent neutrophil chemoattractant in the lung (80). Although various cell types, including airway epithelial cells, T cells, and macrophages can secrete CXCL8, neutrophils themselves can produce this chemokine, promoting further neutrophil recruitment to the airways (81). Interestingly, neutrophils from asthmatics express high-affinity IgE receptors (FcεRI), whose engagement leads to the release of CXCL8 from the neutrophils (82). CXCL8 is also induced by IL-17, which shows crosstalk between neutrophils and Th17 cells (83). Moreover, neutrophils can produce CXCL10, which induces Th1 cell recruitment. The IFN-γ produced by Th1 cells has also been implicated in the chemotaxis of neutrophils (84) Thus, it is possible that Th1 and Th17 cells establish a communication network in the airways of some severe asthmatics.

Recent hierarchical transcriptomics clustering analysis of sputum identified different clusters that allowed classifying asthmatic subjects (85). One cluster was associated with the highest level of sputum neutrophilia (>90%) accompanied by increased expression of CXCR1/2 and members of the IFN (both type I and type II IFN-inducible genes) and TNF families. This cluster was related to ILC-1 and ILC-3, as well as with inflammasome signatures, suggesting that type-I and II IFNs and the inflammasome are critical drivers of this endotype.

- Th2 High (Th2/IL-4/IL-13/IL-5)

Th2-high asthma is related to eosinophilic inflammation (10). The cytokines produced by Th2 cells, chiefly IL-4, IL-5, and IL-13, orchestrate this inflammatory profile. IL-4 activates IgE production by B lymphocytes. Eosinophil recruitment and survival depend mainly on IL-5, whereas IL-13 has multiple effects in the lungs, including a relevant role in the development of airway hyperreactivity (AHR) and tissue remodeling (86).

Previous studies suggest that HDM-specific Th2 cells have an essential role in the allergic inflammatory response to HDM allergens by inducing the production of specific IgE, the permissiveness of endothelium for the recruitment of inflammatory cells to lungs like eosinophils, production of mucus, and modulation of the ASM contraction (86).

Recent hierarchical clustering analysis of sputum transcriptomics identified different clusters to classify patients with asthma (87). One cluster was associated with eosinophilic sputum and the Th2 genes IL1RL1 and CCR3, genes also related to systemic inflammation by elevating C-reactive protein (CRP) and IL-6 levels in the blood. Another cluster, related to moderate-to-high sputum eosinophils counts, comprises genes associated with metabolic pathways, ubiquitination, and mitochondrial function.

2.1.5. Cytokine targets

- IL-4/IL-13

The cytokines involved in the Th2 response are encoded in the IL-4 gene cluster in chromosome region 5q23-31, containing the genes encoding IL-4, IL-5, IL-9, IL-13, and GM-CSF (88). The IL-4 promotes B-cell isotype switching to IgE, the upregulation of adhesion molecules, eotaxin production, and the development of AHR and goblet cell metaplasia. IL-13 has an effect on ASM cell cycle by upregulating the RhoA protein. IL-4 and IL-13 together induce cytokine and chemokine production by the airway epithelium (i.e., TSLP, GM-CSF, and CCL20) (89).

- IL-5

IL-5 is the key cytokine to eosinophil growth, maturation, activation, and survival. For this reason, it has a significant effect on acute and sustained pulmonary eosinophilia and changes in lung function.

- IL-9

IL-9 can induce ILC2s to boost the production of IL-5 and IL-13 (90). Mice with IL-9 overexpression in the lung have increased airway inflammation and AHR (91).

- IL-17/IL-22

The IL-17 family: IL-17A, IL-17F, and IL-22 are produced by the $CD4^+$ Th17 lineage. In mice, allergic sensitization followed by airway challenge induces a robust Th17 response that causes AHR and airway remodeling by direct interaction of IL-17 with bronchial smooth muscle cells (92, 93). Additionally, IL-17 can also induce steroid insensitivity in bronchial epithelial cells (94). In mouse asthma models, IL-22 exert a dual role, their inhibition, reduces eosinophil recruitment and helps epithelial repair by Th2 cytokine production; but at the same time, IL-22 inhibition in allergen challenge induced lung inflammation and an increased in Th2 cytokine production (95).

- TNF-α

Tumor necrosis factor-alpha (TNF-α) is a cytokine that exerts a variety of effects, such as growth promotion, apoptosis, angiogenesis, cytotoxicity, inflammation, and immunomodulation. TNF-α is mainly produced by activated macrophages, but other immune cells like lymphocytes or NKs, as well as stromal cells like endothelial cells and fibroblasts, lead to increased TNF-α concentrations in BAL from the airways of patients with asthma (96).

- IFN-γ

The role of interferon-gamma (IFN-γ) in asthma is controversial, yet it plays a role in both severe acute and chronic stable asthma, due to having immunomodulatory effects in innate and adaptive immunity. IFN-γ has an important role in asthma due to their importance in AHR enhanced. Interestingly, IFN-γ can up-regulate Cys-LT receptors (Cys-LTR) on smooth muscle cells, modulating the response to LTD4 and increasing smooth muscle stiffness. Moreover, it can also up-regulate Cys-LTR on eosinophils, contributing to inflammation during acute exacerbations of asthma (97).

- Serum IgE

The specific IgE produced in response to allergen exposure binds to its Fc high-affinity receptor (FcεRI), most prominently expressed on mast cells, and to the low-affinity receptor (FcεRII) expressed on antigen presenting cells (APCs) and other cell types. On the mast cell surface, crossing of two or more FcεRI-bound specific IgE molecules by antigen encounter triggers mast cell activation and the release of the early allergic response mediators. The subsequent release of further mediators including Cys-LTs, along with other factors such as increased vascular permeability, induce the late allergic response with the recruitment of other leukocytes, mostly effector $CD4^+$ T cells and eosinophils, and the formation of inflammatory infiltrates (98). Specific IgE also facilitates antigen presentation through enhanced antigen uptake by B cells and DCs. Moreover, data demonstrating the expression of FcεRI on ASM cells show that IgE may directly contribute to airway remodeling (99). Thus, IgE may be involved in airway remodeling in severe asthma.

2.2. Immune responses against allergens

During sensitization, immature DCs encounter allergens at the airway epithelial barrier. Upon allergen uptake, the DC matures and migrates to the regional lymph node to induce differential and clonal expansion of allergen-specific Th2 cells from naive $CD4^+$ T cells. Th2 cell polarization can be facilitated by alarmins (TSLP, IL-33, IL-25) produced by disrupted epithelial cells, which induce OX40L upregulation on DCs and activate ILC2s to produce Th2-type cytokines. In the lymph node, Th2-primed T cells produce IL-4 and IL-13, which initiate immunoglobulin class switching in allergen-specific naive B cells, which evolve into plasma cells producing allergen-specific IgE and memory B cells. The released antigen-specific IgE binds FcεRI receptors expressed by mastocytes and basophils. Upon subsequent allergen encounter (challenge), mast cells and basophils are activated by FcεRI-bound, allergen-specific IgE cross-linking, releasing inflammatory mediators responsible for the early phase of the allergic response. This process induces mast cell degranulation and releases large amounts of histamine, prostaglandin D2 (PGD2), leukotrienes, and the inflammatory cytokine TNF-α. Histamine is a key mediator of the immediate effects of allergic reactions, acting directly on blood vessels to induce an influx of fluid, causing swelling or edema. By contrast, leukotrienes have more lasting actions than histamine and cause smooth muscle contraction, which leads to bronchoconstriction. A late-phase response is initiated upon infiltration of additional effector cells to the site of allergen encounter. The Th2-type response to the allergen is

further maintained and reinforced by stimulated allergen-specific Th2 cells (5). With repeated episodes over time, chronic changes occur. These include the loss of epithelial cells, goblet cell hyperplasia, submucosal collagen accumulation, smooth muscle growth, and an overall thickening of the airway wall, collectively referred to as airway remodeling (**Figure 3**).

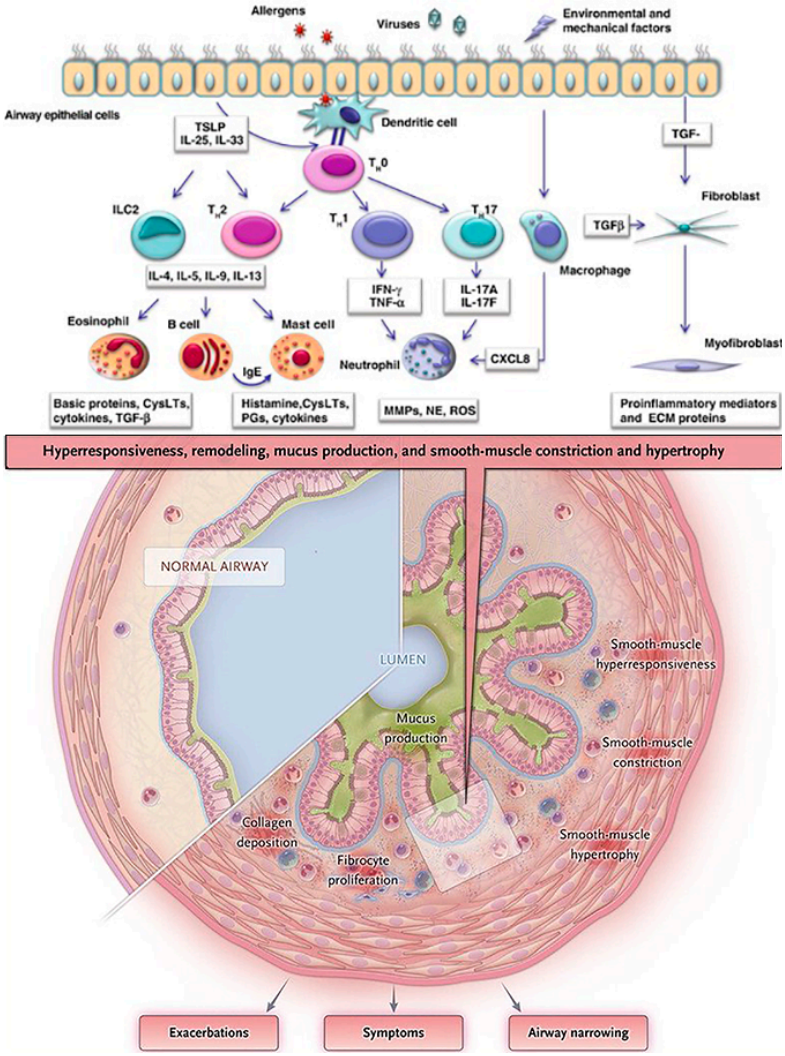

Figure 3. Airway epithelium as the primary interface between lung and the environment. Allergen, viruses and environmental factors trigger the soluble factors released by epithelial cells that recruit and activate immune cells. The signal amplification involves macrophages, Dendritic cells, neutrophils, mast cells, eosinophils and lymphocytes. Both the epithelium and immune cells produce paracrine signals that induce angiogenesis, goblet cell hyperplasia, hypertrophy and hyperplasia of smooth muscle and thickening of the lamina propria due to increased deposition of extracellular matrix. (Modified from Bergeron, C., Tulic, M. K., & Hamid, Q. (2010); and Elliot Israel, M.D., & Helen K. Reddel, M.B., B.S., (2017).

3. Pathophysiology of asthma: structural changes of the airways

The histopathological features of asthma were extensively described by Huber and Koesser in 1922 (100). In necropsy specimens from fatal asthma cases, they observed extensive mucus plugs present along the segmental and subsegmental bronchi, and peripheral airways. The composition of mucus plugs includes necrotic airway epithelial cells, inflammatory cells comprising lymphocytes, granulocytes (mainly neutrophils and eosinophils) (101, 102), plasma protein exudate, and mucins (103, 104). Interestingly,

airway inflammation in severe acute asthma exacerbations is often different from stable, mild or moderate asthma. Mild and moderate asthma is commonly characterized by eosinophilic airway inflammation, whereas prominent neutrophil infiltrates may occur in sudden-onset fatal asthma attacks (100, 105-107). The enlargement of submucosal glands is more characteristic in severe forms of the disease (108), while an increment of the number of goblet cells is related to mild and moderate asthma (109).

Regarding the airway epithelium, signs of airway epithelial repair, such as sloughing of ciliated columnar cells, along with goblet cell and squamous cell metaplasia, are present. Simultaneously, an increased thickness of the subepithelial connective layer, by increased accumulation of extracellular matrix components beneath the basal lamina, is observed (110).

Airway remodeling denotes the pathophysiological modifications of the normal airway wall structure (111). It starts as a repair process in response to the inflammation that causes airway wall injuries. The dysregulation of the repair processes leads to mucus gland hyperplasia (112), airway smooth muscle hypertrophy and hyperplasia (113), and subepithelial thickening adjacent to the reticular basement membrane (110), all of which contribute to the progressive and irreversible loss of lung function (114). These modifications are partly reversible in mild asthma but are mostly irreversible in chronic severe asthma (111).

Asthmatic patients also show airway wall thickening due to an increase in the ASM mass and mucous glands (115). This airway wall thickening is more prominent in severe asthma (116). The airflow limitation is not only due to the airway wall thickening since the increased mucous secretion and the inflammatory exudates also play an essential role (117). Thus, airway remodeling has generally been considered an effect of chronic airway inflammation. Bronchoconstriction itself, without further inflammation, may induce airway remodeling (118). Overall, further work is necessary to better understand the relationship among inflammation. remodeling, and asthma severity (119).

3.1. Airway epithelium – Epithelial cells

The airway epithelium acts as a barrier frontline against environment stimuli but, in the asthmatic epithelium, its function is truncated and allows allergen penetration into the airway tissues due to defective intercellular tight junctions (120). Components of allergens such as house dust mite, cockroach, animal and fungal, can disrupt this epithelial tight junction and activate protease receptors (121). In response to local inflammation at inhaled agents, the associated epithelial cells enter into a continuous injury-repair process (122).

The repair phase is characterized by epithelial cell production of profibrotic mediators as TGF-β, fibroblast growth factor, and endothelin, which induce fibroblasts and myofibroblasts to release collagen, elastic fibers, proteoglycans, and glycoproteins. All these substances accumulate in the airway wall and cause subepithelial fibrosis (110, 123, 124) and the thickening of the inner wall layer, contributing to airway narrowing. Eosinophils can contribute to airway remodeling by the release of factors, as eosinophil-derived TGF-β, cationic proteins, and cytokines that can directly activate the epithelium and mesenchymal cells, developing airway remodeling (125, 126).

As long ago as 1883, Curschman noted the presence of ciliated columnar respiratory tract cells in the sputum of asthmatic patients. Years later (1908), Ellis observed detachment of the bronchial mucosa, considering it to be a mechanical separation consequent upon contraction of the bronchial muscle. The damage on the ciliated respiratory epithelium and the transudation of edema fluid into the bronchial lumen are critical factors in the failure to clear bronchial secretions in asthma (105). Another mechanism for increased production of mucous in the airways is the increased number and hypertrophy of the bronchial mucus glands (105), as well as goblet cell hypertrophy and hyperplasia (127), resulting in overall mucus metaplasia.

3.2. Airway Smooth Muscle

Another mechanism of airway remodeling is the abnormal growth of ASM. Biopsy studies have reported ASM hyperplasia and hypertrophy in children with mild to severe asthma (128). ASM cell proliferation is induced by the matrix metalloproteinase-2 (MMP-2), which is an autocrine factor required for proliferation (129). MMP-2 production by ASM contributes to the extracellular matrix turnover and airway remodeling. ASM can also participate in chronic airway inflammation by producing cytokines and chemoattractants for eosinophils, activated T lymphocytes, and macrophages/monocytes (68). In turn, the eosinophils can contribute to airway remodeling by enhancing ASM cell proliferation (130).

Not only the composition but also the function of the smooth muscle is also essential. ASM contracts by a calcium-dependent cross-bridge activation of actin and myosin, resulting in shortening and contraction (127). The calcium is released by inositol triphosphate (IP3) from sarcoplasmic reticulum stores, then the calcium-calmodulin

complex is formed and activates myosin light chain (MLC) kinase (MLCK), which phosphorylates regulatory MLCs creating phosphorylated-MLC (p-MLC) (131). The RhoA/Rho kinase signaling pathway upregulation increases the level of p-MLC and subsequently increases ASM contraction force. Moreover, acetylcholine or methacholine induce the formation of IP3 (131) and, as a consequence, induce contraction of ASM.

High levels of RhoA protein are found in airway hyperresponsive animal models. This increment is mediated through inflammatory cytokines, such as IL-13 (93) and IL-17A (129) that themselves directly enhance the contractility of ASM through RhoA/Rho kinase signaling change.

3.3. Extracellular Matrix

The airways of asthmatic patients present an excessive accumulation of extracellular matrix components, mainly collagen, in the subepithelial connective tissue and adventitia of the airway wall (132, 133). The accumulated deposition of extracellular matrix in asthmatic patients was described to cause thickening of the basement membrane's *lamina reticularis*, inducing subepithelial fibrosis (110). This subepithelial fibrosis is thought to be partly the consequence of airway epithelium dysfunction and deterioration (134) and has been associated with disease severity (135). ASM and myofibroblasts can contribute to tissue remodeling by altering the extracellular matrix and releasing components such as elastin, fibronectin, and laminin (136).

3.4. Pathophysiology of asthma: airway hyperreactivity

Asthmatic patients have a predisposition to excessively narrow the airways in response to a variety of stimuli, which defines airway hyperreactivity (AHR). Such stimuli would produce little or no effect in healthy subjects (137). Many mediators participate in the development of AHR, although it is unknown which of them are more directly involved. Despite this knowledge gap, it has been seen that the degree of AHR correlates with asthma severity (138, 139). Tests based on bronchoprovocation with methacholine (MCh) or histamine are well established to evaluate AHR in clinical practice, where increasing doses of the bronchoconstrictor agent are inhaled by the subjects until the highest concentration of MCh or histamine has been aerosolized or until there is a ≥20% fall in the forced expiratory volume in 1 second (FEV1) (139).

3.5. Pathophysiology of asthma: airway inflammatory profiles

Airway remodeling is generally believed to be a consequence of chronic airway inflammation in asthmatics. Not only mediators released by structural cells have been implicated in airway remodeling but also those secreted by inflammatory cells, such as TGF-β, a profibrotic cytokine that can be released by epithelial cells, and also by neutrophils and eosinophils, who are considered a significant source of TGF-β in the airways of asthmatics (140, 141).

Despite asthma heterogeneity, three major airway inflammatory profiles have been proposed on the basis of the cell type predominantly involved: eosinophilic, neutrophilic, and paucigranulocytic (12).

3.5.1. Eosinophilic airway inflammation

Eosinophilic asthma refers to the inflammatory profile of asthma, with its associated clinical traits, where a high presence of eosinophils is demonstrated in sputum, airways, or blood (60). Sputum eosinophils levels greater than 2 to 3% are the preferred method to determine eosinophilic asthma (142, 143), as this is believed to directly reflect lung inflammation (144). Moreover, sputum induction is a noninvasive procedure compared to bronchial biopsies.

Allergy is the prominent mechanism in many cases of eosinophilic asthma. This atopic-eosinophilic phenotype is mediated by antigen-specific Th2 cells. their related cytokines like IL-4, IL-5, and IL-13, specific IgE, and eosinophilia (145). IL-5 mediates eosinophil recruitment to the site of antigen exposure. The eotaxins are further chemoattractants mediating eosinophil influx into airways. IL-13, mainly produced by effector Th2 cells and also by eosinophils and other cells, contributes to airway hyperreactivity (146, 147). Additionally, TGF-β produced by eosinophils contributes to the airway remodeling that is related to persistent changes in lung function (148). An important source of IL-5 and IL-13 are the ILC2, present in the airways of patients with eosinophilic asthma, which correlate with persistent airway eosinophilia (149).

Non-atopic eosinophilic airway inflammation is related to innate immune responses that include type-2 inflammatory pathways but, in this case, IgE-mediated signals are not prominently contributing. Factors such as pollutants and microbes may induce airway

epithelial injury, which, in turn, releases IL-25, IL-33, and TSLP, stimulating ILC2s and promoting eosinophilia and airway hyperreactivity (146). To differentiate atopic eosinophilic asthma, the lack of IL-4 production minimizes B-cell switching to IgE, thus showing low levels or absent specific IgE (150).

3.5.2. Neutrophilic airway inflammation

The lack of eosinophils has been used to define non-eosinophilic asthma (151, 152). Combined eosinophilic and neutrophilic infiltrates in the airway wall or sputum are relatively frequent, and this is termed mixed granulocytic asthma. “Pure” neutrophilic asthma, although uncommon, also exists. When very few granulocytes are present, it is called paucigranulocytic asthma (60).

A clinical phenotype related to neutrophilic asthma is less clear than the clinical traits associated with eosinophilic asthma (81, 153). Moreover, on tissue biopsy, many patients with neutrophilic inflammation may have concomitant eosinophilic inflammation, whereas, in sputum, they have a clear predominance of neutrophils. In autopsies of patients who died soon after the onset of a severe exacerbation, the inflammatory profile is often neutrophilic (154-156).

The cause of neutrophilic inflammation in asthma is unknown. External factors such as smoke, occupational exposure to irritants, or viral infections may be involved. The neutrophil activity has been associated with increases in IL-8, neutrophil elastase, and MMP9. Some asthmatics with evidence of neutrophil activity show lower FEV_1 (12).

Although atopy can be present in neutrophilic asthma, asthma with predominant neutrophilic inflammation or the paucigranulocytic subphenotype usually present with a Th2-low inflammatory environment. The pathways involved are mostly related to the neutrophilic inflammation and airway dysfunction. Differential inflammatory pathways through the acquired and innate immune responses distinguish neutrophilic from eosinophilic asthma. The innate immune level is activated during infection (viral, bacterial) or during irritant environmental exposure, such as endotoxin, ozone, and particulate matter exposures. These agents can activate Toll-like receptor 4 and CD14 on epithelial cells and macrophages, leading to nuclear factor (NF)-κβ activation, which in turn initiates a highly proinflammatory state (157, 158). This pathway activation leads to major IL-8 production, hence recruiting neutrophils into the airways. Other pathways

and mechanisms can contribute to airway neutrophilia, like impaired alveolar macrophage phagocytosis of apoptotic cells, leading to persistent airway neutrophilia (159).

Corticosteroids are known to deplete eosinophils and inhibit neutrophil apoptosis, which may favor apparent neutrophilic infiltrates (9). Due to these effects, the use of corticosteroids, especially systemic, to treat severe asthma may complicate the accurate diagnosis of the true inflammatory profile (9). Additionally, NK and NKT cells are a significant source of proinflammatory and cytotoxic mediators, such as IFN-γ or TNF-α, with corticosteroid insensitivity, which may contribute to the development of neutrophilic asthma (160).

Th17 inflammation is also associated with a severe phenotype, frequent exacerbations, steroid resistance, and airway remodeling (161, 162). In asthma, this Th17-type inflammatory pathway can be due to chronic subclinical infection or inhaled exposures that induce IFN-γ and IL-17 production in addition to other proinflammatory cytokines (43, 163, 164).

4. Animal models of experimental asthma

Experimental modeling of allergic airway inflammation, particularly in mice, has contributed dramatically to our understanding of the pathogenesis of asthma. Mouse models offer a wide availability of genetically characterized inbred strains at low cost but, unlike humans, mice do not spontaneously develop asthma (47). Although mouse models provide a good choice to examine allergic asthma traits such as lung inflammation and airway hyperreactivity, conventionally used models involve intraperitoneal antigen administration in conjunction with potent chemical adjuvants (generally aluminum hydroxide). Such coadjuvants allow inducing allergic airway inflammation that does not truly reflect the immunological agents and pathways that elicit allergic sensitization in actual disease. The choice of adjuvants to induce allergic sensitization depends on the nature of the antigen selected (165, 166).

The heterogeneity of asthma indicates that there are different airway mechanisms involved in inflammation. In order to further study these mechanisms, various mouse models were established to mimic the different subtypes of asthma.

One of the classical models is the **atopic eosinophilic asthma** model, induced by intraperitoneal injections of ovalbumin (OVA), followed by repeated inhalation of aerosolized OVA. The pathological findings compared to controls comprise increased eosinophils, elevated levels of Th2 cytokines in BAL fluid, and airway inflammatory infiltrates. A model of **neutrophilic asthma** was established by transtracheal administration of a high dose of lipopolysaccharide (LPS; 10 μg) in combination with OVA sensitization and challenge. This model presents an increased number of neutrophils, elevated levels of Th1 and Th17 cytokines in BAL, and severe inflammation of lung tissues. Another model is **mix-granulocytic asthma**, established by intratracheal administration of low-dose LPS (1μg) in combination with OVA sensitization and challenge. A conjunction of both neutrophilic and eosinophilic asthma characteristics was observed in this model, represented by increased numbers of both eosinophils and neutrophils, elevated levels of Th1, TH2, and Th17 cytokines in BAL, and severe inflammation of lung tissues. Airway hyperresponsiveness, increased bronchial mucus secretion, and elevated serum levels of total and OVA-specific IgE were detected in all three asthma models (167).

The development and characterization of novel animal models representing the different subtypes of asthma is needed to further understand asthma, and to research and target treatment for asthma patients.

4.1. Allergens to induce asthma in mouse models

Murine models have been helpful in understanding the basic cellular and molecular mechanisms of allergic sensitization and acute airway inflammation. However, the mechanisms and implications of chronic airway inflammation and remodeling have been more challenging to study and correlate with human disease.
The main reason for this lies in the type of antigen used and the sensitization route. The antigen most commonly used is the OVA and, although it can cause an inflammatory response, OVA does not lead to chronic airway inflammation. Continuous exposure to OVA results in inhalation tolerance and, in sensitized animals, leads to a reduction or complete abrogation of AHR (168).

- HDM

House dust mites are an important source of indoor allergens implicated in a variety of allergic symptoms in 10% of the population (169). The mite-related allergen most frequently associated with respiratory allergy is the *Dermatophagoides pteronyssinus* Derp (169, 170). The Derp extracts mimic everyday's environmental allergen exposure and offer the opportunity to elaborate a pathogenic sequence of events, from initiation to resolution of the immunological response (171).

Some work done in animal models relating to allergy to HDM antigens has been performed in immunologically deficient animals in the form of a humanized severe combined immunodeficiency (SCID) mouse model (172, 173) or in guinea pigs in which intraperitoneal injections were required to elicit Th2 sensitization(165).
Exposure to HDM alone generates Th2 sensitization based on the production of Th2 effector molecules and airway eosinophilic inflammation in BALB/C mice (165).

HDM is a major perennial allergen source and a significant cause of allergic rhinitis and allergic asthma. Although comprehensive reviews of HDM allergy exist, the links among exposure, allergenicity, and the pathological effects on the whole airway tract has yet to be thoroughly explored (28).

HYPOTHESIS AND OBJECTIVES

HYPOTHESIS

In the non-Th2-biased C57BL/6 mouse, repeated *i.n*. instillation of an actual aeroallergen such as HDM may lead to an optimized asthma model closely resembling the process of human allergic sensitization and the physiopathology of asthma. The characterization of immune response outcomes in this model, and the tuning of variables to be determined, may lead to model variants resembling a spectrum of asthma inflammatory profiles that may comprise experimental neutrophilic asthma. Further model comparative analyses, and protein matching tests with induced sputum from asthmatic subjects, may support model validation, define immunobiological pathways involved, and facilitate the identification of novel molecular targets of potential diagnostic or therapeutic value.

OBJETIVES

1. To establish an experimental model of asthma in C57BL/6J mice by repeated intranasal instillations of house dust mite (HDM) extract allowing for an optimized approach to the physiopathological mechanisms of human asthma.
    1.1. To develop HDM dose-finding and i.n. instillation timing experiments leading to a model that represents the cardinal asthma traits (airway hyperresponsiveness, inflammation, remodeling) in this non-Th2-biased mouse strain.
    1.2. To analyze the immune response outcomes in this model, including the cellular inflammatory profile, bronchial hyperresponsiveness, and airway remodeling.

2. To evaluate the inflammatory cell subpopulations in the experimental asthma model.
    2.1. To analyze the neutrophil and eosinophil subpopulations based on identified cell surface markers related to different functional phenotypes, including proinflammatory versus immunoregulatory.

3. To perform exploratory kinetics analyses of immune response outcomes through the development of experimental asthma in order to identify the mechanisms leading to a neutrophilic or eosinophilic asthma phenotype.

3.1. To analyze the inflammatory cell subpopulations, cytokine secretion, and immunoglobulin production upon each successive i.n. HDM instillation, and define disease stages.

4. To determine and compare the airway soluble protein profile to facilitate further identification of molecular species with novel diagnostic or therapeutic potential.

4.1. To evaluate the model representativeness by comparing gene expression through proteomics on murine BAL and induced sputum from asthmatic subjects.

4.2. To classify, as per their expression, genes related to an eosinophilic or neutrophilic asthma profile that may offer potential as diagnostic or therapeutic targets.

METHODS

1. Experimental animals

6-12-week-old C57BL/6J females were purchased from Charles River Laboratories Inc. (Lyon, France). The animals were housed at core facilities of the *Institut de Recerca Hospital de la Santa Creu I Sant Pau* (IBB Sant Pau) in individually allergen-free ventilated cages containing a double positive/negative-pressure filtration system (Ebeco, e. Becker & Co. GmbH). Mice were maintained under temperature and humidity-controlled conditions, and a 12/12-hour light/dark cycle. Water and food were supplied ad libitum.

All procedures were approved by the Animal Research Ethics Committee of the *Generalitat de Catalunya*, following European Union Directive 86/609 and Royal Decree 1201/2005 of the Spanish Government.

2. Sensitization groups and treatments

To develop a neutrophilic asthma experimental model, crude extract of House Dust Mite (HDM, *Dermatophagoides pteronyssinus (Der p)*) was used alone or combined to *Staphylococcus Enterotoxin B (SEB),* or *alpha Galceramide (*α-*Galcer).*
First, stock solutions were prepared for each treatment. HDM was dissolved in physiological sterile saline solution (SS) to obtain a stock concentration of 10 mg/mL, and stored at 4ºC during the whole treatment. α-Galcer and SEB were dissolved in SS to obtain a working concentration of 20 ng/mL or 2 mg/mL respectively, and stored at -20ºC.

Then, two groups of HDM were established based on the HDM period of instillations. A model consisting of three instillations per week during four weeks (4W) (**Figure 4 A**); and a model consisting of three instillations per week during six weeks (6W) (**Figure 4 B**). Both were treated with a High or Low HDM dose. The high dose of HDM refers to 15 mg/0.3mL of Derp1 content, and the low dose refers to 7,5 mg/0.3mL of Derp 1.

For *i.n.* treatments to HDM, HDM+α-Galcer*,* HDM+SEB or SS (control), the animals were put into a Plexiglas chamber and anesthetized with 3% of inhaled Isoflurane (AbbVie, Madrid, Spain). Each animal was instilled with 15 µL per nostril and twenty-four hours after the last *i.n.* instillation, animals were sacrificed to perform functional analyses.

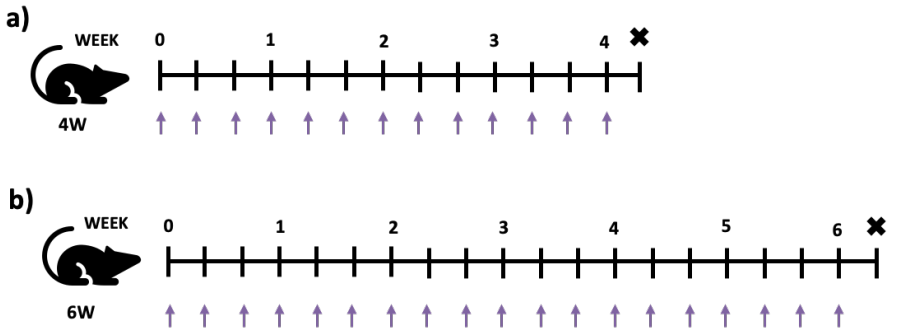

Fig 4. Timeline for allergen exposure in two different HDM models. (a) Chronic 4-week model of HDM-induced airways inflammation. (b) 6-weeks model of HDM.

Subsequently, after the establishment of the allergen-exposure timeline of mice asthmatic model (**Figure 5**), two conditions of HDM extract were used to immune-drive inflammatory disease to neutrophilic or eosinophilic asthma. A freshly reconstituted HDM preserved at -20 degrees (defined as H20), and another one maintained at 4 degrees during twelve days and posteriorly kept at -20 degrees until use. C57BL/6J mice were chronically exposed to H4 or H20, without the provision of exogenous adjuvant, intranasally (15 mg of protein in 0.3mL of saline solution) for 3 days/week for up to four consecutive weeks.

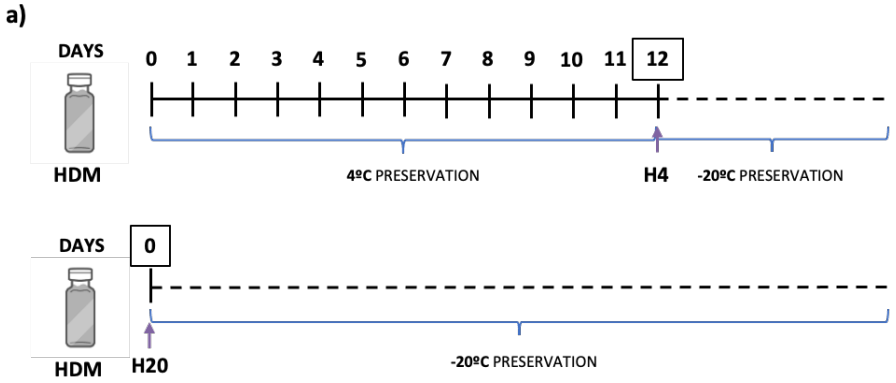

Fig 5. Timeline for HDM extract reconstitution and preservation. (a) HDM maintained at 4 degrees during twelve days and posteriorly kept at -20 degrees (H4). (b) freshly reconstituted HDM preserved at -20 degrees (H20).

3. Inflammatory kinetics development study

108 animals were distributed in three groups (36 mice per group) based on the preservation status of the HDM, starting from 10 mg/mL stock solution. One group was treated with HDM preserved at 4ºC during the whole treatment, defined as HDM. Another group was treated with HDM preserved at 4ºC during twelve days, from there on, preserved at -20ºC, defined as H4. The last group was treated with HDM reconstituted

and subsequently preserved at -20ºC without any variation in the HDM content, defined as H20. All mice were i.n. instilled with the high HDM dose (15 mg/0.3mL) and 24 h after each instillation (1-13), three mice were sacrificed and lung infiltrating populations and the cytokine profile secreted, were studied.
To assess the HDM status at each dose administered given to the mice, HDM samples were obtained before each *i.n* instillation and preserved at -20ºC until protein analysis.

4. Lung function assessment

For assessing lung function, the most common method used is Spirometry. This procedure consists of tracheostomized and cannulating the animals and subjected oscillating forced pressures using the equipment of mechanical ventilation, EMMS eSpira™ (EMMS; London, UK).
The pulmonary function of asthmatic animals was analyzed twenty-four hours after the last *i.n.* instillation. Six increasing concentrations from 0 to 50 mg/mL of Methacholine (MCh; *Acetyl-b-Methyl-Choline Chloride*; Sigma-Aldrich, Madrid, Spain) were administered to mechanically ventilated animals by an ultrasonic nebulizer (Aerogen, Galway, Ireland) coupled to the EMMS eSpira™ inspiratory line.

4.1. Calibration of EMMS eSpira

Calibration of EMMS eSpira should be performed to adequate the airway and cylinder pressure per mouse weight. The airway pressure was calibrated using a 50 mL syringe and a manometer to adjust the lowest point of pressure (0 mmHg) and the highest point of pressure (30 mmHg). To adjust the cylinder pressure, a dynamic tubing calibration was required using a manually close and open cannula, according to the manufacturer's instructions.

4.2. Tracheal cannulation and connection to the mechanical ventilator

Mice were weighed and anesthetized with 75 mg/kg Ketamine (Fatro Ibérica, Barcelona, Spain) and 1 mg/Kg Dexdomitor (Esteve Laboratories, Barcelona, Spain) by intraperitoneal injection (5 µL mix per gram body weight). Anesthesia was verified by the loss of the palpebral and toe-pinch reflexes. During the entire procedure, mice body temperature was controlled, keeping warm constantly with a heating mat for small

animals. Furthermore, vital constants as heart rate, blood pressure, and O_2 saturation were monitored using a pulse oximeter.

All anesthetized mice were cannulated by tracheostomy with a 20 G tracheal cannula (FTC100 Tracheal Cannula, 20G, Ø 0.2 mm, EMMS) between the two upper-third tracheal rings. Posteriorly, mice were attached to the EMMS machine and the program to standard breathing was set. Before starting the EMMS measurements, anesthetized mice receive a muscle relaxant, 1µl/g mouse Rocuronium bromide (Esmeron®-MSD, Madrid, Spain). When the lung function started, the positive end-expiratory pressure (PEEP) was set at 3 mm H_20. Then, the MCh in doses of 20 µL, was administered intratracheally by the nebulizer and airway responsiveness was measured using the EMMS eSpira respirator.

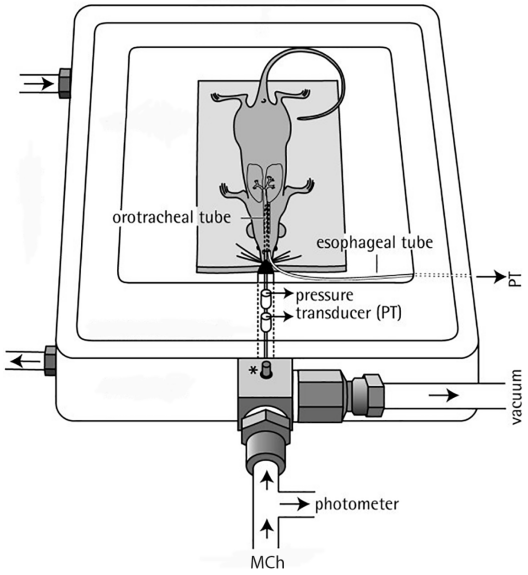

Fig 6. Diagram of orotracheally intubated mice for pulmonary function test. Heating mat ensured a body temperature of 34-35ºC. Defined aerosol concentrations of methacholine, were supplied by the nebulizer into the airways via the orotracheal tube. To calculate the pulmonary resistance (RL), transpulmonary pressure (PTP) was recorded via an esophageal tube, and tidal flow was determined by an acquisition unit attached to the gas interchange unit connected to the orotracheal tube. (Reproduced from Bonnardel, E., Prevel, R., Campagnac, M. *et al.* (2019)).

4.3. Measurement of pulmonary function

Once the anesthetized animal was connected to the ventilator and the ventilation parameters were adjusted, tidal-volume ventilation was carried out until pulmonary function values were stable. Pulmonary function variables were measured using the mathematical model stated by the EMMS eSpira software. To acquire data, tidal-volume was transiently interrupted after each nebulization generating prime pressure waves by the ventilator. The primary variable to analyze was the pulmonary resistance (R_L), measured from 20-second “snap-shot” prime waves, an indicator of airway responsiveness to increasing MCh doses. To establish an increase in pulmonary resistance, a difference was established between the R_L baseline and the maximum MCh concentration.

4.4. Sample collection

4.1.1. Blood serum

Immediately after lung function mice were euthanized by anesthesia overdose. Blood was collected through cardiac puncture using a 25G needle removing approximately 1 mL of blood. The serum was obtained by centrifugation (1200 xg during 10 min) and stored at -80ºC for posterior analyses.

4.1.2. Bronchoalveolar lavage (BAL)

To perform bronchoalveolar lavage, a three-way stopcock was connected to the tracheal cannula, and then lungs were flushed gently twice with a 0,5 mL of Phosphate Buffered Saline 1X (PBS). BAL was collected and centrifuged (650 xg during 5 min) to obtain the supernatant and cell pellet. Both were stored at -80ºC for posterior analyses.

4.1.3. Lung lobes

To obtain individual lungs, a perfusion through the right ventricle with a 5 mL of PBS containing 10 UI/mL heparin (Sodium heparin I; Hospira Invicta S.A., Madrid, Spain) was done. Once the lungs were washed, the left lung was placed in 2,5 mL of RMPI1640 medium and kept on ice until organ disaggregation. The right lung was excised, attached to the cannula, and was fixed by constant infusion of 4% paraformaldehyde (Sigma-Aldrich) at 25 cmH_2O pressure for at least 6 hours. After fixation, the lung was preserved in 70% Ethanol until posterior histological analysis.

5. Single-Cell Suspensions of Lung Tissue

The left lung was transferred into a petri dish in sterile conditions to obtain a single-cell suspension from lung tissue. The lung was cut using a scalpel to obtain a homogeneous paste, then was dissolved in 6 mL of RPMI1640 medium, and incubated in agitation for 30 min at room temperature (RT). After tissue disaggregation, the parenchyma was removed by filtering through a 50 µm cell strainer (Sysmex Partec GmbH, Goerlitz, Germany) into a new 15 ml tube. The single-cell suspension was then centrifuged at 350 xg for 5 min at 4ºC, and the supernatant was discarded. Erythrocytes were lysed by adding 1 mL of RBC lysis buffer (Sigma-Aldrich, Schnelldorf, Germany) to the cell suspension and gently vortex for 2 minutes at room temperature. Immediately, 10 mL of

PBS was added to stop the reaction and centrifuge again. The supernatant was discarded, and RMPI1640 medium was added to the cell suspension to raise 2 mL. Cells were counted using a hemocytometer (Neubauer chamber Zuzi Corp., France), and cell viability was performed with Trypan blue (Sigma-Aldrich). Cell suspension was adjusted to the desired concentration and was used for cytospin, flow cytometry, or cell culture.

6. Cell population profile analysis by flow cytometry

Lung single-cell suspension obtained was used to quantify and classify the cellular infiltrate in the lung parenchyma using specific antibody markers. To achieve this, two antibody labeling panels were established (Table 1).

Table 1. Populations Panel (Granulocytes/Lymphocytes)

Antibody	*Fluorochrome*	*Clone*	*Supplier*	*Panel*
CD3	AlexaFluor 647	17A2	BD	Lymphocytes
CD4	APC-Vio770	REA604	Miltenyi	Lymphocytes
CD8	PE	YTS 169,4	Immunotools	Lymphocytes
CD11B	PerCP-Vio700	M1/70.15.11.5	Miltenyi	Granulocytes
CD11B	PE	CE50-2440	Immunotools	Granulocytes
CD11C	PE-Vio770	N418	Miltenyi	Lymphocytes
CD19	PE-Vio770	REA749	Miltenyi	Lymphocytes
CD19	PE	REA749	Miltenyi	Lymphocytes
CD14	FITC	REA934	Miltenyi	Granulocytes
CD25	FITC	PC61.5.3	Immunotools	Lymphocytes
CD62L	PerCP-Vio700	REA828	Miltenyi	Lymphocytes
CD64	APC	X54-5/7.1	Biolegend	Granulocytes
CD80 (B7-1)	FITC	16-10A1	Immunotools	Lymphocytes
CD86	APC	GL-1	Immunotools	Lymphocytes
CD115	APC	AFS98	Miltenyi	Granulocytes
CD125	APC-Vio770	REA343	Miltenyi	Granulocytes
CD206	AlexaFluor 647	MR5D3	BD	Granulocytes
GR1	PE	RB6-8C5	Immunotools	Granulocytes
LY6C	FITC	REA796	Miltenyi	Granulocytes
LY6G	PE-Vio770	REA526	Miltenyi	Granulocytes
CD184 (CXCR4)	APC	REA107	Miltenyi	Granulocytes
CD193 (CCR3)	APC	REA122	Miltenyi	Granulocytes
MHCII	VioGreen	REA813	Miltenyi	Lymphocytes
SIGLECF	PE	E50-2440	BD	Granulocytes
SIGLECF	PerCP-eFluor 710	1RNM44N	eBioscience	Granulocytes

Cells were blocked with anti-CD16/CD30 (BD, Biosciences, Madrid, Spain) for 10 min at room temperature. After centrifugation, cell concentration was adjusted to $1x10^6$ cells/mL using a staining buffer (PBS + 1% BSA). 100 mL of cell suspension were distributed in as many tubes as needed and stained with Fixable Viability Dye eFluor®450 (eBioscience-Labclinics S.A., Barcelona, Spain) and antibodies, as detailed in Table 1, were added and incubated for 10 min at 4ºC. Finally, cell suspension was centrifuged and resuspended in 200 mL of staining buffer and a three-laser flow cytometer MACSQuant (Miltenyi Biotec, Cologne, Germany) were used to assess cell populations.

Data were analyzed using MACS Quantify software (Miltenyi Biotec, Cologne, Germany) and Flowjo software (TreeStar, Ashland, Oregon, USA).

6.1. ILCs profile analysis by flow cytometry

Innate lymphoid cells (ILCs) can only by identified lack of expression of classical cell-surface markers and cytokine production, multicolor flow cytometry is the most reliable technique to purify and characterize ILCs.

Type 1 ILCs (ILC1) produce interferon (IFN)-γ and express the transcription factor T-bet, type 2 ILCs (ILC2) produce Th2 cell-associated cytokines (IL-4, IL-5, IL-9, and IL-13) and express multiple transcription factors as GATA-3, while as the type 3 ILCs (ILC3) produce IL-17 and/or IL-22 and share expression of the transcription factor RORγt.

Lung single-cell suspension was previously obtained and was used to quantify and classify the infiltrate ILCs in the lung parenchyma using specific antibody markers. First, at least $1x10^6$ cells are resuspended in DPBS containing 2% FBS and blocked 10 min at RT with anti-CD16/CD32 blocking reagent. Cells are then fluorescently labeled for 30 min at 4ºC in the dark with a panel of previously optimized (Table 2). After washing, cells were then fixed by Cytofix/Cytoperm solution during 20 min at 4ºC. After washing, cells were intracellular stained with respectively transcription factor for 30 min at 4ºC. Finally, the cells were washed and resuspended with a staining buffer (DPBS containing 2% FBS) to flow cytometric analysis.

Table 2. ILCs Panel.

Antibody	*Fluorochrome*	*Clone*	*Supplier*
CD45	Viogreen	30F11	Miltenyi
Ly6C	FITC	REA796	Miltenyi
CD19	PE	REA749	Miltenyi
CD19	PE-Vio770	REA749	Miltenyi
SIGLECF	PE-Vio 615	REA798	Miltenyi
CD127	PE-Cy7	SB/199	BD
CD3	AlexaFluor 647	17A2	BD
CD11B	APC-Cy7	M1/70	BD
T-BET	Alexa Fluor 488	O4-46	BD
GATA-3	Alexa Fluor 647	L50-823	BD
RORG	PE	Q31-378	BD

7. Protein Analysis

7.1. ELISA Cytokine determination

IL-17A, IL-13, IL-4, IL-2, IFN-γ cytokines and total immunoglobulin (Ig) IgG and IgE were determined using a quantitative sandwich ELISA kit following the manufacturer's instructions. Detection ranges were 1,56-1500 pg/mL (Table1.). Specific IgE and IgA were determined by adapted indirect ELISA as follows.

High-affinity binding 96-well flat-bottom ELISA plates (ThermoFisher, Nunc A/S, Denmark) were coated with 5 µg of HDM in 100 µL in PBS overnight (ON) at 4ºC. Then, plates were washed five times using a wash buffer (PBS containing 0.05% Tween 20) to remove the antibody excipient and blocked with assay diluent (PBS containing 0.05% Tween 20 and 0.1% of BSA) for 1 hour at RT. After 5 washes, samples were added and incubated ON at 4ºC. After five washes, 100 µL of biotin-anti mouse IgE (1 µg/mL) or anti-mouse IgA (1:3000) (see Table 4) was added and incubated 30 min at RT. The plates were washed again, and 100 µL of horseradish peroxidase streptavidin (HRP; BD Biosciences), diluted 1:200 in ELISA buffer, was added and incubated for 1 hour at RT. Following the last washes, TMB was incorporated to the plate and incubated for 10 min in dark until the coloring reaction was completed. Finally, the reaction was stopped by adding 50 µL 4M H_2SO_4 to each well. Optical density was readed at 450 nm on the ELISA plate reader (Multiskan Plus Microplate Reader; Labsystems, Lima, Peru).

Table 4. Overview of immunoglobulin ELISA antibodies

Antibody	*Detection Range*	*Supplier*
IL17A	5-500 pg/mL	MABTECH
Il13	4-500 pg/mL	INVITROGEN
IgE	15-1500 pg/mL	MABTECH
IFNg	4-400 pg/mL	MABTECH
IL4	4-400 pg/mL	MABTECH
IL2	7-700 pg/mL	MABTECH
IgG	1.56-100 ng/mL	INVITROGEN
sIgE		BIOLEGEND
sIgA		INVITROGEN

7.2. Immunoglobulin isotype determination by Flow cytometry

Six different immunoglobulins (IgG1, IgG2a, IgG2b, IgG3, IgA, IgM) were quantified with LEGENDplex™ Mouse Immunoglobulin Isotyping Panel (Biolegend, San Diego, CA) following the manufacturer's instruction.

LEGENDplex™ assays are based on the same principle as sandwich immunoassays. Consist of a system of two beads with different size and internal fluorescence intensities, conjugated with a specific antibody on the surface used as the capture antibody to recognize a particular analyte. This method is useful to quantify a high number of cytokines simultaneously with high sensitivity.

7.3. HDM status analysis

Protein status of HDM extracts was analyzed using Western blot assay. Briefly, 10 uL of HDM sample from each dose, was reduced with 5 mL of LDS sample buffer 4X (Invitrogen, ThermoFisher, Nunc A/S, Denmark), were denatured by heat and charge into a polyacrylamide gel electrophoresis NuPAGE™4-12% Bis-Tris Gel (Invitrogen, ThermoFisher, Nunc A/S, Denmark). The electrophoresis separation was done at 200V and 300W during 90 min. Gel staining with Blue Coomassie (Invitrogen, ThermoFisher, Nunc A/S, Denmark) was performed to assess the band proteins in each dose of HDM.

7.4. Total Protein Determination in BAL Mouse and Induced Human Sputum

Samples from mouse bronchoalveolar lavage were obtained as previously explained and preserved at -80ºC; while as induced human sputum were obtained following the procedures previously described by our group. Mucus plugs were manually selected and weighed, incubated 15 min at room temperature in 4 times the weight (in ml) of the selected plug (in mg) in 0.1% dithiothreitol (Calbiochem, San Diego, Calif., USA), washed with 4 times the plug weight (in ml) in Dulbecco's PBS, and finally filtered with a 41-µm-pore nylon net filter (Millipore Inc; Billerica, Mass., USA). A Neubauer hemocytometer was used to determine total cell count with Trypan blue viability exclusion. Sample were centrifuged to obtain cell pellet and supernatant. The pellet was used for differential cell counts (macrophages, eosinophils, neutrophils, lymphocytes, and bronchial epithelial cells) performed on May-Grünwald-Giemsa-stained preparations. While as the supernatant was preserved at -80ºC to posterior Proteomic analysis.

Subsequently, all the samples were concentrated by 1400g centrifugation for 5 min at 4ºC. To avoid the interfering substances with the proteins, the samples were running in

a SDS-PAGE system (BioRAD). The protein bands obtained in the process were cutted and fixed for 1 hour in a fixation solution (10% acetic acid + 40% ethanol) and then were washed three times with miliQ water. Mass spectrometry was performed by the Barcelona Science Park in the Proteomics Platform, a member institution of the ProteoRed-ISCIII network.

7.6.1. Protein Digestion

Gel bands containing the proteins of interest were washed with ammonium bicarbonate (50 mM NH4HCO3) and acetonitrile (ACN) and subsequently, were reduced with DTT 20 mM during 60 min at 60ºC. After this, the samples were alkylated with Iodoacetamide 55 mM, during 30 min at 25ºC, protected from the light. Moreover, Trypsin solution (sequence grade modified Trypsin, Promega) was used at 37ºC ON to digest the proteins. The resulting peptide mixture was finally extracted from the gel with a first solution exposition of 4% of formic acid (FA) in 50% of ACN, and subsequently a 100% ACN solution. Finally, the peptide digests were dried-down in a SpeedVac vacuum system and stored at -201C until the LC-MS analyses.

7.6.2. LC-MS analysis

The peptide mixtures were analyzed in a nanoAcquity liquid chromotographer (Waters) coupled to a LTQ-Orbitrap Velos (Thermo Scientific) mass spectrometer.

The tryptic digests were resuspended in 1% FA solution and an aliquot of each sample was injected for chromatographic separation. Peptides were trapped on a Symmetry C18TM trap column (5 µm x 180 µm x 20mm; Waters), and were separated using a C18 reverse- phase capillary column (ACQUITY UPLC BEH column; 130Å, 1.7µm, 75 µm x250 mm, Waters). The gradient used for the elution of the peptides was 1 to 40% B through 30 minutes, followed by 40% to 60% A in 5 min (A: 0.1% FA; B: 100% ACN, 0.1% FA; flow rate: 250 nL/min).

The eluted peptides were subjected to electrospray ionization in an emitter needle (PicoTipTM, New Objective) with an applied voltage of 2000 V. Peptide masses (m/z

300- 1700) were analyzed in data dependent mode where a full Scan MS was acquired in the Orbitrap with a resolution of 60,000 FWHM at 400m/z. Up to the 15th most abundant peptides (minimum intensity of 500 counts) were selected from each MS scan, and then fragmented in the linear ion trap using CID (38% normalized collision energy) with helium as the collision gas. The scan time settings were: Full MS: 250 ms (1 microscan) and MSn: 120 ms. Generated *.raw* data files were collected with Thermo Xcalibur (v.2.2).

7.6.3. Database search

The *.raw* data files obtained from the mass spectrometry analyses were used for a search against all murinae or human entries present in the Uniprot public database. The search was performed with SequestHT search engine using Thermo Proteome Discover (v.1.4.1.14).

The following search parameters were applied:

- Database/Taxonomy: Uniprot_refprot_mmusculus_UP000000589_cont
- Enzyme: Trypsin
- Missed cleavage: 2
- Fixed modification: carbamidomethyl of cysteine
- Variable modifications: oxidation of methionine deamidation of asparagine, deamidation of glutamine
- Peptide tolerance: 10 ppm and 0.6 Da (respectively for MS and MS/MS spectra)

- Percolator:

- Target FDR (Strict): 0.01
- Target FDR (Relaxed): 0.05
- Validation based on q-Value

To improve the sensitivity of the database search, Percolator (semi-supervised learning machine) was used in order to discriminate correct from incorrect peptide spectrum matches. Percolator assigns a q-value to each spectrum, which is defined as the minimal FDR at which the identification is deemed correct. These q-values are estimated using the distribution of scores from the

decoy database search. The results have been filtered, so only proteins identified with at least 2 medium confidence peptides (FDR≤ 0.05) are included in the list.

8. Histologic lung analysis

Wright-Giemsa staining was performed for leukocyte differential counts on lung cell samples cytocentrifuge slides.

To identify inflammatory infiltrates in the lungs (Haematoxylin-eosin), mucus production by goblet cells (Periodic acid-Schiff), extracellular matrix and collagen deposition (Masson's trichrome), and contractile airway tissue (Alpha-smooth muscle actin) lung sagittal slices were introduced into histological cassettes, immersed in 70% ethanol (Panreac, Barcelona, Spain), and processed for paraffin embedding at the IIB Sant Pau Histopathology core facilities. Mouse fixed lungs were deparaffinized with xylene, and four-micron cuts were made. The slides were passed through several changes of alcohol to remove the xylene, then were thoroughly rinsed in water. The sample was hydrated, so aqueous reagents can penetrate the cells and tissue elements.

8.1. Wright-Giemsa

The Wright-Giemsa stain is based on the "Romanowsky effect" to stain the cellular components differentially. This procedure allows a three-color stain by the combination of a basic dye (azure B from Methylene blue) and an acidic dye (Eosin). The leukocyte nuclei being acid are purple, while the cytoplasm is sky blue. The eosinophils containing basic granules are red-orange, while the neutrophil granules are lilac. However, Giemsa is not required to produce the Romanowsky effect, which was added to intensify nuclear features and neutrophil granulation.

Cytocentrifuged BAL samples were fixed with Methanol. Then they were stained with the Wright solution (Merck, Darmstadt, Germany) and followed by the Giemsa solution (Merck, Darmstadt, Germany). Finally, the samples were dried and were mounted with a DePlex mounting medium (Merck, Darmstadt, Germany).

8.2. Haematoxylin-eosin

Hematoxylin is a basic day that has a deep blue-purple color with acidic cellular components like the nucleus, while Eosin is an acidic day that has varying degrees of pink color to basic cytoplasmic components including collagen and elastic fibers, muscle fibers, and red blood cells. These stains combinations lead to the interpretation of morphological changes associated with this disease.

First, the slides were stained with hematoxylin (Sigma-Aldrich) for 5 min. After rinsing in tap water, to convert the hematoxylin into a dark blue color. Next, the eosin (Panreac) counterstain was applied for 30 seconds. Following the eosin stain, the slide is passed through several changes of alcohol to remove all traces of water, then rinsed in several bats of xylene, which clears the tissue and renders it completely transparent. A thin layer of polystyrene mounting was applied, followed by a glass coverslip.

8.3. Periodic acid-Schiff

The Periodic acid-Schiff (PAS) reaction was introduced by McManus and described by Hotchkiss. This reaction consists of the principle that glycols are oxidized to aldehydes when treated with periodic acid. Together with the release of the pararosaniline adduct after reaction with Schiff's reagent, this adducts stains pink to red the glycol-containing cellular elements like cellular components as glycogen, basement membrane, certain epithelial sulfomucins and sialomucins, and neutral mucosubstances.
PAS stain was performed with a commercial kit for clinical diagnosis (Panreac) following manufacturer's instructions.

8.4. Masson's trichrome

Masson's Trichrome (MT) staining owes its name to the combination of three stains. **Weigert's Hematoxylin**, an iron hematoxylin dye, is used to stain the nuclei. **Biebrich scarlet-acid fuchsin** solution stains all the acidic tissues such as the cytoplasm, muscle, and collagen. **Phosphomolybdic** acid is used as a decolorizing agent, making the Biebrich Scarlet-acid fuchsin to diffuse out of the collagen fibers. This leaves the muscle cells staining red. Aniline blue stains the collagen along which 1% acetic acid is added to show a difference in tissue sections. The collagen fibers stain blue, and the nuclei

stain black, with a red background. Also, Bouin's solutions were used to improve the quality of MT stain.
The MT stain was performed with a commercial kit for clinical diagnosis (Panreac) following manufacturer's instructions.

8.5. Alpha-smooth muscle actin immunohistochemistry

Alpha-smooth muscle actin (α-SMA) is an isoform of actin, positive in muscular fibers. Alpha actin is the major constituent of the contractile apparatus found in skeletal muscle. Actin exists as a ubiquitous protein involved with filament formation that makes up large portions of the cytoskeleton. Actin filaments interact with myosin to assist in muscle contraction. Smooth muscle actin is found on smooth muscle vessel walls.
Lung sections were stained with rabbit anti-mouse α-SMA (Abcam) using Methyl green (Sigma-Aldrich) as counterstain. The slides were examined under a fluorescence microscope.

9. Quantitative Image Analysis

Lung histology sections were acquired with a fluorescence microscope (BX50; Olympus) equipped with a digital camera (DP21; Olympus), that includes 10X, 20X and 40X magnifications. Image processing for quantitative morphology was performed with ImagJ software (v.1.43m; National Institutes of Health, USA).

After digitization of slides, inflammatory leukocytes were counted in H&E-stained lung tissue sections at 20X magnification in random regions along major airways (30 mm length). A constant airway size reference independently from the airway contraction or relaxation status, known as the basement membrane perimeter squared (P_{BM}^2) was used to adjust the counting regions.

The mass of the region or substance of interest, was quantified by color particles in a section surface, and calculated by the division of this surface by the P_{BM}^2 in case of muco-substances and collagen deposition, measured by PAS and MT respectively.
In case of airway contractile tissue quantification, the α-SMA immunofluorescent signal was digitally thresholder, extracted and measured as particle surface area summation divided by the P_{BM}^2.

10. Data Analysis

Statistical analysis was performed using GraphPad Prism (version 8.0; GraphPad Software, La Jolla, CA). Data are represented as the mean ± standard error of the mean (SEM). Binary comparisons were made using Student t test or Mann-Whitney test, as appropriate. Multiple group comparisons were made using one-way ANOVA, with post hoc comparisons via Tukey's or Kruskal-Wallis post hoc test, as appropriate. Two-way ANOVA was used to compare individual dose differences between the MCh dose-response relationships, and to compare time point of treatment and compare between H4 and H20 treatments.

RESULTS

1. Establishment of an allergic asthma model in non-Th2-biased C57BL/6J mice by airway allergen exposure

To better understand the poorly studied characteristics of the neutrophilic subtype of asthma, we aimed at establishing a mouse model with allergic asthma by primary allergic sensitization of the airways with intranasal instillations of the complete extract of *D. pteronyssinus* HDM. For this, two doses were proposed, a low of 7.5 µg and a high of 15 µg; in addition, they were analyzed for a short period of time (4 weeks; 4W) and for a long period of time (6 weeks, 6W). In addition to a control group treated with saline solution (SS).

1.1. Repeated airway exposure to HDM for short periods elicits airway hyperresponsiveness

To study airway hyperreactivity in all conditions of the mouse model, lung resistance (R_L) was assessed by Methacholine (MCh) challenge, 24 hours after the last HDM instillation.

Repeated HDM instillations during 4W, independently of delivering Low or High HDM doses, induced significantly increased R_L at 50 mg/mL MCh compared with control group (SS). The highest R_L increment was observed with Low HDM doses (P<0.0001 versus SS). The High doses also led to a significant R_L increase (P=0.0140 versus SS). In contrast, no significant difference was observed in the mice treated with Low or High doses for six weeks compared to the control group (**Figure 7 and Table S1**). These data show that the airway hyperresponsiveness induced by primary airway HDM exposure is present after four weeks of repeated instillations but falls spontaneously at six weeks of allergen exposure.

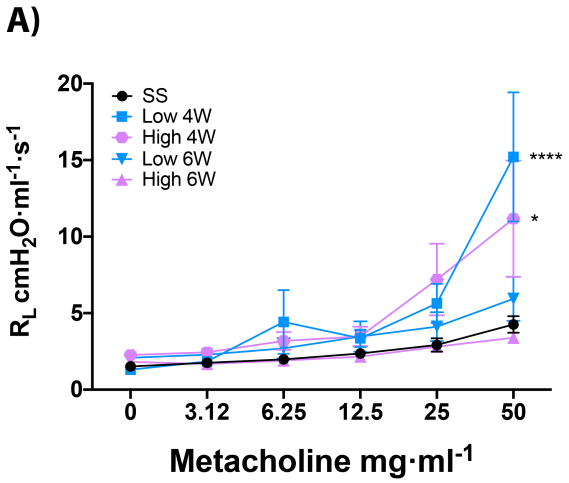

Figure 7. Repeated HDM intranasal instillation causes changes in lung resistance. C57BL/6J mice were sensitized with *i.n* saline solution (SS) or House Dust Mite (HDM) at Low (7,5 µg/mL) or High (15 µg/mL) doses, three times per week, during 4 weeks (4W) or 6 weeks (6W). Lung resistance (R_L) ($cmH_2O \cdot ml^{-1} \cdot s^{-1}$) was assessed by airway challenge with increasing methacholine (MCh) concentration (0-50 $mg \cdot mL^{-1}$). R_L is represented as mean±SEM and was analyzed by 2-way ANOVA. Group size: SS, n=7; Low 6W, n=8; High 6W, n=11; Low/High 4W, n=12. *P<0.05; ***P<0.0002.

1.2. Inflammatory cell recruitment to lung tissues after primary airway exposure to HDM

To study the inflammatory cell infiltration in the lung tissues, flow cytometry was performed on cell suspensions from lung homogenates 24 h after the last HDM exposure using primary antibodies against leukocyte surface antigens.

A stepwise gating procedure was used to classify the different leukocyte populations present in the lung homogenates, including lymphocytes, granulocytes, macrophages, and monocytes (**Figure S3**). The first step to gating was to obtain a single live Leukocyte population. Subsequently, the populations were gated by granularity into lymphocytes, macrophages/monocytes (MacroMon), neutrophils, and eosinophils. Then, the CD3 and CD19 markers were used to identify T and B lymphocytes, respectively. Thereafter, T lymphocytes were classified as $CD4^+$ and $CD8^+$. Macrophages and monocytes were classified by MHC-II and CD11c expressions ($MHC\text{-}II^+CD11c^+$ for macrophages and $MHC\text{-}II^-CD11c^+$ for monocytes). The granulocytes were identified by Siglec-F expression for the eosinophils and Ly6G for the neutrophils.

We quantitatively analyzed the infiltrated leukocyte subpopulations as percentage (**Figure 8**) and absolute numbers (**Figure 9**) The corresponding numerical data and *P* values are in **Table S2** and **Table S3**, respectively. Intranasal delivery of saline did not yield any inflammatory response. The lungs from mice exposed to HDM showed significantly increased $CD3^+$ T lymphocytes in the High 4W group and in both 6W groups (**Figure 8A**). The percentage of $CD4^+$ T lymphocytes was increased in the 4W groups, independently of Low or High HDM, dose but not in the 6W groups (**Figure 8B**). There was no significant effect of any dose regime on the $CD8^+$ T-cell (**Figure 8C**) nor $CD19^+$ B-cell (**Figure 8D**) percentages. The percentage of macrophages and monocytes dropped in all groups of HDM-instilled mice (**Figure 8E**). A significant increment of neutrophils was observed in the High 4W and High 6W groups (**Figure 8F**). The eosinophils were increased in the High 4W group only (**Figure 8G**).

The analysis of the absolute cell numbers paralleled the $CD3^+$ T-cell increment in the High 4W, and in both doses of the 6W groups (**Figure 9A**). $CD4^+$ T cells (**Figure 9B**) were significantly higher in all HDM-instilled groups. $CD8^+$ T cells (**Figure 9C**) and $CD19^+$ B cells (**Figure 9D**) were significantly increased only in the High 4W group. No significant effects were observed in the monocytes/macrophages (**Figure 9E**). The neutrophils

were significantly increased in all HDM-exposed groups (**Figure 9F**). The eosinophils were significantly higher in the High 4W group only (**Figure 9G**).

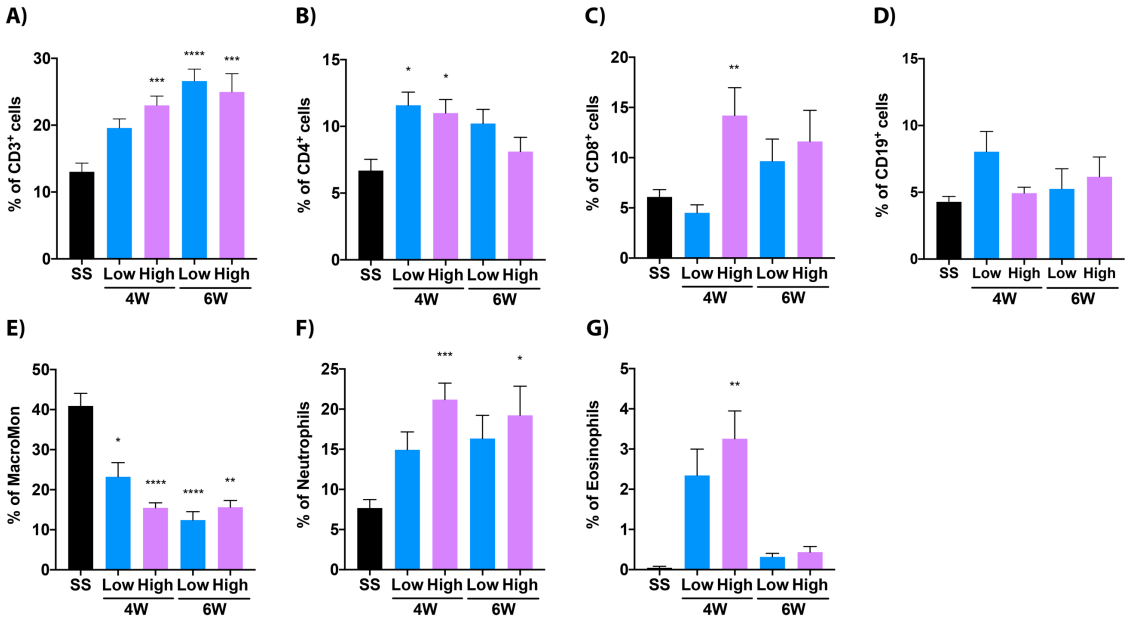

Figure 8. Inflammatory cell recruitment to lung tissues by repeated airway HDM instillations, relative frequencies. C57BL/6J mice were sensitized *i.n* with saline solution (SS) or House Dust Mite (HDM) at Low (7,5 µg/mL) or High (15 µg/mL) dose, during 4 or 6 weeks (4W or 6W respectively), three times per week. The cell percentages are shown for $CD3^+$ cells (**A**), $CD4^+$ T lymphocytes (**B**), $CD8^+$ T lymphocytes (**C**), B lymphocytes (**D**), macrophages and monocytes (**E**), neutrophils (**F**), and eosinophils (**G**). Data are presented as mean±SEM and were analyzed by Ordinary one-way ANOVA. Group size: SS n=13; Low 4W= 16; High 4W, n=22; Low/High 6W, n=12. **P<0.05*; ****P<0.0002*; *****P<0.0001*.

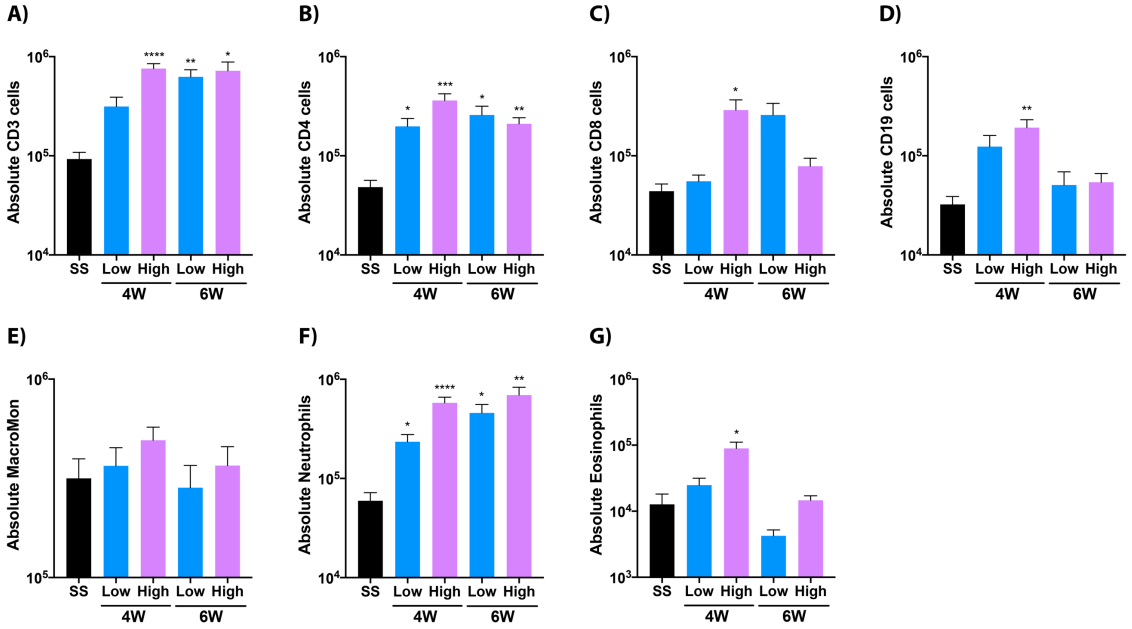

Figure 9. Inflammatory cell recruitment to lung tissues by repeated airway HDM instillations, absolute counts. C57BL/6J mice were sensitized *i.n* with saline solution (SS) (n=13) or House Dust Mite (HDM) at Low (7,5 µg/mL) or High (15 µg/mL) dose, during 4 or 6 weeks (4W or 6W respectively), three times per week. The absolute numbers of leukocyte populations are shown: $CD3^+$ cells (**A**), $CD4^+$ T lymphocytes (**B**), $CD8^+$ T lymphocytes (**C**), B lymphocytes (**D**), macrophages and Monocytes (**E**), neutrophils (**F**), and eosinophils (**G**). Data are presented as mean±SEM and analyzed by Ordinary one-way ANOVA test. Group size: SS n=12; Low 4W n=16; High 4W, n=20; Low/High 6W n=12. **P<0.05*; ***P<0.0021*; ****P<0.0002*.

1.3. Airway inflammatory microenvironment after HDM exposure

To study the inflammatory milieu in the airways, we determined BAL cytokine and immunoglobulin concentrations by ELISA (**Figure 10**; numerical data in **Table S4**). IL-4 (**Figure 10B**) was increased in the Low 4W group (*P*=0.0363 versus SS). IL-17A (**Figure 10D**) was increased in all HDM-instilled groups (*P*<0.05 versus SS), independently of the dose or duration of HDM exposure. IgG (**Figure 10E**) was higher in all HDM-instilled groups (*P*<0.05 versus SS) with a tendency to higher concentration in the 6W groups. Total BAL IgE (**Figure 10F**) was increased in the Low-HDM doses independently of exposure time, and in the High dose only at 4W. HDM-specific IgE (**Figure 10G**) was significantly higher in the Low-dose only, with a significant difference in the High 4W group. HDM-specific IgA (**Figure 10H**) was significantly increased in both doses at 4W (P<0.0021 versus SS).

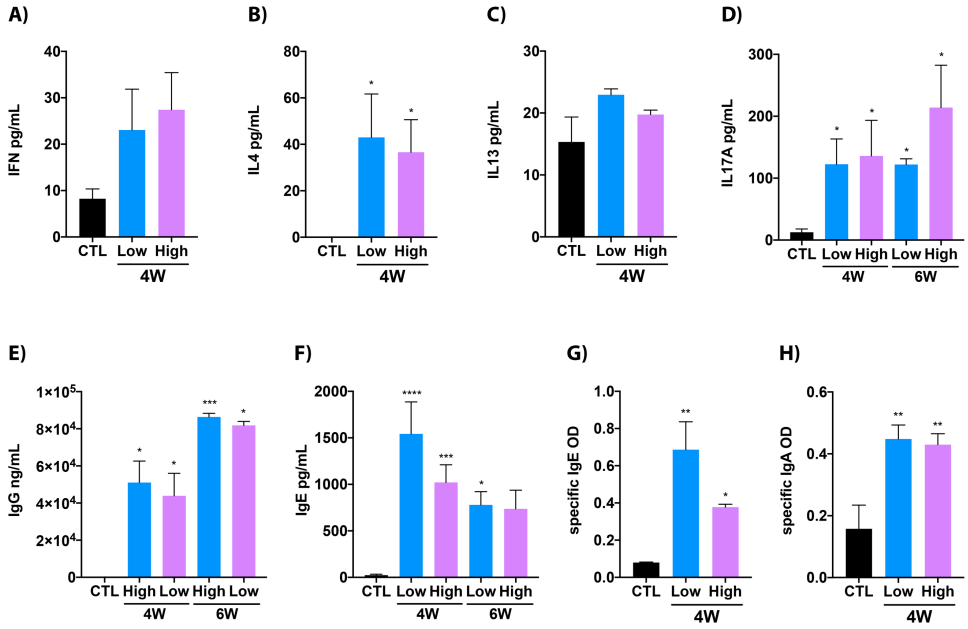

Figure 10. Increased cytokine and immunoglobulin secretion in bronchoalveolar lavage after HDM airway exposure. C57BL/6J mice were sensitized *i.n* with saline solution (SS) or House Dust Mite (HDM) at Low (7,5 µg/mL) or High (15 µg/mL) dose, during 4 or 6 weeks (4W or 6W respectively), three times per week. Total protein of IFN-γ (**A**), IL-4 (**B**), IL-13 (**C**), IL-17A (**D**), IgG (**E**), IgE (**F**), expressed as pg/mL, plus specific IgE (**G**) and specific IgA (**H**) in optical density (OD), are represented. Data are mean±SEM and were analyzed by one-way ANOVA test. Group size:SS n=9; Low 4W n=11; High 4W n=13; Low/High 6W n=6. **P<0.05*; ***P<0.0021*; ****P<0.0002*; *****P<0.0001*.

1.4. Lung histopathology after HDM exposure

Lung sections from HDM or SS-instilled mice were analyzed by histological stains to examine inflammatory cell infiltration and airway remodeling traits including goblet cell hyperplasia, mucus hyperproduction, and subepithelial fibrosis (**Figure 11**).

Hematoxylin-eosin was used to evaluate the cell infiltration. Consistent with the flow-cytometry data indicating lung inflammation, we found peribronchial inflammatory cell infiltration, especially in the High 4W group. No changes were observed in goblet cells or mucus production by PAS staining. Although slight peribronchial collagen deposition was observed, no obvious subepithelial fibrosis was seen by Masson's trichrome staining.

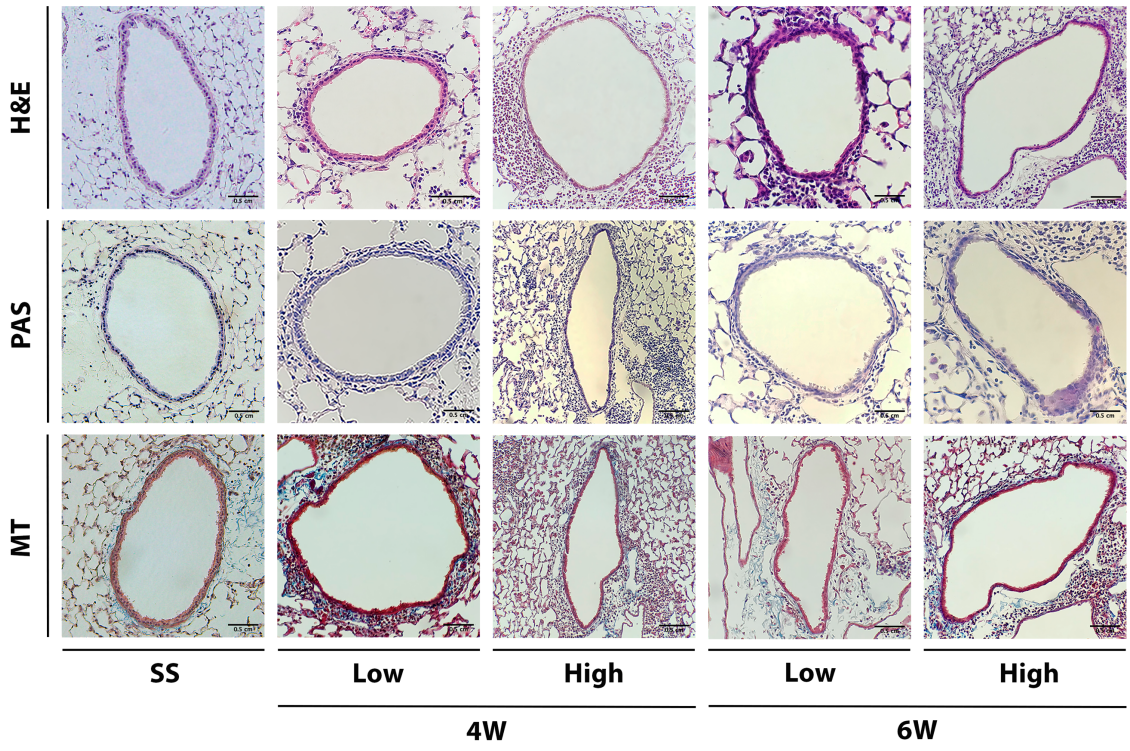

Figure 11. Lung histopathology after repeated HDM intranasal instillation. C57BL/6J mice were sensitized *i.n* with saline solution (SS) or House Dust Mite (HDM) at Low (7,5 µg/mL) or High (15 µg/mL) dose during 4 or 6 weeks (4W or 6W respectively), three times per week. The micrographs show representative airway sections from the experimental groups and histological stains as indicated. H&E, hematoxylin-eosin. PAS, periodic acid-Schiff. MT, Masson's trichrome.

2. Role of *Staphylococcus aureus* enterotoxin-B (SEB) and α-galceramyde (α-Galcer) adjuvants in the murine, C57BL/6J-based allergic asthma model

From the previous dose and time-finding experiments, the High 4W group was selected for further model development because it showed HDM-specific IgE as evidence of allergic sensitization, airway hyperresponsiveness, and the strongest granulocytic, mixed eosinophilic-neutrophilic inflammatory infiltration. We next aimed at achieving a solid representation of airway remodeling, a cardinal asthma feature. For this purpose, we employed two adjuvants along with HDM, namely SEB and α-Galcer.

2.1. SEB and α-Galcer modulate HDM-induced airway hyperresponsiveness

We instilled mice with High-dose HDM plus SEB or α-Galcer (HDM+SEB and HDM+α-Galcer groups, respectively) following the 4W schedule. We employed the existing High 4W HDM and SS groups (**Figure 12**, **Table S5**) as positive and negative disease controls, respectively. Both the HDM+SEB and HDM+α-Galcer groups showed an R_L reduction to a non-significant level over the SS group. Therefore, the HDM+SEB and HDM+α-Galcer combinations abrogated airway hyperresponsiveness to MCh. In the case of HDM+α-Galcer, the R_L was brought down to the SS level (**Figure 6 and Table 5**).

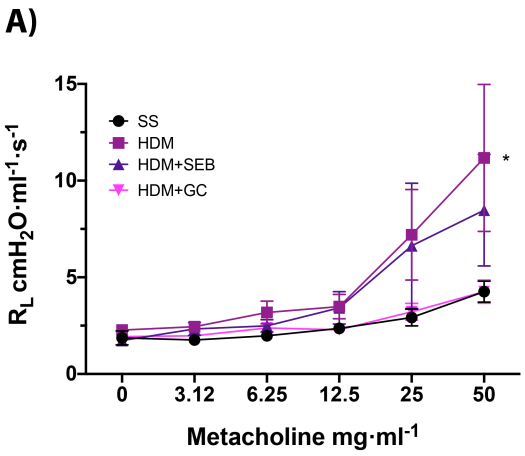

Figure 12. *Staphylococcus aureus* enterotoxin-B (SEB) and α-galceramyde (α-Galcer) adjuvants abrogate HDM-induced airway hyperresponsiveness. C57BL/6J mice were sensitized *i.n* with saline solution (SS), House Dust Mite (HDM) alone (15 µg/mL), or HDM combined with SEB (2 mg/mL) (HDM+SEB) or α-Galcer (20 ng/mL) (HDM+ α-Galcer). Lung resistance (R_L) ($cmH_2O \cdot ml^{-1} \cdot s^{-1}$) was assessed in response to airway challenge with increasing methacholine (MCh) concentrations (0-50 $mg \cdot ml^{-1}$). Data are presented as mean±SEM and were analyzed by 2-way ANOVA. Group size: SS n=8; HDM n=12; HDM+SEB n=8; HDM+ α-Galcer n=4. *$P<0.05$.

2.2. Effect of HDM or α-Galcer addition on lung inflammatory infiltrates

We evaluated the effect of SEB and α-Galcer on the inflammatory infiltrates from homogenized lungs as relative frequencies (**Figure 13**) and absolute cell numbers (**Figure 14**). The corresponding numerical data and *P* values are in **Tables S6 and S7**, respectively. The addition of SEB had a depleting effect on T cells overall by bringing down to nonsignificant values over SS, in relative and absolute numbers consistently, the $CD3^+$ (**Figures 13A** and **14A**), $CD4^+$ (**Figures 13B** and **14B**), and $CD8^+$ (**Figures 13C** and **14C**) cells in the HDM+SEB group. Conversely, HDM+α-Galcer caused an increase in all T cells ($CD3^+$, $CD4^+$, and $CD8^+$; same figure panels), which reached statistical significance versus HDM and HDM+SEB in the relative frequencies. Both HDM+SEB and HDM+α-Galcer increased the $CD19^+$ B cells significantly over SS (**Figures 13D and 14D**).

On monocytes/macrophages, neither the effects of SEB or α-Galcer were consistent between relative frequencies and absolute cell numbers (**Figures 7E and 8E**). SEB did not modify the effect of HDM on neutrophils or eosinophils. On the contrary, the addition of α-Galcer brought down the eosinophils significantly in the HDM+α-Galcer group. A depleting effect of the addition of α-Galcer on neutrophil relative frequency was not reflected in the absolute counts (**Figures 13 F-G and 14 F-G**).

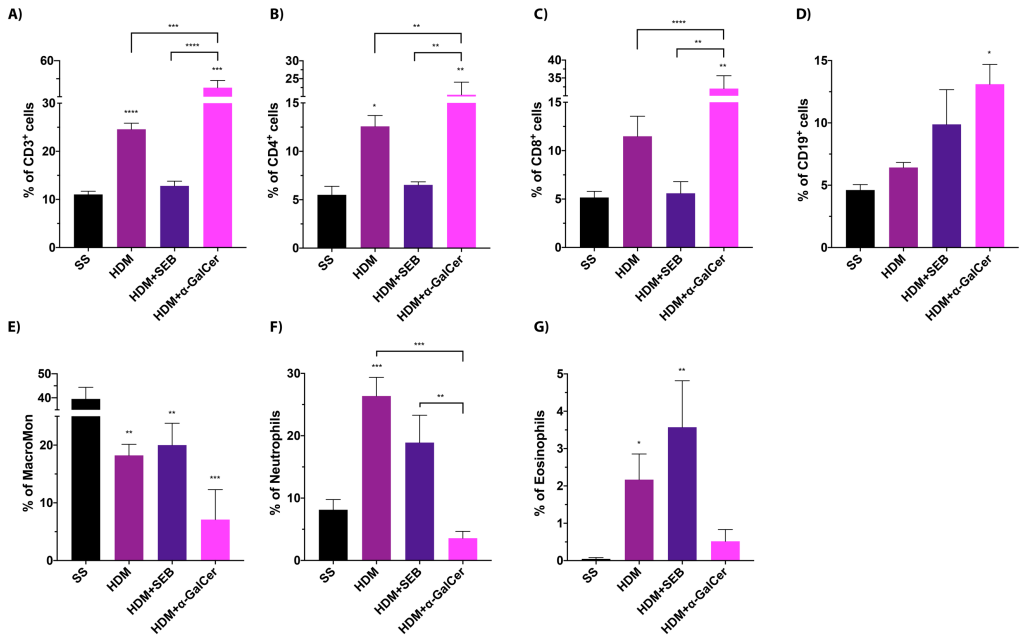

Figure 13. Effect of *Staphylococcus aureus* enterotoxin-B (SEB) and α-galceramyde (α-Galcer) addition on the pulmonary inflammatory infiltrates, relative cell frequencies. C57BL/6J mice were sensitized *i.n* with saline solution (SS), House Dust Mite alone (15 μg/mL) (HDM), or HDM with SEB (2 mg/mL) (HDM+SEB) or α-Galcer (20 ng/mL) (HDM+ α-Galcer). The panels show the percentage of $CD3^+$ T cells (**A**), $CD4^+$ T cells (**B**), $CD8^+$ T cells (**C**), B cells (**D**), macrophages and monocytes (**E**), neutrophils (**F**), and eosinophils (**G**). Data are presented as mean±SEM and were analyzed by one-way ANOVA. The asterisks mark the differences versus the SS group unless otherwise signaled by bars between groups as indicated. Group size: SS n=13; HA n=22; HA+SEB n=8; HA+ α-Galcer n=4. **P<0.05*; ***P<0.0021*; ****P<0.0002*; *****P<0.0001*.

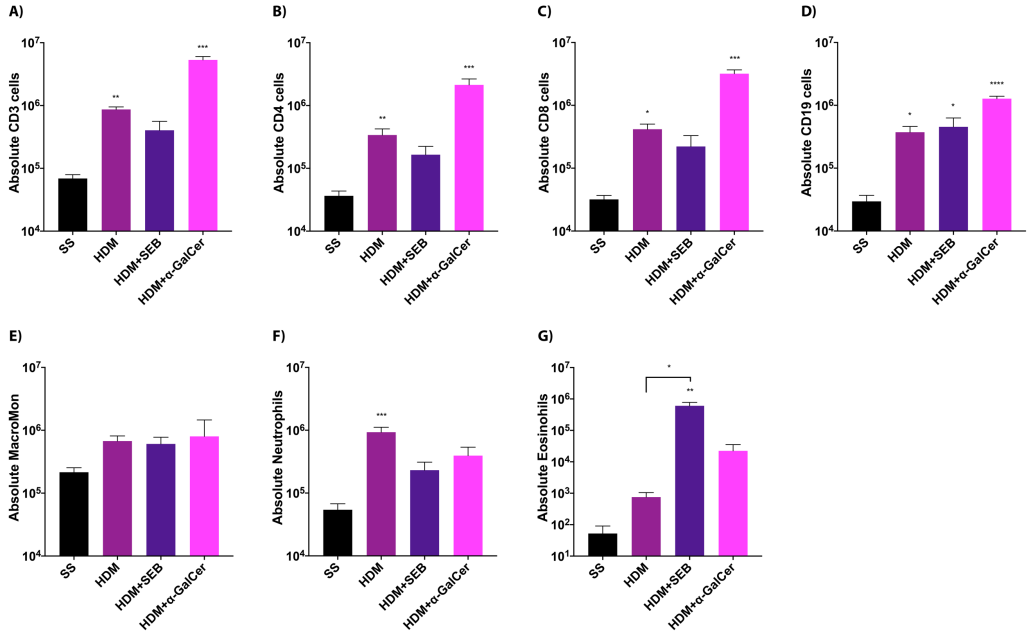

Figure 14. Effect of *Staphylococcus aureus* enterotoxin-B (SEB) and α-galceramyde (α-Galcer) addition on the pulmonary inflammatory infiltrates, absolute cell counts. C57BL/6J mice were sensitized *i.n* with saline solution (SS), House Dust Mite alone (15 µg/mL) (HDM), or HDM with SEB (2 mg/mL) (HDM+SEB) or α-Galcer (20 ng/mL) (HDM+ α-Galcer). The panels show the absolute numbers of $CD3^+$ T cells (**A**), $CD4^+$ T cells (**B**), $CD8^+$ T cells (**C**), B cells (**D**), macrophages and monocytes (**E**), neutrophils (**F**), and eosinophils (**G**). Data are presented as mean±SEM and analyzed by ordinary one-way ANOVA. The asterisks mark the differences versus the SS group unless otherwise signaled by bars between groups as indicated. Group size: SS n=12; HDM n=20; HDM+SEB n=8; HDM+ α-Galcer n=4. **P<0.05*; ***P<0.0021*; ****P<0.0002*.

2.3. HDM with SEB but not with α-Galcer induces airway remodeling

The HDM High 4W results in Section 1 showed that HDM alone induces an increase of peribronchial cell infiltration as seen with H&E stain, without apparent changes in the goblet cells or mucous mass by PAS stain nor subepithelial fibrosis by Masson's trichrome. In the subsequent experiments, the instillation of HDM combined to SEB elicited remodeling of the airways as reflected by goblet cells hyperplasia, increased mucous mass, and fibrosis in subepithelial and peribronchial location. In contrast, the combination of HDM with α-Galcer did not lead to any observable changes in the airway wall compared with HDM alone (**Figure 15**).

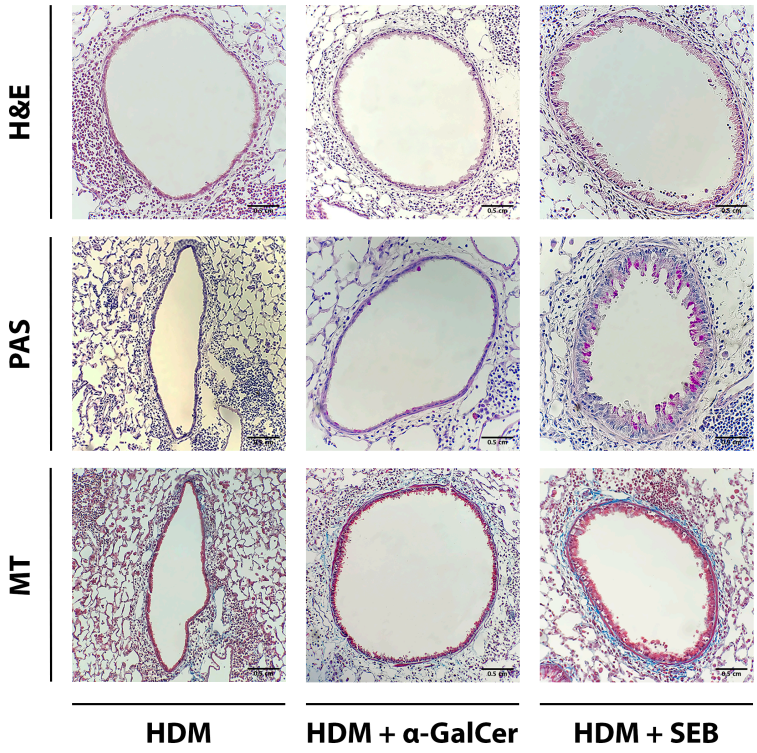

Figure 15. HDM combined with *Staphylococcus aureus* enterotoxin-B (SEB) induces airway remodeling. C57BL/6J mice were sensitized *i.n* with saline solution (SS), House Dust Mite alone (15 µg/mL) (HDM), or HDM with SEB (2 g/mL) (HDM+SEB) or α-Galcer (20 ng/mL) (HDM+ α-Galcer). The micrography's show representative airway sections from the experimental groups and histological stains as indicated. H&E, hematoxylin-eosin. PAS, Periodic acid-Schiff. MT, Masson's trichrome.

3. Assessment of the airway inflammatory response kinetics upon repeated HDM dosing

To study the pattern of lung inflammatory infiltration during successive development stages of experimental asthma, we carried out an exploratory analysis of leukocyte subpopulation kinetics by sampling cutoffs after each HDM instillation following the High 4W protocol. We divided the model sequence into two stages: a first stage encompassing

the first two weeks of antigen exposure through the first six instillations, and a second stage for the last two weeks with the remaining seven instillations. We analyzed the infiltrating leukocyte subpopulations by percentage and absolute numbers in lung homogenates and cytokines in bronchoalveolar lavage.

3.1. Primary airway exposure to HDM elicits and modulates airway inflammatory cell recruitment

During the first stage of the High 4W experimental asthma model, the relative frequency of the cells involved in the $CD4^+$ T-cell-driven adaptive immune response with immunoglobulin production was close to steady state with some limited tendency to increase. This pattern involved the $CD3^+$ and $CD4^+$ T cells, and $CD19^+$ B cells (**Figures 16 A-B and 15C**). The $CD8^+$ T cells showed an early peak upon the second HDM dose, and then steady state (**Figure 16C**). The baseline percentage of monocytes/macrophages dropped (**Figure 16E**), an effect attributable to the increasing percentages of most of the other cell types in view of the absolute numbers (see below). Differently from T and B cells, the granulocyte percentages experienced their main increase during this stage. The neutrophil percentage increased and plateaued after the third HDM instillation (**Figure 16F**). The eosinophils showed a close-to-linear increase for the entire first stage, reaching about 20% of the leukocytes (**Figure 16G**).

During the second stage, the relative frequencies of lymphocytes and granulocytes behaved inversely. All adaptive immunity lymphocytes ($CD3^+$, $CD4^+$ and $CD8^+$ T cells, and $CD19^+$ B cells) showed their major increase during the second stage (**Figures 16 A-D**). However, the $CD3^+$ and $CD4^+$ T cells showed an abrupt drop following the last (13^{th}) instillation, associated with a decrease in B cells as well, whereas the CD8+ T cells had a tendency to increase at this point. The monocyte/macrophage percentage continued at its lowest level (**Figure 16 E**). Contrary to the lymphocytes, the neutrophils and eosinophils dropped (**Figure 16 F-G**).

The absolute cell counts of $CD3^+$, $CD4^+$ and $CD8^+$ T cells, and $CD19^+$ B cells (**Figure 17 A-D**) were consistent with the tendencies shown by their relative frequencies. The absolute macrophages and monocytes (**Figure 17 E**) maintained their baseline during the first stage and increased notably in the second phase. The absolute neutrophils and

eosinophils (**Figure 17 F-G**) increased through the first stage and remain approximately constant during the second stage.

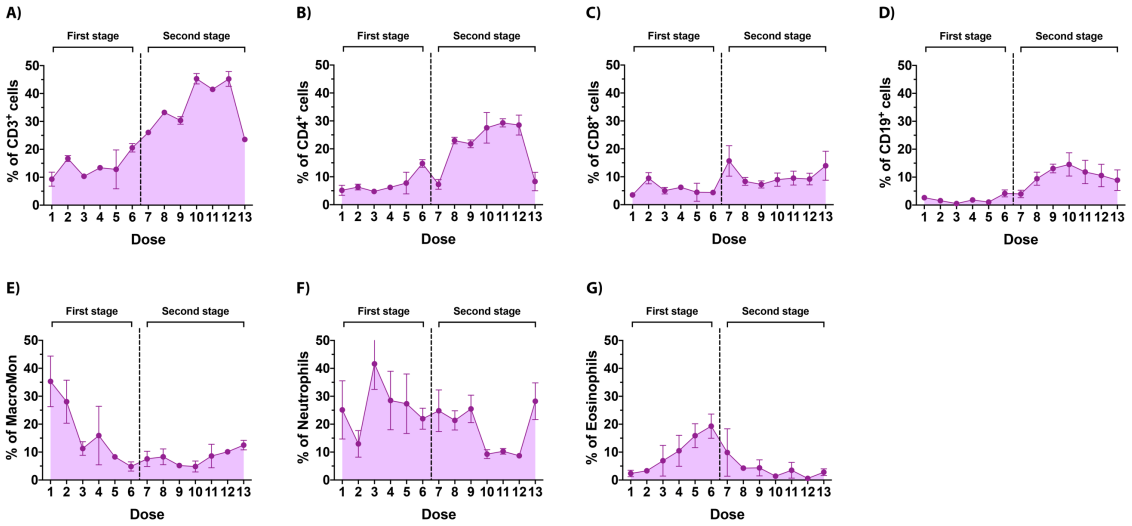

Figure 16. Exploratory kinetics of inflammatory cells across repeated house dust mite (HDM) instilations in High 4W regime, relative frequencies. Thirty-nine C57BL/6J mice were sensitized *i.n.* with HDM (15 µg/mL), three mice per dose cutoff for the 13 doses as per the High 4W scheme, and sacrificed 24 hours after the last instillation. The panels show the percentage of $CD3^+$ T cells (**A**), $CD4^+$ T cells (**B**), $CD8^+$ T cells (**C**), $CD19^+$ B cells (**D**), macrophages/monocytes (**E**), neutrophils (**F**), and eosinophils (**G**).

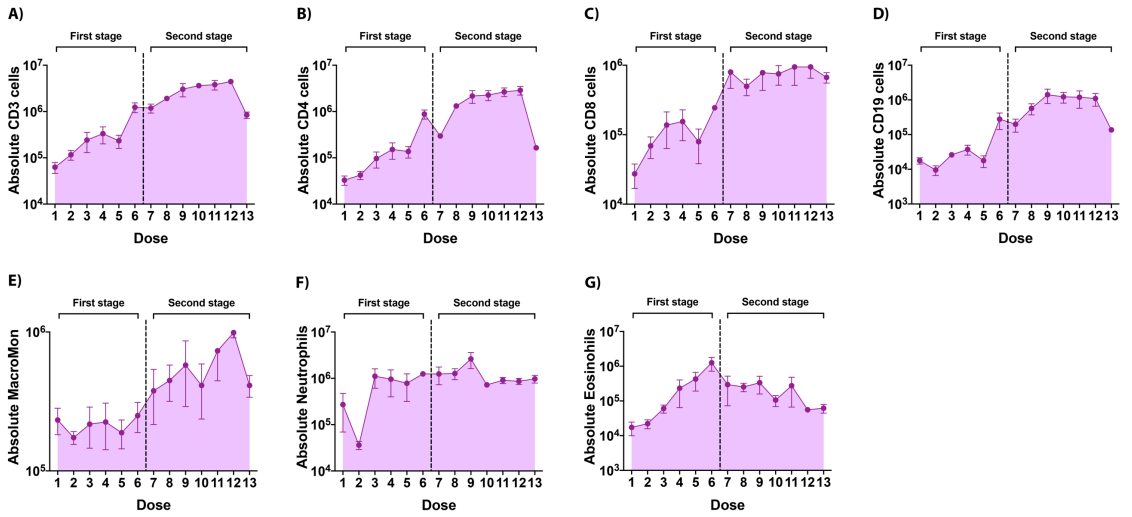

Figure 17. Exploratory kinetics of inflammatory cells across repeated house dust mite (HDM) instilations in High 4W regime, absolute cell counts. Thirty-nine C57BL/6J mice were sensitized *i.n.* with HDM (15 µg/mL), three mice per dose cutoff for the 13 doses as per the High 4W scheme, and sacrificed 24 hours after the last instillation. The panels show the percentage of $CD3^+$ T cells (**A**), $CD4^+$ T cells (**B**), $CD8^+$ T cells (**C**), $CD19^+$ B cells (**D**), macrophages/monocytes (**E**), neutrophils (**F**), and eosinophils (**G**).

3.2. Effect of primary airway exposure to HDM on soluble inflammatory mediators

We measured BAL cytokines and immunoglobulins in the inflammatory response kinetics mice. IFN-γ and IL-4 peaked in the first stage (**Figure 18 A-B**), whereas IL-17A increased progressively through both stages and had its peak in the second stage with a drop after the 13th HDM instillation (**Figure 18C**). All immunoglobulin classes showed a response. Increased total IgE was detected from the 4th instillation, peaking in the early second stage and subsequently declining (**Figure 18D**). HDM-specific IgE had cyclic peaks (**Figure 18H**), the first of which coincided with the initial rise of total IgE. IgA and IgM were the immunoglobulin classes reaching the highest concentration, with their response concentrating within the second stage and followed by an end decline in both cases (**Figure 18 E-F**). The IgG had a sharp rise from the 2nd instillation and maintained its increased concentration until declining by mid second stage (**Figure 18 G**).

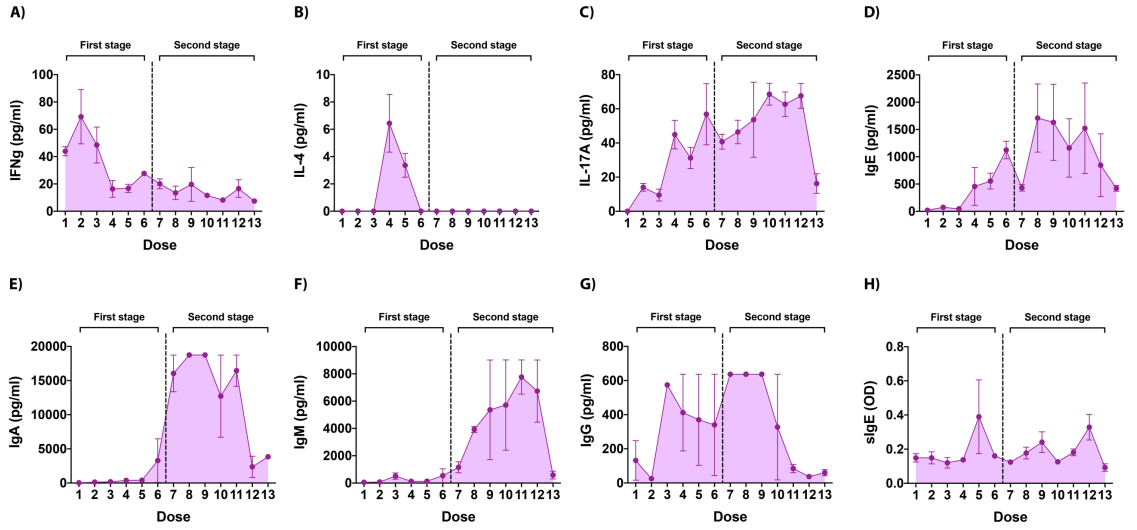

Figure 18. Exploratory BAL cytokine and immunoglobulin kinetics across repeated house dust mite (HDM) instilations in High 4W regime. Thirty-nine C57BL/6J mice were sensitized *i.n.* with HDM (15 µg/mL), three mice per dose cutoff for the 13 doses as per the High 4W scheme, and sacrificed 24 hours after the last instillation. The panels show total protein concentration for IFN-γ (**A**), IL-4 (**B**), IL-17A (**C**), total IgE (**D**), IgA (**E**), IgM (**F**), IgG (**G**), and HDM-specific IgE (**H**). OD: optical density. Data are mean±SEM.

4. HDM antigen status shifts experimental asthma towards an eosinophilic or neutrophilic profile

4.1. The protein content of standardized HDM extract varies over time following reconstitution

The changes produced in the lung inflammatory cell populations (**Figures 16 and 17**) and the cytokine trends (**Figure 18**) observed during the disease kinetics were induced by repeated HDM exposure. However, changes in the state of preservation of the HDM antigens may carry dosing variations that modify the immunological response. To determine whether such changes in HDM protein content occur, we performed Western blot analysis. For this purpose, a sample of reconstituted HDM was kept for each *i.n.* instillation delivered to the mice. The Western blot was then performed with the corresponding 13 samples (**Figure 13**).

The bands corresponding to the 25-kDa Derp1 and 14-kDa Derp2 proteins faded from the 6th instillation, which corresponds to 12 days after HDM reconstitution and storage at 4ºC (**Figure 19**).

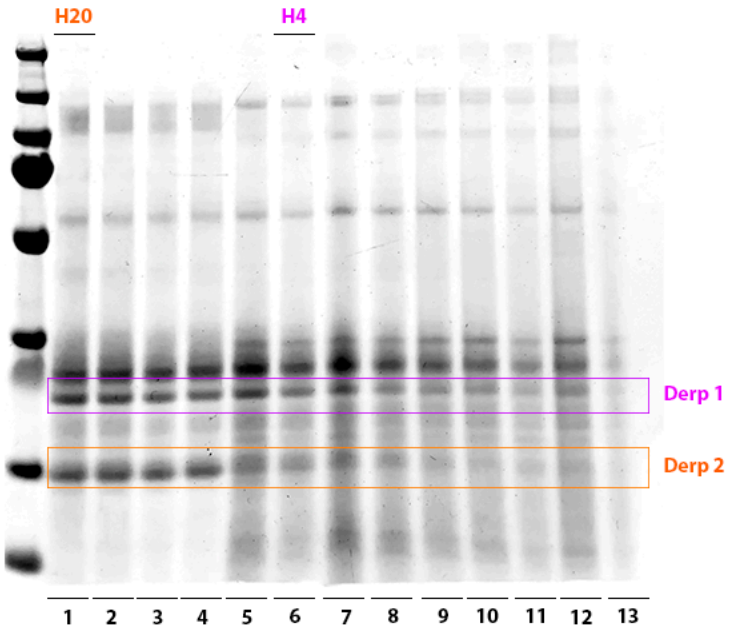

Figure 19. DerP1 and DerP2 protein content through each consecutive HDM instillation as per regular procedure in the High 4W model. Lyophilized, standardized HDM extract was reconstituted and its protein extract assayed by SDS-PAGE through the timing corresponding to each *i.n.* instillation (1 to 13) of the High 4W regime.

5. Experimental asthma develops differently with varying HDM antigen status

In accordance with the results obtained from the Western blot, we generated an asthma model following the established High 4W dose and timing, but taking into account HDM status For this purpose, we used two different HDM sources: freshly reconstituted HDM, preserved at -20ºC to avoid degradation (named **H20** hereinafter); and HDM partially degraded by preservation for 12 days at 4ºC after reconstitution and then stored at -20ºC (named **H4**), whose condition is that of the 6th instillation as per regular procedures. As done in the previous experiments, we analyzed R_L, lung leukocyte populations, BAL cytokines and immunoglobulins, and histopathology.

5.1. Primary airway exposure to H4 and H20 elicits airway hyperresponsiveness

Both H4 and H20 instillations induced airway hyperresponsiveness, as reflected by significantly increased R_L (P<0.005 versus SS from 25 mg/mL MCh) (**Figure 20 and Table S8**). No significant difference was observed between H4 and H20.

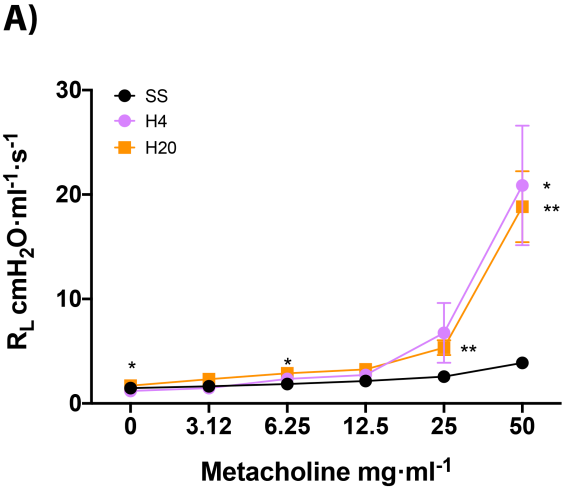

Figure 20. H4 and H20-induced airway hyperresponsiveness. C57BL/6J mice were sensitized *i.n* with saline solution (SS) or House Dust Mite (HDM) (15 µg/mL) with protein degradation (H4) or with frozen-preserved extract (H20), through 4 weeks, three times per week. Lung resistance (R_L) ($cmH_2O \cdot ml^{-1} \cdot s^{-1}$) was assessed by methacholine (MCh) challenge (0-50 $mg \cdot ml^{-1}$). Data are mean±SEM and were analyzed by 2-way ANOVA. Group size: SS n=7; H4 n=7; H20 n=10. **P<0.05*; ***P<0.002.*

5.2. H4 induces neutrophilic, and H20 eosinophilic, inflammatory recruitment in the lung and BAL

We evaluated the leukocyte subpopulations in lung homogenates (**Figures 21 and 22**; numerical data and *P* values in **Tables S9 and S10**, respectively). In terms of relative cell frequencies, H4 led to increased $CD3^+$ and $CD4^+$ T cells (**Figure 21A-B**), in addition to a large increase in neutrophils (**Figure 21F**), all significant versus the SS control. In contrast, H20 induced increased B cells (**Figure 21D**), neutrophils (**Figure 21F**), and a large eosinophil increment (**Figure 21F**). The comparison between H4 and H20 shows a higher $CD3^+$ T-cell percentage for H4 versus H20 (**Figure 21A**). It is remarkable that H4 induces a large increment of neutrophils versus H20, whereas H20 shows a large number of eosinophils versus H4. Both compounds decreased $CD8^+$ T cells and monocytes/macrophages similarly.

The absolute cell counts were consistent with the relative frequencies for the $CD3^+$ and $CD4^+$ T cells, neutrophils, and eosinophils (**Figure 22 A-B, F-G**). The $CD4^+$ T cell increase reached significance for H4 over H20 in this case. H4 also induced a significant increase of $CD19^+$ B cells over SS, similar to H20 (**Figure 22D**). Different from the relative frequencies, H4 induced a significant $CD8^+$ T-cell and monocyte/macrophage increment over SS and H20 (**Figure 22 C, E**), whereas H20 had no effect. As a supplementary data analysis, we compared H4 versus H20 with the leukocyte counts normalized by lung weight (**Figure S1**; numerical data and *P* values in **Table S11**). The result was consistent with the absolute cell counts except for the loss of the significant difference for the monocytes/macrophages.

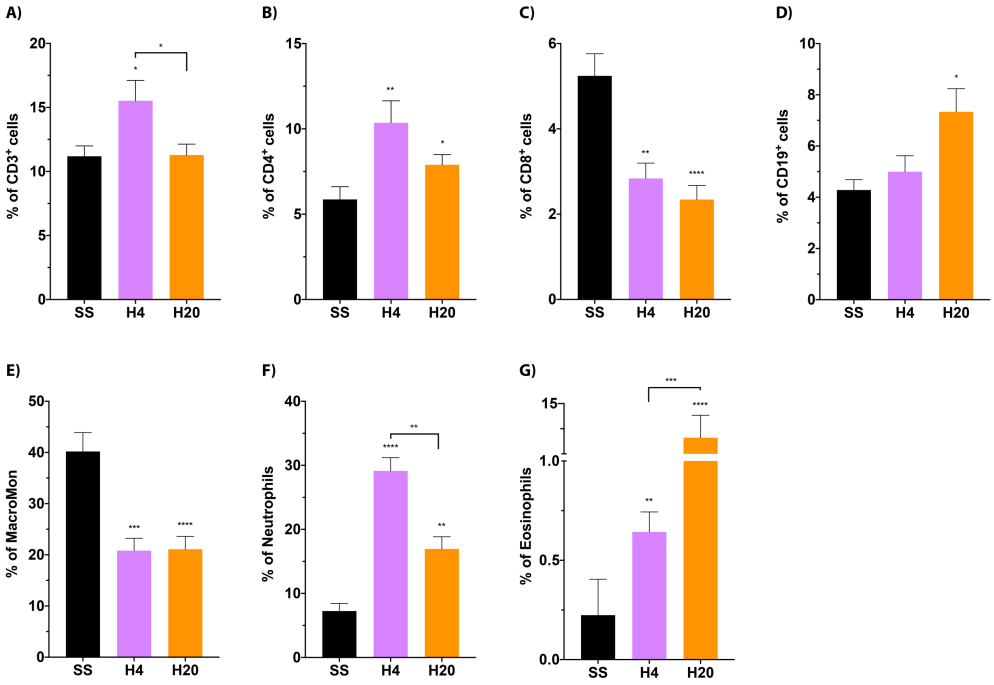

Figure 21. Lung inflammatory cell infiltration induced by H4 and H20, relative frequencies. C57BL/6J mice were sensitized *i.n* with saline solution (SS) or House Dust Mite (HDM) (15 µg/mL) with protein degradation (H4) or with frozen-preserved extract (H20), through 4 weeks, three times per week. The panels show the percentage of $CD3^+$ T cells (**A**), $CD4^+$ T cells (**B**), $CD8^+$ T cells (**C**), $CD19^+$ B cells (**D**), macrophages/monocytes (**E**), neutrophils (**F**), and eosinophils (**G**). Data are mean±SEM and were analyzed by one-way ANOVA. Group size: SS n=10; H4 n=12; H20 n=20. **P<0.05*; ***P<0.0021*; ****P<0.0002*; *****P<0.0001*. (n=12).

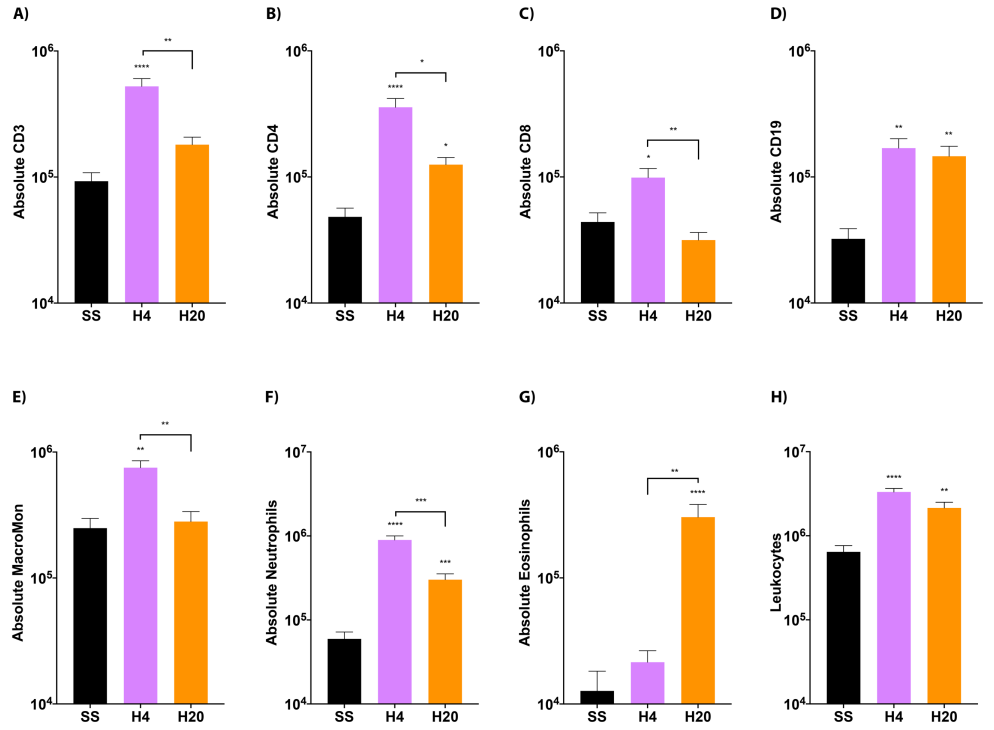

Figure 22. Lung inflammatory cell infiltration induced by H4 and H20, absolute counts. C57BL/6J mice were sensitized *i.n* with saline solution (SS) or House Dust Mite (HDM) (15 µg/mL) with protein degradation (H4) or with frozen-preserved extract (H20), through 4 weeks, three times per week. The panels show the percentage of $CD3^+$ T cells (**A**), $CD4^+$ T cells (**B**), $CD8^+$ T cells (**C**), $CD19^+$ B cells (**D**), macrophages/monocytes (**E**), neutrophils (**F**), eosinophils (**G**), and total leukocytes (**H**). Data are mean±SEM and were analyzed by one-way ANOVA. Group size: SS n=10; H4 n=12; H20 n=20. **P<0.05*; ***P<0.0021*; ****P<0.0002*; *****P<0.0001*.

Comparing treatments H4 and H20, we observed how in the H4 model the neutrophil population predominates both in the BAL (**Figure 23 C and D**) and in the lungs (**Figure 23 E and F)**, while in the H20 model the eosinophil population predominates (**Figure 23 C, D and E, F**). Whereas when comparing the granules present in the BAL versus those found in the lung parenchyma, we see the predominant eosinophils in the BAL both in the neutrophilic model (**Figure 23 A**) and in the eosinophilic (**Figure 23 B**).

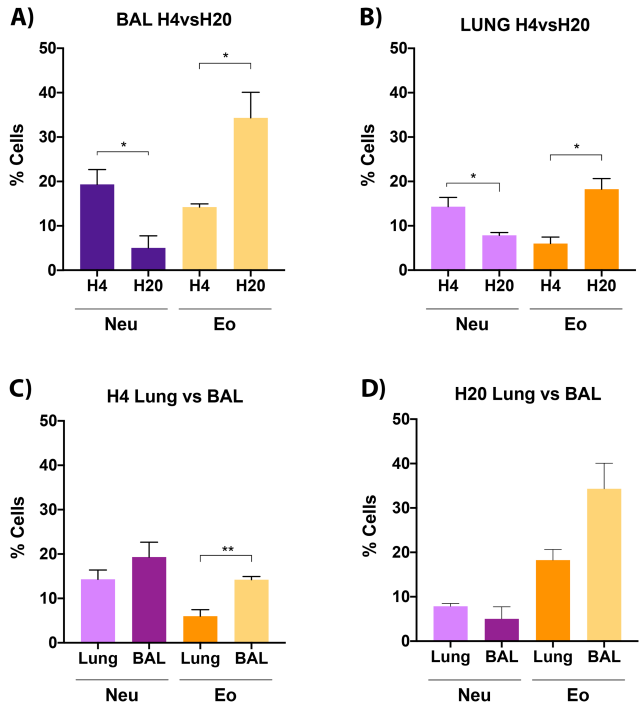

Figure 23. BAL and Lung inflammatory cell infiltration induced by H4 and H20. C57BL/6J mice were sensitized *i.n* with saline solution (SS) or House Dust Mite (HDM) (15 µg/mL) with protein degradation (H4) or with frozen-preserved extract (H20), through 4 weeks, three times per week. The panels show the comparative Lung vs BAL in H4 model (**A**), comparative Lung vs BAL in H20 model (**B**), BAL absolute number cells (**C**), BAL cells (**D**), Lung cells (**E**), Lung absolute number cells (**F**). Data are mean±SEM and were analyzed by t test. Group size: H4 n=3; H20 n=3. **P<0.05*.

5.3. BAL cytokines and immunoglobulins upon H4 and H20 instillations

We measured BAL cytokines and immunoglobulins (**Figure 24**; numerical data and *P* values in **Table S12**). H4 induced significantly increased concentrations of IFN-γ, IL-4, IL-13, and IL-17A (**Figure 18 A-D**), whereas H20 had no significant effect on any of these cytokines. Both H4 and H20 induced increased IgG, total IgE, specific IgE, and specific IgA (**Figure 18 E-H**) with no difference between them.

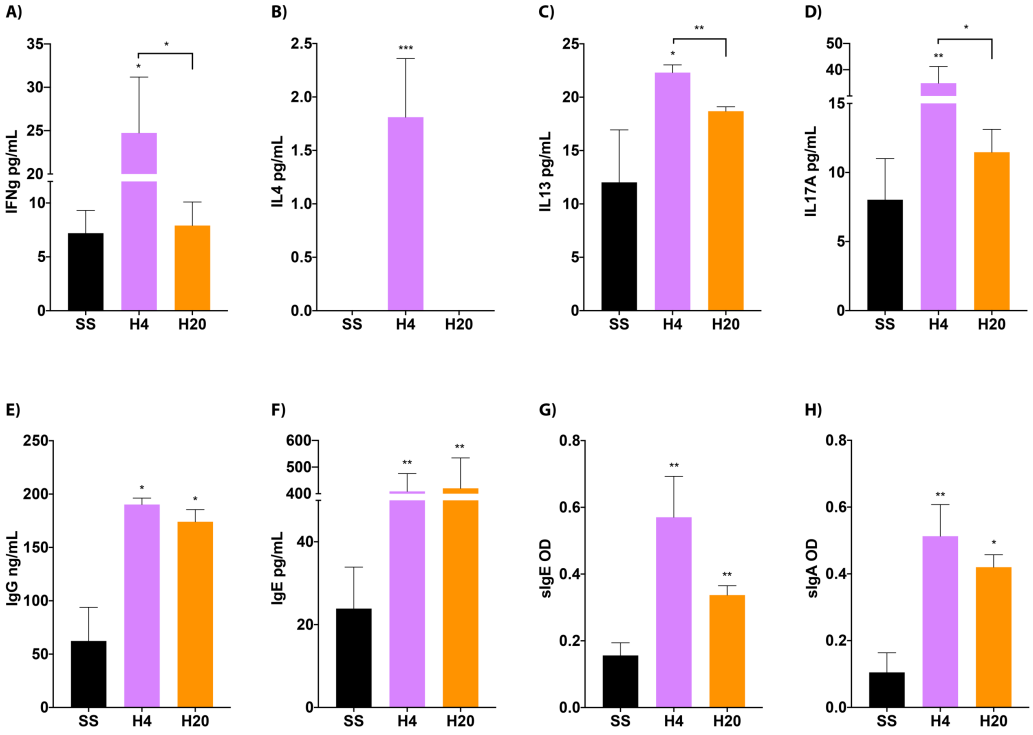

Figure 24. BAL cytokines and immunoglobulins upon H4 and H20 instillations, High 4W regime. C57BL/6J mice were sensitized *i.n* with saline solution (SS) or House Dust Mite (HDM) (15 µg/mL) with protein degradation (H4) or with frozen-preserved extract (H20), through 4 weeks, three times per week. IFN-γ (**A**), IL-4 (**B**), IL-13 (**C**), IL-17A (**D**), IgG (**E**), IgE (**F**), HDM-specific IgE (**G**), and HDM-specific IgA (**H**) were measured. OD: optical density**.** Data are mean±SEM and were analyzed by one-way ANOVA. Group size: SS n=10; H4 n=12; H20 n=20. **P<0.05*; ***P<0.0021*; ****P<0.0002*; *****P<0.0001*. (n=9).

5.4. Primary exposure with HDM induces changes in lung histopathology

An increase in the infiltration of leukocytes in the lung parenchyma was observed, either by counting by optical microscopy or flow cytometry. The peribronchial infiltration of cells in the histological sections of the lungs was evaluated by HE staining. For this purpose, the nuclei were selected and counted automatically using ImageJ software. A tendency to increase the peribronchial infiltrate was observed in H20 treatment compared to the control group (**Figure 25A, C and D, and Table S14**). However, the H4 group showed a significant difference in cell infiltrate either compared to the H20 group or compared to the control group (**Figure 25A-B and D, and Table 14**) (P=0.0096).

PAS staining and quantification by color extraction were performed to evaluate the mucus-producing cells. PAS staining did not reveal detectable mucus in the control and H4 groups (**Figure 26 A-B and D, and Table S14**). However, the H20 treatment presents a significantly greater amount of mucus in the epithelial cells (**Figure 26 C and D, and Table S13**) (P=0.006).

Subepithelial fibrosis was analyzed by Masson's trichrome. In the H20 group, higher levels of extracellular mass (ECM) were observed compared to the control group (**Figure 27 A, C and D, and Table S14**). The H4 group showed significantly increased ECM mass versus the control group and the H20 group (**Figure 27 A-B and D, and Table S14**) (P=0.0379).

The amount of smooth muscle alpha-actin was analyzed using immunofluorescence. We observed that H20 showed the highest amount and intensity of smooth muscle alpha-actin compared to the H4 and control groups (**Figure 28 and Table S14**) (P=0.0024 and P=0.0409).

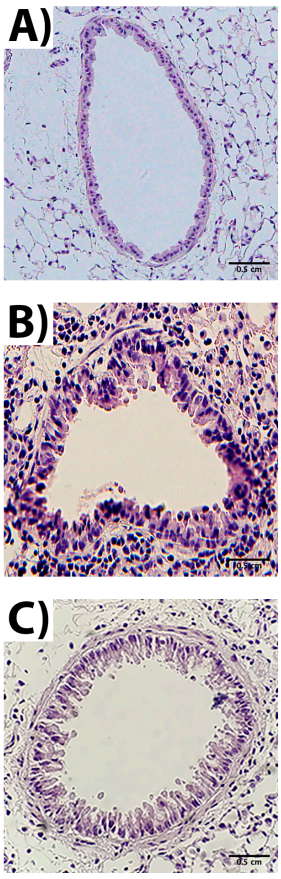

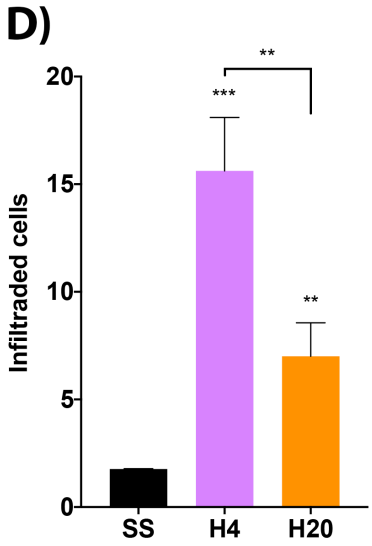

Figure 25. Lung cell inflammatory infiltration induced by H4 and H20 stimuli. C57BL/6J mice were sensitized *i.n* with saline solution (SS) or House Dust Mite (HDM) (15 µg/mL) with protein degradation (H4) or with whole extract (H20), during 4 weeks, three times per week. Peribronchial lung cell infiltration was determined by HE**.** Microscopy pictures show representative airways of bronchial SS (**A**), H4 (**B**), and H20 (**C**). Infiltration was quantified of each histological section, and data were represented to compare each treatment (**D**). Data are represented as mean±SEM and analyzed by Mann-Whitney or Unpaired t-test. **P<0.05*; ***P<0.0021.* (n=9).

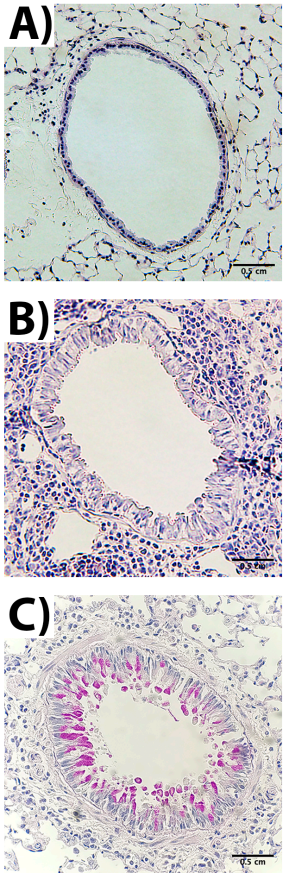

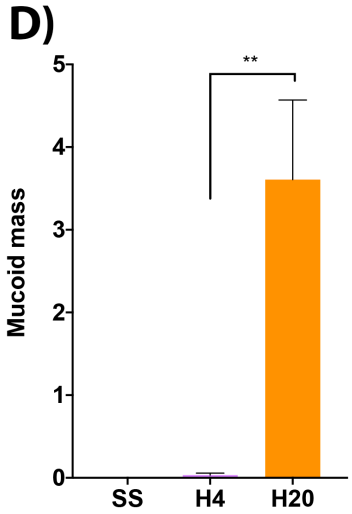

Figure 26. C57BL/6J mice were sensitized *i.n* with saline solution (SS) or House Dust Mite (HDM) (15 µg/mL) with protein degradation (H4) or with whole extract (H20), during 4 weeks, three times per week. PAS stain from lung histological sections was used to evaluate goblet cell number and hyperplasia and moreover were quantified mucus load. Microscopy pictures show representative airways of bronchial SS (**A**), H4 (**B**), and H20 (**C**). Mucus load quantification between treatments (**D**). Data are represented as mean±SEM and analyzed by Mann-Whitney or Unpaired t-test. ***P<0.0021*. (n=5).

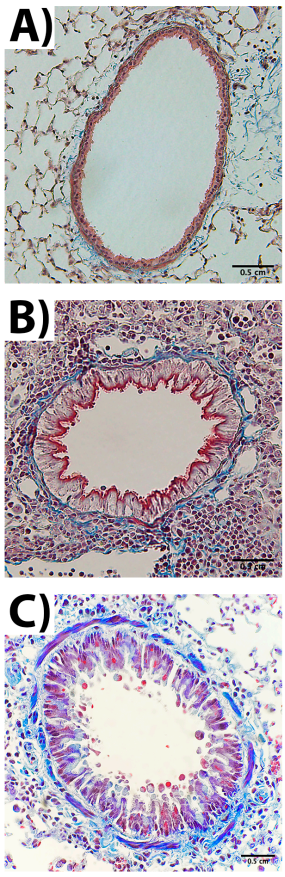

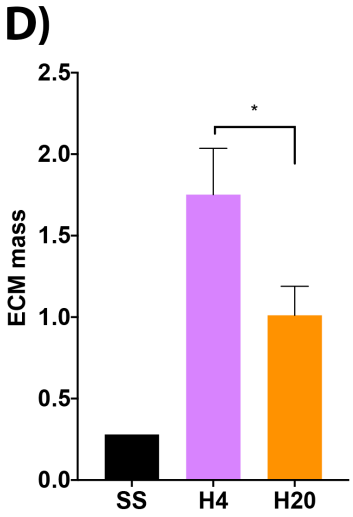

Figure 27. C57BL/6J mice were sensitized *i.n* with saline solution (SS) or House Dust Mite (HDM) (15 µg/mL) with protein degradation (H4) or with whole extract (H20), during 4 weeks, three times per week. Subepithelial fibrosis was evaluated by quantification of extracellular matrix mass (ECM). Microscopy pictures show representative airways of bronchial of SS (**A**), H4 (**B**), and H20 (**C**). The extracellular matrix was stained blue, and the ECM mass was calculated by digital color extraction (**D**). Data are represented as mean±SEM and analyzed by Mann-Whitney or Unpaired t-test. **P<0.05*. (n=12).

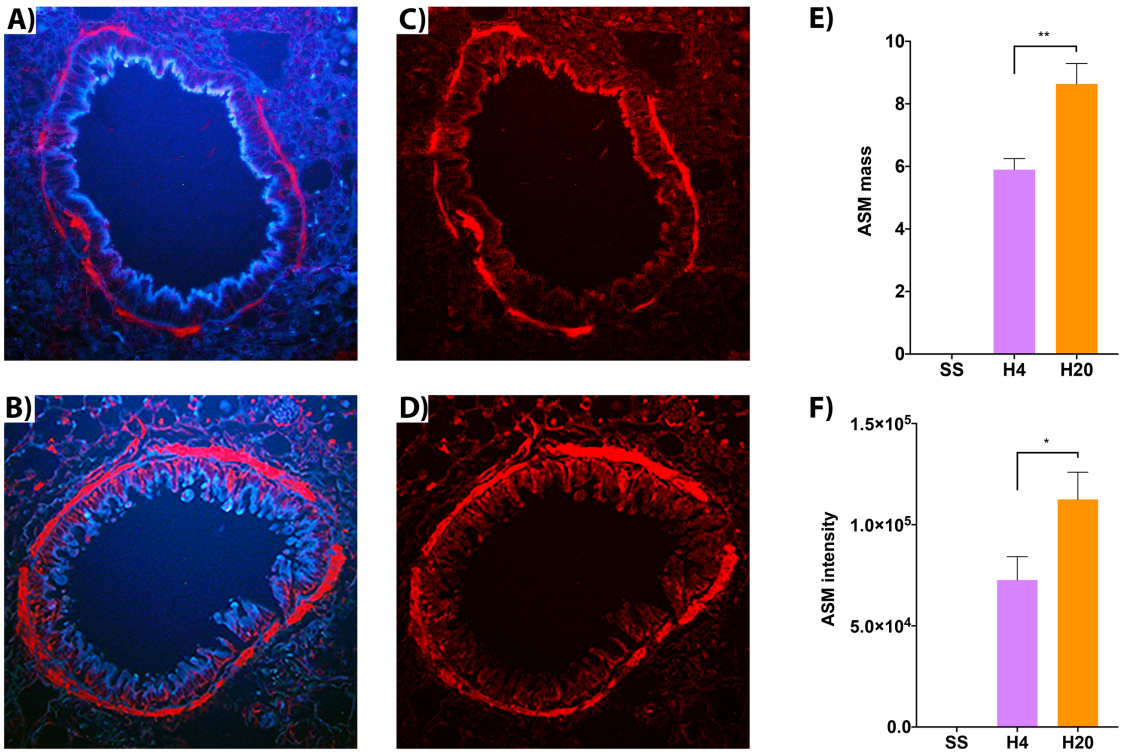

Figure 28. H4 and H20 stimuli increase airway smooth muscle cells. C57BL/6J mice were sensitized *i.n* with saline solution (SS) or House Dust Mite (HDM) (15 µg/mL) with protein degradation (H4) or with whole extract (H20), during 4 weeks, three times per week. Airway contractile tissue mass (ASM mass) was evaluated by alpha-SMC quantification by immunofluorescence detection in airway sections. Microscopy pictures show representative airways of bronchial H4 (**B** and **E**) and H20 (**A** and **D**). ASM mass was analyzed in each group by digital color extraction (**C**), and the alpha-SMC intensity was also quantified (**F**). Data are represented as mean±SEM and analyzed by Mann-Whitney or Unpaired t-test. **P<0.05*; ***P<0.0021*. (n=6).

5.5. Relationship of leukocyte infiltration with airway remodeling with H4 and H20 antigen sources

To analyze if there was a relationship between the cells mainly present in the lung as analyzed by flow cytometry and the remodeling features observed through the histological sections, statistical correlations were carried out (**Figure 29**). In the H4 treatment, we observed a positive correlation between the increase in the airway cell infiltrates and the presence of neutrophils (**Figure 29 A and Table S15**) (P=0.0015). There is also a positive correlation between the amount of smooth muscle and the presence of neutrophils (**Figure 29 B and Table S15**) (P=0.0046). However, in the case of subepithelial fibrosis, an inverse correlation is observed between fibrosis and the neutrophil infiltrate (**Figure 29 C and Table S15**) (P=0.0462). In the H20 treatment, where the dominant infiltrating cells are eosinophils, there is a positive correlation between the amount of mucoid mass and the number of infiltrating eosinophils (**Figure 29 D and Table S15**) (P=0.0462).

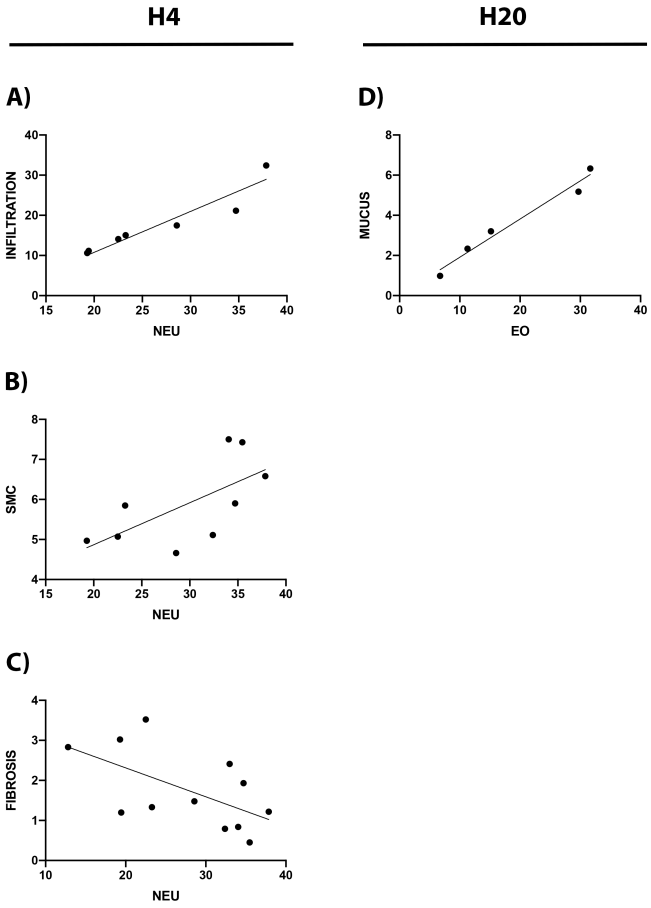

Figure 29. Lung inflammatory cell infiltration and airway remodeling correlation in H4 and H20 models. The panels show the correlation of lung cell infiltration count by H&E and neutrophil counts by Flow cytometry in H4 model (**A**), correlation of smooth muscle cell mass by αSMC and neutrophil counts by Flow cytometry in H4 model (**B**), correlation of collagen deposition count by Masson's Trichrome and neutrophil counts by Flow cytometry in H4 model (**C**)**,** correlation of mucus mass count by Acid Periodic Schiff and neutrophil counts by Flow cytometry in H20 model (**D**). Data are mean±SEM and were analyzed by Pearson r correlation. Group size: H4 n=6-12; H20 n=5.

6. Kinetics of eosinophilic and neutrophilic inflammatory infiltration across the High 4W model upon H4 and H20 antigen sources

After establishing eosinophilic (H20) and neutrophilic (H4) asthma models, kinetics with both antigen sources were performed from the first to the last dose of the 4-week model to compare the differences along the development of the disease.

6.1. Primary airway exposure to HDM elicits and modulates airway cell recruitment

As we have seen previously, there was a fluctuation between innate and adaptive immunity throughout the disease, with granulocyte populations being predominant to a greater extent.

Comparing the initial stage and the late stage of the disease under the two HDM sources, changes were observed at the percentage level in the infiltrating lung populations. In the case of adaptive immunity, the behavior in both treatments was quite similar in the first phase of the disease (**Figure 30 A-D**). Although in H4, a significant fluctuation of $CD8^+$

T lymphocytes was observed (**Figure 30 C and Table S16**). Regarding innate immunity, the most remarkable difference between both treatments was found at the level of granulocytes. Significantly higher levels of neutrophils (**Figure 30 E and Table S16**) were observed in H4 compared to H20 at different points, both in the first and second phase of the disease. In contrast, eosinophils (**Figure 30 G and Table S16**) predominated significantly during the entire disease process in H20 compared to H4, where these were in very low percentages.

In the second stage of the disease, we observed that the numbers of $CD4^+$ and $CD8^+$ T lymphocytes (**Figure 30 B-C and Table S17**) were significantly higher in the H4 treatment than in H20 at different points. For B lymphocytes (**Figure 30 D and Table S17**), differences were observed only in a single dose in the first stage, where there was a greater number in H4 compared to H20. As for innate immunity, H4 presents higher numbers of macrophages and monocytes (**Figure 30 E and Table S17**), in addition to neutrophils (**Figure 30 F and Table S17**) throughout the two stages compared to H20. However, H20 presents higher numbers of eosinophils along to the entire disease (**Figure 30G and Table S17**).

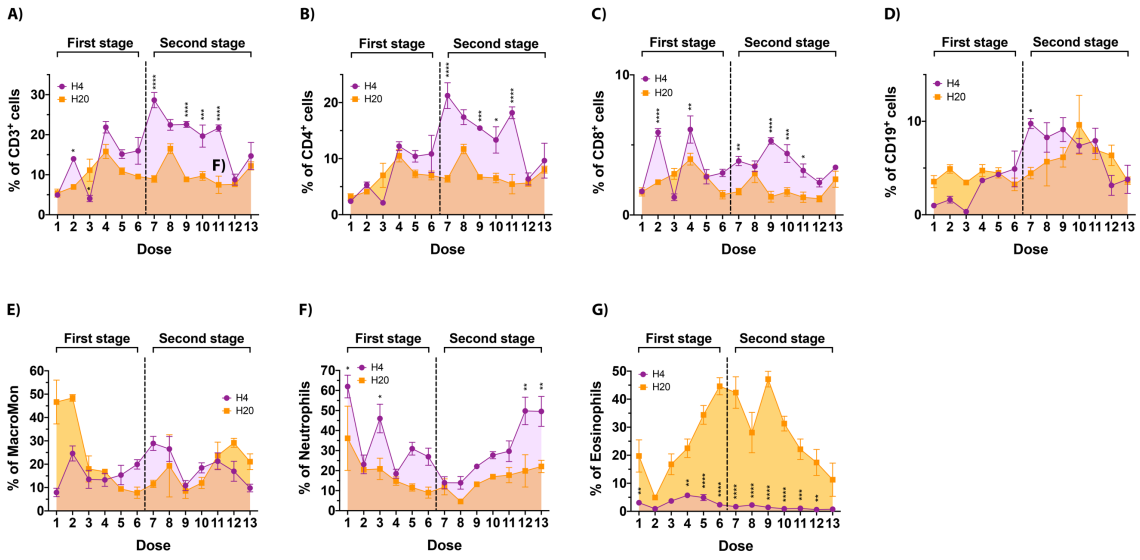

Figure 30. The effect of H4 and H20 challenge on the percentage of cell recruitment in lung tissue during the development of asthma. 39 C57BL/6J mice were *i.n* sensitized with House Dust Mite (HDM) (15 µg/mL) with protein degradation (H4) or with whole extract (H20), three mice per dose during 13 doses. Percentage of CD3 cells (**A**), CD4 T lymphocytes cells (**B**), CD8 T lymphocytes cells (**C**), B lymphocytes cells (**D**), Macrophage and Monocytes (**E**), Neutrophils (**F**), and Eosinophils (**G**). Data are represented as mean±SEM and analyzed by 2-way ANOVA test. **P<0.05*; ***P<0.0021*; ****P<0.0002*; *****P<0.0001*. (n=3).

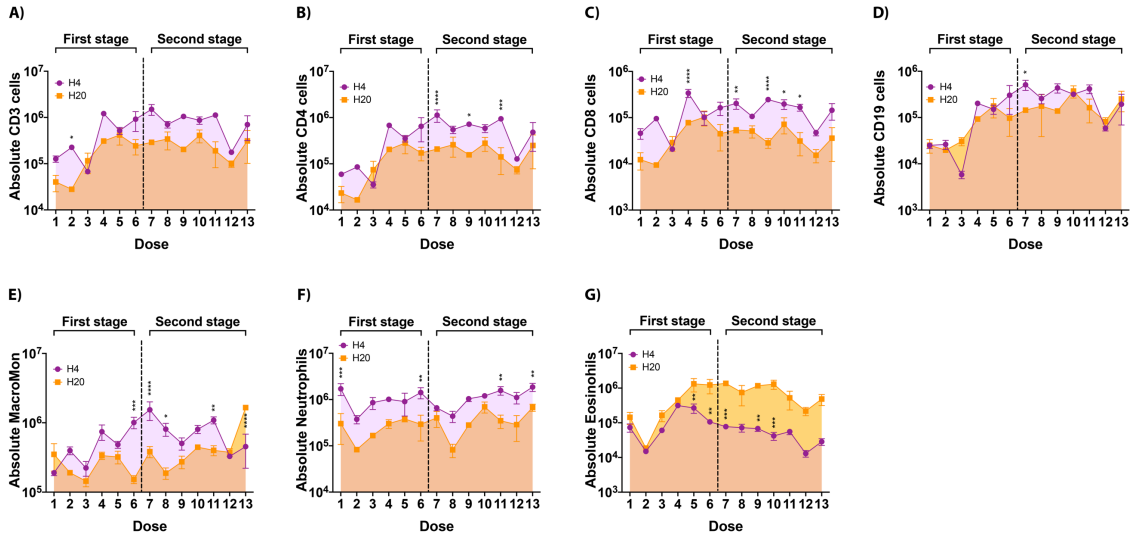

Figure 31. The effect of H4 and H20 challenge on absolute numbers of cell recruitment in lung tissue during the development of asthma. 39 C57BL/6J mice were *i.n* sensitized with House Dust Mite (HDM) (15 µg/mL) with protein degradation (H4) or with whole extract (H20), three mice per dose during 13 doses. Absolute numbers of leukocyte populations are showed: CD3 cells (**A**), CD4 T lymphocytes cells (**B**), CD8 T lymphocytes cells (**C**), B lymphocytes cells (**D**), Macrophage, and Monocytes (**E**), Neutrophils (**F**), and Eosinophils (**G**). Data are represented as mean±SEM and analyzed by 2-way ANOVA test. *$P<0.05$; **$P<0.0021$; ***$P<0.0002$; ****$P<0.0001$. (n=3).

6.2. Primary airway exposure to HDM elicits and modulates airway inflammation

Due to the fluctuation of cell populations previously described, we compared the cytokine profile in BAL of the H4 and H20 mice.

In the first stage of the disease, we observed that the levels of IFN-γ (**Figure 32 A and Table S19**) and IL-13 (**Figure 32 C and Table S19**) increased in H20 but not in H4. IL-4 (**Figure 32 B and Table S19**) and IgE (**Figure 32 E and Table S19**) appeared earlier with H4. In the case of IL-17A (**Figure 32D and Table S19**), it is present throughout the disease at significantly higher levels with H4 compared to H20. As for specific immunoglobulins, both s-IgE (**Figure 32 F and Table S19**) and s-IgA (**Figure 32 G and Table S19**) had a similar profile during the first stage of the disease, showing a peak in both treatments but earlier with H4 than H20. In the second stage of the disease, a slight peak of specific IgE was observed with H20 but not in H4, while specific IgA presented a peak earlier with H20 than H4 (**Figure 32 F-G and Table S19**).

To check if the cytokines quantified in BAL were secreted by HDM memory cells present in the lung, cells from the lungs of treated mice were isolated and stimulated *in vitro* with HDM and with PMA+IO as a nonspecific stimulus. When the cells were stimulated with their specific stimulus (HDM), as previously observed in BAL, the cells restimulated from

H20-instilled mice secreted IFN-γ (**Figure 33 A and Table S20)** in the first stage of the disease compared to H4. Similarly in BAL cytokines, IL-17A (**Figure 33C and Table S19**) levels were higher at the second stage of the disease in H4 than H20 but, at the last HDM exposure, the levels were inverted for H20 versus H4. The results obtained for IgE (**Figure 33 D and Table S20**) were more discrepant due to higher levels present in the H20 treatment compared to H4.

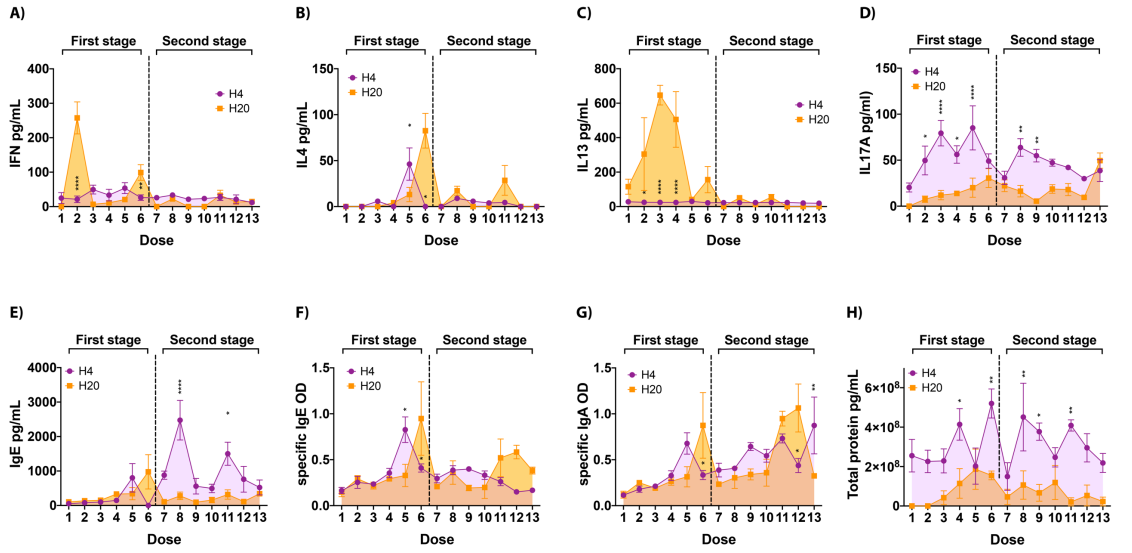

Figure 32. H4 and H20 stimuli change the cytokine and immunoglobulin profile in bronchoalveolar lavage. 39 C57BL/6J mice were sensitized *i.n* with House Dust Mite (HDM) (15 µg/mL) with protein degradation (H4) or with whole extract (H20), three mice per dose during 13 doses. Total protein of interferon-gamma (**A**), interleukin 4 (**B**), interleukin 13 (**C**), interleukin 17A (**D**), immunoglobulin E (**E**) and total protein (**H**) are represented as pg/mL; and specific immunoglobulin E (**F**) and specific immunoglobulin A (**G**) in optical density (OD). Data are represented as mean±SEM and analyzed by 2-way ANOVA test. **P<0.05*; ***P<0.0021*; ****P<0.0002*; *****P<0.0001*. (n=3).

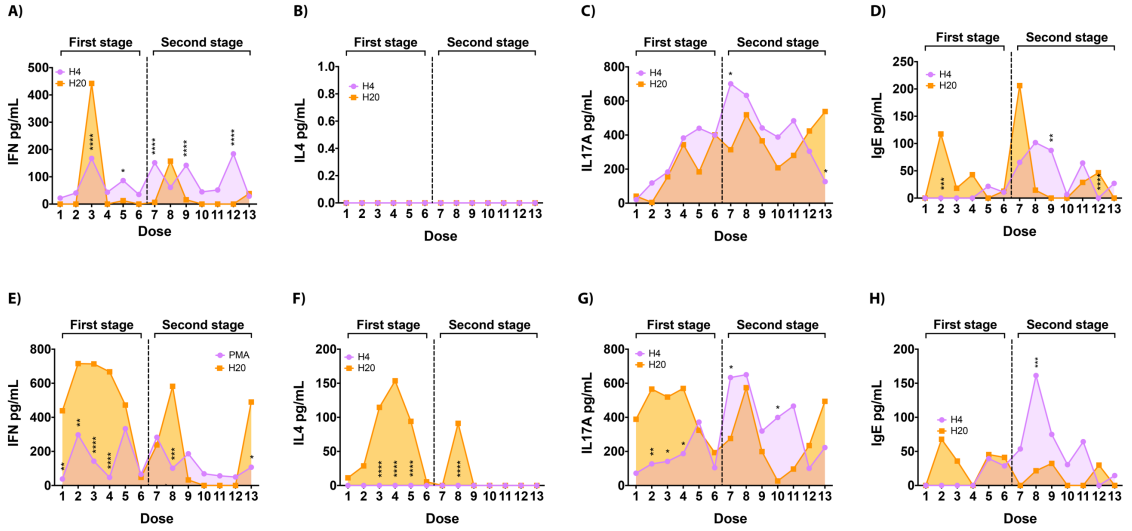

Figure 33. Cytokine supernatant determination from HDM and PMA restimulated lung cells. 39 C57BL/6J mice were *i.n* sensitized with HDM (15 µg/mL) with protein degradation (H4) or with whole extract (H20), three mice per dose during 13 doses(n=3). Lung cells were *in vitro* stimulated with H4 or H20 depending on mice treatment and PMA with IO (PMA/IO). Twelve hours post-stimulation, the supernatant was preserved for posterior ELISA analysis. Total protein of interferon gamma (**A** and **E**), interleukin 4 (**B** and **F**), interleukin 17A (**C** and **G**), immunoglobulin E (**D** and **H**) represented as pg/mL. Data are represented as mean±SEM and analyzed by 2-way ANOVA test. **P<0.05*; ***P<0.0021*; ****P<0.0002*; *****P<0.0001*. (n=3).

6.3. Different neutrophil and eosinophil subpopulations present along with the H4/H20 experimental asthma development

Since the populations of neutrophils and eosinophils were varying along the neutrophilic and eosinophilic experimental asthma, we aimed at studying if there was also variation in their activation state and, therefore, different subpopulations based on these markers and the morphology of these cells. For this purpose, the cells were analyzed on the basis of their granularity (side-scatter flow cytometry parameter, SSC) and activation markers including CD11b, Ly6C, and Ly6G for neutrophils and Siglec-F for eosinophils.

We observed three neutrophil populations based on CD11b and cell granularity, classified as $CD11b^{Lo}SSC^{Hi}$ (A), $CD11b^{Hi}SSC^{Lo}$ (B), and $CD11b^{M}SSC^{M}$ (C). Two other populations were detected based on Ly6C and CD11b expression, classified as $Ly6C^{+}CD11b^{Lo}$ (D) and $Ly6C^{+}CD11b^{Hi}$ (E). The neutrophilic model showed an increase in Ly6G expression greater than in the eosinophilic model, showing its maximum intensity during the third dose (1st phase) and during the ninth (2nd phase). While in the eosinophilic model, the MFI remains constant throughout all kinetics (F) (**Figure 34**).

Regarding the eosinophils, we also observe two populations based on the CD11b expression, a $CD11b^{Lo}$ (A) and $CD11b^{Hi}$ (B). Moreover, other subpopulations were observed based on the coexpression of CD11b and $Ly6C^{Hi}$ expression named $Ly6C^{High}$ (C). In the eosinophilic model, according to their size (FSC) a big size was observed at the initial stage, at the 3rd dose fall abruptly and a slight increase is observed in the final stage, reaching its smallest size in the last dose (D). Regarding their granularity, we observe that there are two large peaks in which the eosinophils reach their maximum granularity (3rd and 10th doses), while during the rest of the response they remain less granular, obtaining the lowest granularity at the final dose (E). In the case of the neutrophilic model, the size and granularity of the eosinophils remains more oscillating throughout the entire response. Focusing on the expression of SiglecF by MFI in the H20 model, we see that this increases until the 4th dose and then remains fairly constant throughout the disease; while in the H4 model it behaves in a similar way, but always with a lower intensity throughout the disease (E) (**Figure 35**).

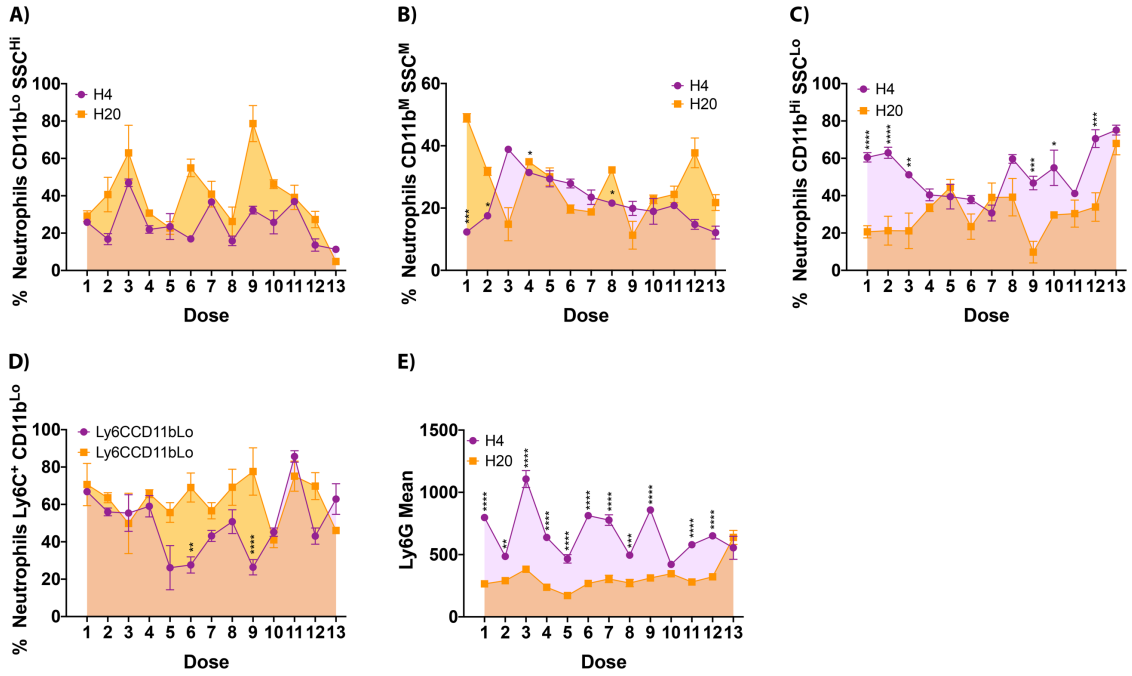

Figure 34. Neutrophil subpopulations on the different stages of asthma development. C57BL/6J mice were *i.n* sensitized with HDM (15 µg/mL) with protein degradation (H4) (n=39) or with whole extract (H20) (n=39), three mice per dose during 13 doses. Percentage of Neutrophils CD11bLow SSCHigh **A)**, Neutrophils CD11bHigh SSCLow **B)**, Neutrophils CD11bMild SSCMild **C)**, Neutrophils Ly6C+CD11bHigh **D)**, Neutrophils Ly6C+CD11bLow **E)**. Data are represented as mean±SEM. (n=3)

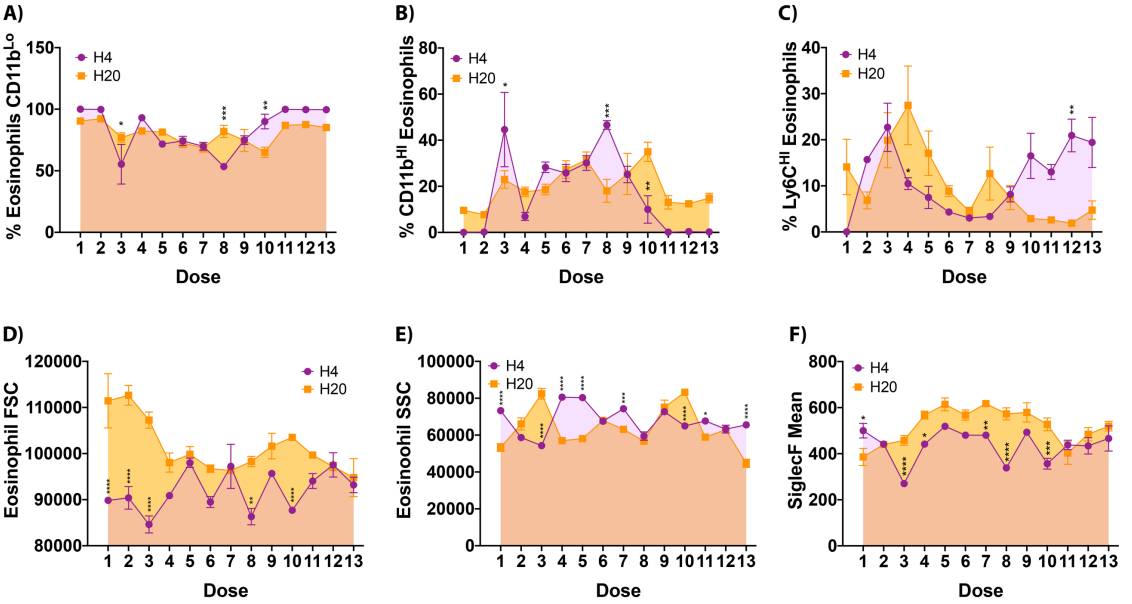

Figure 35. Eosinophil subpopulations on the different stages of asthma development. C57BL/6J mice were *i.n* sensitized with HDM (15 µg/mL) with protein degradation (H4) (n=39) or with whole extract (H20) (n=39), three mice per dose during 13 doses. Percentage of Eosinophils CD11b High **A)**, Eosinophils Ly6C High **B)**, Size of Eosinophils (Forward Scatter) **C)**, Granularity of Eosinophils (Side Scatter) **D)**. Data are represented as mean±SEM and analyzed by 2-way ANOVA test. **P<0.05*; ***P<0.0021*; ****P<0.0002*; *****P<0.0001*. (n=3).

6.4. ILC profile present at the initial and final in the H4/H20 asthma development

To observe how the response of the innate immune system varied throughout the development of asthma, ILC1, 2 and 3 were determined at the first and last points of each treatment.

We observed that ILC1 and 2 (A, B) were in a lower percentage at the beginning of treatment, however both increased at the end point of the disease. In the case of ILC3 (C) there is a slight decrease at the beginning of treatment and a slight increase at the final dose. Comparing the neutrophilic model with the eosinophilic, no differences were observed. However, neutrophilic has a tendency to ILC3 response; while the eosinophilic has a higher frequency of IL1 and ILC2 response (**Figure 36**).

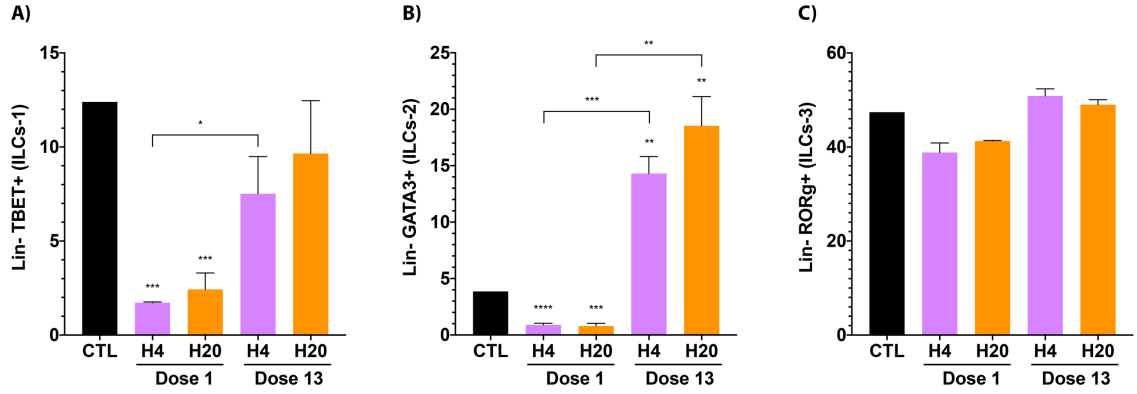

Figure 36. Lung ILCs infiltration induced by H4 and H20, relative frequencies. C57BL/6J mice were sensitized *i.n* with saline solution (SS) or House Dust Mite (HDM) (15 µg/mL) with protein degradation (H4) or with frozen-preserved extract (H20), with 1 dose or through 4 weeks, three times per week (13 doses). The panels show the percentage of ILC1 (**A**), ILC2 (**B**) and ILC3 (**C**)**.** Data are mean±SEM and were analyzed by one-way ANOVA. Group size: SS n=3; H4 n=3; H20 n=3 for each Dose. **P<0.05*; ***P<0.0021*; ****P<0.0002*; *****P<0.0001*.

7. Proteomic profile in BAL of experimental eosinophilic and neutrophilic asthma and human induced sputum supernatant

To evaluate the airway protein profile among the eosinophilic versus neutrophilic inflammatory phenotypes, in mice models and asthma patients, a comprehensive qualitative proteomic profiling of BAL mice and human sputum using LTQ-Orbitrap Velos MS/MS was performed.

To study the proteome and establish the protein profile characterizing both the onset of neutrophilic or eosinophilic inflammation and the endpoint of our murine asthma model, we independently evaluated BAL samples collected from each of the inflammatory profiles 24 hours after the 1st and 13th instillations. Sputum samples were analyzed according to the patient's neutrophilic or eosinophilic inflammatory phenotype, regardless of disease stage.

The proteomic assessment yielded a total of 98 proteins after the 1st HDM instillation of the H4-driven neutrophilic model (H4.1), 117 after the 1st dose of the H20-driven eosinophilic model (H20.1), 134 after the 13th dose of the neutrophilic model (H4.13), and 143 after the 13th dose of the eosinophilic model (H20.13). The human induced sputum analyses yielded a total of 315 proteins in neutrophilic asthma and 222 in eosinophilic asthma.

After the 1st HDM instillation, the proteomic assessment yielded a total of 98 proteins in BAL of the H4-driven neutrophilic model (H4.1), and 117 in H20-driven eosinophilic model (H20.1). After the 13th HDM dose, 134 proteins in the neutrophilic model (H4.13), and 143 to eosinophilic model (H20.13) were identifies. The human induced sputum analyses yielded a total of 315 proteins in neutrophilic asthma and 222 in eosinophilic asthma.

7.1. Biological processes identified in proteins from BAL and Sputum

To determine protein functionalities, all proteomics data were mapped according to biological processes (Figure 37) using the PANTHER (Protein Analysis Through Evolutionary Relationships) Classification System (264), part of the Gene Ontology Project. A total of 15 biological processes were identified for BAL and sputum analyzed

samples. A large amount of the proteins detected were related to cellular and metabolic processes, biological regulation, response to stimuli (*i.e.*, HDM), localization, and immune system processes (**Figure 37 and Table S1-6**).

To study the role of the innate immune system in the asthmatic response, we first evaluated all proteins founded in BAL and sputum involved in the immunological system. Mice treated with 1 dose of HDM (H4.1 and H20.1) showed a lower proportion of proteins related to the immunological system, in both the neutrophilic and eosinophilic models, compared to the 13th dose (H4.13 y H20.13, respectively) as shown in **Tables S1-4** (**Figure 37**). The biological processes related to the proteins detected in humans were similar to those observed in the first's doses of the murine models (H4.1 and H20.1) (**Tables S5-6**) (**Figure 37**).

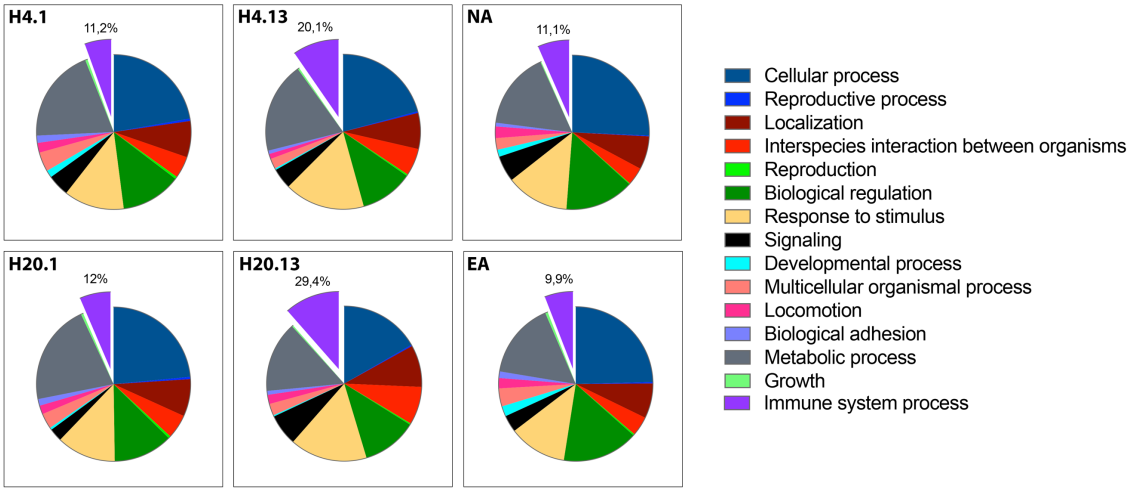

Figure 37. Comparison between the different biological processes in which the proteins analyzed in the BAL mice or sputum human of neutrophilic and eosinophilic asthmatics participate. The different proteins obtained from BAL mice and sputum human by mass spectrophotometry were analyzed using the Panther database to see their involvement in each of the biological processes. The values were represented by a diagram showing the samples of the animal models after a first exposure to the allergen for the neutrophilic model (**H4.1**) and for the eosinophilic model (**H20.1**), in addition to the last exposure to the allergen for the neutrophilic model (**H4.13**) and the eosinophilic model (**H20.13**). The biological processes obtained in sputum samples from neutrophilic (**NA**) and eosinophilic (**EA**) patients are also shown.

7.2. Assessment of pathway proteins

A more exhaustive analysis was done through Reactome software (265) to distinguish the enriched pathways of the innate and adaptive immune system in which these proteins are involved. The proteins measured in murine BAL or human sputum underwent a statistical hypergeometric distribution test using Reactome software (265) to establish which pathways were overrepresented (enriched). This test produces a probability score for every pathway, which was corrected for false discovery rate (FDR) using the

Benjamani-Hochberg method (266). *p*-values and FDR enriched pathways were selected and represented in a heat map. Pathway analysis showed an enrichment in neutrophil degranulation, complement cascade, post-transcriptional phosphorylation, response to elevated platelet cytosolic Ca2+, antimicrobial peptides, regulation of Insulin-like Growth Factor (RIGF) and glutathione conjugation in all BAL mice analyses regardless of the treatment (**Figure 38**). In human sputum samples, only neutrophil degranulation, complement cascade, antimicrobial peptides and Fc gamma receptor (FcGR)-dependent phagocytosis showed differences in both the eosinophilic and neutrophilic asthma (**Figure 39**).

The murine BAL analyses showed major variability in the proteins' role in the different pathways. Comparing the initial stage of asthma in neutrophilic and eosinophilic mice (H4.1 and H20.1) with the final ones (H4.13 and H20.13). We observed that the proteins related to the pathways of surfactant metabolism, binding and uptake of ligands by scavenger receptors (RSCV), FCGR activation and calnexin/calreticulin cycle did not shown differences on their FDR at the initial instillations compared to the final ones. A deeper analysis of the extracellular matrix degradation pathway showed a greater difference in the neutrophilic model at H4.1 compared to H4.13. By contrast, in the eosinophilic model, no differences were observed at H20.1, while a minor FDR was observed at H20.13. Another pathway to highlight is the CD22-mediated B-cell receptor (BCR) regulation, which presents a major difference in the eosinophilic model independent of the dose with respect to the neutrophilic model (**Figure 38**).

The results from human sputum showed their main differences in the pathways related to degradation of the extracellular matrix, regulation of TLR, and HSP90 chaperone in RSHR, which were more enriched in eosinophilic asthma. By contrast, the CD22-mediated BCR regulation and FcεRI signaling were more enriched in neutrophilic asthma (**Figure 39**).

These results show that although the proteins present in the different experimental asthma-inducing regimes may participate in the same pathways or present the same significance respect to the database, the detected proteins involved within each pathway may differ between models. To evaluate this, all the proteins involved in each pathway were selected using the Reactome software (**see Annexed Table 1 and 2**). The comparisons among the different proteins involved at the initial and final instillations (1 or 13) and within HDM sources (H4 or H20) were made using Venn diagrams (267). The

proteins from the human sputum samples were also compared to pinpoint those exclusive for neutrophilic and eosinophilic asthma (see Section 7.3 below).

To match the pathways involved in the development of a neutrophilic or eosinophilic model, exclusive proteins from each group of mice and type of human asthma were compared, discarding the differing ones that could be conditioned to the species or another type of pathway not relevant to the development of asthma. Finally, proteins common to humans and mice were selected. A comparison between the proteins presents in human sputum with those in murine BAL associated with the initial and the final instillations was performed, obtaining the proteins shown in the table (**Annexed Table 3**).

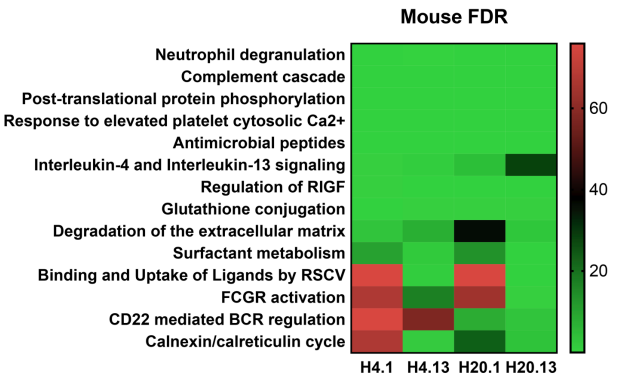

	H4.1		H20.1		H4.13		H20.13	
Pathway	FDR	p-value	FDR	p-value	FDR	p-value	FDR	p-value
Neutrophil degranulation	1,58E-11	1.11E-16	1,53E-11	1.11E-16	8,09E-12	1.11E-16	1,67E-11	1.11E-16
Complement cascade	1,47E-02	6.19E-7	8,89E-04	3.88E-8	2,77E-06	7.62E-11	1,97E-07	4.34E-12
Post-translational protein phosphorylation	1,05E-03	2.95E-8	1,65E-05	4.8E-10	3,02E-06	1.24E-10	8,08E-06	2.69E-10
Response to elevated platelet cytosolic Ca2+	1,32E-07	2.78E-12	5,65E-09	1.23E-13	4,20E-10	8.64E-14	2,12E-05	8.48E-10
Antimicrobial peptides	3,20E-03	1.8E-6	5,07E-02	3.34E-6	1,11E-01	7.63E-6	1,32E-01	1.32E-5
Interleukin-4 and Interleukin-13 signaling	2,58E-01	2.37E-5	4,02E+00	6.49E-4	9,53E-01	1.21E-4	2,82E+01	1.66E-2
Regulation of RIGF	2,41E-01	2.04E-5	4,68E-03	2.72E-7	3,13E-03	1.51E-7	5,03E-03	3.33E-7
Glutathione conjugation	8,20E-02	1.44E-4	2,88E-01	2.3E-5	4,48E-01	4,00E-05	4,62E-01	5.8E-5
Degradation of the extracellular matrix	2,67E+00	6.5E-4	3,64E+01	4.04E-2	7,40E+00	1.38E-1	2,10E+00	9.14E-3
Surfactant metabolism	1,05E+01	3.88E-3	1,36E+01	5.08E-3	1,54E+00	2.24E-4	7,15E-02	6.51E-6
Binding and Uptake of Ligands by RSCV	7,59E+01	7.59E-1	7,59E+01	7.59E-1	9,53E-01	1.25E-4	2,76E-02	2.03E-6
FCGR activation	6,69E+01	3.74E-1	6,41E+01	1.63E-1	1,72E+01	4.53E-3	3,79E-01	4.31E-5
CD22 mediated BCR regulation	7,59E+01	7.59E-1	7,80E+00	7.8E-1	5,73E+01	2.6E-2	2,72E+00	4.39E-4
Calnexin/calreticulin cycle	6,69E+01	9.64E-2	2,33E+01	1.88E-2	1,50E+00	3.43E-3	3,14E+00	5.24E-4

Figure 38. Variation in pathway involvement between the beginning and the end of development of the neutrophilic or eosinophilic asthmatic mouse model. The different proteins obtained from BAL mice by mass spectrophotometry were analyzed using the Reactome database and the different pathways with the greatest significance were represented by false discovery rate (FDR) using a heat map where the mice exposed to a first dose of the allergen of the neutrophilic model (**H4.1**) and the eosinophilic model (**H20.1**), were compared to the last dose of exposure after 4 weeks of treatment of the neutrophilic model (**H4.13**) and the eosinophilic model (**H20.13**).

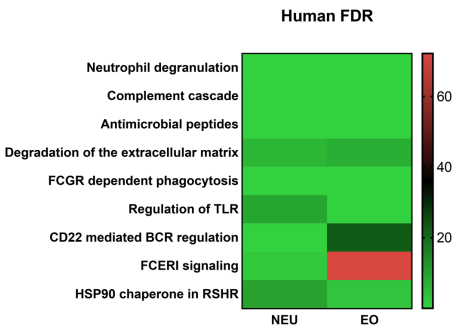

	Neutrophilic		Eosinophilic	
Pathway	FDR	p-value	FDR	p-value
Neutrophil degranulation	3,20E-13	1.11E-16	2,38E-12	1.11E-16
Complement cascade	4,80E-13	2.22E-16	2,38E-12	1.11E-16
Antimicrobial peptides	1,37E-04	1.83E-8	7,54E-05	7.54E-9
Degradation of the extracellular matrix	5,78E+00	3.04E-3	7,18E+00	2.89E-3
FCGR dependent phagocytosis	5,07E-05	6.51E-9	1,13E-02	2.51E-6
Regulation of TLR	8,76E+00	5.15E-3	7,34E-03	1.53E-6
CD22 mediated BCR regulation	7,87E-03	1.33E-6	2,27E+01	1.14E-2
FCERI signaling	1,66E+00	6.63E-4	7,22E+01	2.11E-1
HSP90 chaperone in RSHR	9,53E+00	6.35E-3	2,76E+00	9.85E-4

Figure 39. Variation in pathway participation between neutrophilic and eosinophilic patients. The different proteins obtained from sputum patients by mass spectrophotometry were analyzed using the Reactome database and the different pathways with the greatest significance were represented by false discovery rate (FDR) using a heat map where a neutrophilic asthmatic patient (**NA**) is compared with another eosinophilic (**EA**).

7.3. Diagnostic markers for asthma phenotypes

In order to identify hallmarks for neutrophilic or eosinophilic asthma that improve diagnosing one type of inflammation or another, those proteins exclusive for humans and absent in mice were classified for each type of asthma. The resulting proteins were analyzed through STRING (268) in order to infer the interactions among them, and to study their implication in the development of the disease.

Table 5. Neutrophilic asthma

GEN	PROTEIN NAME	FUNCTION
CD63	CD63 antigen	-Functions as cell surface receptor for TIMP1 and plays a role in the activation of cellular signaling cascades. -Promotes cell survival, reorganization of the actin cytoskeleton, cell adhesion, spreading and migration. -Plays a role in VEGFA signaling. - Index of basophil degranulation (271). -CD63 has been identified as an activation marker for basophils and mast cells (272). - CD63 expression is rapidly upregulated following allergen challenge (273).
CD9	CD9 antigen	-Upregulated during allergy season (274). -Degranulation of human eosinophils as well as increased survival (275).
CTSD	Cathepsin D	Cathepsins play a role in ECM remodeling, with cathepsin D, H and K being associated with lung diseases (276).
CTSG	Cathepsin G	Has antibacterial activity against the Gram-negative bacterium cathepsin G (CG) is a novel key player in chronic lung inflammation, neutrophils secrete cathepsin G (278, 279)
EEF1A1	Elongation factor 1-alpha 1	With PARP1 and TXK, forms a complex that acts as a T helper 1 (Th1) cell-specific transcription factor and binds the promoter of IFN-gamma to directly regulate its transcription, and is thus involved importantly in Th1 cytokine production.
FCN1	Ficolin-1	Extracellular lectin functioning as a pattern-recognition receptor in innate immunity. Binds the sugar moieties of pathogen-associated molecular patterns (PAMPs) displayed on microbes and activates the lectin pathway of the complement system. May also activate monocytes through a G protein-coupled receptor, FFAR2, inducing the secretion of interleukin-8/IL-8. -Inside of gelatinase granules secreted by neutrophils (280, 282).
GRB2	Growth factor receptor-bound protein 2	IL-5 activates a signal transduction pathway utilizing the adapter proteins Shc and Grb2 in the human eosinophil (283).
ITGAM	Integrin alpha-M	-Integrin ITGAM/ITGB2 is implicated in various adhesive interactions of monocytes, macrophages and granulocytes as well as in mediating the uptake of complement-coated particles. It is identical with CR-3, the receptor for the iC3b fragment of the third complement component. -Regulates neutrophil migration. In association with beta subunit ITGB2/CD18.

LGALS3	Galectin-3	-Galactose-specific lectin which binds IgE. May mediate with the alpha-3, beta-1 integrin the stimulation by CSPG4 of endothelial cells migration. Together with DMBT1, required for terminal differentiation of columnar epithelial cells during early embryogenesis. -In the nucleus: acts as a pre-mRNA splicing factor. Involved in acute inflammatory responses including neutrophil activation and adhesion, chemoattraction of monocytes macrophages, opsonization of apoptotic neutrophils, and activation of mast cells. - Act as neutrophil chemoattractant (284). - Regulates the Th1/Th2 response (285).
LTA4H	Leukotriene A-4 hydrolase	-Epoxide hydrolase that catalyzes the final step in the biosynthesis of the proinflammatory mediator leukotriene B4. Has also aminopeptidase activity. -Produced by eosinophils in severe asthma. -LTA4H catalyzes the final critical step in the biosynthesis of the proinflammatory compound LTB4. -Recently identified as a key signal-relay molecule during neutrophil chemotaxis and swarming (286, 287).
PSMA1, 2, 4, 7 PSMB1, 2		The complement activation modulates key adoptive immune responses, which stimulates and/or suppress pulmonary allergic reactions during airway tissue remodeling (288).
PYCARD	Apoptosis-associated speck-like protein containing a CARD	Functions as key mediator in apoptosis and inflammation CARD-containing signaling molecules within the inflammasome (289).
RHOA	Transforming protein RhoA	-Involved in a microtubule-dependent signal that is required for the myosin contractile ring formation during cell cycle cytokinesis. -Key protein in the contraction of smooth muscles, including airway smooth muscles (290, 291).
TAGLN2	Transgelin-2	TG2 is an abundant protein in smooth muscle cells and participates in muscle relaxation (292).
TTN	Titin	Key component in the assembly and functioning of vertebrate striated muscles.

Table 6. Eosinophilic asthma

GEN	PROTEIN NAME	FUNCTION
ELANE	Neutrophil elastase	-Modifies the functions of natural killer cells, monocytes and granulocytes. Inhibits C5a-dependent neutrophil enzyme release and chemotaxis. - Neutrophils capture allergens and release NE and further promote eosinophil infiltration and amplify type 2 immune responses to initiate asthmatic inflammation (293).
EPX	Eosinophil peroxidase	-Mediates tyrosine nitration of secondary granule proteins in mature resting eosinophils. -Causes histamine release and degranulation from mast cells; inactivates leukotrienes, damages respiratory epithelium, provokes bronchospasm in primates. Generates reactive oxidants and free radicals (294).

FGB	Fibrinogen beta chain	-Functions during the early stages of wound repair to stabilize the lesion and guide cell migration during re-epithelialization. -Fibrinogen is a specific trigger for cytolytic eosinophil degranulation (295).
FN1	Fibronectin type III domain containing	Fibronectin is a mechanically sensitive protein which is organized in the extracellular matrix as a network of interacting fibrils (296).
MMP9	Matrix metalloproteinase-9	-May play an essential role in local proteolysis of the extracellular matrix and in leukocyte migration. -Induce ASM hypertrophy and collagen deposition under the respiratory epithelium, which leads to the airway tissue remodeling and repair of lower airways (297, 298).
MPO	Myeloperoxidase;	Part of the host defense system of polymorphonuclear leukocytes markers of neutrophil activation. (299)
PRG2	Bone marrow proteoglycan *Proteoglycan 3, pro eosinophil major basic protein 2*	Induce non-cytolytic histamine release from human basophils. Involved in antiparasitic defense mechanisms and immune hypersensitivity reactions
PRG3	Proteoglycan 3	Assesses similar cytotoxic and cytostimulatory activities to PRG2/MBP. In vitro, stimulates neutrophil superoxide production and IL8 release, and histamine and leukotriene C4 release from basophils.
VTN	Vitronectin	Multifunctional glycoprotein involved in coagulation, inhibition of the formation of the membrane attack complex (MAC), cell adhesion and migration, wound healing, and tissue remodeling. (301).

7.4. Asthma therapeutic targets based on mouse models

Once the proteins common to humans and mice were identified, a functional exploration was carried out with STRING to infer the interactions among them.

A comparison between human neutrophilic asthma and the H4 neutrophilic mouse model at its initial (1st) and final (13th) instillations showed more proteins in common in the first instillation (20 proteins) than in the final one (10 proteins). As shown in Figure 40, proteins related to the recruitment or function of neutrophils, neutrophil elastase (*ELANE*), the matrix metalloproteinase-9 (*MMP9*), myeloperoxidase (*MPO*), and protein S100-AB (*S100AB*), the latter also involved in the regulation of inflammatory processes and immune responses, stand out from the rest in the 1st instillation. Others are also involved in the innate immune system, such as peptidoglycan recognition protein 1 (*PGLYRP1*). Proteins related to wound repair and cell migration guiding during re-epithelization also stand out, such as the fibrinogen beta and gamma chains (*FGB* and

FGG, respectively). We also observed proteins involved in the adaptive immune system and tissue remodeling, with a role in the Th2 response and inflammation mediated by IL-13, regulating sensitization to allergens such as chitinase-3-like protein (*CHIL3L1*). We also identified proteins involved in angiogenesis such as tissue factor (*TF*) and plasma protease C1 inhibitor (*SERPING1*), a regulator of vascular permeabilization.

Among the common proteins associated with the 13th murine instillation, we also found the peptidoglycan recognition protein 1 (*PGLYRP1*), S100-AB protein (*S100AB*), and the plasma protease C1 inhibitor (*SERPING1*). In this case, the presence of the glucose-6-phosphate isomerase (*GPI*), responsible for stimulating the motility of endothelial cells as an angiogenic factor, is remarkable.

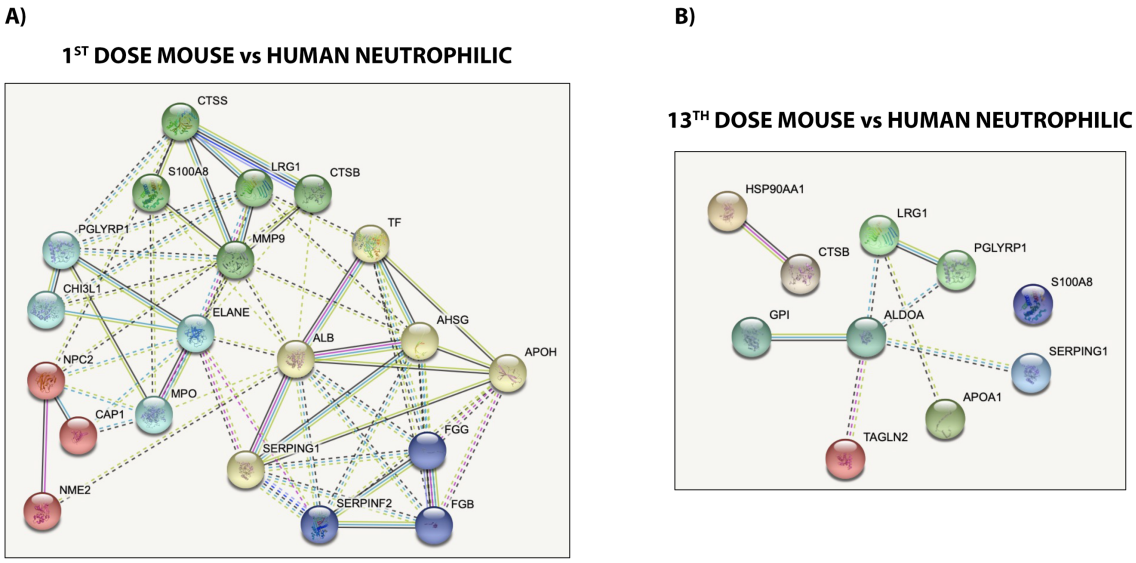

Figure 40. Variation between the proteins involved between an earlier stage and a later stage in the development of neutrophilic asthma. Once the proteins common to human and mouse exclusive of neutrophilic inflammation were extracted, they were interconnected by STRING for the proteins present in the first dose for the mice common to humans **A)** and for the proteins present in the last dose for the mice common to humans **B)**.

In the case of the proteins common to human eosinophilic asthma and the H20 eosinophilic model, we did not find any exclusive proteins related to the eosinophils. However, at its initial stage, we found some proteins related to the innate immune system such as BPI fold-containing family B member 1 (*BPIFB1*) and the complement components C5 and C6 (*C5, C6*). We also found histidine-rich glycoprotein (*HRG*), involved in the regulation of immune complexes, pathogen clearance, and cell chemotaxis. Another protein also involved in cell migration, during re-epithelialization in this case, is the fibrinogen alpha chain (*FGA*). Other proteins observed to be common to human eosinophilic asthma were the elongation factor 1-alpha 1 (*EEF1A1*), responsible for forming a complex that acts as a promoter in the Th1 response and IFN-γ production. Also noteworthy is kininogen-1 (*KNG1*), involved in smooth muscle contraction and a

mediator of inflammation, and alpha-1-acid glycoprotein 1 (*ORM1*), responsible for modulating the immune system during the acute reaction phase.

As already observed in the H4 neutrophilic model, we also saw protein shares between the initial and final instillations in the eosinophilic model, such as the fibrinogen alpha chain (*FGA*), the complement components C5 and C6 (*C6*), kininogen-1 (*KNG1*), alpha-1-acid glycoprotein 1 (*ORM1*), and Histidine-rich glycoprotein (*HRG*). Proteins exclusive to final instillation were also found, such as the inter-alpha-trypsin inhibitor heavy chain H4 (*ITIH4*), related to the type-II acute-phase protein involved in inflammatory responses to trauma, and cathepsin D (*CTSD*), involved in extracellular matrix remodeling.

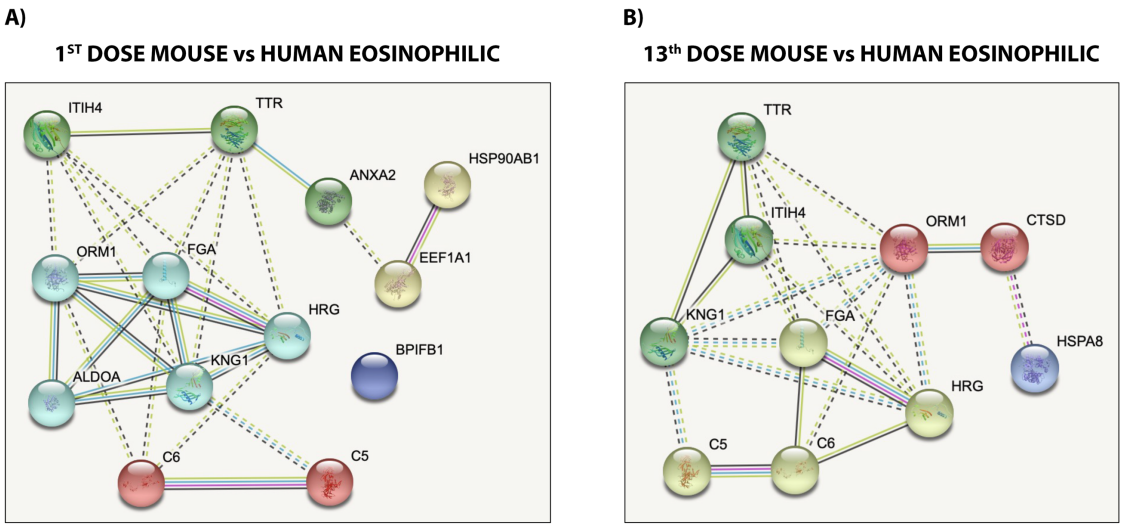

Figure 41. Variation between the proteins involved between an earlier stage and a later stage in the development of eosinophilic asthma. Once the proteins common to human and mouse exclusive of eosinophilic inflammation were extracted, they were interconnected by STRING for the proteins present in the first dose for the mice common to humans **A)** and for the proteins present in the last dose for the mice common to humans **B)**.

DISCUSSION

Animal models of allergic airway inflammation are helpful tools to study the pathogenesis of asthma and potential therapeutic interventions. Despite the long use of experimental asthma models and the undoubtful validity of much information harvested from them, some of which paved the way for the development of new approved therapies, animal asthma models have always been limited by factors that made them distant from the pathogenesis and physiopathology of the actual disease. The large variability of clinical asthma traits and their combinations (originating the so-called asthma "phenotypes", with repeatedly inconclusive classification attempts) and their underlying disease mechanisms ("endotypes", with no better comprehensive outcome than for the "phenotypes" so far) adds major challenges to animal asthma modeling. All such a mixture of successes and pitfalls converges in the outstanding need for *moldable models* that get closer to the human disease and allow reflecting its natural complexity and varying outcomes.

Aside from occupational asthma models based on low-molecular weight haptens (32, 174-176), most asthma models have been based on "allergic" sensitization. Most models employ rodents, largely mice, which do not develop any known asthma-like disease naturally. Therefore, the experimental disease must be induced, which brings about the modeling toolbox with all of its virtues and problems. The factors that have at once been tools and limitations for antigen sensitization-induced asthma modeling fall really into a handful of main aspects. One is the rodent strain employed, something that has both favored and hindered the development of models through the "trick" of largely employing inbred strains with a constitutively Th2-biased immune system. The C57BL/6J mouse strain, our choice for the work presented here, has possibly the poorest susceptibility to allergen sensitization compared with its usual asthma modeling counterpart, the BALB/c mouse, which bears such Th2 immune response deviation (177-179). In classical approaches employing OVA as an allergen for sensitization and airway challenge, the intensity of the modeled asthma features such as goblet cell hyperplasia, airway hyperresponsiveness, BAL Th2 cytokines, and serum OVA-specific IgE concentration was significantly lower in C57BL76J mice than in BALB/c (166, 180, 181). Another aspect is the antigen source for allergic sensitization and its delivery route. A great deal of information on allergic airway inflammation has been generated from murine experimental systems using OVA, not an aeroallergen causing airway allergic disease in humans, as a surrogate allergen. However, inhaled OVA elicit tolerance, which led to devising OVA-driven asthma models based on procedures very distant from human allergic sensitization, *i.e.*, systemic delivery of OVA along with strong adjuvants (165).

The subsequent trend has been shifting towards aeroallergen-based models, mostly HDM as a common source of indoor allergens, delivered directly into the rodent airways, usually by *i.n*. instillation. However, despite how obvious this methodological principle is, relatively little information is available regarding the airway immune inflammatory responses to HDM in murine systems. The main HDM allergen antigen, namely Derp1, is a cysteine and serine protease capable of modulating both the adaptive and innate immune system (182-184). Studies in an acute murine model of airway inflammation demonstrated that the proteolytic activity of Derp1 enhances its allergenicity by degrading the airway epithelial barrier, as it was found to disrupt tight junctions and increase permeability between epithelial cells (185, 186). Another major allergen present in HDM is Derp2, a molecule capable of establishing a specific IgE-response with eosinophilic lung inflammation (36, 186). As a result of the knowledge on HDM allergens, some studies employed single isolated allergens or their epitopes but this reductionist approach led to some paradox results; *e.g.*, isolated Derp1 is known to elicit inhalational tolerance (7). Conversely, quite limited work has been done in systems using whole mite extracts. Although whole mite extracts are complex from an immunological perspective, they are ultimately more representative of real-world aeroallergen exposure. Thus, for the work presented here, we deemed it important to study the responses to whole HDM as closer to real-world methodology. One more factor is protocol variation since the distinct allergic airway inflammation models available to date have used a wide range of doses and exposition frequency (6), which, combined with the previous aspects, has resulted in differently enhanced asthma features and varying degrees of airway inflammation, hyperresponsiveness, and remodeling. Finally, whereas the hapten-induced models of occupational asthma are neutrophilic (31, 32, 174, 175), the available allergen-induced, Th2-driven models are polarized towards eosinophilic inflammation leaving the true airway inflammometric scope seen in clinical practice almost entirely underrepresented.

The global aim of this work has been to expand the murine asthma model portfolio into innovative variants adhering to close-to-real pathogenetic procedures and allowing to represent different airway inflammatory profiles as seen in clinical practice, with their associated cardinal disease traits, so as to provide an extended set of tools for the comparative investigation of disease mechanisms and, eventually, the identification of novel therapeutic targets. Our first move in this direction was to choose the mouse strain portrayed as most unfavorable to develop allergic airway inflammatory disease, *i.e.*, the C57BL/6 mouse (187). As an overall itinerary over the work done, of which further discussion follows, we first started by dose-finding experiments combined with allergen

exposure length testing. As most relevant outcomes, we found evidence of a T-cell driven adaptive immune response in the High-dose, 4-week (4W) setup as per an increased presence of $CD3^+CD4^+$ T cells and the production of HDM-specific IgE, along with mixed eosinophilic and neutrophilic inflammatory infiltrates in a balanced fashion, and airway hyperresponsiveness to MCh. Despite this consistent response, airway remodeling did not develop in these animals. In the 6-week (6W) setup, the T-cell response declined along with an abrogation of the airway hyperresponsiveness and the eosinophilic infiltrates, with persisting neutrophils, all suggesting the development of immunoregulatory mechanisms acting on the Th2 arm. The synchrony between the early presence of eosinophils and airway hyperresponsiveness, and the late abrogation of both together despite continuing neutrophilic infiltration, is remarkable. From the data of these experiments, we chose the High-dose 4W protocol scheme for further development. Aiming at representing airway remodeling, we performed the next sets of experiments with the aim of boosting the responses by delivering the HDM extract with added SEB and α-Galcer. SEB is a naturally occurring superantigen known to be involved in human allergic sensitization. α-Galcer is an NKT-cell stimulator with which we intended a nonspecific reinforcement of innate immunity in this model. The addition of SEB, but not α-Galcer, succeeded to elicit airway remodeling. However, both SEB and α-Galcer failed to originate consistent models because the resulting inflammatory profiles lacked clear translation to asthma patterns and, importantly, because they both inhibited airway hyperresponsiveness. We next questioned whether the HDM antigen preservation status would play some role in modulating sensitization and its outcomes. In usual laboratory procedures, lyophilized, standardized HDM extract is reconstituted and kept at 4-8°C, and this vial is the source for successive *i.n*. installations through a complete protocol. Despite being whole HDM extract, this method adds one more deviation from real-world conditions since the environmental HDM fecal pellets, the source of allergens in actual disease, may contain antigens in different states of degradation at room temperature. Our original High-dose 4W scheme following HDM extract reconstitution as per manufacturer's indications led to mixed granulocytic inflammation. However, our Western blot data showed progressive degradation of the DerP1 and DerP2 proteins from the midpoint of the *i.n*. instillations schedule. By controlling antigen preservation in the reconstituted HDM, the use of partially degraded allergens (H4 model) induced dominant neutrophilic inflammation, whereas preserved antigens (H20 model) elicited dominant eosinophilic inflammation, being the neutrophilic versus eosinophilic shift significant between these two variants. All three models (bare High-dose 4W, H4, and H20) showed evidence of a $CD4^+$ T cell-driven adaptive immune response with Th2 functionality leading to HDM-specific IgE production. Although all of

these models showed both neutrophils and eosinophils in their inflammatory profile, we are referring to the H4 and H20 models as “neutrophilic” and “eosinophilic”, respectively, based on the significant, clear cutoff dominance of each effector cell. None of these models represents “pure" neutrophilic asthma, which is nonatopic in most cases and of low relative prevalence (188, 189). Yet a large proportion of the asthmatics termed as “neutrophilic” or “eosinophilic” show some mixed increase of the counterpart granulocyte despite the dominance that guides their mainstream inflammometric classification (190). Therefore, our model diversion encompasses a wide representation of inflammometric profiles seen in real-world clinical practice, from balanced eosinophilic-neutrophilic, to dominant neutrophilic with concomitant allergic sensitization, and the more typical atopy-driven eosinophilic. As for associated cardinal asthma traits linking to clinical features, all three models developed airway hyperresponsiveness, yet airway remodeling was dissociated in its components. It is of particular interest that the eosinophilic-dominant H20 model presented with prominent mucoid mass (a quantitative composite of goblet cell hyperplasia and functional hypertrophy) and significantly greater airway contractile tissue mass, whereas the neutrophilic-dominant H4 developed subepithelial fibrosis that extended to the adventitia through the *lamina propria*. These experimental outcomes match clinical observations linking neutrophilic airway inflammation with a fibrogenic airway remodeling pattern (191, 192) and eosinophilic inflammation with airway mucus plugging and increased airway smooth muscle (65, 193). In summary, we ended with respective models of neutrophilic and eosinophilic asthma, both with airway hyperresponsiveness as an in vivo enveloping outcome, showing varying inflammatory and airway remodeling profiles that reasonably match clinically identifiable asthma “phenotypes”. The final research step in this work was to employ these models for comparative proteomics in murine BAL and human induced sputum.

In our initial experiments aimed at dose and time finding, we carried out 7.5 μg and 15 μg HDM instillations 3 days a week for 4 or 6 weeks. Acute models of allergic airway inflammation, normally induced in less than 3 weeks, often manifest the AHR and airway inflammation features but not remodeling (165). Although the observation of some aspects of airway remodeling such as goblet cell hyperplasia has been reported in a 2-week model (194), airway remodeling with increased collagen deposition rarely occurs with an allergen exposure of less than 5 to 12 weeks, which requires a significant investment in time and resources (6, 171, 195). The High 4W model chosen for further development showed combined eosinophilic and neutrophilic inflammation along with a concordant, mixed BAL cytokine profile with increased IL-4 and IL-17A, and presented with airway hyperresponsiveness. Despite these features, we did not observe any signs

of airway remodeling. We did not pursue laborious and costly quantitative morphology because, in our experience, quantitative morphology of airway remodeling is unlikely to yield relevant results, of biological significance and with meaningful clinical translation, in the absence of obvious changes visible upon qualitative histopathological examination. Previous studies have shown that animals must be exposed to the allergen for at least 5 weeks to develop airway remodeling (6, 171, 195). Furthermore, the C25BL/6 mouse is the strain less prompted to develop airway remodeling (187). In our long, High and Low-dose 6W models, there was also absence of remodeling, accompanied by a decline of granulocyte infiltration and an abrogation of airway hyperresponsiveness. Therefore, the absence of airway remodeling caused by the sole exposure to HDM was not an issue related to the length of exposure.

The mechanisms originating airway remodeling have been largely attributed to Th2 responses and the associated inflammatory infiltrations by eosinophils (42). Innate immunity also has a relevant role in the development of asthma (33, 34). It is likely involved in airway remodeling as well, although the data are still scarce due to the recent evolvement of this field. The failure of the High 4W model to develop airway remodeling in response to HDM alone brought up next research questions on whether the use of adjuvants would enhance this asthma feature and how the inflammatory profile would behave. Our point here was to employ inhaled adjuvants along with the HDM extract since naturally acquired allergic sensitization is likely aided by the presence of molecules other than the allergens that act as adjuvants (196-198). For this purpose, we developed respective sets of experiments with SEB and α-Galcer.

SEB, the *S. aureus* enterotoxin B, is an enhancer of chronic airway inflammation in murine experimental allergic asthma and is postulated to also play such a role in humans (160, 199, 200). In mice, SEB breaks tolerance to inhaled and contact allergens due to its capacity for polyclonal T-cell stimulation by acting as a superantigen (160, 199, 201). It induces the production of proinflammatory and Th2-polarizing cytokines such as IL-4, IL-5, IL13 (201, 202). Little is known about its interaction with the innate immune system. However, SEB increases the levels of eotaxin, a potent chemoattractant and survival factor for eosinophils (202). In our experiments, the addition of SEB to HDM succeeded to induce airway remodeling on the basis of the High 4W model scheme, accompanied by eosinophilic inflammation. However, the evidence of a $CD4^+$ T-cell mediated response seen in bare HDM-driven High 4W model was lost, and also airway hyperresponsiveness since there was a weak, nonsignificant response to MCh. It is unclear why the addition

of SEB elicited airway remodeling while the model got otherwise weakened in other essential allergic asthma traits.

α-Galcer, α-galactosylceramide, an α-galactosylated sphingolipid originally isolated from the sea sponge *Agelas mauritanius* (203), has no physiological role but provides utility in innate immune system research. This glycolipid is presented by CD1d, a non-classical MHC-I molecule expressed by NKT cells, which, although arguably, may play some assistive role in the development of allergic asthma (204-206). α-Galcer induces NKT proliferation and secretion of IFN-γ and IL-4 (207), thus supporting the induction of innate and adaptive immunity (166). These cytokines, respectively related to the Th1 and Th2 responses, together with the association of NKT and airway neutrophils (208), made α-Galcer an attractive choice as a potential adjuvant to model neutrophilic asthma. Since neutrophilic asthma is related to a Th2-Low response, the induction of mixed Th1/Th2 profiles by α-Galcer in combination with the Th17 activation observed in our High 4W model led as to study the effect of combined HDM and α-Galcer on the development of airway remodeling. However, the results did not meet our expectations. Consistent with the known role of α-Galcer in adaptive immunity, we observed a strong increase in $CD4^+$ and $CD8^+$ T cells, and B cells. Discordant with this response, granulocyte infiltration was absent, affecting both neutrophils and eosinophils. Moreover, airway hyperresponsiveness was fully inhibited to control level and the animals did not develop airway remodeling. The reasons for this wide inhibitory effect associated with α-Galcer are unclear and amenable to a separate study.

The failure of the SEB and α-Galcer-assisted modeling to provide plausible choices of inflammatory patterns associated with both airway hyperresponsiveness and remodeling, as required asthma traits for model validity, brought us back to the drawing board. In search of clues to better understand the initial High 4W model, and optimize its outcomes, we performed exploratory kinetics of the cellular inflammatory profiles and BAL cytokines across the successive HDM instillations comprising, respectively, 13 cutoff analysis points. This was a labour-intensive aim that, due to its exploratory nature and cost, was limited to HDM-instilled series in the absence of a control sequence, and to a n=3 size per cutoff point. The mixed eosinophilic-neutrophilic inflammatory profile originally seen in this model was an end-point outcome following the complete course of *i.n*. instillations. Our aim at this point was to profile possible variations of the inflammatory profile through the course of the experimental disease. The relationship between eosinophilia and airway remodeling has been well defined (193, 209) but the direct effect of neutrophils is more controversial (106). The inflammatory kinetics sequence showed

early peaks of BAL IFN-γ and IL-4 and a late dominance of IL-17 along with an overall steady progression of $CD4^+$ and $CD8^+$ T cells, and B cells. Immunoglobulin production occurred late in the model, involving all classes analyzed (IgM, IgG, IgA, and IgE). These curves are coherent with an early activation of a mixed Th1/Th2 response that then rolls through the model, along with the addition of a later Th17 response. Whereas the interpretation is uneasy, the overall data suggest that, in the non-Th2-biased C57BL/6 mouse, repeated HDM inhalational exposure elicits a complex, mixed adaptive immune response beyond a Th2 response with HDM-specific IgE production. The associated granulocyte response had oscillations through the model with some percentual shifts of eosinophil versus neutrophil dominance, to end with the mixed profile originally seen. Such oscillations may link the importance of the time point where induced sputum samples are taken for inflammometrics in human asthma (210). In those centers enabled for induced sputum processing in clinical practice, a patient's inflammometric classification is often based on a single sampling point; two at the most in some cases. Serial sampling is unusual. Despite the recent trend to class “eosinophilic” asthma as per absolute blood eosinophil counts, particularly for the indication of anti-IL-5 or anti-IL5Rα biologics, induced sputum remains the unique noninvasive procedure that allows diagnosing neutrophilic asthma, cases of eosinophilic asthma with uncorrelated blood eosinophil counts, and mixed inflammatory profiles. Our experimental data suggest that the immune response to aeroallergens may oscillate as allergen exposure persists and varying effector and counterregulatory pathways get involved, and this intra-subject variability may be largely underrepresented in usual clinical practice.

Since the stability and conformational status of antigens may vary over time as the allergens age under environmental conditions, we probed the stability of DerP1 and DerP2 as the reconstituted HDM extract aged through the 4W instillations protocol. The Western blot analysis demonstrated nonlinear degradation of both DerP1 and DerP2; therefore, in the High 4W model, the mice received allergen antigens undergoing conformational modifications and a changing effective dose particularly through the second half of the 4W instillation protocol. To analyze the effect of inhaled exposure to degrading versus preserved HDM antigens, we developed the models termed H20 and H4. Both models were based on the High 4W protocol. In the H20 model, the HDM extract was preserved at -20ºC from its reconstitution. In the H4 model, the reconstituted HDM extract was kept at 4ºC for 12 days and then frozen-preserved at -20ºC. As summarized earlier, the H20 and H4 outcomes diverged widely. The H20 model led to eosinophilic inflammatory infiltration with increased mucoid and airway contractile tissue mass, whereas the H4 model elicited neutrophilic infiltration with a fibrogenic

airway remodeling pattern. The analyses of the cellular inflammatory infiltrates, plus cytokine and immunoglobulin concentrations in BAL, suggest that both models, despite their diverging granulocyte inflammatory profile, were HDM sensitization-driven. The development of an adaptive immune response directed towards IgE production is reflected by the finding, in both models, of $CD4^+$ T-cell and $CD19^+$ B-cell infiltration, large increases of total BAL IgE, and HDM-specific IgE. However, beyond this congruent IgE response pathway, the data suggest complex involvement of further pathways that are either common or diverge. In both models, total BAL IgG was significantly increased as an expected part of the response (211-213) and HDM-specific BAL IgA was present. The detection of the latter was surprising since there is a lack of a demonstrated pathway linking specific IgA production with IgE-producing Th2 responses. Besides, the BAL cytokine profile was quite different. The H4 model showed significantly increased IFN-γ, IL-4, IL-13, and IL-17A. The joint production of IFN-γ, IL-4, and IL-13 suggests that the Th2 pathway leading to IgE production is mixed with a Th1 component, as demonstrated in some asthmatics (214-216). The presence of IL-17A is consistent with the activation of Th17 cells and the dominant neutrophilic infiltration in this model (67, 79, 216, 217). On the contrary, the cytokine profile of the H20 model resulted undetermined, yet this unclear outcome for the BAL cytokines gets clarified in the kinetics study (see below). The H20 model reflected otherwise the traits of atopic asthma including the evidence of a Th2 response leading to specific IgE production, the eosinophilic infiltration, and the airway remodeling pattern. Together, the H4 and H20 models encompass a spectrum of possibilities for translational research wider than the available allergen-driven models. A relevant proportion of subjects with severe asthma show mixed inflammatory patterns involving both eosinophils and neutrophils (11, 12), and approximately 15% of asthmatics with such mixed profiles in sputum are resistant to corticosteroids (128).

The H20 and H4 model outcomes just discussed are endpoints measured after the last *i.n*. instillation. However, the oscillations observed in the exploratory kinetics previously performed in the basic High 4W model led us to undertake the same type of serial analyses in the H20 and H4 models. Whereas it has been proposed that the validity of eosinophil numbers in asthma is limited by single time-point sampling within variable factors, some lines of evidence suggest otherwise. Some studies have shown that eosinophilic inflammation increases with disease severity, but other reports disagree (218-221). In one study, about 50% of patients with severe asthma that had previously been identified as non-eosinophilic had eosinophilic inflammation in the distal lung (222). Previously published findings show that most animal models exhibit peak eosinophilia after 3 weeks of allergen exposure, followed by a plateau or non-significant increases in

eosinophils after that, up to 7 weeks (171, 223). Therefore, although some controversy appears to exist, factors such as sampling procedure and single time-point sampling may deviate the inflammometric classification of some asthmatics. Our kinetics study in the H20 and H4 models showed a different pattern of the eosinophilic and neutrophilic components across time. The strong eosinophilic infiltration observed in the H20 model had a tendency to a relatively late onset with a steep rise through the second week of *i.n*. instillations and its percentage declined by the last week. The rise of eosinophilic infiltration coincided, approximately, with the first peak of HDM-specific IgE and IgA in BAL. Conversely, the dominant neutrophilic infiltration in the H4 model peaked from the earliest instillations and followed through successive peaks with no end decline. Concordant with the neutrophils and different from the H20 model, the eosinophilic component in the H4 model was present from the first instillations and continued with a wavy pattern that had an approximately flat average. Together, these data suggest that the pathways directing granulocyte infiltration may have been different in the H20 and H4 models. In the H20 model, the eosinophilic infiltration seems dependent on the adaptive immune response leading to HDM-specific IgE production, *i.e*., it matches the pattern of "classical", Th2-driven eosinophilia associated with atopy. By contrast, the mixed neutrophilic-eosinophilic infiltration seen in the H4 model, with neutrophilic dominance, appears attributable to innate immunity in its onset. The data also suggest that a complex adaptive immune response steps in later in the H4 model. Whereas a Th2 pathway leading to IgE production is functional in this model, the kinetics data show an overlapping and sustained Th17 response that accounts in part for the dominant neutrophilia. The strong rise of $CD4^+$ T cells in this model is consistent with the relevance of the adaptive immune mechanisms in this model. It is noteworthy that the concentration of BAL IL-17A rises very early through the initial *i.n*. instillations, suggesting that Th17 activation, although an adaptive immune response pathway, may develop faster than the classical Th2 and Th1 responses. In all, the data suggest that the neutrophilic H4 model is driven by successive, overlapping pathways starting with a direct and significant role of the innate immune system and a subsequent yet early development of a complex adaptive immune response. With regard to the cytokine kinetics in the H20 model, where the end-point measurements were inconclusive, the kinetics show earlier IL-4 and IL-13 peaks, mainly within the first stage of the instillations sequence, consistent with the activation of the Th2 response at this point. The presence of a very early IFN-γ peak, ahead of Th2 activation, has no clear explanation and is noteworthy. In summary, the kinetics of inflammatory cells, cytokines and immunoglobulins show that the models evolve through dynamic changes involving different immunobiological pathways and time windows within them, where particular activation phases may be missed if

measured out of their time intervals. These observations have implications for both experimental modeling and clinical translation. In experimental disease, most animal models are profiled and interpreted as per measurements done at final endpoints where significant facts may be missed. As for the clinical translation, asthma “phenotypes” are often classed according to single or very limited determinations, particularly inflammometric for obvious logistics reasons. Whereas the contribution of such limited determinations to asthma management has still been notable, much information is most likely missed, and this gap most likely originates misunderstood variability and confusion in our understanding of asthma. Should we be able to perform extensive kinetic studies across the years of disease evolution, we would possibly view asthma, and airway inflammatory disease more widely, as physiopathological and clinical traits moving and combining across fuzzy spectra, rather than trying to define closed categorical classes such as “atopic”, “nonatopic”, “eosinophilic”, “non-eosinophilic”, “neutrophilic”, “pauci-inflammatory”, etc.

The previous results are consistent with the relevance of the innate immune system in allergen-driven responses (33, 34). To further explore the mechanisms, involved in these responses, the kinetics study showing the fluctuations of the granulocyte populations was followed by an analysis of cellular phenotypes of the neutrophils and eosinophils. While the concept of granulocyte heterogeneity is not new (224, 225), there is renewed interest in understanding the effector function of neutrophils and eosinophils as proinflammatory or regulatory cells, which may add translational value to stratify patients for specific therapies. The classical characterization of neutrophils and eosinophils and their precursors is based on histological examination of shape, size, nuclear morphology, and granular content, limited by subjective observational factors. Recently, with an expanding marker coverage by flow cytometry and single-cell level sequencing of granulocyte populations, novel phenotypes are now becoming clearer, thus transforming the previously known populations into heterogeneous cells in health and disease (224, 225). Although neutrophils and eosinophils express different sets of granular proteins and play different functional roles in innate immunity, there are also overlaps in their functions, as they both contribute to proinflammatory cascades and tissue remodeling. Some factors that considerably influence the phenotypic and functional plasticity of granulocytes are generated by the tissue microenvironment, in which different inflammatory stimuli are found (217(226).

Ly6G proteins are expressed in a lineage-specific fashion, and their expression is related to stages of differentiation (227). The Ly6G molecule is expressed on neutrophils, while

Ly6C is also expressed in neutrophils, but also on macrophages and eosinophils (228, 229). Although the physiology of most Ly6 proteins is not well understood, the knowledge of their role in neutrophil function is increasing, since Ly6G expression is typically higher in circulating than bone-marrow neutrophils, and higher in cells recruited to inflamed sites, indicating a role in migration (227, 230). While the Ly6G expression does not appear inducible, Ly6C surface markers can be inducible by IFNs response. A potential role of Ly6C in signal transduction establishes roles in neutrophil migration and activation, supporting a proinflammatory role of Ly6C (227).

Neutrophils have been traditionally regarded as proinflammatory innate immune cells, but recent studies demonstrate an important role as immunomodulatory in adaptive immune responses, mainly in T-cell responses (231). This potential of neutrophils was attributed to plasticity of conventional neutrophils and a new suppressive myeloid cell phenotype, named as myeloid-derived suppressor cells (MDSCs) (232). MDSCs represent heterogeneous groups of myeloid cells defined by the surface expression of CD11b and Ly6G (PMN-MDCs, characterized by $Ly6G^{Hi}CD11b^{+}Ly6C^{Int}$) (226, 233, 234). A study showed this MDSCs population as an anti-inflammatory role in a HDM-induced model of airway inflammation (235, 236). Another study also shown neutrophil heterogeneity on spleen after *S.pneumoniae* infection defined an immobilized, immature Ly6G-intermediate ($CD11^{+}Ly6C^{Lo}$) population and a mature Ly6G-high ($CD11b^{Hi}Ly6C^{Hi}$) population of neutrophils that scans the tissue (237). $Ly6G^{Hi}$ $Ly6C^{Hi}$ neutrophils are rapidly recruited to sites of infection, and are responsible for cytokine production and host defense during pulmonary infection with *Legionella pneumophila* (238).
Throughout our kinetics studies, we characterized three subtypes of neutrophils based on the CD11b expression and cell granularity. In addition, were classified two populations based on the level of expression of CD11b together with Ly6C. We also analyzed the fluctuation of the Ly6G intensity. In the case of eosinophils, we analyzed CD11b expression and its coexpression with Ly6C. Furthermore, the size, granularity and intensity of SiglecF in these populations were studied separately. CD11b is essential for the migration of neutrophils into tissues in response to inflammatory stimuli. Previous studies showed that the expression of CD11b by neutrophils is associated with asthma severity and airway neutrophilia (239, 240).

Focusing on eosinophil populations, a study in mice showed that, in the normal lung, there is a resident $SiglecF^{Int}$ eosinophil population with ring-shaped nucleus with a regulatory-homeostatic function. However, during HDM-induced allergy, this population

remains unchanged and a new population is recruited, named inflammatory eosinophils, which are SiglecF^{Hi} and have a segmented nucleus (241, 242).

In our analyses, we found a subpopulation of Ly6G^{+}Ly6C^{Hi}CD11b^{Hi} neutrophils present only in neutrophilic inflammation, while the Ly6G^{+}Ly6C^{+}CD11b^{Lo} population was found in both the H4 and H20 models. It is also worth noting the intensity of Ly6G expression in neutrophils of the H4 model, where we found high intensity at the beginning and at the end of the kinetics series, while it remained fairly constant in the H20 model. We observed that the populations fluctuate throughout the kinetics of the asthmatic model, highlighting the subpopulation of Ly6G^{+}CD11b^{Hi}SSC^{Lo} neutrophils at the beginning and at the end of the kinetics. As for CD11b expression in eosinophils, no relevant changes seemed obvious between both models, yet we can still classify populations with lower and higher expression, respectively. By analyzing Ly6C in the eosinophils, we observed how, in the H20 model, it increases to its maximum value in the first stage of the disease, then having a slight peak in the second stage, while in the H4 model it presents an initial peak and a final peak. With regard to the size and granularity of the eosinophils, we observed greater size in the H20 model versus H4. The granularity fluctuated in two peaks marked at the beginning and end of the H20 kinetics with respect to the H4, where it presents greater fluctuation. In the case of the intensity of expression of SiglecF, it appears greater in almost the entire kinetic series in the H20 model compared to the H4 model. This characterization of neutrophil and eosinophil subpopulations still lacks functional interpretation. For example, knowing whether particular subpopulations migrate to the airway lumen with a cytokine secretory function that promotes inflammation or, on the contrary, whether they remain in the tissues interacting with other cell types. More studies are needed to profile these granulocyte subpopulations and eventually provide them with diagnostic or therapeutic value.

Since the H4 and H20 models were neatly diverging, with their respective neutrophilic and eosinophilic dominance as overall endpoints, we aimed, as the next and closing data set for this work, at exploring their molecular maps through proteomics. Due to the clinical heterogeneity that resides in asthma together with the related mechanisms (243), the identification of the genes involved and their functional association with the pathways involved in the disease mechanisms offers potential for translation into various aspects of disease management including the discovery of novel therapeutic targets. The mix of variable factors influencing asthma and the different treatments applied, may mask relevant biological pathways. Although the *IL4*, *IL13*, *CD14*, the β2 adrenergic receptor (*ADRB2*), *FCER1B*, *TNF, ADAM33* and serine peptidase inhibitor, Kazal type 5

(*SPINK5*) genes have been the most studied in relation to asthma and atopy (244-246), there is likely another large spectrum of unknown genes left aside, leading to a burden of inconsistencies in the genes that have been associated with disease phenotypes and the direction of their effects (244). Moreover, the well-studied genes named, failed to show an association with asthma or allergy in several studies (245, 246) or when the studies are replicated, have small effects on the phenotypic variance (244). The asthma susceptibility genes studied are classified in four main groups: genes associated with innate immunity and immunoregulation; genes associated with Th2-cell differentiation and effector functions; genes associated with epithelial biology and mucosal immunity; and genes associated with lung function, airway remodeling and disease severity (244). Our results from murine BAL proteomics showed that the main gene expression detected fell in the pathways related with innate immunity and immunoregulation including neutrophil degranulation (*i.e.,* SA100), complement cascade (C5), regulation of TLR (CD14), adaptive immunity and antigen presentation (MHC-II), lung function (GSTM1); and airway remodeling (*i.e.* MMP9). In induced sputum from patients, we observed gene expression related to some pathways not found in mice, such as regulation of phagocytosis and FcεRI signaling, which participate in innate immunity and immunoregulation, genes related with BCR signal related with adaptive immunity and antigen presentation; genes related to cellular response to stimuli (HSP90 chaperone in RSHR); and genes related to smooth muscle contraction. The profile of gene expression found in induced sputum and murine BAL was not related with the existing definition of the differentiation and effector function of Th2 cells. However, newly discovered asthma genes such as the complement factor 5 (*C5*) which is related to Th2 differentiation, were present in both of the asthma phenotypes that we studied. Recently it has been reported that C5 provides a crucial bridge between the innate and the adaptive immune systems, as C5 regulates the Th1 immune responses through the modulation of IL-12 (179). Also in recent studies, it was demonstrated that the complement was associated with pathways of allergen induced (247), pollutant induced (248) and virally induced (249) experimental asthma (179). Moreover, although expression of the *IL4* and *IL13* genes, was not present at the initial or final point in our mouse model, the corresponding cytokines levels were detected along asthma development in the mouse model, mainly in the eosinophilic phenotype. Several studies show strong associations between specific MHC-II and allergen-specific IgE responses (243). Allergen-specific IgE binds to mast cells in the skin and lungs through a high-affinity Fc receptor (FcεRI, encoded by *FCERI*). The S100A calcium-binding proteins are often secreted in response to inflammation and have a wide range of immunological actions (250), related to asthma severity (251). S100A2 is a chemotactic agent for eosinophils (252), S100A8 is a

chemotactic agent for leukocytes (253-255), S100A9 is a chemotactic factor to neutrophils (251) and S100A12 has pro-inflammatory activity on endothelial and inflammatory cells (256, 257). We observed the presence of S100A8/A9 in both human asthma phenotypes, and in mice at the initial and final stages in the neutrophilic model only, while it was just present at the first allergen challenge in the eosinophilic model. Compared to other previous studies, we found genes related to a group of glutathione-S transferases involved in lung function. These are GSTP1, only found in humans both neutrophilic and eosinophilic; and GSTM1 present in both humans and mouse models at the final stage of the disease. Induced sputum as obtained from humans, is affected by several factors, while mouse BAL originates from mice that are under exact control of the dose and exposure time to the antigen, which makes human versus murine model samples differ. Nevertheless, animal models may still help us estimate the human's disease state. Comparisons between molecules at the beginning and the end of the experimental disease show some proteins differing between models, whereas others remain constant, which may pinpoint particular proteins as markers to classify asthma phenotypes regardless of the disease stage. In the case of the H4 neutrophilic model, the exclusive proteins at the beginning of the disease were related to the innate immune system, while those upon the final instillation were rather related to the adaptive immune response, which is congruent. However, we observed common proteins for both stages of the disease (PGLYRPA1, S100AB, SERPING1, GPI). In the H20 eosinophilic model, the number of exclusive molecules was reduced, with only two of them presents at each disease stage and the majority in both stages (FGA, C5-C6, KNG1, ORM1, HRG). This suggests that eosinophilic asthma has better traceability, since it presents a more homogeneous response at the genetic level. This supports that the models developed in this thesis are driven by responses close to those in humans. The implication of the genes differing between phenotypes may be further studied to identify therapeutic targets. There are previously identified genes that we share in our study, associated with asthma or atopy phenotypes (245). On the other hand, when analyzing the genes that we did not find in the mice, we found that all of them fell outside the published literature. These discrepancies do not imply that such genes have less relevance in the pathophysiology of the disease, but rather that their study would be more difficult as their expression is absent in animal models. However, they may offer potential phenotypic markers to deepen our knowledge of neutrophilic asthma.

CONCLUSIONS

CONCLUSIONS

1. In the non-Th2-biased C57BL/6 mouse, a short (4-week) course of 15-μg HDM i.n. instillations induce an IgE-producing, CD4+ T-cell driven adaptive immune response with mixed eosinophilic-neutrophilic inflammatory infiltration, airway hyperresponsiveness, and absence of airway remodeling. An extended (6-week) i.n. instillation course leads to a T-cell response decline, and abrogation of airway hyperresponsiveness and eosinophilic infiltrates, with persisting neutrophilic infiltration, suggesting immunoregulation of the Th2 arm.

2. The addition of SEB to HDM elicits airway remodeling and mucus hyperproduction and preserves a mixed eosinophilic-neutrophilic inflammatory profile but inhibits airway hyperresponsiveness and $CD4^+$ T-cell infiltration.

3. The addition of α-Galcer to HDM induces increased $CD4^+$ and $CD8^+$ T cells and B cells but fails to reproduce translatable asthma traits such as granulocyte infiltration, airway hyperresponsiveness, and remodeling.

4. The components of cellular and humoral immunity to inhaled HDM, and associated cytokine release, oscillate through the course of experimental asthma, likely due to varying effector and counterregulatory pathways. This exploratory kinetics suggest that the immune response to aeroallergens may also fluctuate in human disease, and this variability may be underrepresented in clinical practice.

5. The DerP1 and DerP2 antigens undergo degradation in standardized, reconstituted HDM extract. Aeroallergen antigens may, therefore, undergo spontaneous degradation in environmental conditions leading to conformational changes that may modify the immune response.

6. Different conditions of HDM preservation status lead to divergent experimental asthma profiles encompassing eosinophilic versus neutrophilic inflammatory infiltration and differing airway remodeling patterns, i.e., mucoid with increased airway contractile tissue mass versus fibrotic. These divergent outcomes are associated with complex, differing patterns of adaptive immune response and innate immune system intervention evolving through varying

time windows. This model diversion encompasses a broad representation of inflammometric profiles seen in real-world clinical practice.

7. Kinetic phenotyping of the infiltrating eosinophils and neutrophils according to cell surface markers related to maturation, migration, and proinflammatory versus immunomodulatory activity (Ly6, CD11b, SiglecF) identifies subpopulations that vary between the eosinophilic and neutrophilic models and fluctuate across time. These changing subpopulations likely involve functional implications not yet identified.

8. Proteomics of murine BAL and induced sputum from asthmatics identify immune response-related gene expression with some molecular species differing from those previously linked to atopic asthma and some differing between eosinophilic and neutrophilic patterns. Overall, the proteomics data support that the developed models are driven by responses close to those in humans. Further study of gene expression differing between inflammatory profiles may point towards potential disease-management targets.

BIBLIOGRAPHY

1. Standards for the diagnosis and care of patients with chronic obstructive pulmonary disease (COPD) and asthma. This official statement of the American Thoracic Society was adopted by the ATS Board of Directors, November 1986. Am Rev Respir Dis. 1987;136(1):225-44.
2. Holgate ST, Lackie PM, Davies DE, Roche WR, Walls AF. The bronchial epithelium as a key regulator of airway inflammation and remodelling in asthma. Clin Exp Allergy. 1999;29 Suppl 2:90-5.
3. Masoli M, Fabian D, Holt S, Beasley R, Global Initiative for Asthma P. The global burden of asthma: executive summary of the GINA Dissemination Committee report. Allergy. 2004;59(5):469-78.
4. Bousquet J, Clark TJ, Hurd S, Khaltaev N, Lenfant C, O'Byrne P, et al. GINA guidelines on asthma and beyond. Allergy. 2007;62(2):102-12.
5. Voskamp AL, Kormelink TG, van Wijk RG, Hiemstra PS, Taube C, de Jong EC, et al. Modulating local airway immune responses to treat allergic asthma: lessons from experimental models and human studies. Semin Immunopathol. 2020;42(1):95-110.
6. Woo LN, Guo WY, Wang X, Young A, Salehi S, Hin A, et al. A 4-Week Model of House Dust Mite (HDM) Induced Allergic Airways Inflammation with Airway Remodeling. Sci Rep. 2018;8(1):6925.
7. Hoyne GF, O'Hehir RE, Wraith DC, Thomas WR, Lamb JR. Inhibition of T cell and antibody responses to house dust mite allergen by inhalation of the dominant T cell epitope in naive and sensitized mice. J Exp Med. 1993;178(5):1783-8.
8. Kudo M, Ishigatsubo Y, Aoki I. Pathology of asthma. Front Microbiol. 2013;4:263.
9. Wang M, Gao P, Wu X, Chen Y, Feng Y, Yang Q, et al. Impaired anti-inflammatory action of glucocorticoid in neutrophil from patients with steroid-resistant asthma. Respir Res. 2016;17(1):153.
10. Kuruvilla ME, Lee FE, Lee GB. Understanding Asthma Phenotypes, Endotypes, and Mechanisms of Disease. Clin Rev Allergy Immunol. 2019;56(2):219-33.
11. Ray A, Kolls JK. Neutrophilic Inflammation in Asthma and Association with Disease Severity. Trends Immunol. 2017;38(12):942-54.
12. Wenzel SE. Asthma: defining of the persistent adult phenotypes. Lancet. 2006;368(9537):804-13.
13. Devereux G ME, Burney PGJ. Epidemiology of Asthma and Allergic Airway Diseases. Middleton's Allergy. 2014;754-789.
14. Peters U, Dixon AE, Forno E. Obesity and asthma. J Allergy Clin Immunol. 2018;141(4):1169-79.
15. ST W. Obesity: insight into the origins of asthma. Nature Immunology. 2005;6:537–539.
16. Beuther DA, Weiss ST, Sutherland ER. Obesity and asthma. Am J Respir Crit Care Med. 2006;174(2):112-9.
17. Burney P, Malmberg E, Chinn S, Jarvis D, Luczynska C, Lai E. The distribution of total and specific serum IgE in the European Community Respiratory Health Survey. J Allergy Clin Immunol. 1997;99(3):314-22.
18. Weinmayr G, Genuneit J, Nagel G, Bjorksten B, van Hage M, Priftanji A, et al. International variations in associations of allergic markers and diseases in children: ISAAC Phase Two. Allergy. 2010;65(6):766-75.
19. Bousquet PJ, Chinn S, Janson C, Kogevinas M, Burney P, Jarvis D, et al. Geographical variation in the prevalence of positive skin tests to environmental aeroallergens in the European Community Respiratory Health Survey I. Allergy. 2007;62(3):301-9.
20. COLLOFF MJ. DUST MITES: Springer; 2009.
21. U Wahn SL, R Bergmann, M Kulig, J Forster, K Bergmann, C P Bauer, I Guggenmoos-Holzmann. Indoor allergen exposure is a risk factor for sensitization during the first three years of life. J Allergy Clin Immunol. 1997.

22. Jongepier H BH, Dijkstra A, et al. Polymorphisms of the ADAM33 gene are associated with accelerated lung function decline in asthma. . Clin Exp Allergy. 2004;34: 757–60.
23. Pulleyn LJ NR, Adcock IM, Barnes PJ. TGFbeta1 allele association with asthma severity. Hum Genet. 2001;109: 623–27.
24. Sandford AJ CT, Zhu S, et al. Polymorphisms in the IL4, IL4RA, and FCERIB genes and asthma severity. J Allergy Clin Immunol 2000;106: 135–40.
25. Shang Y, Das S, Rabold R, Sham JS, Mitzner W, Tang WY. Epigenetic alterations by DNA methylation in house dust mite-induced airway hyperresponsiveness. Am J Respir Cell Mol Biol. 2013;49(2):279-87.
26. Iijima H, Kaneko Y, Yamada H, Yatagai Y, Masuko H, Sakamoto T, et al. A distinct sensitization pattern associated with asthma and the thymic stromal lymphopoietin (TSLP) genotype. Allergol Int. 2013;62(1):123-30.
27. Davis MF, McCormack MC, Matsui EC. Growing Concerns with Staphylococcus aureus and Asthma: New Territory for an Old Foe? J Allergy Clin Immunol Pract. 2019;7(2):616-7.
28. Calderon MA, Linneberg A, Kleine-Tebbe J, De Blay F, Hernandez Fernandez de Rojas D, Virchow JC, et al. Respiratory allergy caused by house dust mites: What do we really know? J Allergy Clin Immunol. 2015;136(1):38-48.
29. Custovic A, Woodcock H, Craven M, Hassall R, Hadley E, Simpson A, et al. Dust mite allergens are carried on not only large particles. Pediatr Allergy Immunol. 1999;10(4):258-60.
30. Casset A, Marchand C, Purohit A, le Calve S, Uring-Lambert B, Donnay C, et al. Inhaled formaldehyde exposure: effect on bronchial response to mite allergen in sensitized asthma patients. Allergy. 2006;61(11):1344-50.
31. Olga Meca Ma-JsC, Mónica Sánchez-Ortiz Francisco-Javier González- Barcala4 Iñigo Ojanguren, Xavier Munoz. Do Low Molecular Weight Agents Cause More Severe Asthma than High Molecular Weight Agents? PLoS One. 2016.
32. Baur X, Akdis CA, Budnik LT, Cruz MJ, Fischer A, Forster-Ruhrmann U, et al. Immunological methods for diagnosis and monitoring of IgE-mediated allergy caused by industrial sensitizing agents (IMExAllergy). Allergy. 2019;74(10):1885-97.
33. Wang JY. The innate immune response in house dust mite-induced allergic inflammation. Allergy Asthma Immunol Res. 2013;5(2):68-74.
34. Jacquet A. Innate immune responses in house dust mite allergy. ISRN Allergy. 2013;2013:735031.
35. Gregory LG, Lloyd CM. Orchestrating house dust mite-associated allergy in the lung. Trends Immunol. 2011;32(9):402-11.
36. Pacciani V, Corrente S, Gregori S, Pierantozzi A, Silenzi R, Chianca M, et al. Correlation of Der p 2 T-cell responses with clinical characteristics of children allergic to house dust mite. Ann Allergy Asthma Immunol. 2012;109(6):442-7.
37. Thomas WR. Geography of house dust mite allergens. Asian Pac J Allergy Immunol. 2010;28(4):211-24.
38. Simpson A, Simpson B, Custovic A, Cain G, Craven M, Woodcock A. Household characteristics and mite allergen levels in Manchester,UK. Clin Exp Allergy. 2002;32(10):1413-9.
39. Laprise C, Laviolette M, Boutet M, Boulet LP. Asymptomatic airway hyperresponsiveness: relationships with airway inflammation and remodelling. Eur Respir J. 1999;14(1):63-73.
40. Fish JE, Peters SP. Airway remodeling and persistent airway obstruction in asthma. J Allergy Clin Immunol. 1999;104(3 Pt 1):509-16.
41. Knight D. Epithelium-fibroblast interactions in response to airway inflammation. Immunol Cell Biol. 2001;79(2):160-4.

42. Trifilieff A, Fujitani Y, Coyle AJ, Kopf M, Bertrand C. IL-5 deficiency abolishes aspects of airway remodelling in a murine model of lung inflammation. Clin Exp Allergy. 2001;31(6):934-42.
43. Carr TF, Kraft M. Chronic Infection and Severe Asthma. Immunol Allergy Clin North Am. 2016;36(3):483-502.
44. Trompette A, Divanovic S, Visintin A, Blanchard C, Hegde RS, Madan R, et al. Allergenicity resulting from functional mimicry of a Toll-like receptor complex protein. Nature. 2009;457(7229):585-8.
45. Perros F, Hoogsteden HC, Coyle AJ, Lambrecht BN, Hammad H. Blockade of CCR4 in a humanized model of asthma reveals a critical role for DC-derived CCL17 and CCL22 in attracting Th2 cells and inducing airway inflammation. Allergy. 2009;64(7):995-1002.
46. Klose CS AD. Innate lymphoid cells as regulators of immunity, inflammation and tissue homeostasis. Nature Immunology. 2016;17(7):765–774.
47. Kips JC, Anderson GP, Fredberg JJ, Herz U, Inman MD, Jordana M, et al. Murine models of asthma. Eur Respir J. 2003;22(2):374-82.
48. Nauseef WMaB, N. Neutrophils at work. Nature Immunology. 2014;15, 602–611
49. Soehnlein O, Weber C, Lindbom L. Neutrophil granule proteins tune monocytic cell function. Trends Immunol. 2009;30(11):538-46.
50. Brinkmann V, Zychlinsky A. Beneficial suicide: why neutrophils die to make NETs. Nat Rev Microbiol. 2007;5(8):577-82.
51. Nadel JA. Role of neutrophil elastase in hypersecretion during COPD exacerbations, and proposed therapies. Chest. 2000;117(5 Suppl 2):386S-9S.
52. Anticevich SZ, Hughes JM, Black JL, Armour CL. Induction of hyperresponsiveness in human airway tissue by neutrophils--mechanism of action. Clin Exp Allergy. 1996;26(5):549-56.
53. Stanescu D, Sanna A, Veriter C, Kostianev S, Calcagni PG, Fabbri LM, et al. Airways obstruction, chronic expectoration, and rapid decline of FEV1 in smokers are associated with increased levels of sputum neutrophils. Thorax. 1996;51(3):267-71.
54. Hough KP, Curtiss ML, Blain TJ, Liu RM, Trevor J, Deshane JS, et al. Airway Remodeling in Asthma. Front Med (Lausanne). 2020;7:191.
55. Meghan Cundall M, Yongchang Sun, MD, Christina Miranda, MS, PA,, John B.Trudeau B, Stephen Barnes, BS, and Sally E.Wenzel, MD. Neutrophil-derived matrix metalloproteinase-9 is increased in severe asthma and poorly inhibited by glucocorticoids. J Allergy Clin Immunol. 2003;112.
56. Cundall Mea. Neutrophil-derived matrix metalloproteinase-9 is increased in severe asthma and poorly inhibited by glucocorticoids. J Allergy Clin Immunol. 2003;112, 1064–1071
57. Vignola AM, Bonanno A, Mirabella A, Riccobono L, Mirabella F, Profita M, et al. Increased levels of elastase and alpha1-antitrypsin in sputum of asthmatic patients. Am J Respir Crit Care Med. 1998;157(2):505-11.
58. Erlewyn-Lajeunesse MD, Hunt LP, Pohunek P, Dobson SJ, Kochhar P, Warner JA, et al. Bronchoalveolar lavage MMP-9 and TIMP-1 in preschool wheezers and their relationship to persistent wheeze. Pediatr Res. 2008;64(2):194-9.
59. Pothoven KL, Norton JE, Suh LA, Carter RG, Harris KE, Biyasheva A, et al. Neutrophils are a major source of the epithelial barrier disrupting cytokine oncostatin M in patients with mucosal airways disease. J Allergy Clin Immunol. 2017;139(6):1966-78 e9.
60. Carr TF, Zeki AA, Kraft M. Eosinophilic and Noneosinophilic Asthma. Am J Respir Crit Care Med. 2018;197(1):22-37.
61. Fulkerson PC, Rothenberg ME. Targeting eosinophils in allergy, inflammation and beyond. Nat Rev Drug Discov. 2013;12(2):117-29.
62. McBrien CN M-GA. The biology of eosinophils and their role in asthma. Frontiers in Medicine. 2017;4:93.

63. Shamri R, Xenakis JJ, Spencer LA. Eosinophils in innate immunity: an evolving story. Cell Tissue Res. 2011;343(1):57-83.
64. Durrani SR VR, Busse WW. What effect does asthma treatment have on airway remodeling? J Allergy Clin Immunol. 2011;128(3):439–448.
65. Chung KF. Airway smooth muscle cells: contributing to and regulating airway mucosal inflammation? Eur Respir J. 2000;15(5):961-8.
66. Krug N, Madden J, Redington AE, Lackie P, Djukanovic R, Schauer U, et al. T-cell cytokine profile evaluated at the single cell level in BAL and blood in allergic asthma. Am J Respir Cell Mol Biol. 1996;14(4):319-26.
67. Wang YH, Voo KS, Liu B, Chen CY, Uygungil B, Spoede W, et al. A novel subset of CD4(+) T(H)2 memory/effector cells that produce inflammatory IL-17 cytokine and promote the exacerbation of chronic allergic asthma. J Exp Med. 2010;207(11):2479-91.
68. Li BWS, Stadhouders R, de Bruijn MJW, Lukkes M, Beerens D, Brem MD, et al. Group 2 Innate Lymphoid Cells Exhibit a Dynamic Phenotype in Allergic Airway Inflammation. Front Immunol. 2017;8:1684.
69. Moore WC MD, Wenzel SE, Teague WG, Li H, Li X, D'Agostino R Jr, Castro M, Curran-Everett D, Fitzpatrick AM, Gaston B, Jarjour NN, Sorkness R, Calhoun WJ, Chung KF, Comhair SA, Dweik RA, Israel E, Peters SP, Busse WW, Erzurum SC, Bleecker ER. Identification of asthma phenotypes using cluster analysis in the severe asthma research program. Am J Respir Crit Care Med. 2010;181(4):315–323
70. Guo FH, Uetani K, Haque SJ, Williams BR, Dweik RA, Thunnissen FB, et al. Interferon gamma and interleukin 4 stimulate prolonged expression of inducible nitric oxide synthase in human airway epithelium through synthesis of soluble mediators. J Clin Invest. 1997;100(4):829-38.
71. Ray A, Raundhal M, Oriss TB, Ray P, Wenzel SE. Current concepts of severe asthma. J Clin Invest. 2016;126(7):2394-403.
72. Curtis MM, Rowell E, Shafiani S, Negash A, Urdahl KB, Wilson CB, et al. Fidelity of pathogen-specific CD4+ T cells to the Th1 lineage is controlled by exogenous cytokines, interferon-gamma expression, and pathogen lifestyle. Cell Host Microbe. 2010;8(2):163-73.
73. Mosmann TR, Coffman RL. TH1 and TH2 cells: different patterns of lymphokine secretion lead to different functional properties. Annu Rev Immunol. 1989;7:145-73.
74. B. Defrance PC, G. Billian, J. Guillemot, S. A. Minty, and S. D. Caput. Interleukin 13 Is a B Cell Stimulating Factor. J Exp Med. 1994;179.
75. Annunziato F, Cosmi L, Santarlasci V, Maggi L, Liotta F, Mazzinghi B, et al. Phenotypic and functional features of human Th17 cells. J Exp Med. 2007;204(8):1849-61.
76. Bettelli E, Carrier Y, Gao W, Korn T, Strom TB, Oukka M, et al. Reciprocal developmental pathways for the generation of pathogenic effector TH17 and regulatory T cells. Nature. 2006;441(7090):235-8.
77. Ye P, Rodriguez FH, Kanaly S, Stocking KL, Schurr J, Schwarzenberger P, et al. Requirement of interleukin 17 receptor signaling for lung CXC chemokine and granulocyte colony-stimulating factor expression, neutrophil recruitment, and host defense. J Exp Med. 2001;194(4):519-27.
78. Fossiez F, Djossou O, Chomarat P, Flores-Romo L, Ait-Yahia S, Maat C, et al. T cell interleukin-17 induces stromal cells to produce proinflammatory and hematopoietic cytokines. J Exp Med. 1996;183(6):2593-603.
79. Bullens DM, Truyen E, Coteur L, Dilissen E, Hellings PW, Dupont LJ, et al. IL-17 mRNA in sputum of asthmatic patients: linking T cell driven inflammation and granulocytic influx? Respir Res. 2006;7:135.
80. Kunkel SL, Standiford T, Kasahara K, Strieter RM. Interleukin-8 (IL-8): the major neutrophil chemotactic factor in the lung. Exp Lung Res. 1991;17(1):17-23.

81. Gibson PG, Simpson JL, Saltos N. Heterogeneity of airway inflammation in persistent asthma : evidence of neutrophilic inflammation and increased sputum interleukin-8. Chest. 2001;119(5):1329-36.
82. Gounni AS, Lamkhioued B, Koussih L, Ra C, Renzi PM, Hamid Q. Human neutrophils express the high-affinity receptor for immunoglobulin E (Fc epsilon RI): role in asthma. FASEB J. 2001;15(6):940-9.
83. Pelletier Mea. Evidence for a cross-talk between human neutrophils and Th17 cells. Blood. 2010;115, 335-343.
84. Bonecchi R, Polentarutti N, Luini W, Borsatti A, Bernasconi S, Locati M, et al. Up-regulation of CCR1 and CCR3 and induction of chemotaxis to CC chemokines by IFN-gamma in human neutrophils. J Immunol. 1999;162(1):474-9.
85. Kuo CS, Pavlidis S, Loza M, Baribaud F, Rowe A, Pandis I, et al. T-helper cell type 2 (Th2) and non-Th2 molecular phenotypes of asthma using sputum transcriptomics in U-BIOPRED. Eur Respir J. 2017;49(2).
86. Galli SJ, Tsai M, Piliponsky AM. The development of allergic inflammation. Nature. 2008;454(7203):445-54.
87. Kuo CSea. T-helper cell type 2 (Th2) and non-Th2 molecular phenotypes of asthma using sputum transcriptomics in U-BIOPRED. Eur Respir J. 2017.
88. Bowen H, Kelly A, Lee T, Lavender P. Control of cytokine gene transcription in Th1 and Th2 cells. Clin Exp Allergy. 2008;38(9):1422-31.
89. Reibman J, Hsu Y, Chen LC, Bleck B, Gordon T. Airway epithelial cells release MIP-3alpha/CCL20 in response to cytokines and ambient particulate matter. Am J Respir Cell Mol Biol. 2003;28(6):648-54.
90. Rabinovitch N, Liu AH, Zhang L, Rodes CE, Foarde K, Dutton SJ, et al. Importance of the personal endotoxin cloud in school-age children with asthma. J Allergy Clin Immunol. 2005;116(5):1053-7.
91. Bisgaard H, Hermansen MN, Buchvald F, Loland L, Halkjaer LB, Bonnelykke K, et al. Childhood asthma after bacterial colonization of the airway in neonates. N Engl J Med. 2007;357(15):1487-95.
92. Wang YH, Voo, K. S., Liu, B., Chen, C. Y., Uygungil, B., Spoede, W., et al. . A novel subset of CD4(+) T(H)2 memory/effector cells that produce inflammatory IL-17 cytokine and promote the exacerbation of chronic allergic asthma. J Exp Med. 2010;207, 2479–2491.
93. Kudo M, Melton AC, Chen C, Engler MB, Huang KE, Ren X, et al. IL-17A produced by alphabeta T cells drives airway hyper-responsiveness in mice and enhances mouse and human airway smooth muscle contraction. Nat Med. 2012;18(4):547-54.
94. Zijlstra GJ, Ten Hacken NH, Hoffmann RF, van Oosterhout AJ, Heijink IH. Interleukin-17A induces glucocorticoid insensitivity in human bronchial epithelial cells. Eur Respir J. 2012;39(2):439-45.
95. Pennino D, Bhavsar PK, Effner R, Avitabile S, Venn P, Quaranta M, et al. IL-22 suppresses IFN-gamma-mediated lung inflammation in asthmatic patients. J Allergy Clin Immunol. 2013;131(2):562-70.
96. Broide DH, Lotz M, Cuomo AJ, Coburn DA, Federman EC, Wasserman SI. Cytokines in symptomatic asthma airways. J Allergy Clin Immunol. 1992;89(5):958-67.
97. Teixeira LK, Fonseca BP, Barboza BA, Viola JP. The role of interferon-gamma on immune and allergic responses. Mem Inst Oswaldo Cruz. 2005;100 Suppl 1:137-44.
98. Brown JM, Wilson TM, Metcalfe DD. The mast cell and allergic diseases: role in pathogenesis and implications for therapy. Clin Exp Allergy. 2008;38(1):4-18.
99. Samitas K, Delimpoura V, Zervas E, Gaga M. Anti-IgE treatment, airway inflammation and remodelling in severe allergic asthma: current knowledge and future perspectives. Eur Respir Rev. 2015;24(138):594-601.
100. SEYMOUR B. CREPEA MD, ” AND JOHN W. HARMAN, M.D.,** MADISON, Wrs. The pathology of bronchial asthma. Arch Int Med. 1955.

101. Carroll N, Cooke C, James A. The distribution of eosinophils and lymphocytes in the large and small airways of asthmatics. Eur Respir J. 1997;10(2):292-300.
102. Hamid Q, Song Y, Kotsimbos TC, Minshall E, Bai TR, Hegele RG, et al. Inflammation of small airways in asthma. J Allergy Clin Immunol. 1997;100(1):44-51.
103. Bullen SS. Correlation of clinical and autopsy findings in 176 cases of asthma. J Allergy. 1952;23(3):193-203.
104. Messer J. PGA, Bennet W. A. Cause of death and pathological findings in 304 cases of bronchial asthma. Chest. 1960.
105. Dunnill MS. The pathology of asthma, with special reference to changes in the bronchial mucosa. J Clin Pathol. 1960;13:27-33.
106. Lamblin C, Gosset P, Tillie-Leblond I, Saulnier F, Marquette CH, Wallaert B, et al. Bronchial neutrophilia in patients with noninfectious status asthmaticus. Am J Respir Crit Care Med. 1998;157(2):394-402.
107. Ordonez CL, Shaughnessy TE, Matthay MA, Fahy JV. Increased neutrophil numbers and IL-8 levels in airway secretions in acute severe asthma: Clinical and biologic significance. Am J Respir Crit Care Med. 2000;161(4 Pt 1):1185-90.
108. Dunnill MS, Massarella GR, Anderson JA. A comparison of the quantitative anatomy of the bronchi in normal subjects, in status asthmaticus, in chronic bronchitis, and in emphysema. Thorax. 1969;24(2):176-9.
109. C.L. Ordonez RK, H.H. Wong, et al. Mild and moderate asthma is associated with airway goblet cell hyperplasia and abnormalities in mucin gene expression. Am J Respir Crit Care Med. 2001;163.
110. Roche WR, Beasley R, Williams JH, Holgate ST. Subepithelial fibrosis in the bronchi of asthmatics. Lancet. 1989;1(8637):520-4.
111. Vignola AM, Mirabella F, Costanzo G, Di Giorgi R, Gjomarkaj M, Bellia V, et al. Airway remodeling in asthma. Chest. 2003;123(3 Suppl):417S-22S.
112. Aikawa T, Shimura S, Sasaki H, Ebina M, Takishima T. Marked goblet cell hyperplasia with mucus accumulation in the airways of patients who died of severe acute asthma attack. Chest. 1992;101(4):916-21.
113. Carroll N, Elliot J, Morton A, James A. The structure of large and small airways in nonfatal and fatal asthma. Am Rev Respir Dis. 1993;147(2):405-10.
114. Lazaar AL PRJ. Is airway remodeling clinically relevant in asthma? . Am J Med. 2003;115:652–659.
115. Johns DP, Wilson J, Harding R, Walters EH. Airway distensibility in healthy and asthmatic subjects: effect of lung volume history. J Appl Physiol (1985). 2000;88(4):1413-20.
116. Awadh N, Muller NL, Park CS, Abboud RT, FitzGerald JM. Airway wall thickness in patients with near fatal asthma and control groups: assessment with high resolution computed tomographic scanning. Thorax. 1998;53(4):248-53.
117. Chiappara G, Gagliardo R, Siena A, Bonsignore MR, Bousquet J, Bonsignore G, et al. Airway remodelling in the pathogenesis of asthma. Curr Opin Allergy Clin Immunol. 2001;1(1):85-93.
118. Grainge CL, Lau LC, Ward JA, Dulay V, Lahiff G, Wilson S, et al. Effect of bronchoconstriction on airway remodeling in asthma. N Engl J Med. 2011;364(21):2006-15.
119. Bento AM, Hershenson MB. Airway remodeling: potential contributions of subepithelial fibrosis and airway smooth muscle hypertrophy/hyperplasia to airway narrowing in asthma. Allergy Asthma Proc. 1998;19(6):353-8.
120. Xiao C, Puddicombe SM, Field S, Haywood J, Broughton-Head V, Puxeddu I, et al. Defective epithelial barrier function in asthma. J Allergy Clin Immunol. 2011;128(3):549-56 e1-12.
121. Jacquet A. Interactions of airway epithelium with protease allergens in the allergic response. Clin Exp Allergy. 2011;41(3):305-11.

122. Bousquet J, Jeffery PK, Busse WW, Johnson M, Vignola AM. Asthma. From bronchoconstriction to airways inflammation and remodeling. Am J Respir Crit Care Med. 2000;161(5):1720-45.
123. Holgate ST, Davies DE, Lackie PM, Wilson SJ, Puddicombe SM, Lordan JL. Epithelial-mesenchymal interactions in the pathogenesis of asthma. J Allergy Clin Immunol. 2000;105(2 Pt 1):193-204.
124. Brewster CE, Howarth PH, Djukanovic R, Wilson J, Holgate ST, Roche WR. Myofibroblasts and subepithelial fibrosis in bronchial asthma. Am J Respir Cell Mol Biol. 1990;3(5):507-11.
125. Aceves S. S. BDH. Airway fibrosis and angiogenesis due to eosinophil trafficking in chronic asthma. Curr Mol Med. 2008;8 350–358.
126. Kariyawasam HH, Robinson DS. The role of eosinophils in airway tissue remodelling in asthma. Curr Opin Immunol. 2007;19(6):681-6.
127. Gunst SJ, Tang DD. The contractile apparatus and mechanical properties of airway smooth muscle. Eur Respir J. 2000;15(3):600-16.
128. Regamey N, Ochs M, Hilliard TN, Muhlfeld C, Cornish N, Fleming L, et al. Increased airway smooth muscle mass in children with asthma, cystic fibrosis, and non-cystic fibrosis bronchiectasis. Am J Respir Crit Care Med. 2008;177(8):837-43.
129. Johnson S, Knox A. Autocrine production of matrix metalloproteinase-2 is required for human airway smooth muscle proliferation. Am J Physiol. 1999;277(6):L1109-17.
130. Halwani R, Vazquez-Tello A, Sumi Y, Pureza MA, Bahammam A, Al-Jahdali H, et al. Eosinophils induce airway smooth muscle cell proliferation. J Clin Immunol. 2013;33(3):595-604.
131. Chen C, Kudo M, Rutaganira F, Takano H, Lee C, Atakilit A, et al. Integrin alpha9beta1 in airway smooth muscle suppresses exaggerated airway narrowing. J Clin Invest. 2012;122(8):2916-27.
132. Kuwano K, Bosken CH, Pare PD, Bai TR, Wiggs BR, Hogg JC. Small airways dimensions in asthma and in chronic obstructive pulmonary disease. Am Rev Respir Dis. 1993;148(5):1220-5.
133. Gillis HL, Lutchen KR. Airway remodeling in asthma amplifies heterogeneities in smooth muscle shortening causing hyperresponsiveness. J Appl Physiol (1985). 1999;86(6):2001-12.
134. Holgate ST. Epithelium dysfunction in asthma. J Allergy Clin Immunol. 2007;120(6):1233-44; quiz 45-6.
135. Chetta A, Foresi A, Del Donno M, Bertorelli G, Pesci A, Olivieri D. Airways remodeling is a distinctive feature of asthma and is related to severity of disease. Chest. 1997;111(4):852-7.
136. Vignola AM, Kips J, Bousquet J. Tissue remodeling as a feature of persistent asthma. J Allergy Clin Immunol. 2000;105(6 Pt 1):1041-53.
137. Chapman DG, Irvin CG. Mechanisms of airway hyper-responsiveness in asthma: the past, present and yet to come. Clin Exp Allergy. 2015;45(4):706-19.
138. Cockcroft DW, Ruffin RE, Dolovich J, Hargreave FE. Allergen-induced increase in non-allergic bronchial reactivity. Clin Allergy. 1977;7(6):503-13.
139. Tomaki M, Ichinose M. [Measurement of airway hyperresponsiveness]. Nihon Rinsho. 2001;59(10):1945-9.
140. Halwani R, Al-Muhsen S, Al-Jahdali H, Hamid Q. Role of transforming growth factor-beta in airway remodeling in asthma. Am J Respir Cell Mol Biol. 2011;44(2):127-33.
141. Chu HW, Trudeau JB, Balzar S, Wenzel SE. Peripheral blood and airway tissue expression of transforming growth factor beta by neutrophils in asthmatic subjects and normal control subjects. J Allergy Clin Immunol. 2000;106(6):1115-23.

142. Arron JR, Choy DF, Scheerens H, Matthews JG. Noninvasive biomarkers that predict treatment benefit from biologic therapies in asthma. Ann Am Thorac Soc. 2013;10 Suppl:S206-13.
143. Berry M, Morgan A, Shaw DE, Parker D, Green R, Brightling C, et al. Pathological features and inhaled corticosteroid response of eosinophilic and non-eosinophilic asthma. Thorax. 2007;62(12):1043-9.
144. Szefler SJ, Wenzel S, Brown R, Erzurum SC, Fahy JV, Hamilton RG, et al. Asthma outcomes: biomarkers. J Allergy Clin Immunol. 2012;129(3 Suppl):S9-23.
145. Woodruff PG, Modrek B, Choy DF, Jia G, Abbas AR, Ellwanger A, et al. T-helper type 2-driven inflammation defines major subphenotypes of asthma. Am J Respir Crit Care Med. 2009;180(5):388-95.
146. Lambrecht BN, Hammad H. The immunology of asthma. Nat Immunol. 2015;16(1):45-56.
147. Kaur D, Gomez E, Doe C, Berair R, Woodman L, Saunders R, et al. IL-33 drives airway hyper-responsiveness through IL-13-mediated mast cell: airway smooth muscle crosstalk. Allergy. 2015;70(5):556-67.
148. Minshall EM, Leung DY, Martin RJ, Song YL, Cameron L, Ernst P, et al. Eosinophil-associated TGF-beta1 mRNA expression and airways fibrosis in bronchial asthma. Am J Respir Cell Mol Biol. 1997;17(3):326-33.
149. Smith SG, Chen R, Kjarsgaard M, Huang C, Oliveria JP, O'Byrne PM, et al. Increased numbers of activated group 2 innate lymphoid cells in the airways of patients with severe asthma and persistent airway eosinophilia. J Allergy Clin Immunol. 2016;137(1):75-86 e8.
150. Fallon PG, Ballantyne SJ, Mangan NE, Barlow JL, Dasvarma A, Hewett DR, et al. Identification of an interleukin (IL)-25-dependent cell population that provides IL-4, IL-5, and IL-13 at the onset of helminth expulsion. J Exp Med. 2006;203(4):1105-16.
151. Fowler SJ, Tavernier G, Niven R. High blood eosinophil counts predict sputum eosinophilia in patients with severe asthma. J Allergy Clin Immunol. 2015;135(3):822-4 e2.
152. Westerhof GA, Vollema EM, Weersink EJ, Reinartz SM, de Nijs SB, Bel EH. Predictors for the development of progressive severity in new-onset adult asthma. J Allergy Clin Immunol. 2014;134(5):1051-6 e2.
153. Wenzel SE SL, Langmack EL, et al. Evidence that severe asthma can be divided pathologically into two inflammatory subtypes with distinct physiologic and clinical characteristics. Am J Respir Crit Care Med. 1999;160: 1001–08.
154. Wenzel SE, Szefler SJ, Leung DY, Sloan SI, Rex MD, Martin RJ. Bronchoscopic evaluation of severe asthma. Persistent inflammation associated with high dose glucocorticoids. Am J Respir Crit Care Med. 1997;156(3 Pt 1):737-43.
155. Sur S, Crotty TB, Kephart GM, Hyma BA, Colby TV, Reed CE, et al. Sudden-onset fatal asthma. A distinct entity with few eosinophils and relatively more neutrophils in the airway submucosa? Am Rev Respir Dis. 1993;148(3):713-9.
156. James AL, Elliot JG, Abramson MJ, Walters EH. Time to death, airway wall inflammation and remodelling in fatal asthma. Eur Respir J. 2005;26(3):429-34.
157. Green BJ, Wiriyachaiporn S, Grainge C, Rogers GB, Kehagia V, Lau L, et al. Potentially pathogenic airway bacteria and neutrophilic inflammation in treatment resistant severe asthma. PLoS One. 2014;9(6):e100645.
158. Wood LG, Baines KJ, Fu J, Scott HA, Gibson PG. The neutrophilic inflammatory phenotype is associated with systemic inflammation in asthma. Chest. 2012;142(1):86-93.
159. Simpson JL, Gibson PG, Yang IA, Upham J, James A, Reynolds PN, et al. Impaired macrophage phagocytosis in non-eosinophilic asthma. Clin Exp Allergy. 2013;43(1):29-35.

160. Huvenne W, Callebaut I, Plantinga M, Vanoirbeek JA, Krysko O, Bullens DM, et al. Staphylococcus aureus enterotoxin B facilitates allergic sensitization in experimental asthma. Clin Exp Allergy. 2010;40(7):1079-90.
161. Cosmi L, Liotta F, Annunziato F. Th17 regulating lower airway disease. Curr Opin Allergy Clin Immunol. 2016;16(1):1-6.
162. Ricciardolo FLM, Sorbello V, Folino A, Gallo F, Massaglia GM, Favata G, et al. Identification of IL-17F/frequent exacerbator endotype in asthma. J Allergy Clin Immunol. 2017;140(2):395-406.
163. Acosta-Rodriguez EV, Rivino L, Geginat J, Jarrossay D, Gattorno M, Lanzavecchia A, et al. Surface phenotype and antigenic specificity of human interleukin 17-producing T helper memory cells. Nat Immunol. 2007;8(6):639-46.
164. Bettelli E, Korn T, Oukka M, Kuchroo VK. Induction and effector functions of T(H)17 cells. Nature. 2008;453(7198):1051-7.
165. Cates EC, Fattouh R, Wattie J, Inman MD, Goncharova S, Coyle AJ, et al. Intranasal exposure of mice to house dust mite elicits allergic airway inflammation via a GM-CSF-mediated mechanism. J Immunol. 2004;173(10):6384-92.
166. Kawano T, Cui J, Koezuka Y, Toura I, Kaneko Y, Motoki K, et al. CD1d-restricted and TCR-mediated activation of valpha14 NKT cells by glycosylceramides. Science. 1997;278(5343):1626-9.
167. Liyan Chen CL, Min Peng, Jiaxing Xie, Kefang Lai & Nanshan Zhong Establishment of a mouse model with all four clinical features of eosinophilic bronchitis. Sci Rep. 2020;10.
168. Swirski FK, Sajic D, Robbins CS, Gajewska BU, Jordana M, Stampfli MR. Chronic exposure to innocuous antigen in sensitized mice leads to suppressed airway eosinophilia that is reversed by granulocyte macrophage colony-stimulating factor. J Immunol. 2002;169(7):3499-506.
169. Neeno T, Krco CJ, Harders J, Baisch J, Cheng S, David CS. HLA-DQ8 transgenic mice lacking endogenous class II molecules respond to house dust allergens: identification of antigenic epitopes. J Immunol. 1996;156(9):3191-5.
170. O'Brien RM, Thomas WR, Wootton AM. T cell responses to the purified major allergens from the house dust mite Dermatophagoides pteronyssinus. J Allergy Clin Immunol. 1992;89(5):1021-31.
171. Johnson JR, Wiley RE, Fattouh R, Swirski FK, Gajewska BU, Coyle AJ, et al. Continuous exposure to house dust mite elicits chronic airway inflammation and structural remodeling. Am J Respir Crit Care Med. 2004;169(3):378-85.
172. Duez C, Tsicopoulos A, Janin A, Tillie-Leblond I, Thyphronitis G, Marquillies P, et al. An in vivo model of allergic inflammation: pulmonary human cell infiltrate in allergen-challenged allergic Hu-SCID mice. Eur J Immunol. 1996;26(5):1088-93.
173. Herz U, Schnoy N, Borelli S, Weigl L, Kasbohrer U, Daser A, et al. A human-SCID mouse model for allergic immune response bacterial superantigen enhances skin inflammation and suppresses IgE production. J Invest Dermatol. 1998;110(3):224-31.
174. de Homdedeu M, Cruz M, Sanchez-Diez S, I O, Romero-Mesones C, J V, et al. The immunomodulatory effects of diesel exhaust particles in asthma. Environ Pollut. 2020;263(Pt A):114600.
175. Hu C, Cruz MJ, Ojanguren I, de Homdedeu M, Gonzalez-Barcala FJ, Munoz X. Specific inhalation challenge: the relationship between response, clinical variables and lung function. Occup Environ Med. 2017;74(8):586-91.
176. Iga Meca Ma-JsC, Mónica Sánchez-Ortiz, Francisco-Javier González- Barcala, Iñigo Ojanguren, Xavier Munoz. Do Low Molecular Weight Agents Cause More Severe Asthma than High Molecular Weight Agents? PLoS One. 2016.
177. De Vooght V, Vanoirbeek JA, Luyts K, Haenen S, Nemery B, Hoet PH. Choice of mouse strain influences the outcome in a mouse model of chemical-induced asthma. PLoS One. 2010;5(9):e12581.

178. Watanabe H, Numata K, Ito T, Takagi K, Matsukawa A. Innate immune response in Th1- and Th2-dominant mouse strains. Shock. 2004;22(5):460-6.
179. Wills-Karp M, Ewart SL. Time to draw breath: asthma-susceptibility genes are identified. Nat Rev Genet. 2004;5(5):376-87.
180. Whitehead GS, Walker JK, Berman KG, Foster WM, Schwartz DA. Allergen-induced airway disease is mouse strain dependent. Am J Physiol Lung Cell Mol Physiol. 2003;285(1):L32-42.
181. Takeda K, Haczku A, Lee JJ, Irvin CG, Gelfand EW. Strain dependence of airway hyperresponsiveness reflects differences in eosinophil localization in the lung. Am J Physiol Lung Cell Mol Physiol. 2001;281(2):L394-402.
182. John RJ, Rusznak C, Ramjee M, Lamont AG, Abrahamson M, Hewitt EL. Functional effects of the inhibition of the cysteine protease activity of the major house dust mite allergen Der p 1 by a novel peptide-based inhibitor. Clin Exp Allergy. 2000;30(6):784-93.
183. Wan H, Winton HL, Soeller C, Taylor GW, Gruenert DC, Thompson PJ, et al. The transmembrane protein occludin of epithelial tight junctions is a functional target for serine peptidases from faecal pellets of Dermatophagoides pteronyssinus. Clin Exp Allergy. 2001;31(2):279-94.
184. Wan H, Winton HL, Soeller C, Gruenert DC, Thompson PJ, Cannell MB, et al. Quantitative structural and biochemical analyses of tight junction dynamics following exposure of epithelial cells to house dust mite allergen Der p 1. Clin Exp Allergy. 2000;30(5):685-98.
185. Gough L, Campbell E, Bayley D, Van Heeke G, Shakib F. Proteolytic activity of the house dust mite allergen Der p 1 enhances allergenicity in a mouse inhalation model. Clin Exp Allergy. 2003;33(8):1159-63.
186. Johansson L, Svensson L, Bergstrom U, Jacobsson-Ekman G, Arner ES, van Hage M, et al. A mouse model for in vivo tracking of the major dust mite allergen Der p 2 after inhalation. FEBS J. 2005;272(13):3449-60.
187. Shinagawa K, Kojima M. Mouse model of airway remodeling: strain differences. Am J Respir Crit Care Med. 2003;168(8):959-67.
188. Lawson JA, Chu LM, Rennie DC, Hagel L, Karunanayake CP, Pahwa P, et al. Prevalence, risk factors, and clinical outcomes of atopic and nonatopic asthma among rural children. Ann Allergy Asthma Immunol. 2017;118(3):304-10.
189. Knudsen TB, Thomsen SF, Nolte H, Backer V. A population-based clinical study of allergic and non-allergic asthma. J Asthma. 2009;46(1):91-4.
190. Bullone M, Carriero V, Bertolini F, Folino A, Mannelli A, Di Stefano A, et al. Elevated serum IgE, oral corticosteroid dependence and IL-17/22 expression in highly neutrophilic asthma. Eur Respir J. 2019;54(5).
191. Haddad A, Gaudet M, Plesa M, Allakhverdi Z, Mogas AK, Audusseau S, et al. Neutrophils from severe asthmatic patients induce epithelial to mesenchymal transition in healthy bronchial epithelial cells. Respir Res. 2019;20(1):234.
192. Ding L, Yang J, Zhang C, Zhang X, Gao P. Neutrophils Modulate Fibrogenesis in Chronic Pulmonary Diseases. Front Med (Lausanne). 2021;8:616200.
193. Foley SC, Prefontaine D, Hamid Q. Images in allergy and immunology: role of eosinophils in airway remodeling. J Allergy Clin Immunol. 2007;119(6):1563-6.
194. Piyadasa H, Altieri A, Basu S, Schwartz J, Halayko AJ, Mookherjee N. Biosignature for airway inflammation in a house dust mite-challenged murine model of allergic asthma. Biol Open. 2016;5(2):112-21.
195. Abbring S, Verheijden KAT, Diks MAP, Leusink-Muis A, Hols G, Baars T, et al. Raw Cow's Milk Prevents the Development of Airway Inflammation in a Murine House Dust Mite-Induced Asthma Model. Front Immunol. 2017;8:1045.
196. Cook DN. Role of Environmental Adjuvants in Asthma Development. Curr Allergy Asthma Rep. 2020;20(9):42.

197. Wilson RH, Maruoka S, Whitehead GS, Foley JF, Flake GP, Sever ML, et al. The Toll-like receptor 5 ligand flagellin promotes asthma by priming allergic responses to indoor allergens. Nat Med. 2012;18(11):1705-10.
198. Arae K, Morita H, Unno H, Motomura K, Toyama S, Okada N, et al. Chitin promotes antigen-specific Th2 cell-mediated murine asthma through induction of IL-33-mediated IL-1beta production by DCs. Sci Rep. 2018;8(1):11721.
199. Krysko O, Maes T, Plantinga M, Holtappels G, Imiru R, Vandenabeele P, et al. The adjuvant-like activity of staphylococcal enterotoxin B in a murine asthma model is independent of IL-1R signaling. Allergy. 2013;68(4):446-53.
200. Bachert C, Zhang N, Patou J, van Zele T, Gevaert P. Role of staphylococcal superantigens in upper airway disease. Curr Opin Allergy Clin Immunol. 2008;8(1):34-8.
201. Hellings PW, Hens G, Meyts I, Bullens D, Vanoirbeek J, Gevaert P, et al. Aggravation of bronchial eosinophilia in mice by nasal and bronchial exposure to Staphylococcus aureus enterotoxin B. Clin Exp Allergy. 2006;36(8):1063-71.
202. Kim DW, Khalmuratova R, Hur DG, Jeon SY, Kim SW, Shin HW, et al. Staphylococcus aureus enterotoxin B contributes to induction of nasal polypoid lesions in an allergic rhinosinusitis murine model. Am J Rhinol Allergy. 2011;25(6):e255-61.
203. N. Woods KN, R. Acevedo, J. Igoli, N.A. Altwaijry, J. Tusiimire, A.I. Gray, D.G. Watson, and V.A. Ferro. Natural Vaccine Adjuvants and Immunopotentiators Derived From Plants, Fungi, Marine Organisms, and Insects. Immunopotentiators in Modern Vaccines. 2017;211–229.
204. Akbari O, Stock P, Meyer E, Kronenberg M, Sidobre S, Nakayama T, et al. Essential role of NKT cells producing IL-4 and IL-13 in the development of allergen-induced airway hyperreactivity. Nat Med. 2003;9(5):582-8.
205. Jae-Ouk Kim D-HK, Woo-Sung Chang, Se-Ho Park, Sanghee Kim, Chang-Yuil Kang,. Asthma is induced by intranasal coadministration of allergen and natural killer T-cell ligand in a mouse model. Journal of allergy and clinical immunology. 2004;114.
206. Das J, Eynott P, Jupp R, Bothwell A, Van Kaer L, Shi Y, et al. Natural killer T cells and CD8+ T cells are dispensable for T cell-dependent allergic airway inflammation. Nat Med. 2006;12(12):1345-6; author reply 7.
207. Borg NA, Wun KS, Kjer-Nielsen L, Wilce MC, Pellicci DG, Koh R, et al. CD1d-lipid-antigen recognition by the semi-invariant NKT T-cell receptor. Nature. 2007;448(7149):44-9.
208. Matangkasombut P, Pichavant M, Dekruyff RH, Umetsu DT. Natural killer T cells and the regulation of asthma. Mucosal Immunol. 2009;2(5):383-92.
209. Brown JR, Kleimberg J, Marini M, Sun G, Bellini A, Mattoli S. Kinetics of eotaxin expression and its relationship to eosinophil accumulation and activation in bronchial biopsies and bronchoalveolar lavage (BAL) of asthmatic patients after allergen inhalation. Clin Exp Immunol. 1998;114(2):137-46.
210. George L, Brightling CE. Eosinophilic airway inflammation: role in asthma and chronic obstructive pulmonary disease. Ther Adv Chronic Dis. 2016;7(1):34-51.
211. Lambrecht BN, Hammad H, Fahy JV. The Cytokines of Asthma. Immunity. 2019;50(4):975-91.
212. Snapper CM, Finkelman FD, Paul WE. Regulation of IgG1 and IgE production by interleukin 4. Immunol Rev. 1988;102:51-75.
213. Haniuda K, Kitamura D. Multi-faceted regulation of IgE production and humoral memory formation. Allergol Int. 2021;70(2):163-8.
214. Truyen E, Coteur L, Dilissen E, Overbergh L, Dupont LJ, Ceuppens JL, et al. Evaluation of airway inflammation by quantitative Th1/Th2 cytokine mRNA measurement in sputum of asthma patients. Thorax. 2006;61(3):202-8.
215. Magnan AO, Mely LG, Camilla CA, Badier MM, Montero-Julian FA, Guillot CM, et al. Assessment of the Th1/Th2 paradigm in whole blood in atopy and asthma. Increased IFN-gamma-producing CD8(+) T cells in asthma. Am J Respir Crit Care Med. 2000;161(6):1790-6.

216. Sze E, Bhalla A, Nair P. Mechanisms and therapeutic strategies for non-T2 asthma. Allergy. 2020;75(2):311-25.
217. Linden A. Role of interleukin-17 and the neutrophil in asthma. Int Arch Allergy Immunol. 2001;126(3):179-84.
218. Wenzel SE, Schwartz LB, Langmack EL, Halliday JL, Trudeau JB, Gibbs RL, et al. Evidence that severe asthma can be divided pathologically into two inflammatory subtypes with distinct physiologic and clinical characteristics. Am J Respir Crit Care Med. 1999;160(3):1001-8.
219. The ENFUMOSA cross-sectional European multicentre study of the clinical phenotype of chronic severe asthma. European Network for Understanding Mechanisms of Severe Asthma. Eur Respir J. 2003;22(3):470-7.
220. ten Brinke A, Zwinderman AH, Sterk PJ, Rabe KF, Bel EH. Factors associated with persistent airflow limitation in severe asthma. Am J Respir Crit Care Med. 2001;164(5):744-8.
221. Louis R, Lau LC, Bron AO, Roldaan AC, Radermecker M, Djukanovic R. The relationship between airways inflammation and asthma severity. Am J Respir Crit Care Med. 2000;161(1):9-16.
222. Balkissoon RC BS, Rhodes D, Trudeau JB, Wenzel S. Eosinophils persist in the distal lung of severe asthma despite low numbers in proximal airways. American Thoracic Society; San Diego, CA, USA2006.
223. Southam DS, Ellis R, Wattie J, Inman MD. Components of airway hyperresponsiveness and their associations with inflammation and remodeling in mice. J Allergy Clin Immunol. 2007;119(4):848-54.
224. Berdnikovs S. The twilight zone: plasticity and mixed ontogeny of neutrophil and eosinophil granulocyte subsets. Semin Immunopathol. 2021;43(3):337-46.
225. Panettieri RA, Jr. Neutrophilic and Pauci-immune Phenotypes in Severe Asthma. Immunol Allergy Clin North Am. 2016;36(3):569-79.
226. Galli SJ, Borregaard N, Wynn TA. Phenotypic and functional plasticity of cells of innate immunity: macrophages, mast cells and neutrophils. Nat Immunol. 2011;12(11):1035-44.
227. Lee PY, Wang JX, Parisini E, Dascher CC, Nigrovic PA. Ly6 family proteins in neutrophil biology. J Leukoc Biol. 2013;94(4):585-94.
228. Gumley TP, McKenzie IF, Sandrin MS. Tissue expression, structure and function of the murine Ly-6 family of molecules. Immunol Cell Biol. 1995;73(4):277-96.
229. Fleming TJ, Fleming ML, Malek TR. Selective expression of Ly-6G on myeloid lineage cells in mouse bone marrow. RB6-8C5 mAb to granulocyte-differentiation antigen (Gr-1) detects members of the Ly-6 family. J Immunol. 1993;151(5):2399-408.
230. Wang JX, Bair AM, King SL, Shnayder R, Huang YF, Shieh CC, et al. Ly6G ligation blocks recruitment of neutrophils via a beta2-integrin-dependent mechanism. Blood. 2012;120(7):1489-98.
231. Leliefeld PH, Koenderman L, Pillay J. How Neutrophils Shape Adaptive Immune Responses. Front Immunol. 2015;6:471.
232. Pillay J, Tak T, Kamp VM, Koenderman L. Immune suppression by neutrophils and granulocytic myeloid-derived suppressor cells: similarities and differences. Cell Mol Life Sci. 2013;70(20):3813-27.
233. Talmadge JE, Gabrilovich DI. History of myeloid-derived suppressor cells. Nat Rev Cancer. 2013;13(10):739-52.
234. Gabrilovich DI, Nagaraj S. Myeloid-derived suppressor cells as regulators of the immune system. Nat Rev Immunol. 2009;9(3):162-74.
235. Nowroozilarki N, Oz HH, Schroth C, Hector A, Nurnberg B, Hartl D, et al. Anti-inflammatory role of CD11b(+)Ly6G(+) neutrophilic cells in allergic airway inflammation in mice. Immunol Lett. 2018;204:67-74.

236. Ma H, Guo S, Luo Y, Wang Y, Wang H, He J, et al. MicroRNA-20b promotes the accumulation of CD11b+Ly6G+Ly6C(low) myeloid-derived suppressor cells in asthmatic mice. Cent Eur J Immunol. 2017;42(1):30-8.
237. Deniset JF, Surewaard BG, Lee WY, Kubes P. Splenic Ly6G(high) mature and Ly6G(int) immature neutrophils contribute to eradication of S. pneumoniae. J Exp Med. 2017;214(5):1333-50.
238. Casson CN, Doerner JL, Copenhaver AM, Ramirez J, Holmgren AM, Boyer MA, et al. Neutrophils and Ly6Chi monocytes collaborate in generating an optimal cytokine response that protects against pulmonary Legionella pneumophila infection. PLoS Pathog. 2017;13(4):e1006309.
239. Yeatts KB, E. Svendsen, N. E. Alexis, W. Reed, S. Harder, J. Lay, P A. Bromberg, L Neas, AND R B. Devlin. CD11B EXPRESSION IN THE AIRWAY IS ASSOCIATED WITH ASTHMA SEVERITY, AIRWAY INFLAMMATION, AND REDUCED PERCENTAGE OF CD-54POSITIVE BLOOD LYMPHOCYTES IN ASTHMATICS. American Thoracic Society; San Diego, CA2005.
240. Mann BS, Chung KF. Blood neutrophil activation markers in severe asthma: lack of inhibition by prednisolone therapy. Respir Res. 2006;7:59.
241. Mesnil C, Raulier S, Paulissen G, Xiao X, Birrell MA, Pirottin D, et al. Lung-resident eosinophils represent a distinct regulatory eosinophil subset. J Clin Invest. 2016;126(9):3279-95.
242. Kanda A, Yun Y, Bui DV, Nguyen LM, Kobayashi Y, Suzuki K, et al. The multiple functions and subpopulations of eosinophils in tissues under steady-state and pathological conditions. Allergol Int. 2021;70(1):9-18.
243. Shiina T, Inoko H, Kulski JK. An update of the HLA genomic region, locus information and disease associations: 2004. Tissue Antigens. 2004;64(6):631-49.
244. Vercelli D. Discovering susceptibility genes for asthma and allergy. Nat Rev Immunol. 2008;8(3):169-82.
245. Ober C, Hoffjan S. Asthma genetics 2006: the long and winding road to gene discovery. Genes Immun. 2006;7(2):95-100.
246. Hersh CP, Raby BA, Soto-Quiros ME, Murphy AJ, Avila L, Lasky-Su J, et al. Comprehensive testing of positionally cloned asthma genes in two populations. Am J Respir Crit Care Med. 2007;176(9):849-57.
247. Humbles AA, Lu B, Nilsson CA, Lilly C, Israel E, Fujiwara Y, et al. A role for the C3a anaphylatoxin receptor in the effector phase of asthma. Nature. 2000;406(6799):998-1001.
248. Walters DM, Breysse PN, Schofield B, Wills-Karp M. Complement factor 3 mediates particulate matter-induced airway hyperresponsiveness. Am J Respir Cell Mol Biol. 2002;27(4):413-8.
249. Polack FP, Teng MN, Collins PL, Prince GA, Exner M, Regele H, et al. A role for immune complexes in enhanced respiratory syncytial virus disease. J Exp Med. 2002;196(6):859-65.
250. Donato R. S100: a multigenic family of calcium-modulated proteins of the EF-hand type with intracellular and extracellular functional roles. Int J Biochem Cell Biol. 2001;33(7):637-68.
251. Lee TH, Jang AS, Park JS, Kim TH, Choi YS, Shin HR, et al. Elevation of S100 calcium binding protein A9 in sputum of neutrophilic inflammation in severe uncontrolled asthma. Ann Allergy Asthma Immunol. 2013;111(4):268-75 e1.
252. Komada T, Araki R, Nakatani K, Yada I, Naka M, Tanaka T. Novel specific chemtactic receptor for S100L protein on guinea pig eosinophils. Biochem Biophys Res Commun. 1996;220(3):871-4.
253. Passey RJ, Xu K, Hume DA, Geczy CL. S100A8: emerging functions and regulation. J Leukoc Biol. 1999;66(4):549-56.

254. Lackmann M, Rajasekariah P, Iismaa SE, Jones G, Cornish CJ, Hu S, et al. Identification of a chemotactic domain of the pro-inflammatory S100 protein CP-10. J Immunol. 1993;150(7):2981-91.
255. Cornish CJ, Devery JM, Poronnik P, Lackmann M, Cook DI, Geczy CL. S100 protein CP-10 stimulates myeloid cell chemotaxis without activation. J Cell Physiol. 1996;166(2):427-37.
256. Hofmann MA, Drury S, Fu C, Qu W, Taguchi A, Lu Y, et al. RAGE mediates a novel proinflammatory axis: a central cell surface receptor for S100/calgranulin polypeptides. Cell. 1999;97(7):889-901.
257. Cookson W. The immunogenetics of asthma and eczema: a new focus on the epithelium. Nat Rev Immunol. 2004;4(12):978-88.

SUPPLEMENTARY DATA

Table S1. R_L responsiveness to 50 mg/mL MCh airway challenge in High or Low doses of HDM.

	Treatment				
MhC	**SS**	**Low 4W**	**High 4W**	**Low 6W**	**High 6W**
50 mg/mL	4.259±0.544	15.21±4.215 ******P<0.0001***	11.17±3.799 ****P=0.0140***	5.939±1.434 *P=0.9551*	3.398±0.242 *P=0.9951*

Data are mean ± standard error of the mean. C57BL/6J data are shown. SS: respective to sensitized *i.n* with saline solution; Low: respective to sensitized *i.n* 7,5 µg/mL HDM; High: respective to sensitized *i.n* 15 µg/mL HDM; 4W: respective to 4 weeks of sensitization; 6W: respective to 6 weeks of sensitization. P values are from post-2-ANOVA multiple comparisons followed by Tukey's post hoc test for inter-group comparisons. Group size: SS, n=7; Low 6W, n=8; High 6W, n=11; Low/High 4W, n=12. **P*<0.05; ****P<0.0002*.

Table S2. Frequencies of lung leucocyte populations from Low or High doses of HDM.

	Treatment				
% Populations	**SS**	**Low 4W**	**High 4W**	**Low 6W**	**High 6W**
CD3	13.03±1.291	19.58±1.362 *P=0.0911*	22.97±1.387 ******P=0.0005***	26.6±1.796 *******P<0.0001***	24.97±2.739 ******P=0.0002***
CD4	6.687±0.8433	11.58±0.9855 ****P=0.0142***	11±1.020 ****P=0.0245***	10.21±1.066 *P=0.1941*	8.108±1.073 *P=9015*
CD8	6.091±0.7282	4.504±0.8023 *P=0.9787*	9.093±1.92 *P=0.7759*	9.648±2.208 *P=0.7529*	11.61±3.097 *P=0.3496*
CD19	4.282±0.4047	8.039±1.518 *P=0.1902*	5.698±0.6174 *P=0.8990*	5.253±1.511 *P=0.9817*	6.165±1.478 *P=0.8125*
MacroMon	40.91±3.136	23.22±3.532 *******P<0.001***	15.47±1.254 *******P<0.0001***	12.42±2.094 *******P<0.0001***	15.64±1.664 *******P<0.0001***
Neutrophils	7.672±1.063	14.93±2.221 *P=0.2363*	21.18±2.058 ******P=0.0009***	16.34±2.891 *P=0.1665*	19.23±3.631 ****P=0.0226***
Eosinophils	0.04571±0.03637	2.343±0.6555 *P=0.1473*	3.255±0.6935 ****P=0.0101***	0.3173±0.08752 *P=0.9989*	0.4358±0.1376 *P=0.9954*

Data are mean ± standard error of the mean. C57BL/6J data are shown. SS: respective to sensitized *i.n* with saline solution; Low: respective to sensitized *i.n* 7,5 µg/mL HDM; High: respective to sensitized *i.n* 15 µg/mL HDM; 4W: respective to 4 weeks of sensitization; 6W: respective to 6 weeks of sensitization. P values are from one way ANOVA followed by Tukey's post hoc test for inter-group comparisons. Group size: SS n=13; Low 4W= 16; High 4W n=22; Low/High 6W, n=12. **P<0.05*; ****P<0.0002*; *****P<0.0001*.

Table S3. Absolute numbers analysis of lung leucocyte populations from Low or High doses of HDM.

	Treatment				
Absolute Nº	**SS**	**Low 4W**	**High 4W**	**Low 6W**	**High 6W**
CD3	92676±15575	314112±75463 *P=0.7027*	757705±92194 ******P<0.0006***	626013±111627 ****P=0.00152***	720786±161413 *****P=0.0026***
CD4	48258±8333	198192±39839 ****P=0.0186***	360761±61184 ******P=0.0006***	258310±57947 ****P=0.0227***	210085±31977 *****P=0.0013***
CD8	43958±7931	55395±8470 *P>0.9999*	2888852±77311 ****P=0.0431***	258071±79720 *P=0.1303*	78373±16100 *P=0.9964*
CD19	32274±6591	123614±36578 *P=0.2645*	192068±39073 *****P=0.0036***	50711±18187 *P=0.9943*	54102±12193 *P=0.9899*
MacroMon	315936±80436	365199±85279 *P=0.9955*	491892±80645 *P=0.6188*	283684±83457 *P=0.9991*	366741±89727 *P=0.9949*
Neutrophils	59527±12377	234436±42820 *P=0.7081*	579623±79643 *****P=0.0018***	457869±98846 ****P=0.0382***	693419±138397 ******P=0.0002***
Eosinophils	12695±5501	24799±6770 *P=0.9803*	89160±21745 *****P=0.0029***	4237±971.2 *P=0.9952*	14611±2523 *P>0.9999*

Data are mean ± standard error of the mean. C57BL/6J data are shown. SS: respective to sensitized *i.n* with saline solution; Low: respective to sensitized *i.n* 7,5 µg/mL HDM; High: respective to sensitized *i.n* 15 µg/mL HDM; 4W: respective to 4 weeks of sensitization; 6W: respective to 6 weeks of sensitization. Group size: SS n=12; Low 4W n=16; High 4W n=20; Low/High 6W n=12. **P<0.05*; ***P<0.0021*; ****P<0.0002*. P values are from one way ANOVA followed by Tukey's post hoc test for inter-group comparisons.

Table S4. BAL cytokine determination from Low or High doses of HDM.

	Treatment				
CK levels	**SS**	**Low 4W**	**High 4W**	**Low 6W**	**High 6W**
IgE	23.87±10.02	1543±342.9 *******P<0.0001***	1021±188.9 ******P=0.0008***	779.3±142.3 ****P=0.0448***	736.7±200.2 *P=0.0604*
IL17A	12.58±5.254	122.5±40.73 ****P=0.0434***	135.8±57.58 ****P=0.0421***	122±9.183 ****P=0.0115***	213.9±68.5 ****P=0.0014***
IL4	0	43±18.69 ****P=0.0286***	36.61±13.97 ****P=0.0286***		
IgG	91.87±40.6	43901±12105 ****P=0.0317***	51034±11580 ****P=0.0308***	81836±2119 ******P=0.0303***	86353±1949 ****P=0.0003***
sIgE	0.07925±0.002750	0.6865±0.1499 *****P=0.0286***	0.3775±0.01545 ****P=0.0286***		
sIgA	0.1575±0.07666	0.4480±0.04511 *****P=0.084***	0.4297±0.03536 *****P=0.0071***		

Data are mean ± standard error of the mean. C57BL/6J data are shown. SS: respective to sensitized *i.n* with saline solution; Low: respective to sensitized *i.n* 7,5 µg/mL HDM; High: respective to sensitized *i.n* 15 µg/mL HDM; 4W: respective to 4 weeks of sensitization; 6W: respective to 6 weeks of sensitization. Group size: SS n=9; Low 4W n=11; High 4W n=13; Low/High 6W n=6. **P<0.05*; ***P<0.0021*; ****P<0.0002*; *****P<0.0001*. P values are one way ANOVA followed by Kruskal Wallis post hoc test or Mann-Whitney test for inter-group comparisons.

Table S5. R_L responsiveness to 50 mg/mL MCh airway challenge from HDM alone or with adjuvants.

	Treatment			
MhC	**SS**	**HDM**	**HDM+SEB**	**HDM+ α-Galcer**
50 mg/mL	4.259±0.544	11.174±3.799 ***P=0.0098**	8.471±2.886 *P=0.5229*	4.258±0.602 *P>0.9999*

Data are mean ± standard error of the mean. C57BL/6J data are shown. SS: respective to sensitized *i.n* with saline solution; HDM: respective to sensitized *i.n* 15 µg/mL HDM; HDM+SEB: representative to combination of HDM together with 2mg/mL of *Staphylococcus aureus enterotoxin-B*; HDM+ α-Galcer: representative to HDM together with 20 ng/mL of *alpha-Galceramyde*. Group size: SS n=8; HDM n=12; HDM+SEB = 8; HDM+ α-Galcer = 4. **P<0.05*. P values are from post-2-ANOVA multiple comparisons followed by Bonferroni's post hoc test for inter-group comparisons.

Table S6. Frequencies of lung leucocyte populations from HDM alone or with adjuvants.

	Treatment			
% Populations	**SS**	**HDM**	**HDM+SEB**	**HDM+ α-Galcer**
CD3	13.03±1.291	22.97±1.387 ****P<0.0001	12.82±0.9794 *P=0.9997*	52.52±2.004 ****P<0.0001
			+++P=0.0001	++++P<0.0001
CD4	6.687±0.8433	11±1.020 *P=0.0253	6.529±0.3163 *P=0.9998*	20.47±3.551 ****P<0.0001
				+++P=0.0008
CD8	6.091±0.7282	9.093±1.923 *P=0.5993*	5.599±1.202 *P=0.9985*	32.03±3.591 ****P<0.0001
				++++P<0.0001
CD19	4.282±0.4047	5.698±0.6174 *P>0.9999*	9.885±2.780 *P=0.0288	13.11±1.579 **P=0.0035
				+P=0.0117
MacroMon	40.91±3.136	15.47±1.254 ****P<0.0001	20.01±3.797 *P=0.0223	7.095±5.199 ***P=0.0005
Neutrophils	7.672±1.063	21.18±2.058 ***P=0.0003	18.91±4.373 *P=0.0295	3.570±1.091 *P=0.8402*
				++P=0.0029
Eosinophils	0.0457±0.0363	3.255±0.6935 **P=0.0060	3.571±1.246 *P=0.0108	0.5175±0.3151 *P>0.9999*

Data are mean ± standard error of the mean. C57BL/6J data are shown. SS: respective to sensitized *i.n* with saline solution; HDM: respective to sensitized *i.n* 15 µg/mL HDM; HDM+SEB: representative to combination of HDM together with 2mg/mL of SEB; HDM+ α-Galcer: representative to HDM together with 20 ng/mL of α-Galcer. Group size: SS n=13; HDM n=22; HDM+SEB n=8; HDM+ α-Galcer n=4. **P<0.05*; ***P<0.0021*; ****P<0.0002*; *****P<0.0001*. P values are from one way ANOVA followed by Tukey or Kruskal Wallis post hoc test for inter-group comparisons. * compared with SS group; + compared with HDM.

Table S7. Absolute numbers analysis of lung leucocyte populations from HDM alone or with adjuvants.

	Treatment			
Absolute Nº	**SS**	**HDM**	**HDM+SEB**	**HDM+ α-Galcer**
CD3	92676±15575	757705±92194 *****P=0.0059***	403918±155713 *P=0.7220*	5320021±704315 *******P<0.0001***
				++++P<0.0001
CD4	48258±8333	360761±61184 ******P=0.0004***	164987±58828 *P=0.8709*	2131033±516592 *******P<0.0001***
CD8	43958±7931	288852±77311 ****P=0.0419***	221469±108351 *P>0.9999*	3186650±480028 ******P=0.0003***
CD19	32274±6591	227568±51246 *****P=0.0065***	454701±175031 ****P=0.0120***	1276962±116834 *******P<0.0001***
MacroMon	315936±80436	491892±80645 *P=0.7684*	606070±169461 *P=0.7450*	799287±661658 *P=0.3480*
Neutrophils	59527±12377	579623±79643 *******P<0.0001***	231479±78986 *P=0.6845*	394616±142832 *P=0.1523*
Eosinophils	12695±5501	89160±21745 *P=0.1937*	606070±169461 *****P=0.0016***	22311±12957 *P>0.9999*

Data are mean ± standard error of the mean. C57BL/6J data are shown. SS: respective to sensitized *i.n* with saline solution; HDM: respective to sensitized *i.n* 15 µg/mL HDM; HDM+SEB: representative to combination of HDM together with 2mg/mL of SEB; HDM+ α-Galcer: representative to HDM together with 20 ng/mL of α-Galcer. Group size: SS n=12; HDM n=20; HDM+SEB = 8; HDM+ α-Galcer = 4. **P<0.05*; ***P<0.0021*; ****P<0.0002*; *****P<0.0001*. P values are from one way ANOVA followed by Bonferroni or Kruskal Wallis post hoc test for inter-group comparisons. * Compared with SS group; + compared with HDM.

Table S8. R_L responsiveness to MCh airway challenge from H4 or H20 treatment.

	Treatment		
MhC	**SS**	**H4**	**H20**
0 mg/mL	1.465±0.079	1.193±0.047 ***P=0.0284***	1.705±0.252 *P=0.7677*
6.25 mg/mL	1.853±0.081	2.342±0.138 ***P=0.0252***	22.879±0.434 *P=0.0684*
25 mg/mL	2.560±0.283	6.754±2.863 *P=0.3885*	5.336±0.716 ****P=0.0076***
50 mg/mL	3.875±0.444	20.88±5.732 ***P=0.05***	18.84±3.397 ****P=0.0033***

Data are mean ± standard error of the mean. C57BL/6J data are shown. SS: respective to saline solution; H4: respective to HDM with protein degradation; H20: representative to whole extract of HDM. Group size: SS n=7; H4 n=7; H20 n=10. **P<0.05*; ***P<0.002.* P values are from post-2-ANOVA multiple comparisons followed by Tukey's post hoc test for inter-group comparisons.

Table S9. Frequencies of lung leucocyte populations from H4 or H20 treatment.

	Treatment			
% Populations	**SS**	**H4**	**H20**	**H4vsH20**
CD3	11.19±0.8124	15.52±1.587 ****P=0.0487***	11.29±0.8528 *P=0.9979*	****P=0.0209***
CD4	5.864±0.7493	10.36±1.288 *****P=0.0051***	7.897±0.5967 ****P=0,0233***	*P=0.1048*
CD8	5.2421±0.5187	2.838±0.3594 *****P=0.0011***	2.343±0.3290 *******P<0.0001***	*P=0.6346*
CD19	4.282±0.4047	4.998±0.6221 *P=0.8316*	7.333±0.9037 ****P=0.0242***	*P=0.1023*
MacroMon	40.19±3.688	20.81±2.413 *****P=0.0003**	21.08±2.534 ******P<0.0001**	P=0.9977
Neutrophils	7.256±1.183	29.14±2.059 *******P<0.0001***	16.95±1.888 *****P=0.0046***	*****P=0.0002***
Eosinophils	0.2238±0.1808	0.6430±0.1005 *****P=0,0056***	11.61±2.230 *******P<0.0001***	******P=0.0009***

Data are mean ± standard error of the mean. C57BL/6J data are shown. SS: respective to saline solution; H4: respective to HDM with protein degradation; H20: representative to whole extract of HDM. Group size: SS n=10; H4 n=12; H20 n=20. **P<0.05*; ***P<0.0021*; ****P<0.0002*; *****P<0.0001.* P values are from one way ANOVA followed by Tukey or Kruskal Wallis post hoc test for inter-group comparisons.

Table S10. Absolute numbers analysis of lung leucocyte populations from H4 or H20 treatment.

	Treatment			
Absolute Nº	**SS**	**H4**	**H20**	**H4vsH20**
CD3	92676±15575	524020±79909 ******P<0.0001**	180624±26686 P=0.1413	****P=0.0053**
CD4	48258±8333	357063±62108 ******P<0.0001**	125330±17326 ***P=0.0294**	***P=0.0181**
CD8	43958±7931	98736±17898 ***P=0.0388**	31560±4681 P=0.4640	****P=0.0089**
CD19	32274±6591	169342±31564 ****P=0.0033**	145911±29034 ****P=0.0030**	P=0.9275
MacroMon	248691±48350	751192±100894 ****P=0.0011**	280821±56025 P=0.9614	****P=0.0021**
Neutrophils	59527±12377	895314±106263 ******P<0.0001**	301744±51724 *****P=0.0005**	*****P=0.0004**
Eosinophils	12695±5501	21438±5008 P=0.8557	303255±78873 *****P<0.0001**	****P=0.0059**

Data are mean ± standard error of the mean. C57BL/6J data are shown. SS: respective to saline solution; H4: respective to HDM with protein degradation; H20: representative to whole extract of HDM. Group size: SS n=10; H4 n=12; H20 n=20. **P<0.05*; ***P<0.0021*; ****P<0.0002*; *****P<0.0001*. P values are from one way ANOVA followed by Bonferroni or Kruskal Wallis post hoc test for inter-group comparisons.

Table S11. Cells per milligram analysis of lung leucocyte populations from H4 or H20 treatment.

	Treatment	
c/mg	**H4**	**H20**
CD3	1611±326.1	638.5±142.6
	***P=0.0104**	
CD4	1063±232.6	470.9±114.7
	***P=0.0290**	
CD8	354.9±175.7	96.93±53.65
	****P=0.0055**	
CD19	589.6±131.5	405.7±100.4
	P=0.2782	
MacroMon	2672±520.3	1943±486.6
	P=0.3171	
Neutrophils	3130±482.3	1201±168.7
	****P=0.0010**	
Eosinophils	95.10±23.76	1004±233
	****P=0.0013**	

Data are mean ± standard error of the mean. C57BL/6J data are shown. H4: respective to HDM with protein degradation; H20: representative to whole extract of HDM. (n=12). **P<0.05*; ***P<0.0021*; ****P<0.0002*; *****P<0.0001*. P values are from Unpaired t-test for inter-group comparisons.

Table S12. BAL cytokine determination from H4 or H20 treatment.

	Treatment			
CK levels	**SS**	**H4**	**H20**	**H4vsH20**
IgE	23.87±10.02	408.7±66.86 ****P=0.0012**	420.2±114.3 ****P=0.0037**	P>0.9999
IFNg	7.201±2.106	24.74±6.434 ***P=0.0193**	7.908±2.184 P=0.9926	***P=0.0307**
IL17A	8.026±2.980	34.88±6.354 ****P=0.0040**	11.47±1.649 P>0.9999	***P=0.0394**
IL13	12.02±4.917	22.31±0.7238 ***P=0.0495**	18.69±0.4181 P>0.9999	****P=0.0100**
IL4	0±0	1.811±0.5488 *****P=0.0008**		
IgG	62.31±31.57	190.2±6.067 ***P=0.0115**	174.1±11.35 ***P=0.0247**	P=0,5330
sIgE	0.1561±0.03787	0.5703±0.1225 ****P=0.014**	0.3370±0.02815 **P=0.1365**	P=0.0523
sIgA	0.1050±0.05876	0.5128±0.09473 ****P=0.011**	0.4201±0.03722 ****P=0.0095**	P=0.3597

Data are mean ± standard error of the mean. C57BL/6J data are shown. SS: respective to saline solution; H4: respective to HDM with protein degradation; H20: representative to whole extract of HDM. (n=9). **P<0.05*; ***P<0.0021*; ****P<0.0002*; *****P<0.0001. P* values are from one way ANOVA followed by Tukey's post hoc test or unpaired t test (to sIgE and sIgA) for inter-group comparisons.

Table S13. Cytokine production analyses by CD4+ and CD8+ T cells in lung from H4 and H20 treatments.

	Treatment			
	HDM		PMA+IO	
CD4	**H4**	**H20**	**H4**	**H20**
IL10	5.323±1.155	2.097±0.5668	6.860±0.7910	2.907±0.8497
	P=0.0662		***P=0.0271***	
IL17A	16.97±0.7623	14.38±2.953	17.30±1.790	11.34±0.9040
	P=0.4441		***P=0.0411***	
IFNg	2.083±0.1220	0.4867±0.1146	3.470±0.4996	2.163±0.7993
	****P=0.0007***		*P=0.2379*	
	HDM		**PMA+IO**	
CD8	**H4**	**H20**	**H4**	**H20**
IL10	7.527±1.448	1.620±0.5552	14.24±2.525	4.220
	P=0.0190		***P=0.0182***	
IL17A	15.20±1.626	8.270±1.971	15.25±2.165	7.907±1.768
	P=0.0534		*P=0.0584*	
IFNg	3.490±0.3272	0.7267±0.1434	7.950±0.5312	12.36±3.331
	P=0.0015		*P=0.2614*	

Data are mean ± standard error of the mean. C57BL/6J data are shown. H4: respective to HDM with protein degradation; H20: representative to whole extract of HDM. Lymphocytes from asthmatic lung mice were restimulated in vitro with PMA and IO (20 ng/mL and 200 ng/mL) (PMA/IO) or HDM (3 µg/mL) during 12 hours and after analyzed by flow cytometry. (n=3). **P<0.05*; ***P<0.0021*; ****P<0.0002*; *****P<0.0001*. P values are from Unpaired t test for inter-group comparisons.

Table S14. Quantitative morphology of lungs from H4 and H20 treatments.

	Treatment		
	H4	**H20**	**H4vsH20**
Infiltrated cells	15.62±2.482	7.007±1.555	***P=0.0096**
Mucoid mass	0.033±0.02427	3.606±0.9634	***P=0.006**
ECM mass	1.752±0.2841	1.011±0.1784	**P=0.0379**
ASM mass	5.897±0.3551	8.637±0.6545	***P=0.0024**
ASM intensity	72649±11541	112504±13411	**P=0.0409**

Data are mean ± standard error of the mean. C57BL/6J data are shown.H4: respective to HDM with protein degradation; H20: representative to whole extract of HDM. Infiltrated cells n=9; Mucoid mass n=5; Extracellular matrix (ECM) mass n=12; alpha smooth muscle cell (ASM) mass n=6. **P<0.05*; ***P<0.0021*. P values are from Mann-Whitney or Unpaired t test for inter-group comparisons.

Table S15. Quantitative morphology and cell infiltrated correlation from H4 and H20 treatments.

	Treatment	
	H4	H20
Infiltration Neutrophils	*P=0.0015*	
ASM Neutrophils	*P=0.0462*	
Fibrosis Neutrophils	*P=0.0462*	
Mucus Eosinophils	*P=0.0462*	

Data are mean ± standard error of the mean. C57BL/6J data are shown. H4: respective to HDM with protein degradation; H20: representative to whole extract of HDM. Infiltration correlated with neutrophils n=6; alpha smooth muscle cell (ASM) mass correlated with neutrophils n=9; Fibrosis correlated with neutrophils n=12; Mucus correlated with eosinophils n=5. *$P<0.05$; **$P<0.0021$. P values are from Pearson r correlation.

Table S16. Frequencies of lung leucocyte populations during asthma development from H4 or H20 model.

	CD3		CD4		CD8		CD19		MacroMon		Neu		Eo	
%	H4	H20	H4	H20	H4	H20	H4	H20	H4	H20	H4	H20	H4	H20
1	4.490±0.396	5.413±0.989	2.413±0.415	3.150±0.592	1.680±0.142	1.647±0.291	0.987±0.124	3.547±0.644	7.907±1.814	46.653±9.391	61.973±5.680	36.140±16.039	3.067±0.909	19.730±5.747
	P>0,9999		*P>0,9999*		*P>0,9999*		*P=0,6913*		*P=0,6430*		***P=0,0119***		****P=0,0051***	
2	13.970±0.596	6.950±0.306	5.3±0.533	4.120±0.150	5.897±0.277	2.340±0.115	1.620±0.361	4.903±0.453	24.607±3.214	48.407±1.452	23.117±4.646	20.423±0.908	0.927±0.038	4.940±0.502
	P=0,0380		*P>0,9999*		*****P<0,0001***		*P=0,0719*		*P=0,1091*		*P>0,9999*		*P>0,9999*	
3	4.063±0.783	11.137±2.767	2.127±0.456	7.030±2.163	1.263±0.238	2.933±0.386	0.337±0.041	3.457±0.244	13.543±3.853	17.980±5.574	46.023±7.132	20.870±5.310	3.693±0.874	16.770±3.720
	P=0,0355		*P=0,2145*		*P=0,0659*		*P=0,0655*		*P>0,9999*		***P=0,0158***		*P=0,0575*	
4	21.877±1.455	15.813±1.754	12.223±0.787	10.5±1.091	6.1±0.970	3.987±0.421	3.680±0.070	4.733±0.639	13.307±2.795	16.830	18.463±2.253	14.790±2.135	5.713±0.379	22.5±3.321
	P=0,1221		*P>0,9999*		****P=0,0067***		*P>0,9999*		*P>0,9999*		*P=0,0158*		****P=0,0046***	
5	15.157±1.092	10.883±0.826	10.420±1.031	7.270±0.681	2.727±0.511	2.733±0.132	4.310±0.085	4.490±0.548	15.373±4.171	9.437±1.058	30.933±3.207	11.583±1.829	4.920±1.074	34.407±3.346
	P=0,8168		*P>0,9999*		*P>0,9999*		*P>0,9999*		*P>0,9999*		*P=0,1443*		*****P<0,0001***	
6	15.973±3.356	9.553±0.670	10.853±3.312	7±0.789	3.003±0.267	1.447±0.299	4.9±1.920	3.253±0.672	19.933±2.003	7.777±2.431	26.937±4.291	9.020±2.756	2.363±0.754	44.610±3.036
	P=0,0799		*P=0,7398*		*P=0,1126*		*P>0,9999*		*P=0,2524*		*P=0,2366*		*****P<0,0001***	
7	28.640±1.911	8.940±0.826	21.243±2.299	6.417±0.602	3.853±0.332	1.667±0.231	9.760±0.528	4.460±0.613	28.923	11.580±1.547	13.943±3.002	11.910±3.978	1.653±0.427	42.370±5.633
	****P<0,0001***		*****P<0,0001***		****P=0,0045***		***P=0,0394***		*P=0,1932*		*P>0,9999*		*****P<0,0001***	
8	22.453±1.341	16.513±1.229	17.397±1.328	11.723±0.935	3.473±0.382	2.963±0.649	8.273±1.582	5.687±2.6	26.537±5.362	19.287±13.339	13.910±3.160	4.603±0.895	2.250±0.337	28.073±7.221
	P=0,1410		*P=0,0776*		*P>0,9999*		*P>0,9999*		*P>0,9999*		*P>0,9999*		*****P<0,0001***	
9	22.577±0.738	8.850±0.473	15.437±0.370	6.720±0.098	5.287±0.228	1.303±0.390	9.113±1.278	6.15±1.051	10.843±2.164	8.577±3.230	22.097±1.006	13.157±1.084	1.433±0.105	47.150±2.8
	*****P<0,0001***		****P=0,0007***		****P<0,0001***		*P>0,9999*		*P>0,9999*		*P>0,9999*		*****P<0,0001***	
10	19.660±2.755	9.693±1.096	13.340±2.350	6.543±0.847	4.387±0.632	1.267±0.368	7.377±0.791	9.627±3.152	18.447±2.171	11.967±2.4	27.697±1.781	16.957±1.052	0.930±0.146	31.283±2.632
	****P=0.0006***		***P=0,0152***		***P=0,0002***		*P>0,9999*		*P>0,9999*		*P>0,9999*		*****P<0,0001***	

11	21.663±0.788	7.483±2.166	18.173±1.062	5.453±1.736	3.173±0.469	1.267±0.368	7.917±0.791	6.957±1.045	21.277±3.576	23.730±5.759	29.663±5.185	17.750±3.784	1.073±0.192	22.137±3.659
	****P<0,0001		****P<0,0001		****P=0,0201		P>0,9999		P>0,9999		P>0,9999		***P=0,0002	
12	8.783±1.381	7.610±0.376	6.377±1.078	5.667±0.619	2.313±0.313	1.157±0.221	3.143±1.074	6.357±1.096	16.980±4.292	29.157±1.925	49.797±6.877	19.883±8.097	0.6±0.035	17.420±4.630
	P>0,9999		P>0,9999		P=0,6210		P>0,9999		P>0,9999		**P=0,0021		**P=0,0045	
13	14.693±3.388	12.210±1.002	9.647±3.111	8.037±0.631	3.397±0.122	2.553±0.575	3.790±1.505	3.657±0.392	9.793±1.652	21.070±3.368	49.570±7.469	22.087±3.096	0.750±0.098	11.267±5.927
	P>0,9999		P>0,9999		P>0,9999		P>0,9999		P=0,7756		**P=0,0060		P=0,2643	

Data are mean ± standard error of the mean. C57BL/6J data are shown. H4: respective to HDM with protein degradation; H20: representative to whole extract of HDM. (n=39, 3 per dose). *$P<0.05$; **$P<0.0021$; ***$P<0.0002$; ****$P<0.0001$. P values are from 2-way ANOVA followed by Bonferroni post hoc test for inter-group comparisons.

Table S17. Absolute numbers of lung leucocyte populations during asthma development from H4 or H20 model.

	CD3		CD4		CD8		CD19		MacroMon		Neu		Eo	
NºAbs	H4	H20	H4	H20	H4	H20	H4	H20	H4	H20	H4	H20	H4	H20
1	127013,9±19748,54	40259,77±15604,86	59529,18 ± 4699,38	23359,3± 8991,89	45901,02 ± 11880	12353,56 ± 5010,67	24974,15 ± 3635,88	25217,37± 8222,62	189868,38± 17142,47	350559,42± 149218,35	1707688,62± 490173,61	302124,03± 195248,91	73154,75 ± 19571,14	144138,39± 55322,42
	P=0,3690		*P>0,9999*		*P>0,9999*		*P>0,9999*		*P>0,9999*		*****P=0,0004***		*P>0,9999*	
2	225706,99± 9166,90	28008,31± 909,88	85584,49 ± 8639,69	16612,7± 422,74	95267,3± 4290,81	9432,28± 356,79	26248,97 ± 5854,72	19732,29± 1597,60	397338,69± 51096,54	190389,16± 1046,87	373914,17± 76076,92	82790,72 ± 4597,53	14981,67 ± 661,88	18705,81 ± 1436,08
	****P=0,0256***		*P>0,9999*		*P=0,5538*		*P>0,9999*		*P>0,9999*		*P>0,9999*		*P>0,9999*	
3	67367,82± 7305,01	115321,02± 54195,1	35337,34 ± 5355,96	74344,85 ± 38898,82	20818,70 ± 1396,15	28824,31 ± 10147,8	5826,243 ± 1067,44	30644,63± 6138,03	223139,45± 53833,7	144388,2 ± 24944,29	857908,68± 249123,57	166704,69± 15850,9	60391,09 ± 7543,24	165274,46± 58047,17
	P>0,9999		*P>0,9999*		*P>0,9999*		*P>0,9999*		*P>0,9999*		*P=0,3910*		*P>0,9999*	
4	1213637,57± 132730,58	308984,15± 7492,31	677475,1 ± 68555,28	205426,33± 5422,38	339987,83± 67483,94	78049,38 ± 3327,64	202694,89± 5238,18	92903,58± 10920,3	744482,98± 186374,03	336416,59± 40563,65	1010539,75± 99297,94	302185,72± 64933,33	313902,28± 12885,62	450911,89± 87700,99
	P=0,2675		*P=0,1716*		*******P<0,0001***		*P>0,9999*		*P=0,4699*		*P=0,3431*		*P>0,9999*	
5	518617,6± 90171,97	416725,5± 164474,08	352729,1 ± 56846,5	281940,678± 117241,46	101045,75± 32854,96	102344,37± 36594,97	151106,29± 33604,66	177580,3667± 79775,05	484180,51± 55509,46	321927,34± 66801,51	904895,52± 465152,06	380872,76± 51601,18	267353,72± 80118,92	1327522,1± 555302,68
	P>0,9999		*P>0,9999*		*P>0,9999*		*P>0,9999*		*P>0,9999*		*P>0,9999*		*****P=0,0085***	
6	918426,97± 420737,25	243381,35± 88824,51	647138,02± 348489,85	171915,02± 56257,3	163089,18± 52196,62	44880,1± 25882,85	304292,83± 187277,52	97311,80± 58209,86	1009709,21± 190020,81	152570,29± 20255,65	1417843,91± 384248,18	293004,703± 166076,26	106229,69± 13786,55	1229471,07± 546814,29
	P>0,9999		*P=0,1642*		*P=0,0785*		*P=0,8079*		******P=0,0005***		******P=0,0084***		*****P=0,0043***	
7	1505411,99± 394922,16	290536,99± 23908,33	1129545,24± 341102,23	208254,84± 14964,31	202907,11± 51669,02	54359,91 ± 7758,72	511009,87± 125722,2	144481,79 ± 16495,79	1540673,14± 462087,58	383301,83± 70248,53	660146,94± 86795,75	401704,83± 153345,09	77480,84 ± 6884,62	1367089,05± 138507,57

	P>0,9999		*******P<0,0001***		*****P=0,0093***		****P=0,0182***		*******P<0,0001***		*P>0,9999*		******P=0,0007***	
8	704966,32± 114248,24	342221,59± 143829,16	549697,82± 101043,17	258198,87± 119353,83	106462,5 ± 13646,61	51328,55 ± 15141,67	257965,89± 60470,22	176052,07 ± 137345	809467,64± 171634,41	188086,96± 35161,32	436874,24± 118674,29	81778,86 ± 26370,7	72281,11 ± 18541,24	747968,04± 440011,21
	P>0,9999		*P>0,9999*		*P>0,9999*		*P>0,9999*		****P=0,0245***		*P>0,9999*		*P=0,3228*	
9	1052719,44± 89472,47	204124,18± 3888,8	720421,96± 62404,57	156336,41± 9122,13	246405,90± 21122,41	28472,62 ± 6926,42	436435,35± 99013,01	138271,89 ± 14089,2	504001,09 ± 100859,44	273758,43± 56326,92	1037261, 03± 131693,11	281172,20± 16072,15	68017,03 ± 11600,01	1165490, 26± 83626,21
	P=0,1407		****P=0,0446***		*******P<0,0001***		*P=0,1074*		*P>0,9999*		*P=0,2360*		*****P=0,0057***	
10	869649,53± 159723,62	408977,19± 127238,27	587041,33± 113422,65	278955,61± 93773,51	197157,41± 46629,51	71830,26 ± 27411,74	318569,49± 22554,09	374072,35 ± 110299,38	806410,98± 108495,4	444561,62 ± 16843,49	1199622, 88± 31667,34	697348,3 ± 187560,63	41958,89 ± 10826,88	1298833, 72± 382482,35
	P>0,9999		*P>0,9999*		****P=0,0488***		*P>0,9999*		*P=0,8061*		*P>0,9999*		******P=0,0010***	
11	1123680,4± 16567,54	189930,8± 108150,43	940754,88± 13835,01	141024,94± 82548,64	166382,62± 28458,11	31197,28 ± 16288,03	417644,36± 89582,14	163355,64 ± 86648,04	1090318, 1± 127175,94	400919,68± 66064,56	1567944, 81± 327148,92	348181,31± 111995,85	55593,47 ± 10063,34	523246,76± 288968,67
	P=0,1520		******P=0,0008***		****P=0,0246***		*P=0,2996*		*****P=0,0083***		*****P=0,0032***		*P>0,9999*	
12	176859,29± 14860,71	98982,5± 15649,19	127570,64± 7839,34	73796,117± 13323,12	47405,743± 7020,09	15408,733± 4874,76	58881,33 ± 7711,73	81544,017 ± 17488,39	328316,57± 15549,56	374659,40± 48190,65	1110619, 66± 309114,2	287566,14± 163422,94	13014,13 ± 2820,74	218289,39± 57908,28
	P=0,2949		*P>0,9999*		*P>0,9999*		*P>0,9999*		*P>0,9999*		*P=0,1363*		*P>0,9999*	
13	700812,97± 385950,30	311372,96± 209711,14	483208,50± 297424,23	249515,88± 171563,67	144540,037± 56367,57	35933,72 ± 24677,12	194215,9 ± 125274,26	252030,89 ± 118901,63	453943,02 ± 232878,32	1655349, 72± 82897,78	1865787, 03± 372182,97	674273,49 ± 118158,45	28477,5± 6236,47	483193,1 ± 169822,11
	P>0,9999		*P>0,9999*		*P=0,1456*		*P>0,9999*		*******P<0,0001***		*****P=0,0043***		*P>0,9999*	

Data are mean ± standard error of the mean. C57BL/6J data are shown. H4: respective to HDM with protein degradation; H20: representative to whole extract of HDM. (n=39, 3 per dose). **P<0.05*; ***P<0.0021*; ****P<0.0002*; *****P<0.0001.* P values are from 2-way ANOVA followed by Bonferroni post hoc test for inter-group comparisons.

Table S18. Cells per milligram analysis of lung leucocyte populations during asthma development from H4 or H20 model.

	CD3		CD4		CD8		CD19		MacroMon		Neu		Eo	
c/mg	H4	H20	H4	H20	H4	H20	H4	H20	H4	H20	H4	H20	H4	H20
1	466,37± 62,79	161,84± 63,63	219,75± 13,85	94,15± 36,83	167,41 ± 40,62	49,12± 20,07	91,52± 9,98	95,45± 31,5	699,11± 35,17	1348,88 ± 585,68	6267,95± 1795,06	1164,36± 763,92	266,48± 61,17	598,27± 238,91
	P=0,3526		*P=0,8049*		*P>0,9999*		*P=0,910998*		*P>0,9999*		*P>0,9999*		*P>0,9999*	
2	757,69± 61,12	109,32± 6,59	290,54± 47,82	64,81± 3,45	317,92 ± 8,11	36,835 ± 2,41	90,4± 25,29	77,33± 8,37	1336,06± 202,72	741,465 ± 24,84	1260,58± 266,16	320,77± 8,86	50,33± 4,2	73,285± 7,62
	P=0,1065		*P=0,5387*		***P=0,0044*		*P=0,649433*		*P>0,9999*		*P=0,9299*		*P=0,9764*	
3	163,73± 15,31	369,7± 180,29	84,86± 7,77	239,51 ± 129,91	51,12± 5,74	91,37± 32,4	14,17± 2,31	98,18± 17,69	521,75± 81,81	482,64± 105,74	2199,82± 767,55	538± 17,48	145,3± 8,92	512,9± 170,15
	P>0,9999		*P>0,9999*		*P>0,9999*		*P=0,009256*		*P>0,9999*		*P>0,9999*		*P>0,9999*	
4	3192,96 ± 315,59	1029,04 ± 85,57	1772,14 ± 106,95	684,81 ± 61,45	900,34 ± 175,74	260,67 ± 27,65	537,07± 43,11	305,57± 26,7	1968,75± 470,61	1121,39 ± 155,36	2675,41± 319,25	1027,38± 269,16	757,605 ± 8,24	1538,08± 408,29
	P=0,2003		***P=0,0313*		*P=0,8395*		*P=0,010333*		*P>0,9999*		*P=0,2315*		*P>0,9999*	
5	1181,2± 218,94	770,34± 245,42	803,83± 141,93	519,73 ± 176,98	230,57 ± 75,47	190,18 ± 53,27	343,44± 77,02	326,14± 122,26	1092,25± 106,9	613,75± 80,62	2061,25± 1042,38	731,91± 39,97	445,585 ± 71,77	2455,97± 839,28
	P>0,9999		*P>0,9999*		*P>0,9999*		*P=0,910445*		*P=0,3421*		*P>0,9999*		*P>0,9999*	
6	1860,4± 982,15	622,89± 207,42	1320,28 ± 798,02	442,89 ± 135,64	128,09 ± 128,09	111,72 ±59,22	626,43± 423,52	240,4± 132,65	1979,52± 523,84	398,75± 62,12	2836,99± 951,8	735,28± 385,3	199,37± 11,13	3114,63± 1254,94
	P>0,9999		*P>0,9999*		*P>0,9999*		*P=0,4334*		*P>0,9999*		*P>0,9999*		*P>0,9999*	
7	3268,55 ± 407,63	690,88± 69,63	2439,11 ± 410,95	494,63 ± 41,95	42,21± 42,20	129,57 ±21,06	1109,02± 110,88	343,036± 41,19	3312,91± 533,81	920,54± 198,64	1550,66± 301,71	977,52± 405,06	189,62± 54,81	3226,78± 260,5
	P=0,2801		*P=0,5282*		*P=0,1032*		***P=0,0029*		*P=0,4400*		*P>0,9999*		*P=0,0723*	
8	5436,97 ± 4296,49	979,44± 407,57	4159,83 ± 3266,91	738,51 ± 335,02	714,82 ± 714,82	147,63 ±46,76	2408,38± 2052,33	494,56± 379,52	4157,37± 2465,32	518,59± 70,86	4229,71±3657,73	233,48±76,87	490,11± 366,81	2133,74± 1217,28
	P>0,9999		*P>0,9999*		*P>0,9999*		*P=0,411046*		*P>0,9999*		*P>0,9999*		*P>0,9999*	

9	2107,43 ± 282,71	714,26± 43,46	1444,13 ± 202,38	541,89 ± 11,69	63,51± 63,51	105,90 5 ±32,31	883,56±248,6 5	497,88±88,2 3	1035,43±265,3 5	915± 121,36	2101,39± 411,5	974,865± 22,21	137,73± 31,92	4026,645 ± 32,29
	P=0,4699		*P=0,6030*		*P=0,1638*		*P=0,2176*		*P>0,9999*		*P>0,9999*		*******P<0,0001***	
10	2819,16 ± 568,18	964,81± 190,94	1900,18 ± 388,79	653,8± 142,88	168,46 ± 168,46	166,52 ±44,6	1025,94± 77,58	935,08± 305,19	2606,86± 394,56	1122,76 ± 121,9	3866,97± 199,85	1661,2± 228,51	136,8± 39,05	3076,12± 500,86
	P=0,9105		*P=0,9234*		*P>0,9999*		*P=0,787281*		*P=0,6944*		****P=0,0265***		*P=0,3538*	
11	2491,27 ± 65,86	344,47± 167,8	2084,62 ± 28,22	254,91 ± 128,46	66,08± 66,08	57,51 ±25,93	929,23± 208,17	296,86± 129,26	2409,93± 250,59	787,26± 101,53	3492,14± 757,87	680,77± 216,1	123,29± 22,71	944,43± 430,18
	****P=0,0316***		****P=0,0457***		*P=0,3777*		*P=0,061286*		*P=0,1718*		*P=0,7311*		*P>0,9999*	
12	1572,05 ± 1221,64	206,417 ± 37,38	1159,53 ± 909,45	153,41 ± 29,07	297,26 ± 297,26	32,62 ±11,5	680,32± 582,46	171,46± 42,96	3366,53± 2765,07	780,41± 118,85	5984,07± 3310,60	619,14± 369,77	82,65± 52,78	447,69± 108,44
	P>0,9999		*P>0,9999*		*P>0,9999*		*P=0,432776*		*P>0,9999*		*P>0,9999*		*P=0,7676*	
13	1344,74 ± 590,14	811,84± 562,67	911,62± 470,13	651,45 ± 460,18	75,27± 75,27	93,63 ±66,21	363,41± 202,66	643,38± 312,83	880,21± 346,17	974,73± 519,42	3913,85± 349,4	1739,43± 251,34	59,42± 5,95	1294,19± 471,41
	P>0,9999		*P>0,9999*		*P>0,9999*		*P=0,494366*		*P>0,9999*		*P=0,1207*		*P>0,9999*	

Data are mean ± standard error of the mean. C57BL/6J data are shown. H4: respective to HDM with protein degradation; H20: representative to whole extract of HDM. (n=39, 3 per dose). **P<0.05*; ***P<0.0021*; ****P<0.0002*; *****P<0.0001.* P values are from 2-way ANOVA followed by Bonferroni post hoc test for inter-group comparisons.

Table S19. BAL cytokine determination of lung leucocyte populations during asthma development from H4 or H20 model.

	IFNγ		IL4		IL13		IL17A		IgE		sIgE		sIgA	
%	H4	H20	H4	H20	H4	H20	H4	H20	H4	H20	H4	H20	H4	H20
1	24.7±15.89	0±0	0±0	0±0	27.7±2.27	115.37±43.74	20.37±4.89	0±0	54.8±12.01	105.1±33.83	0.165±0.034	0.148±0.148	0.115±0.021	0.120±0.038
	P>0,9999		*P>0,9999*		*P>0,9999*		*P>0,9999*		*P>0,9999*		*P>0,9999*		*P>0,9999*	
2	21.2±9.58	257.640±46.57	0±0	0±0	24.58±1.42	304.92±211.505	49.67±7.6	7.6±3.48	79.65±21.92	136.46±27.98	0.253±0.065	0.293±0.036	0.180±0.034	0.250±0.027
	*******P<0,0001***		*P>0,9999*		****P=0,0117***		****P=0,0185***		*P>0,9999*		*P>0,9999*		*P>0,9999*	
3	49.37±12.88	6.82±0.25	5.77±2.19	0±0	24.293±646.95	646.95±57.15	79.407±13.898	11.98±5.1	99.77±9.4	153.03±30.96	0.235±0.023	0.219±0.038	0.212±0.009	0.191±0.016
	P=0,3380		*P>0,9999*		*******P<0,0001***		*******P<0,0001***		*P>0,9999*		*P>0,9999*		*P>0,9999*	
4	33.35±11.09	11.09±3.87	0±0	4.19±2.37	24.01±0.98	505.6±161.34	56.18±9.49	13.91±1.51	148.30±42.72	331.75±24.02	0.355±0.051	0.292±0.024	0.328±0.053	0.266±0.043
	P>0,9999		*P>0,9999*		*******P<0,0001***		****P=0,0176***		*P>0,9999*		*P>0,9999*		*P>0,9999*	
5	53.61±20.52	20.52±7.53	46.28±17.57	13.06±7.79	29.97±2.74	41.23±8.94	85.1±23.96	20.09±10.41	801.64±414.61	342.41±177.45	0.827±0.139	0.329±0.121	0.678±0.116	0.315±0.11
	P>0,9999		****P=0,0067***		*P>0,9999*		*******P<0,0001***		*P>0,9999*		****P=0,0249***		*P=0,5532*	
6	26.17±8.1	98.97±22.84	0±0	82.52±18.91	21.45±0	156.1±76.48	49.02±7.82	30.5±10.32	0±0	975.62±498.55	0.410±0.045	0.948±0.4	0.334±0.05	0.874±0.358
	*****P=0,0034***		****P<0,0001***		*P>0,9999*		*P>0,9999*		*P=0,1020*		****P=0,0114***		****P=0,0412***	
7	25.84±2.12	0±0	0±0	0±0	22.87±1.42	0±0	30.79±7,17	22.22±6.4	879.75±119.37	108.06±20.74	0.296±0.048	0.208±0.024	0.388±0.075	0.234±0.001
	P>0,9999		*P>0,9999*		*P>0,9999*		*P>0,9999*		*P=0,4319*		*P>0,9999*		*P>0,9999*	
8	33.53±4.21	22.3±6.38	8.95±2.48	17.28±4.9	22.31±0.85		63.78±9.6	16.32±6.27	1836.09±859.06	279.68±109-72	0.386±0.048	0.360±0.128	0.407±0.025	0.304±0.116
	P>0,9999		*P>0,9999*		*P>0,9999*		*****P=0,0049***		*******P=0,0007***		*P>0,9999*		*P>0,9999*	
9	21.38	3.26	5.77±2.59	0±0	23.16±0.49	12.01±10.96	54.88±6.84	5.48±2.82	560.19±227.05	93.85±36.46	0.399±0.023	0.192±0.031	0.644±0.043	0.340±0.06

	P>0,9999		*P>0,9999*		*P>0,9999*		*****P=0,0030***		*P>0,9999*		*P>0,9999*		*P>0,9999*	
10	23.41±1.64	0±0	3.91±0.21	0±0	23.16±0.98	54.68±16.23	47.28±3.80	18.66±4.73	493.9±122.82	158.36±80.97	0.332±0.046	0.198±0.120	0.544±0.07	0.359±0.147
	P>0,9999		*P>0,9999*		*P>0,9999*		*P=0,3365*		*P>0,9999*		*P>0,9999*		*P>0,9999*	
11	26.9±8.94	32.9±14.8	4.4±2.26	28.5±16.2	23.44±2.43	0±0	42.07±2.17	18.01±6.59	1499.95±334.17	317.55±136.67	0.261±0.044	0.520±0.205	0.732±0.049	0.948±0.08
	P>0,9999		*P=0,1238*		*P>0,9999*		*P=0,7719*		****P=0,0195***		*P>0,9999*		*P>0,9999*	
12	21.19±12.78	13.45±5.12	0±0	0±0	20.6±0	0±0	29.92±2.07	9.61±2.24	760.21±372.45	113.98±7.1	0.150±0.024	0.583±0.074	0.437±0.077	1.063±0.262
	P>0,9999		*P>0,9999*		*P>0,9999*		*P>0,9999*		*P=0,9451*		*P=0,0830*		****P=0,0096***	
13	11.99±5.28	14.56±2.94	0±0	0±0	19.47±0.75	0±0	38.6±11.85	49.52±8.37	523.49±216.61	341.22±63.12	0.168±0.029	0.382±0.038	0.874±0.310	0.324±0.028
	P>0,9999		*P>0,9999*		*P>0,9999*		*P>0,9999*		*P>0,9999*		*P>0,9999*		*****P=0,0355***	

Data are mean ± standard error of the mean. C57BL/6J data are shown. H4: respective to HDM with protein degradation; H20: representative to whole extract of HDM. (n=39, 3 per dose). **P<0.05*; ***P<0.0021*; ****P<0.0002*; *****P<0.0001*. P values are from 2-way ANOVA followed by Bonferroni post hoc test for inter-group comparisons.

Table S20. Cytokine production analyses by memory cells in lung during asthma development from H4 or H20 model.

	HDM								PMA							
	IFNg		IL17A		IL4		IgE		IFNg		IL17A		IL4		IgE	
	H4	H20	H4	H20	H4	H20	H4	H20	H4	H20	H4	H20	H4	H20	H4	H20
1	22.12±12.72	0±0	21.24±3.04	41.19±23.16	0	0	0±0	0±0	38.14±32.87	438.63±183.49	72.14±40.04	389±127.47	0	11.24±7.11	0	0
	P>0,9999		*P>0,9999*				*P<0,0001*		*****P=0,0098***		*P=0,1249*				*P>0,9999*	
2	40.63±1.44	0±0	118.7±46.11	4.68±2.34	0	0	0±0	117.53±0	297.24±46.28	715.45±62.02	126.94±49.24	565.84±60.43	0	28.72±11.66	0	67.8±0
	P>0,9999		*P>0,9999*				******P=0,1635***		*****P=0,0060***		*****P=0,0063***				*P=0,4547*	
3	167.42±2.87	442.16±45.68	183.37±8.19	155.02±74.21	0	0	0±0	18.11±2.05	142.92±96.42	713.53±85.98	141.48±103.93	519.19±36.66	0	114.66±16.56	0	35.86±12.3
	*******P<0,0001***		*P>0,9999*				*P>0,9999*		*******P<0,0001***		****P=0,0300***		*******P<0,0001***		*P>0,9999*	
4	43.48±11.94	0±0	382.84±3.49	343.492±138.08	0	0	0±0	42.96±33.75	47.35±11.24	667.42±80.2	186.85±37.41	569.72±103.86	0	153.63±36.35	0	0
	P=0,9023		*P>0,9999*				*P>0,9999*		*******P<0,0001***		****P=0,0264***		*******P<0,0001***		*P>0,9999*	
5	86.21±33.17	12.56±1.28	439.71±56.54	184.16±71.33	0	0	21.66±8.2	0±0	333.52±146.73	472.22±165.5	372.42±156.59	324.11±100.48	0	94.13±35.04	39.41±6.15	45.33±41.43
	****P=0,0362***		*P=0,4632*				*P>0,9999*		*P>0,9999*		*P>0,9999*		*******P<0,0001***		*P>0,9999*	
6	35.19±8.93	0±0	399.57±51.51	401.2±153.6	0	0	10.89±10.712	12.78±1.03	65.39±24.83	48.07±19.35	104.37±52.43	193.2±13	0	5.41±2.41	28.76±4.1	41.19±19.48
	P>0,9999		*P>0,9999*				*P>0,9999*		*P>0,9999*		*P>0,9999*				*P>0,9999*	
7	151.39±36.46	6.52±3.09	700.6±29.57	313.92±42.63	0	0	65.45±20.74	206.12±67.55	283.06±72.21	238.27±38.4	633.75±62.57	276.03±13	0	0±0	53.61±18.45	0
	*******P<0,0001***		****P=0,0253***				*P>0,9999*		*P>0,9999*		****P=0,0487***				*P>0,9999*	
8	61.16±14.85	157.42±23.54	632.45±39.02	518.76±115.44	0	0	101.746±42.29	14.56±6.15	101.67±33.75	582.27±66.6	650.24±28.21	574.17±151.2	0	91.17±32.56	161.32±93.77	21.66±6.15
	P=0,0019		*P>0,9999*				*P>0,9999*		******P=0,0010***		*P>0,9999*		*******P<0,0001***		******P=0,0006***	
9	142.18±23.31	15.88±0.13	441.663±59.29	365.89±102.2	0	0	87.35±1.03	0±0	186.19±95.24	32.45±1.53	319.47±49.1	198.94±99.63	0	0±0	74.92±8.2	32.31±18.45
	*******P<0,0001***		*P>0,9999*				******P=0,0018***		*P>0,9999*		*P>0,9999*				*P>0,9999*	
10	44.77±2.55	0±0	388.27±60.63	207.56±79.1	0	0	6.62±2.72	0±0	68.89±44.18	0±0	399.55±98.9	26.41±6.96	0	0±0	30.53±11.28	0±0

	P=0,8029		*P>0,9999*				*P>0,9999*		*P>0,9999*		***P=0,0335***				*P>0,9999*	
11	51.58±11.65	0±0	483.77±28.01	280.48±122.46	0	0	64.27±11.42	28.76±6.15	56.74±28.59	0±0	466.19±23.09	96.46±31.8	0	0±0	64.27±18.79	0±0
	P=0,4198		P>0,9999				P=0,9047		P>0,9999		**P=0,0364**				P=0,5880	
12	184.27±16.75	0±0	304.58±23.05	423.88±195.7	0	0	0±0	46.51±0	49.74±11.17	0±0	100.26±12.61	234.54±29.66	0	0±0	0±0	29.94±19.38
	****P<0,0001**		*P>0,9999*				****P<0,0001**		*P>0,9999*		*P>0,9999*				*P>0,9999*	
13	28.75±18.06	38.42±12.63	126.72±53.98	538±147.03	0	0	26.99±5.12	0±0	107.2±20.73	489.67±155.27	222.88±103.2	493.93±139.28	0	0±0	14.56±4.1	0±0
	P>0,9999		***P=0,0136**				*P=0,4448*		***P=0,0160**		*P=0,3312*				*P>0,9999*	

Data are mean ± standard error of the mean. C57BL/6J data are shown. H4: respective to HDM with protein degradation; H20: representative to whole extract of HDM. Lung cells were *in vitro* stimulated with H4 or H20 depending on mice treatment and PMA with IO (PMA/IO). Twelve hours post-stimulation, the supernatant was preserved for posterior ELISA analysis. (n=39, 3 per dose). **P<0.05*; ***P<0.0021*; ****P<0.0002*; *****P<0.0001.* P values are from 2-way ANOVA followed by Bonferroni post hoc test for inter-group comparisons.

Table S1. Biological Function of proteins presents in H4.1 treatment.

	Biological process	Nº genes	**% of gene hit against total *genes**	% gene hit against total *Process hits
1	cellular process	44	**44.9%**	22.2%
2	reproductive process	1	**1.0%**	0.5%
3	localization	15	**15.3%**	7.6%
4	interspecies interaction between organisms	9	**9.2%**	4.5%
5	reproduction	1	**1.0%**	0.5%
6	biological regulation	25	**25.5%**	12.6%
7	response to stimulus	25	**25.5%**	12.6%
8	signaling	9	**9.2%**	4.5%
9	developmental process	3	**3.1%**	1.5%
10	multicellular organismal process	8	**8.2%**	4.0%
11	locomotion	4	**4.1%**	2.0%
12	biological adhesion	3	**3.1%**	1.5%
13	metabolic process	39	**39.8%**	19.7%
14	growth	1	**1.0%**	0.5%
15	immune system process	11	**11.2%**	5.6%

Table S2. Biological Function of proteins presents in H20.1 treatment.

	Biological process	Nº genes	**% of gene hit against total *genes**	% gene hit against total *Process hits
1	cellular process	51	**43.6%**	23.5%
2	reproductive process	1	**0.9%**	0.5%
3	localization	17	**14.5%**	7.8%
4	interspecies interaction between organisms	11	**9.4%**	5.1%
5	reproduction	1	**0.9%**	0.5%
6	biological regulation	27	**23.1%**	12.4%
7	response to stimulus	27	**23.1%**	12.4%
8	signaling	6	**5.1%**	2.8%
9	developmental process	1	**0.9%**	0.5%
10	multicellular organismal process	7	**6.0%**	3.2%
11	locomotion	4	**3.4%**	1.8%
12	biological adhesion	3	**2.6%**	1.4%
13	metabolic process	46	**39.3%**	21.2%
14	growth	1	**0.9%**	0.5%
15	immune system process	14	**12.0%**	6.5%

Table S3. Biological Function of proteins presents in H4.13 treatment.

	Biological process	Nº genes	**% of gene hit against total *genes**	% gene hit against total *Process hits
1	cellular process	58	**43.3%**	20.7%
2	reproductive process	1	**0.7%**	0.4%
3	localization	21	**15.7%**	7.5%
4	interspecies interaction between organisms	16	**11.9%**	5.7%
5	reproduction	1	**0.7%**	0.4%
6	biological regulation	31	**23.1%**	11.1%
7	response to stimulus	47	**35.1%**	16.8%
8	signaling	12	**9.0%**	4.3%
9	developmental process	1	**0.7%**	0.4%
10	multicellular organismal process	6	**4.5%**	2.1%
11	locomotion	3	**2.2%**	1.1%
12	biological adhesion	2	**1.5%**	0.7%
13	metabolic process	53	**39.6%**	18.9%
14	growth	1	**0.7%**	0.4%
15	immune system process	27	**20.1%**	9.6%

Table S4. Biological Function of proteins presents in H20.13 treatment.

	Biological process	Nº genes	**% of gene hit against total *genes**	% gene hit against total *Process hits
1	cellular process	61	**42.7%**	16.7%
2	reproductive process	1	**0.7%**	0.3%
3	localization	32	**22.4%**	8.7%
4	interspecies interaction between organisms	29	**20.3%**	7.9%
5	reproduction	1	**0.7%**	0.3%
6	biological regulation	42	**29.4%**	11.5%
7	response to stimulus	59	**41.3%**	16.1%
8	signaling	24	**16.8%**	6.6%
9	developmental process	1	**0.7%**	0.3%
10	multicellular organismal process	9	**6.3%**	2.5%
11	locomotion	7	**4.9%**	1.9%
12	biological adhesion	3	**2.1%**	0.8%
13	metabolic process	54	**37.8%**	14.8%
14	growth	1	**0.7%**	0.3%
15	immune system process	42	**29.4%**	11.5%

Table S5. Biological Function of proteins presents in NA Human.

	Biological process	Nº genes	**% of gene hit against total *genes**	% gene hit against total *Process hits
1	cellular process	136	**43.2%**	25.6%
2	reproductive process	1	**0.3%**	0.2%
3	localization	37	**11.7%**	7.0%
4	interspecies interaction between organisms	20	**6.3%**	3.8%
5	reproduction	1	**0.3%**	0.2%
6	biological regulation	77	**24.4%**	14.5%
7	response to stimulus	70	**22.2%**	13.2%
8	signaling	29	**9.2%**	5.5%
9	developmental process	8	**2.5%**	1.5%
10	multicellular organismal process	13	**4.1%**	2.4%
11	locomotion	13	**4.1%**	2.4%
12	biological adhesion	4	**1.3%**	0.8%
13	metabolic process	86	**27.3%**	16.2%
14	growth	1	**0.3%**	0.2%
15	immune system process	35	**11.1%**	6.6%

Table S6. Biological Function of proteins presents in EA Human.

	Biological process	Nº genes	**% of gene hit against total *genes**	% gene hit against total *Process hits
1	cellular process	92	**41.4%**	24.8%
2	reproductive process	1	**0.5%**	0.3%
3	localization	27	**12.2%**	7.3%
4	interspecies interaction between organisms	15	**6.8%**	4.0%
5	reproduction	1	**0.5%**	0.3%
6	biological regulation	59	**26.6%**	15.9%
7	response to stimulus	45	**20.3%**	12.1%
8	signaling	13	**5.9%**	3.5%
9	developmental process	8	**3.6%**	2.2%
10	multicellular organismal process	14	**6.3%**	3.8%
11	locomotion	8	**3.6%**	2.2%
12	biological adhesion	5	**2.3%**	1.3%
13	metabolic process	59	**26.6%**	15.9%
14	growth	2	**0.9%**	0.5%
15	immune system process	22	**9.9%**	5.9%

Figure S1.

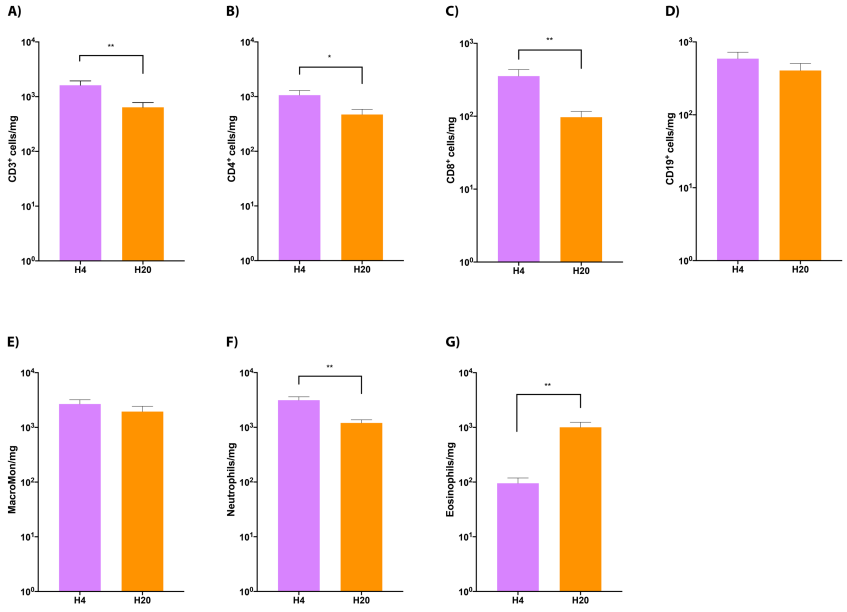

Comparison of lung infiltrating leukocytes, H4 versus H20, normalized by lung weight. C57BL/6J mice were sensitized *i.n* with saline solution (SS) or House Dust Mite (HDM) (15 µg/mL) with protein degradation (H4) or with frozen-preserved extract (H20), through 4 weeks, three times per week. The panels show the percentage of $CD3^+$ T cells (**A**), $CD4^+$ T cells (**B**), $CD8^+$ T cells (**C**), $CD19^+$ B cells (**D**), macrophages/monocytes (**E**), neutrophils (**F**), and eosinophils (**G**). Data are mean±SEM and were analyzed by Mann-Whitney or Unpaired t-test. Group size: SS n=10; H4 n=12; H20 n=20. **P<0.05*; ***P<0.0021*; ****P<0.0002*; *****P<0.0001*.

Figure S2.

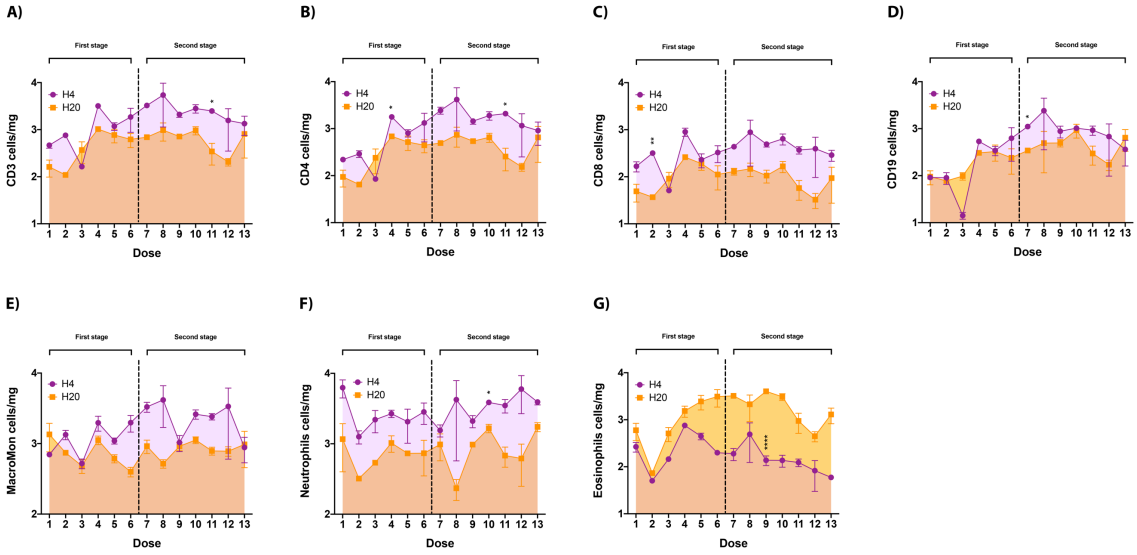

The effect of H4 and H20 challenge on cells per milligram of the lung during the development of asthma. 39 C57BL/6J mice were *i.n* sensitized with HDM (15 µg/mL) with protein degradation (H4) or with whole extract (H20), three mice per dose during 13 doses. Cell per milligram of lung weight of CD3 cells (**A**), CD4 T lymphocytes cells (**B**), CD8 T lymphocytes cells (**C**), B lymphocytes cells (**D**), Macrophage and Monocytes (**E**), Neutrophils (**F**), and Eosinophils (**G**). Data are represented as mean±SEM and analyzed by 2-way ANOVA test. **P<0.05*; ***P<0.0021*; ****P<0.0002*. (n=3).

Figure S3.

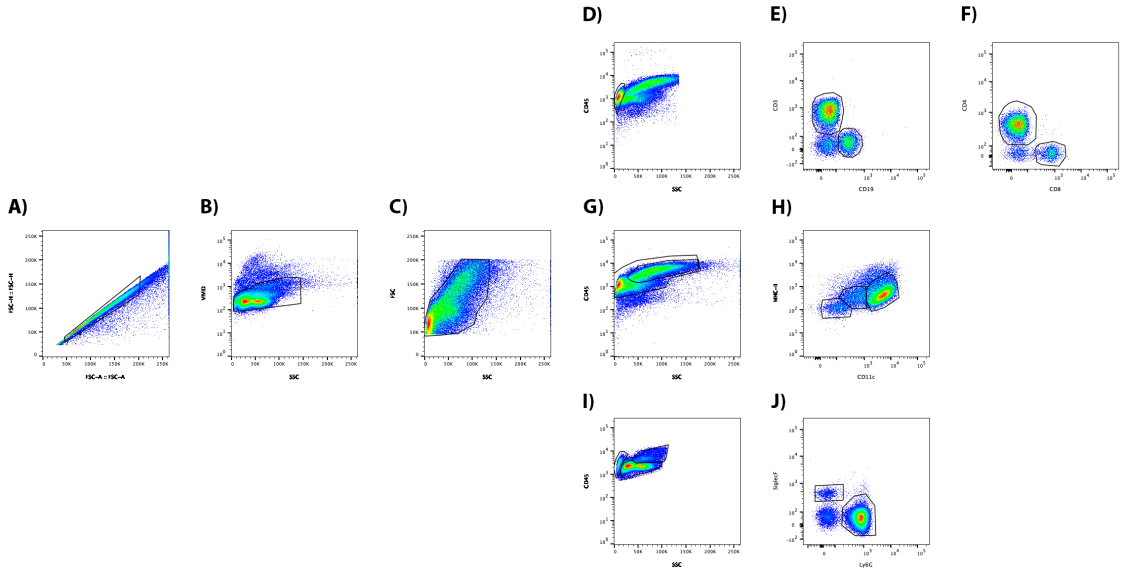

Flow cytometry gating strategy comparison between H4 and H20 treatment. Total leukocytes were first gated by single cells **A)** on a forward scatter (FSC)/side scatter (SS) plot **B)**, selected by live cells **C)** and then gated on the $CD45^{+}$ population. These were then gated based on granularity subsets in lymphocytes **D)** Macrophages and Monocytes **G)** and Granulocytes **I)**. After these gates, populations were separated according to specific markers as CD3/CD19 **E)** to classify T lymphocytes and B lymphocytes, respectively; CD4+ and CD8+ T lymphocytes **F)**. Macrophages and Monocytes were classified by MHC-II and CD11c expression **H)**. Granulocytes were phenotyped according to Siglec-F and Ly6G expression to classify Eosinophils and Neutrophils **J)**. Data were analyzed using FlowJow software, and population frequencies were expressed as a percent of the parent population.

Figure S4.

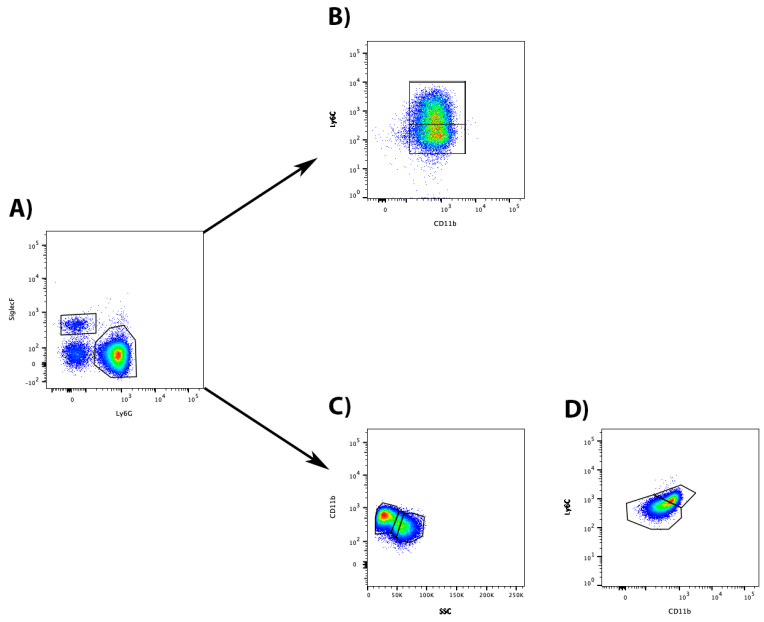

Flow cytometry gating strategy to analyze lung subpopulation in H4 and H20 treatment. Total granulocytes were first gated by SiglecF+ (Eosinophils) or Ly6G+ (Neutrophils) markers **A).** Then subsets of eosinophils were selected by Ly6C and CD11b markers, classified as Ly6CHi or CD11b+ **B)**. Neutrophils were classified by CD11b marker and granularity (SSC) in three populations, CD11bHighSSCLow, CD11bMediumSSCMedium, and CD11bLowSSCHigh **C)** and finally gated also by Ly6C and CD11b expression as Ly6GHigh (Ly6CHigh and CD11bHigh) and Ly6Glow (Ly6Clow and CD11b Low) population.

Figure S5.

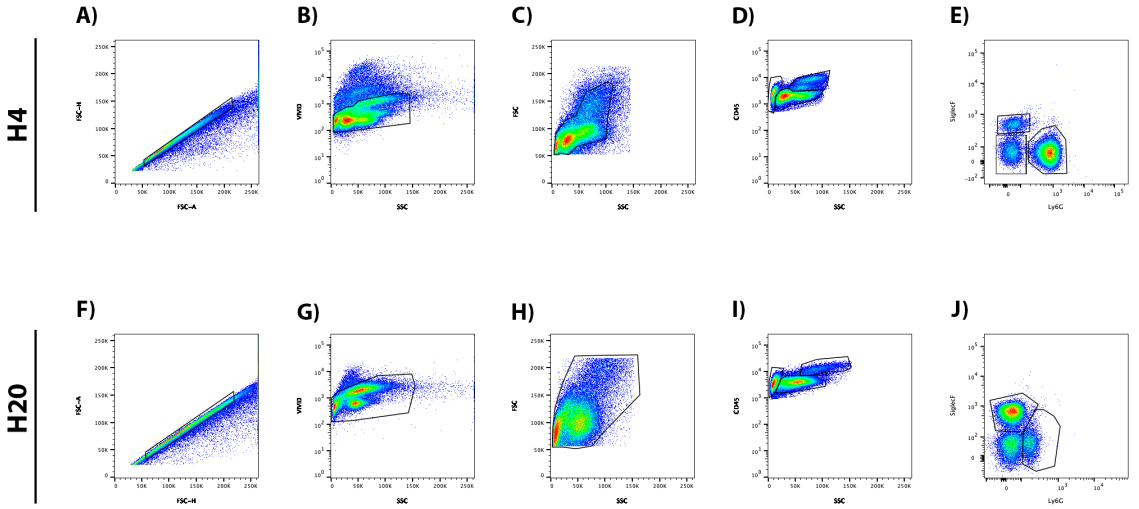

Flow cytometry lung population comparison between H4 and H20 treatment. Total leukocytes were first gated by singlets cells **A),** selected by live cells **B)**, on a forward scatter (FSC)/side scatter (SS) plot **C)** and then gated on the CD45+ and granularity in Granulocyte population **D)**. Granulocytes were phenotype according to Siglec-F and Ly6G expression to classify Eosinophils and Neutrophils **J)**. Data were analyzed using FlowJow software, and population frequencies were expressed as a percent of the parent population.

ANNEXES

Table Annexed 1. Mouse pathways

Neutrophil degranulation

Neutrophilic (H4)		Eosinophilic (H20)		1st Dose		13th Dose	
1st Dose	13th Dose	1st Dose	13th Dose	Neutrophilic	Eosinophilic	Neutrophilic	Eosinophilic
CAP1	ALDOA	ALDOA	CFP	CAP1	ALDOA	ALDOA	COTL1
CD44	ANXA2	ASAH1	COTL1	CD44	ASAH1	GPI	CTSD
CTSD	EAR2	CTSH	EAR1	ELANE	CTSH	HSP90AA1	EAR1
ELANE	EEF1A1	GPI	JUP	MMP9	IDH1	IDH1	FTH1
MMP9	HSP90AA1	IDH1	PPIA	MPO	ANXA2	PKM	JUP
MPO	HSP90AB1	S100A8	PSAP	CFP	EAR2	S100A8	NME2
NME2	IDH1	SERPINB1A			EEF1A1		PSAP
SERPINB1A	PKM				FTH1		
	PPIA				HSP90AB1		

Complement cascade

Neutrophilic (H4)		Eosinophilic (H20)		1st Dose		13th Dose	
1st Dose	13th Dose	1st Dose	13th Dose	Neutrophilic	Eosinophilic	Neutrophilic	Eosinophilic
ELANE	C4B	C4B	C7	ELANE	C4B	C4B	C6
	F2		CFP	CFP	C6	SERPING1	C7
	IGHG3		IGHV1-69	SERPING1	F2		IGHV1-69
	IGHV3-6		IGHV3-6		IGHG3		IGHV5-17
	IGHV4-1		IGHV4-1				IGLC3
	IGKV13-84		IGHV5-17				
			IGKV13-84				
			IGLC3				

Post-transcriptional protein phosphorylation

Neutrophilic (H4)		Eosinophilic (H20)		1st Dose		13th Dose	
1st Dose	13th Dose	1st Dose	13th Dose	Neutrophilic	Eosinophilic	Neutrophilic	Eosinophilic
FGG	APOA1	C4B	ITIH2		C4B	APOA1	FGA
	C4B	FGG	MFGE8		KNG2	C4B	MFGE8
	ITIH2	FN1	P4HB		FGA	FN1	QSOX
	P4HB	KNG2	QSOX			QSOX1	SPP1
		QSOX1	SPP1				

Response to elevated platelet cytosolic Ca2+

Neutrophilic (H4)		Eosinophilic (H20)		1st Dose		13th Dose	
1st Dose	13th Dose	1st Dose	13th Dose	Neutrophilic	Eosinophilic	Neutrophilic	Eosinophilic
CAP1	ALDOA	ALDOA	PLG	CAP1	ALDOA	ALDOA	FGA
FGB	ANXA5	FGG	PPIA	FGB	LGALS3BP	APOA1	PSAP
FGG	APOA1	FN1	PSAP	PLG	ANXA5	FN1	
	PPIA	LGALS3BP	SERPINF2	PZP	FGA	PZP	
	SELENOP		SOD3	SERPINF2		SELENOP	
	TAGLN2		TAGLN2	SERPING1		SERPING1	
			TF	SOD3			
				TF			

Antimicrobial Peptides

Neutrophilic (H4)		Eosinophilic (H20)		1st Dose		13th Dose	
1st Dose	13th Dose	1st Dose	13th Dose	Neutrophilic	Eosinophilic	Neutrophilic	Eosinophilic
ELANE	BPIFB1	S100A8	EAR1	ELANE	BPIFB1	S100A8	EAR1

Neutrophilic (H4)		Eosinophilic (H20)		Neutrophilic Vs Eosinophilic		13th Dose	
1st Dose	13th Dose	1st Dose	13th Dose	1st Dose		Neutrophilic	Eosinophilic
FGB	SFTPA1			FGB	FGA	S100A8	FGA
				S100A8	SFTPA1	UBC	PSAP
				UBC	PSAP		

Neutrophilic (H4)		Eosinophilic (H20)		1st Dose		13th Dose	
1st Dose	13th Dose	1st Dose	13th Dose	Neutrophilic	Eosinophilic	Neutrophilic	Eosinophilic
MMP9		FN1		MMP9		FN1	
						HSP90AA1	

Regulation of IGF transport and uptake by IGFBPs

Neutrophilic (H4)		Eosinophilic (H20)		1st Dose		13th Dose	
1st Dose	13th Dose	1st Dose	13th Dose	Neutrophilic	Eosinophilic	Neutrophilic	Eosinophilic
FGG	APOA1	C4B	ITIH2		C4B	APOA1	FGA
SERPINC1	C4B	FGG	MFGE8		KNG2	C4B	MFGE8
	F2	FN1	P4HB		F2	FN1	SERPINC1
	ITIH2	KNG2	SPP1		FGA		SPP1
	P4HB						

Glutation conjugation

Neutrophilic (H4)		Eosinophilic (H20)		1st Dose		13th Dose	
1st Dose	13th Dose	1st Dose	13th Dose	Neutrophilic	Eosinophilic	Neutrophilic	Eosinophilic
GSTA4	GSTA3			GSTA4			
	GSTM1						
	GSTO1						
	NPC2						

Degradation of the extracellular matrix

Neutrophilic (H4)		Eosinophilic (H20)		1st Dose		13th Dose	
1st Dose	13th Dose	1st Dose	13th Dose	Neutrophilic	Eosinophilic	Neutrophilic	Eosinophilic
CD44		FN1	CDH1	CD44	CTSD	FN1	CDH1
CTSD		PZP	CTSL	ELANE	CTSB	PZP	CTSD
ELANE			SPP1	MMP9	CTSS		CTSL
MMP9					FN1		SPP1
					PLG		
					PZP		

Surfactant metabolism

Neutrophilic (H4)		Eosinophilic (H20)		1st Dose		13th Dose	
1st Dose	13th Dose	1st Dose	13th Dose	Neutrophilic	Eosinophilic	Neutrophilic	Eosinophilic
	SFTPA1	NAPSA	SFTPB	SFTPB	NAPSA		CTSD
		CTSH	PSAP	SFTPD	CTSH		PSAP
			SFTPD		CTSD		
					SFTPA1		

Binding and Uptake and Ligands by Scavender Receptors

Neutrophilic (H4)		Eosinophilic (H20)		1st Dose		13th Dose	
1st Dose	13th Dose	1st Dose	13th Dose	Neutrophilic	Eosinophilic	Neutrophilic	Eosinophilic
						APOA1	IGHV1-69
						HSP90AA1	IGHV5-17
							IGLC3
							JCHAIN
							FTH1

Fc gamma receptor (FCGR) dependent phagocytosis

Neutrophilic (H4)		Eosinophilic (H20)		1st Dose		13th Dose	
1st Dose	13th Dose	1st Dose	13th Dose	Neutrophilic	Eosinophilic	Neutrophilic	Eosinophilic
	IGHV4-1		IGHV4-1		IGHG3	HSP90AA1	IGHV1-69
	HSP90AA1		IGHV1-69		HSP90AB1	IGKV13-84	IGHV5-17
	IGHG3		IGHV5-17				
	HSP90AB1		IGHV3-6				
	IGHV3-6						
	IGKV13-84						

CD22 mediated BCR regulation

Neutrophilic (H4)		Eosinophilic (H20)		1st Dose		13th Dose	
1st Dose	13th Dose	1st Dose	13th Dose	Neutrophilic	Eosinophilic	Neutrophilic	Eosinophilic
	IGHM		IGHM		IGHV1-69		IGHV1-69
	IGHV3-6		IGHV4-1		IGHV5-17		IGHV5-17
	IGKV13-84		IGKV13-84		IGLC3		IGLC3
	IGHV4-1		IGHV1-69				
			IGHV5-17				
			IGLC3				
			IGHV3-6				

Calnexin/Calreticulin cycle

Neutrophilic (H4)		Eosinophilic (H20)		1st Dose		13th Dose	
1st Dose	13th Dose	1st Dose	13th Dose	Neutrophilic	Eosinophilic	Neutrophilic	Eosinophilic
	CALR		CALR	UBC	UBB	UBC	PDIA3
			PDIA3				UBB

Table Annexed 2. Human pathways

Asthmatic Humans: Pathway Analysis

Neutrophil degranulation

Neutrophilic		Eosinophilic
RNASET2	NME2	TTR
FCN1	CTSS	PGAM1
PGLYRP1	PSMA2	CRISP3
LRG1	STOM	HRNR
CYBB	CEACAM8	PRG3
ITGB2	CDA	
PYGL	CHI3L1	
PSAP	ALDH3B1	
HEXB	SERPINB10	
CTSB	RHOA	
GUSB	NPC2	
CTSG	RAC1	
CD63	HBB	
CTSH	FABP5	
LTA4H	ASAH1	
ALDOC	OLFM4	
ITGAM	GGH	
EEF2	CPPED1	
GNS	RETN	
LGALS3	PYCARD	
PSMB1	CAB39	

Complement cascade

Neutrophilic	Eosinophilic
FCN1	IGKV1-12
IGKV1-5	C5
IGKV3-15	IGHV3-13
IGLV3-19	C1QB
IGLV3-25	C1QC
IGHV1-46	C4BPA
IGHV3-7	VTN
IGHV3-9	CPN2
IGHV4-59	CFHR1
IGKV2-30	

Response to elevated platelet cytosolic Ca2+

Neutrophilic	Eosinophilic
PSAP	KNG1
PLEK	FGA
CD63	FN1
HSPA5	ORM1
CD9	HRG
CFL1	ITIH4
ACTN2	
TAGLN2	
TTN	

CD22 mediated BCR regulation

Neutrophilic		Eosinophilic
PSMA7	IGHV4-59	IGKV1-12
IGKV1-5	IGKV2-30	IGHV3-13
IGKV3-15	PSMB1	PSME1
IGLV3-19	PSMA1	
IGLV3-25	PSMA2	
IGHV1-46	PSMA4	
IGHV3-7	PSMB2	
IGHV3-9	GRB2	

Antimicrobial Peptides

Neutrophilic	Eosinophilic
PGLYRP1	
CTSG	

Regulation of TLR by endogenous ligand

Neutrophilic	Eosinophilic
	FGA
	APOB

FCGR dependent phagocytosis

Neutrophilic		Eosinophilic
IGKV1-5	IGHV4-59	IGKV1-12
IGKV3-15	IGKV2-30	IGHV3-13
IGLV3-19	CFL1	ARPC4
IGLV3-25	CDC42	
IGHV1-46	GRB2	
IGHV3-7	RAC1	
IGHV3-9		

FC gamma receptor dependent phagocytosis

Neutrophilic		Eosinophilic
PSMA7	IGKV2-30	IGKV1-12
IGKV1-5	PSMB1	IGHV3-13
IGKV3-15	PSMA1	PSME1
IGLV3-19	PSMA2	
IGLV3-25	PSMA4	
IGHV1-46	PSMB2	
IGHV3-7	GRB2	
IGHV3-9	RAC1	
IGHV4-59		

Smooth Muscle Contraction

Neutrophilic	Eosinophilic
MYL6	ITGA1
TPM4	ANXA6

Striated Muscle Contraction

Neutrophilic	Eosinophilic
ACTN2	ACTC1
VIM	

RFCG dependent phagocytosis

Neutrophilic	Eosinophilic
PSMA7	PSMA4
GSR	PSMB2
SOD2	HBB
CYBB	HBA2
PSMB1	CYCS
PSMA1	TXNRD1
PSMA2	

Formation of Fibrin Clot

Neutrophilic	Eosinophilic
	KNG1
	FGA
	KLKB1
	SERPIND1

Table Annexed 3. Common pathways

Mouse Model 1st Dose vs Asthmatic Humans: Pathway Analysis in common

Neutrophil degranulation

Neutrophilic	Eosinophilic
CAP1	ANXA2
ELANE	EEF1A1
MMP9	HSP90AB1
MPO	TTR
NME2	
CHI3L1	
CTSB	
CTSS	
LRG1	
NPC2	
PGLYRP1	

Response to elevated platelet cytosolic Ca2+

Neutrophilic	Eosinophilic
CAP1	FGA
FGB	HRG
FGG	ITIH4
AHSG	KNG1
ALB	ORM1
APOH	
SERPINF2	
SERPING1	
TF	

Complement Cascade

Neutrophilic	Eosinophilic
ELANE	C5
SERPING1	C6
	IGHG3

Antimicrobial Peptides

Neutrophilic	Eosinophilic
ELANE	BPIFB1
PGLYRP1	

Regulation of TLR by endogenous ligand

Neutrophilic	Eosinophilic
FGB	FGA
S100A8	

Asthmatic Mouse Model 13th Dose vs Asthmatic Humans: Pathway Analysis in common

Neutrophil degranulation

Neutrophilic	Eosinophilic
CTSB	CTSD
GPI	HSPA8
HSP90AA1	TTR
LRG1	
PGLYRP1	
S100A8	

Response to elevated platelet cytosolic Ca2+

Neutrophilic	Eosinophilic
ALDOA	FGA
APOA1	HRG
SERPING1	ITIH4
TAGLN2	KNG1
	ORM1

Complement Cascade

Neutrophilic	Eosinophilic
SERPING1	C5
	C6

Antimicrobial Peptides

Neutrophilic	Eosinophilic
PGLYRP1	

Regulation of TLR by endogenous ligand

Neutrophilic	Eosinophilic
S100A8	

FCGR dependent phagocytosis

Neutrophilic	Eosinophilic
HSP90AA1	

CD22 mediated BCR regulation

Neutrophilic	Eosinophilic
IGKC	

Table Annexed 4. Mouse proteins 1st Dose

MOUSE H4.1		
PROTEIN	**PROTEIN NAME**	**GEN**
A0A075B5P3	Immunoglobulin heavy constant gamma 2B	*IGHG2B*
A0A0N4SV66	Histone H2A	*H2AJ*
A0A0R4J0I1	Serine protease inhibitor A3K	*SERPINA3K*
A0A1B0GR60	Ferritin	*FTL1*
A0A2I3BQ03	14-3-3 protein zeta/delta	*YWHAZ*
A0A2K6EDJ7	Inter alpha-trypsin inhibitor, heavy chain 4	*ITIH4*
A2AJD1	BPI1 domain-containing protein	*BPIFB9B*
A2ATR8	Plasma protease C1 inhibitor	*SERPING1*
A2BIN0	Major urinary protein 11	*MUP9*
A8DUK4	GLOBIN domain-containing protein	*HBB-BS*
B7ZNJ1	Fibronectin	*FN1*
D3YTY9	Kininogen-1	*KNG1*
D3YY36	RIKEN cDNA 1300017J02 gene	*1300017J02RIK*
D3Z0Y2	Peroxiredoxin-6	*PRDX6*
E9Q5F6	Polyubiquitin-C	*UBC*
F6WHQ7	Glutathione S-transferase Mu 1	*GSTM1*
F8WIR1	Cathepsin D	*CTSD*
G3X9T8	Ceruloplasmin	*CP*
O08692	Neutrophilic granule protein	*NGP*
O09049	Regenerating islet-derived protein 3-gamma	*REG3G*
O09131	Glutathione S-transferase omega-1	*GSTO1*
O09164	Extracellular superoxide dismutase [Cu-Zn]	*SOD3*

MOUSE H20.1		
PROTEIN	**PROTEIN NAME**	**GEN**
A0A075B5P3	Immunoglobulin heavy constant gamma 2B	*IGHG2B*
A0A075B5P4	Ig gamma-1 chain C region secreted form	*IGHG1*
A0A075B5P5	Immunoglobulin heavy constant gamma 3	*IGHG3*
A0A075B5V0	Immunoglobulin heavy variable 1-26	*IGHV1-26*
A0A087WR20	Pro-cathepsin H	*CTSH*
A0A0R4J0I1	Serine protease inhibitor A3K	*MCM2*
A0A1B0GR60	Ferritin	*FTL1*
A0A1B0GSR9	L-lactate dehydrogenase	*LDHA*
A0A1C7ZMZ5	Glutathione peroxidase	*GPX3*
A0A1D5RLD8	Glyceraldehyde-3-phosphate dehydrogenase	*GM10358*
A0A2K6EDJ7	Inter alpha-trypsin inhibitor, heavy chain 4	*ITIH4*
A0A5F8MPW1	Angiotensin 1-10	*AGT*
A2AJD1	BPI1 domain-containing protein	*BPIFB9B*
A2BIN1	Lipocln_cytosolic_FA-bd_dom domain-containing protein	*MUP10*
A8DUK4	GLOBIN domain-containing protein	*HBB-BS*
B7ZNJ1	Fibronectin	*FN1*
D3YTK7	Basal cell adhesion molecule	*BCAM*
D3YTY9	Kininogen-1	*KNG1*
D3Z5G7	Carboxylic ester hydrolase	*CES1B*
D6RGQ0	Complement factor H	*CFH*
E0CX80	Selenoprotein P	*SELENOP*
E9PV24	Fibrinogen alpha chain	*PGLYRP1*

O35744	Chitinase-like protein 3	*CHIL3*	E9PVG8	RIKEN cDNA 9530053A07 gene	*9530053A07RIK*
O70370	Cathepsin S	*CTSS*	E9Q4G8	Activated leukocyte cell adhesion molecule	*ALCAM*
O70570	Polymeric immunoglobulin receptor	*PIGR*	E9Q7P0	Dynein heavy chain 17, axonemal	*DNAH17*
O88593	Peptidoglycan recognition protein 1	*PGLYRP1*	F8WIR1	Cathepsin D	*CTSD*
O89020	Afamin	*AFM*	G3X9T8	Ceruloplasmin	*CP*
P00920	Carbonic anhydrase 2	*CA2*	G5E8C3	Retinoic acid-induced protein 3	*GPRC5A*
P01027	Complement C3	*C3*	O08692	Neutrophilic granule protein	*NGP*
P01837	Immunoglobulin kappa constant	*IGKC*	O08709	Peroxiredoxin-6	*PRDX6*
P01868	Ig gamma-1 chain C region secreted form	*IGHG1*	O09043	Napsin-A	*NAPSA*
P01887	Beta-2-microglobulin	*B2M*	O09049	Regenerating islet-derived protein 3-gamma	*REG3G*
P03953	Complement factor D	*CFD*	O09131	Glutathione S-transferase omega-1	*GSTO1*
P04186	Complement factor B	*CFB*	O09164	Extracellular superoxide dismutase [Cu-Zn]	*SOD3*
P06684	Complement C5	*C5*	O35744	Chitinase-like protein 3	*CHIL3*
P06728	Apolipoprotein A-IV	*APOA4*	O70370	Cathepsin S	*CTSS*
P06745	Glucose-6-phosphate isomerase	*GPI*	O70570	Polymeric immunoglobulin receptor	*PIGR*
P06909	Complement factor H	*CFH*	O88593	Peptidoglycan recognition protein 1	*PGLYRP1*
P07309	Transthyretin	*TTR*	O88844	Isocitrate dehydrogenase [NADP] cytoplasmic	*IDH1*
P07724	Albumin	*ALB*	O89020	Afamin	*AFM*
P08071	Lactotransferrin	*LTF*	P00920	Carbonic anhydrase 2	*CA2*
P08074	Carbonyl reductase [NADPH] 2	*CBR2*	P01027	Complement C3	*C3*
P08228	Superoxide dismutase [Cu-Zn]	*SOD1*	P01029	Complement C4-B	*C4B*
P08905	Lysozyme C-2	*LYZ2*	P01837	Immunoglobulin kappa constant	*IGKC*
P09602	Non-histone chromosomal protein HMG-17	*HMGN2*	P01887	Beta-2-microglobulin	*B2M*
P10107	Annexin A1	*ANXA1*	P03953	Complement factor D	*CFD*
P10605	Cathepsin B	*CTSB*	P04186	Complement factor B	*CFB*
P10810	Monocyte differentiation antigen CD14	*CD14*	P05064	Fructose-bisphosphate aldolase A	*ALDOA*

P10853	Histone H2B type 1-F/J/L	*H2BC7*	P06684	Complement C5	*C5*
P11247	Myeloperoxidase	*MPO*	P06728	Apolipoprotein A-IV	*APOA4*
P11672	Neutrophil gelatinase-associated lipocalin	*LCN2*	P06745	Glucose-6-phosphate isomerase	*GPI*
P11680	Properdin	*CFP*	P07309	Transthyretin	*TTR*
P13020	Gelsolin	*GSN*	P07356	Annexin A2	*ANXA2*
P13597	Intercellular adhesion molecule 1	*ICAM1*	P07724	Albumin	*ALB*
P14069	Protein S100-A6	*S100A6*	P08071	Lactotransferrin	*LTF*
P17563	Methanethiol oxidase	*SELENBP1*	P08074	Carbonyl reductase [NADPH] 2	*CBR2*
P17897	Lysozyme C-1	*LYZ1*	P08228	Superoxide dismutase [Cu-Zn]	*SOD1*
P20918	Plasminogen	*PLG*	P08905	Lysozyme C-2	*LYZ2*
P21614	Vitamin D-binding protein	*GC*	P09528	Ferritin heavy chain	*FTH1*
P23953	Carboxylesterase 1C	*CES1C*	P10107	Annexin A1	*ANXA1*
P24549	Retinal dehydrogenase 1	*ALDH1A1*	P10126	Elongation factor 1-alpha 1	*EEF1A1*
P26040	Ezrin	*EZR*	P10605	Cathepsin B	*CTSB*
P26041	Moesin	*MSN*	P10649	Glutathione S-transferase Mu 1	*GSTM1*
P27005	Protein S100-A8	*S100A8*	P10810	Monocyte differentiation antigen CD14	*CD14*
P27784	C-C motif chemokine 6	*SCYA6*	P10853	Histone H2B type 1-F/J/L	*H2BC7*
P28665	Murinoglobulin-1	*MUG1*	P11499	Heat shock protein HSP 90-beta	*HSP90AB1*
P29699	Alpha-2-HS-glycoprotein	*AHSG*	P11672	Neutrophil gelatinase-associated lipocalin	*LCN2*
P30115	Glutathione S-transferase A3	*GSTA3*	P13020	Gelsolin	*GSN*
P31725	Protein S100-A9	*S100A9*	P13597	Intercellular adhesion molecule 1	*ICAM1*
P32261	Antithrombin-III	*SERPINC1*	P14069	Protein S100-A6	*S100A6*
P35700	Peroxiredoxin-1	*PRDX1*	P17563	Methanethiol oxidase	*SELENBP1*
P40124	Adenylyl cyclase-associated protein 1	*CAP1*	P17897	Lysozyme C-1	*LYZ1*
P40142	Transketolase	*TKT*	P19221	Prothrombin	*F2*
P41245	Matrix metalloproteinase-9	*MMP9*	P20918	Plasminogen	*PLG*

P43274	Histone H1.4	*H1-4*	P21614	Vitamin D-binding protein	*GC*
P50404	Pulmonary surfactant-associated protein D	*SFTPD*	P23953	Carboxylesterase 1C	*CES1C*
P50543	Protein S100-A11	*S100A11*	P24472	Glutathione S-transferase A4	*GSTA4*
P60710	Actin, cytoplasmic 1	*ACTB*	P24549	Retinal dehydrogenase 1	*ALDH1A1*
P62806	Histone H4	*H4F16*	P26041	Moesin	*MSN*
P84228	Histone H3.2	*H3C13*	P27005	Protein S100-A8	*S100A8*
P97361	BPI fold-containing family A member 1	*BPIFA1*	P28665	Murinoglobulin-1	*MUG1*
P97821	Dipeptidyl peptidase 1	*CTSC*	P29699	Alpha-2-HS-glycoprotein	*AHSG*
Q01339	Beta-2-glycoprotein 1	*APOH*	P30115	Glutathione S-transferase A3	*GSTA3*
Q01768	Nucleoside diphosphate kinase B	*NME2*	P31725	Protein S100-A9	*S100A9*
Q03734	Serine protease inhibitor A3M	*SERPINA3M*	P32261	Antithrombin-III	*SERPINC1*
Q06318	Uteroglobin	*SCGB1A1*	P35242	Pulmonary surfactant-associated protein A	*SFTPA1*
Q06890	Clusterin	*CLU*	P35700	Peroxiredoxin-1	*PRDX1*
Q3MHH8	Alpha-amylase	*AMY2A*	P40142	Transketolase	*TKT*
Q3U8S1	CD44 antigen	*CD44*	P48036	Annexin A5	*ANXA5*
Q3UP87	Neutrophil elastase	*ELANE*	P50404	Pulmonary surfactant-associated protein D	*SFTPD*
Q504P4	Heat shock cognate 71 kDa protein	*HSPA8*	P50405	Pulmonary surfactant-associated protein B	*SFTPB*
Q60590	Alpha-1-acid glycoprotein 1	*ORM1*	P50543	Protein S100-A11	*S100A11*
Q61129	Complement factor I	*CFI*	P60710	Actin, cytoplasmic 1	*ACTB*
Q61171	Peroxiredoxin-2	*PRDX2*	P62806	Histone H4	*H4F16*
Q61233	Plastin-2	*LCP1*	P63101	14-3-3 protein zeta/delta	*YWHAZ*
Q61247	Alpha-2-antiplasmin	*SERPINF2*	P84228	Histone H3.2	*H3C13*
Q61362	Chitinase-3-like protein 1	*CHI3L1*	P97298	Pigment epithelium-derived factor	*SERPINF1*
Q61599	Rho GDP-dissociation inhibitor 2	*ARHGDIB*	P97361	BPI fold-containing family A member 1	*BPIFA1*
Q61646	Haptoglobin	*HP*	P97425	Eosinophil cationic protein 2	*EAR2*
Q61838	Pregnancy zone protein	*PZP*	P97821	Dipeptidyl peptidase 1	*CTSC*

Q6ZQ29	Serine/threonine-protein kinase TAO2	*TAOK2*
Q80YC5	Coagulation factor XII	*F12*
Q8BND5	Sulfhydryl oxidase 1	*QSOX1*
Q8K0E8	Fibrinogen beta chain	*FGB*
Q8K426	Resistin-like gamma	*RETNLG*
Q8VCM7	Fibrinogen gamma chain	*FGG*
Q91VB8	Alpha globin 1	*HBA-A1*
Q91X72	Hemopexin	*HPX*
Q91XA9	Acidic mammalian chitinase	*CHIA*
Q91XL1	LRRCT domain-containing protein	*LRG1*
Q921I1	Serotransferrin	*TF*
Q93092	Transaldolase	*TALDO1*
Q99PT1	Rho GDP-dissociation inhibitor 1	*ARHGDIA*
Q9D154	Leukocyte elastase inhibitor A	*SERPINB1A*
Q9ESB3	Histidine-rich glycoprotein	*HRG*
Q9QXC1	Fetuin-B	*FETUB*
Q9WUU7	Cathepsin Z	*CTSZ*
Q9WVF5	Receptor protein-tyrosine kinase	*EGFR*
Q9WVL7	C-X-C motif chemokine 15 (Cxcl15)	*SCYB15*
Q9Z0J0	NPC intracellular cholesterol transporter 2	*NPC2*
S4R239	Pulmonary surfactant-associated protein B	*SFTPB*

Q01339	Beta-2-glycoprotein 1	*APOH*
Q01768	Nucleoside diphosphate kinase B	*NME2*
Q03734	Serine protease inhibitor A3M	*SERPINA3M*
Q06318	Uteroglobin	*SCGB1A1*
Q06770	Corticosteroid-binding globulin	*SERPINA6*
Q06890	Clusterin	*CLU*
Q07797	Galectin-3-binding protein	*LGALS3BP*
Q504P4	Heat shock cognate 71 kDa protein	*HSPA8*
Q5SQ27	SEC14-like 3 (S. cerevisiae)	*SEC14L3*
Q5SX22	Polyubiquitin-B	*UBB*
Q60590	Alpha-1-acid glycoprotein 1	*ORM1*
Q61114	BPI fold-containing family B member 1	*BPIFB1*
Q61129	Complement factor I	*CFI*
Q61171	Peroxiredoxin-2	*PRDX2*
Q61233	Plastin-2	*LCP1*
Q61247	Alpha-2-antiplasmin	*SERPINF2*
Q61362	Chitinase-3-like protein 1	*CHI3L1*
Q61646	Haptoglobin	*HP*
Q61838	Pregnancy zone protein	*PZP*
Q62151	Advanced glycosylation end product-specific receptor	*AGER*
Q64437	All-trans-retinol dehydrogenase [NAD(+)] ADH7	*ADH7*
Q64726	Zinc-alpha-2-glycoprotein	*AZGP1*
Q6S9I0	Kininogen 2	*KNG2*
Q8BND5	Sulfhydryl oxidase 1	*QSOX1*
Q8VCM7	Fibrinogen gamma chain	*FGG*
Q8VCT4	Carboxylesterase 1D	*CES1D*

Q91VB8	Alpha globin 1	*HBA-A1*
Q91X70	Complement component 6	*C6*
Q91X72	Hemopexin	*HPX*
Q91XA9	Acidic mammalian chitinase	*CHIA*
Q91XL1	LRRCT domain-containing protein	*LRG1*
Q921I1	Serotransferrin	*TF*
Q93092	Transaldolase	*TALDO1*
Q9D154	Leukocyte elastase inhibitor A	*SERPINB1A*
Q9DBD0	Inhibitor of carbonic anhydrase	*ICA*
Q9DCD0	6-phosphogluconate dehydrogenase, decarboxylating	*PGD*
Q9ESB3	Histidine-rich glycoprotein	*HRG*
Q9QXC1	Fetuin-B	*FETUB*
Q9WUU7	Cathepsin Z	*CTSZ*
Q9WV54	Acid ceramidase	*ASAH1*
Q9WVL7	C-X-C motif chemokine 15	*CXCL15*
Q9Z0J0	NPC intracellular cholesterol transporter 2	*NPC2*

Table Annexed 5. Mouse proteins 13th Dose

MOUSE H4.13		
PROTEIN	**PROTEIN NAME**	**GEN**
A0A075B5N7	Ig-like domain-containing protein	*IGKV6-13*
A0A075B5P3	Immunoglobulin heavy constant gamma 2B	*IGHG2B*
A0A075B5P4	Ig gamma-1 chain C region secreted form	*IGHG1*
A0A075B5P5	Immunoglobulin heavy constant gamma 3	*IGHG3*
A0A075B5R5	Ig-like domain-containing protein	*IGHV4-1*
A0A075B5T4	Ig-like domain-containing protein	*IGHV1-4*
A0A075B5V0	Immunoglobulin heavy variable 1-26	*IGHV1-26*
A0A075B6A3	Immunoglobulin heavy constant alpha	*IGHA*
A0A0A6YXN4	Immunoglobulin heavy variable V1-18	*IGHV1-18*
A0A0A6YY53	Immunoglobulin heavy constant gamma 2C	*IGHG2C*
A0A0A6YYE7	Ig-like domain-containing protein	*IGKV4-57*
A0A0B4J1J7	Ig-like domain-containing protein	*IGHV1-82*
A0A0N4SVV8	L-lactate dehydrogenase	*LDHB*
A0A0R4J0I1	Serine protease inhibitor A3K	*MCM2*
A0A140T8M2	Ig-like domain-containing protein	*IGKV12-44*
A0A140T8N0	Immunoglobulin kappa chain variable 9-120	*IGKV9-120*
A0A140T8N3	Ig-like domain-containing protein	*IGKV13-84*
A0A140T8N7	Ig-like domain-containing protein	*IGKV6-25*
A0A140T8N9	Ig-like domain-containing protein	*IGKV6-32*
A0A1B0GR60	Ferritin	*FTL1*
A0A1B0GSR9	L-lactate dehydrogenase	*LDHA*
A0A1C7ZMZ5	Glutathione peroxidase	*GPX3*

MOUSE H20.13		
PROTEIN	**PROTEIN NAME**	**GEN**
A0A075B5N4	Ig-like domain-containing protein	*IGKV8-27*
A0A075B5N7	Ig-like domain-containing protein	*IGKV6-13*
A0A075B5N9	Ig-like domain-containing protein	*IGKV3-7*
A0A075B5P3	Immunoglobulin heavy constant gamma 2B	*IGHG2B*
A0A075B5P4	Ig gamma-1 chain C region secreted form	*IGHG1*
A0A075B5P5	Immunoglobulin heavy constant gamma 3	*IGHG3*
A0A075B5P6	Immunoglobulin heavy constant mu	*IGHM*
A0A075B5R0	Ig-like domain-containing protein	*IGHV5-16*
A0A075B5R1	Ig-like domain-containing protein	*IGHV5-17*
A0A075B5R5	Ig-like domain-containing protein	*IGHV4-1*
A0A075B5R7	Ig-like domain-containing protein	*IGHV14-2*
A0A075B5W6	Ig-like domain-containing protein	*IGHV1-55*
A0A075B5X7	Ig-like domain-containing protein	*IGHV1-69*
A0A075B5Y1	Ig-like domain-containing protein	*IGHV1-74*
A0A075B5Y4	Ig-like domain-containing protein	*IGHV1-81*
A0A075B5Y5	Immunoglobulin heavy variable 1-84	*IGHV1-84*
A0A075B664	Immunoglobulin lambda variable 2	*IGLV2*
A0A075B680	Ig-like domain-containing protein	*IGHV1-62-2*
A0A075B680	Immunoglobulin heavy variable 1-62-2	*IGHV1-62-2*
A0A075B6A3	Immunoglobulin heavy constant alpha	*IGHA*
A0A0A6YY53	Immunoglobulin heavy constant gamma 2C	*IGHG2C*
A0A0A6YYE7	Ig-like domain-containing protein	*IGKV4-57*

A0A1D5RLD8	Glyceraldehyde-3-phosphate dehydrogenase	*GM10358*
A0A1L1SST0	Peptidyl-prolyl cis-trans isomerase	*PPIA*
A0A2K6EDJ7	Inter alpha-trypsin inhibitor, heavy chain 4	*ITIH4*
B7ZNJ1	Fibronectin	*FN1*
D3YTY9	Kininogen-1	*KNG1*
D6RGQ0	Complement factor H	*CFH*
E0CX80	Selenoprotein P	*SELENOP*
E9Q223	Hemoglobin, beta adult s chain	*HBB-BS*
E9Q5F6	Polyubiquitin-C	*UBC*
E9Q9C6	Fc fragment of IgG-binding protein	*FCGBP*
F6Y6L6	Predicted gene, 49369	*GM49369*
G3X8T9	Serine protease inhibitor A3N	*SERPINA3N*
G3X9T8	Ceruloplasmin	*CP*
O09049	Regenerating islet-derived protein 3-gamma	*REG3G*
O09131	Glutathione S-transferase omega-1	*GSTO1*
O09164	Extracellular superoxide dismutase [Cu-Zn]	*SOD3*
O35744	Chitinase-like protein 3	*CHIL3*
O35945	Aldehyde dehydrogenase, cytosolic 1	*ALDH1A7*
O55226	Chondroadherin	*CHAD*
O70370	Cathepsin S	*CTSS*
O70456	14-3-3 protein sigma	*SFN*
O70570	Polymeric immunoglobulin receptor	*PIGR*
O88593	Peptidoglycan recognition protein 1	*PGLYRP1*
O88844	Isocitrate dehydrogenase [NADP] cytoplasmic	*IDH1*
O89020	Afamin	*AFM*
P00687	Alpha-amylase 1	*AMY1*
A0A0B4J1J2	Ig-like domain-containing protein	*IGKV5-43*
A0A0B4J1J7	Ig-like domain-containing protein	*IGHV1-82*
A0A0B4J1N0	Ig-like domain-containing protein	*IGHV1-76*
A0A0R4IZW5	Cadherin-1	*CDH1*
A0A0R4J0I1	Serine protease inhibitor A3K	*MCM2*
A0A140T8M0	Ig-like domain-containing protein	*IGKV1-117*
A0A140T8M2	Ig-like domain-containing protein	*IGKV12-44*
A0A140T8N3	Ig-like domain-containing protein	*IGKV13-84*
A0A140T8N9	Ig-like domain-containing protein	*IGKV6-32*
A0A140T8P5	Ig-like domain-containing protein	*IGKV8-24*
A0A140T8Q3	Immunoglobulin kappa variable 6-17	*IGKV6-17*
A0A1B0GR60	Ferritin	*FTL1*
A0A1B0GSR9	L-lactate dehydrogenase	*LDHA*
A0A1C7ZMZ5	Glutathione peroxidase	*GPX3*
A0A1D5RLD8	Glyceraldehyde-3-phosphate dehydrogenase	*GM10358*
A0A1D5RLP1	Coactosin-like protein	*COTL1*
A0A1L1SST0	Peptidyl-prolyl cis-trans isomerase	*PPIA*
A0A1Y7VNQ4	Procathepsin L	*CTSL*
A0A2I3BQ03	14-3-3 protein zeta/delta	*YWHAZ*
A0A2K6EDJ7	Inter alpha-trypsin inhibitor, heavy chain 4	*ITIH4*
A0A494B9D4	Ferritin	*FTH1*
B0V2N5	Annexin	*ANXA2*
B9EHT6	Fibronectin	*FIBRONECTIN*
D3YTY9	Kininogen-1	*KNG1*
D3YXF5	Complement component 7	*C7*
D6RGQ0	Complement factor H	*CFH*

P01027	Complement C3	*C3*	E9PV24	Fibrinogen alpha chain	*FGA*
P01029	Complement C4-B	*C4B*	E9PZ00	Prosaposin	*PSAP*
P01631	Ig kappa chain V-II region 26-10	*KV2A7*	E9Q4U7	Protein diaphanous homolog 2	*DIAPH2*
P01638	Ig kappa chain V-V region L6	*KV5A6*	E9Q9C6	Fc fragment of IgG-binding protein	*FCGBP*
P01660	Ig kappa chain V-III region PC 3741/TEPC 111	*KV3A8*	F6ZFS0	EGF-containing fibulin-like extracellular matrix protein 1	*EFEMP1*
P01724	Ig lambda-1 chain V regions MOPC 104E/RPC20/J558/S104	*LV1B*	G3X8T9	Serine protease inhibitor A3N	*SERPINA3N*
P01837	Immunoglobulin kappa constant	*IGKC*	G3X9T8	Ceruloplasmin	*CP*
P01843	Ig lambda-1 chain C region	*LAC1*	H7BXC3	Triosephosphate isomerase	*TPI1*
P01872	Immunoglobulin heavy constant mu	*IGHM*	O09049	Regenerating islet-derived protein 3-gamma	*REG3G*
P01887	Beta-2-microglobulin	*B2M*	O09131	Glutathione S-transferase omega-1	*GSTO1*
P03953	Complement factor D	*CFD*	O09164	Extracellular superoxide dismutase [Cu-Zn]	*SOD3*
P04186	Complement factor B	*CFB*	O35744	Chitinase-like protein 3	*CHIL3*
P05064	Fructose-bisphosphate aldolase A	*ALDOA*	O35945	Aldehyde dehydrogenase, cytosolic 1	*ALDH1A7*
P06684	Complement C5	*C5*	O55226	Chondroadherin	*CHAD*
P06728	Apolipoprotein A-IV	*APOA4*	O70370	Cathepsin S	*CTSS*
P06745	Glucose-6-phosphate isomerase	*GPI*	O70570	Polymeric immunoglobulin receptor	*PIGR*
P07309	Transthyretin	*TTR*	O88312	Anterior gradient protein 2 homolog	*AGR2*
P07356	Annexin A2	*ANXA2*	O88593	Peptidoglycan recognition protein 1	*PGLYRP1*
P07724	Albumin	*ALB*	O89020	Afamin	*AFM*
P07901	Heat shock protein HSP 90-alpha	*HSP90AA1*	P00687	Alpha-amylase 1	*AMY1*
P08071	Lactotransferrin	*LTF*	P00920	Carbonic anhydrase 2	*CA2*
P08074	Carbonyl reductase [NADPH] 2	*CBR2*	P01027	Complement C3	*C3*
P08228	Superoxide dismutase [Cu-Zn]	*SOD1*	P01592	Immunoglobulin J chain	*JCHAIN*
P08905	Lysozyme C-2	*LYZ2*	P01638	Ig kappa chain V-V region L6	*KV5A6*
P09103	Protein disulfide-isomerase	*P4HB*	P01644	Ig kappa chain V-V region HP R16.7	*KV5AB*
P10107	Annexin A1	*ANXA1*	P01801	Ig heavy chain V-III region J606	*HVM32*

P10126	Elongation factor 1-alpha 1	*EEF1A1*
P10605	Cathepsin B	*CTSB*
P10649	Glutathione S-transferase Mu 1	*GSTM1*
P10810	Monocyte differentiation antigen CD14	*CD14*
P11499	Heat shock protein HSP 90-beta	*HSP90AB1*
P11672	Neutrophil gelatinase-associated lipocalin	*LCN2*
P11680	Properdin	*CFP*
P13020	Gelsolin	*GSN*
P13597	Intercellular adhesion molecule 1	*ICAM1*
P14069	Protein S100-A6	*S100A6*
P14152	Malate dehydrogenase, cytoplasmic	*MDH1*
P14211	Calreticulin	*CALR*
P17182	Alpha-enolase	*ENO1*
P17563	Methanethiol oxidase	*SELENBP1*
P17751	Triosephosphate isomerase	*TPI1*
P17897	Lysozyme C-1	*LYZ1*
P18531	Ig heavy chain V region 3-6	*IGHV3-6*
P19221	Prothrombin	*F2*
P20918	Plasminogen	*PLG*
P21614	Vitamin D-binding protein	*GC*
P23953	Carboxylesterase 1C	*CES1C*
P24472	Glutathione S-transferase A4	*GSTA4*
P24549	Retinal dehydrogenase 1	*ALDH1A1*
P26040	Ezrin	*EZR*
P27005	Protein S100-A8	*S100A8*
P27773	Protein disulfide-isomerase A3	*PDIA3*
P01837	Immunoglobulin kappa constant	*IGKC*
P01843	Ig lambda-1 chain C region	*LAC1*
P01845	Ig lambda-3 chain C region	*IGLC3*
P01868	Ig gamma-1 chain C region secreted form	*IGHG1*
P01887	Beta-2-microglobulin	*B2M*
P03953	Complement factor D	*CFD*
P04186	Complement factor B	*CFB*
P04940	Ig kappa chain V-VI region NQ2-17.4.1	*KV6A6*
P06330	Ig heavy chain V region AC38 205.12	*HVM51*
P06684	Complement C5	*C5*
P06728	Apolipoprotein A-IV	*APOA4*
P07309	Transthyretin	*TTR*
P07724	Albumin	*ALB*
P08071	Lactotransferrin	*LTF*
P08074	Carbonyl reductase [NADPH] 2	*CBR2*
P08228	Superoxide dismutase [Cu-Zn]	*SOD1*
P08905	Lysozyme C-2	*LYZ2*
P09103	Protein disulfide-isomerase	*P4HB*
P0CG49	Polyubiquitin-B	*UBB*
P10107	Annexin A1	*ANXA1*
P10126	Elongation factor 1-alpha 1	*EEF1A1*
P10605	Cathepsin B	*CTSB*
P10649	Glutathione S-transferase Mu 1	*GSTM1*
P10810	Monocyte differentiation antigen CD14	*CD14*
P10923	Osteopontin	*SPP1*
P11499	Heat shock protein HSP 90-beta	*HSP90AB1*

P28665	Murinoglobulin-1	*MUG1*	P11672	Neutrophil gelatinase-associated lipocalin	*LCN2*
P29699	Alpha-2-HS-glycoprotein	*AHSG*	P11680	Properdin	*CFP*
P30115	Glutathione S-transferase A3	*GSTA3*	P13020	Gelsolin	*GSN*
P31725	Protein S100-A9	*S100A9*	P13597	Intercellular adhesion molecule 1	*ICAM1*
P32261	Antithrombin-III	*SERPINC1*	P14211	Calreticulin	*CALR*
P35242	Pulmonary surfactant-associated protein A	*SFTPA1*	P17563	Methanethiol oxidase	*SELENBP1*
P35700	Peroxiredoxin-1	*PRDX1*	P17897	Lysozyme C-1	*LYZ1*
P40142	Transketolase	*TKT*	P18242	Cathepsin D	*CTSD*
P47739	Aldehyde dehydrogenase, dimeric NADP-preferring	*ALDH3A1*	P18531	Ig heavy chain V region 3-6	*IGHV3-6*
P47791	Glutathione reductase, mitochondrial	*GSR*	P19221	Prothrombin	*F2*
P48036	Annexin A5	*ANXA5*	P20918	Plasminogen	*PLG*
P50404	Pulmonary surfactant-associated protein D	*SFTPD*	P21614	Vitamin D-binding protein	*GC*
P50543	Protein S100-A11	*S100A11*	P21956	Lactadherin	*MFGE8*
P52480	Pyruvate kinase PKM	*PKM*	P23953	Carboxylesterase 1C	*CES1C*
P60710	Actin, cytoplasmic 1	*ACTB*	P24369	Peptidyl-prolyl cis-trans isomerase B	*PPIB*
P62259	14-3-3 protein epsilon	*YWHAE*	P24472	Glutathione S-transferase A4	*GSTA4*
P62806	Histone H4	*H4F16*	P24549	Retinal dehydrogenase 1	*ALDH1A1*
P63017	Heat shock cognate 71 kDa protein	*HSPA8*	P26040	Ezrin	*EZR*
P63101	14-3-3 protein zeta/delta	*YWHAZ*	P26041	Moesin	*MSN*
P97290	Plasma protease C1 inhibitor	*SERPING1*	P27773	Protein disulfide-isomerase A3	*PDIA3*
P97361	BPI fold-containing family A member 1	*BPIFA1*	P27784	C-C motif chemokine 6	*CCL6*
P97425	Eosinophil cationic protein 2	*EAR2*	P28665	Murinoglobulin-1	*MUG1*
P97821	Dipeptidyl peptidase 1	*CTSC*	P29699	Alpha-2-HS-glycoprotein	*AHSG*
Q00623	Apolipoprotein A-I	*APOA1*	P30115	Glutathione S-transferase A3	*GSTA3*
Q01339	Beta-2-glycoprotein 1	*APOH*	P31725	Protein S100-A9	*S100A9*
Q03734	Serine protease inhibitor A3M	*SERPINA3M*	P32261	Antithrombin-III	*SERPINC1*

Q06318	Uteroglobin	*SCGB1A1*
Q06770	Corticosteroid-binding globulin	*SERPINA6*
Q06890	Clusterin	*CLU*
Q3TQP6	Malic enzyme	*ME1*
Q3UEG7	Inter-alpha-trypsin inhibitor heavy chain H2	*ITIH2*
Q5NC80	Nucleoside diphosphate kinase	*NME1*
Q5SQ27	SEC14-like 3 (S. cerevisiae)	*SEC14L3*
Q60590	Alpha-1-acid glycoprotein 1	*ORM1*
Q61114	BPI fold-containing family B member 1	*BPIFB1*
Q61129	Complement factor I	*CFI*
Q61233	Plastin-2	*LCP1*
Q61247	Alpha-2-antiplasmin	*SERPINF2*
Q61362	Chitinase-3-like protein 1	*CHI3L1*
Q61646	Haptoglobin	*HP*
Q61838	Pregnancy zone protein	*PZP*
Q64437	All-trans-retinol dehydrogenase [NAD(+)] ADH7	*ADH7*
Q6GT24	Peroxiredoxin-6	*PRDX6*
Q6IFZ6	Keratin, type II cytoskeletal 1b	*KRT77*
Q792Z1	Peptidase S1 domain-containing protein	*TRY10*
Q8BND5	Sulfhydryl oxidase 1	*QSOX1*
Q8VCT4	Carboxylesterase 1D	*CES1D*
Q91X72	Hemopexin	*HPX*
Q91XA9	Acidic mammalian chitinase	*CHIA*
Q91XL1	LRRCT domain-containing protein	*LRG1*
Q91Z98	Chitinase-like protein 4	*CHIL4*
Q921I1	Serotransferrin	*TF*

P35242	Pulmonary surfactant-associated protein A	*SFTPA1*
P35700	Peroxiredoxin-1	*PRDX1*
P47739	Aldehyde dehydrogenase, dimeric NADP-preferring	*ALDH3A1*
P48036	Annexin A5	*ANXA5*
P50404	Pulmonary surfactant-associated protein D	*SFTPD*
P50543	Protein S100-A11	*S100A11*
P60710	Actin, cytoplasmic 1	*ACTB*
P62259	14-3-3 protein epsilon	*YWHAE*
P97361	BPI fold-containing family A member 1	*BPIFA1*
P97425	Eosinophil cationic protein 2	*EAR2*
P97426	Eosinophil cationic protein 1	*EAR1*
P97821	Dipeptidyl peptidase 1	*CTSC*
Q01339	Beta-2-glycoprotein 1	*APOH*
Q01768	Nucleoside diphosphate kinase B	*NME2*
Q02257	Junction plakoglobin	*JUP*
Q03404	Trefoil factor 2	*TFF2*
Q03734	Serine protease inhibitor A3M	*SERPINA3M*
Q06318	Uteroglobin	*SCGB1A1*
Q06770	Corticosteroid-binding globulin	*SERPINA6*
Q06890	Clusterin	*CLU*
Q504P4	Heat shock cognate 71 kDa protein	*HSPA8*
Q5SQ27	SEC14-like 3 (S. cerevisiae)	*SEC14L3*
Q60590	Alpha-1-acid glycoprotein 1	*ORM1*
Q61114	BPI fold-containing family B member 1	*BPIFB1*
Q61129	Complement factor I	*CFI*
Q61233	Plastin-2	*LCP1*

Q99PT1	Rho GDP-dissociation inhibitor 1	*ARHGDIA*
Q9CQV8	14-3-3 protein beta/alpha	*YWHAB*
Q9D7Z6	Calcium-activated chloride channel regulator 1	*CLCA1*
Q9DBD0	Inhibitor of carbonic anhydrase	*ICA*
Q9ESB3	Histidine-rich glycoprotein	*HRG*
Q9QXC1	Fetuin-B	*FETUB*
Q9R0H5	Keratin, type II cytoskeletal 71	*KRT71*
Q9WUU7	Cathepsin Z	*CTSZ*
Q9WVA4	Transgelin-2	*TAGLN2*
Q9Z0J0	NPC intracellular cholesterol transporter 2	*NPC2*
S4R2L6	Pulmonary surfactant-associated protein B	*SFTPB*

Q61247	Alpha-2-antiplasmin	*SERPINF2*
Q61362	Chitinase-3-like protein 1	*CHI3L1*
Q61646	Haptoglobin	*HP*
Q61703	Inter-alpha-trypsin inhibitor heavy chain H2	*ITIH2*
Q6GT24	Peroxiredoxin-6	*PRDX6*
Q6IFZ6	Keratin, type II cytoskeletal 1b	*KRT77*
Q80YC5	Coagulation factor XII	*F12*
Q8BND5	Sulfhydryl oxidase 1	*QSOX1*
Q8K196	RNAse_Pc domain-containing protein	*RNASE2A*
Q8VCT4	Carboxylesterase 1D	*CES1D*
Q91X70	Complement component 6	*C6*
Q91X72	Hemopexin	*HPX*
Q91XA9	Acidic mammalian chitinase	*CHIA*
Q91XL1	LRRCT domain-containing protein	*LRG1*
Q91Z98	Chitinase-like protein 4	*CHIL4*
Q921I1	Serotransferrin	*TF*
Q99PT1	Rho GDP-dissociation inhibitor 1	*ARHGDIA*
Q9D1H9	Microfibril-associated glycoprotein 4	*MFAP4*
Q9D7Z6	Calcium-activated chloride channel regulator 1	*CLCA1*
Q9DBD0	Inhibitor of carbonic anhydrase	*ICA*
Q9EP95	Resistin-like alpha	*RETNLA*
Q9ESB3	Histidine-rich glycoprotein	*HRG*
Q9QXC1	Fetuin-B	*FETUB*
Q9WUU7	Cathepsin Z	*CTSZ*
Q9WVA4	Transgelin-2	*TAGLN2*
Q9WVF5	Receptor protein-tyrosine kinase	*EGFR*

Q9WVL7	C-X-C motif chemokine 15	*CXC15*
Q9Z0J0	NPC intracellular cholesterol transporter 2	*NPC2*
S4R2L6	Pulmonary surfactant-associated protein B	*SFTPB*

Table Annexed 6. Human Proteins

HUMAN NEUTROPHILIC		
PROTEIN	**PROTEIN NAME**	**GEN**
A0A075B6I0	Immunoglobulin lambda variable 8-61	*IGLV8-61*
A0A0B4J1U7	Immunoglobulin heavy variable 6-1	*IGHV6-1*
A0A0B4J1V1	Immunoglobulin heavy variable 3-21	*IGHV3-21*
A0A0B4J1Y9	Immunoglobulin heavy variable 3-72	*IGHV3-72*
A0A0C4DH72	Immunoglobulin kappa variable 1-6	*IGKV1-6*
A6NIZ1	Ras-related protein Rap-1b-like protein	*RP1BL*
A8K7I4	Calcium-activated chloride channel regulator 1	*CLCA1*
A8MVU1	Putative neutrophil cytosol factor 1C	*NCF1C*
O00299	Chloride intracellular channel protein 1	*CLIC1*
O00391	Sulfhydryl oxidase 1	*QSOX1*
O00560	Syntenin-1	*SDCBP*
O00584	Ribonuclease T2	*RNASET2*
O00602	Ficolin-1	*FCN1*
O14818	Proteasome subunit alpha type-7	*PSMA7*
O15143	Actin-related protein 2/3 complex subunit 1B	*ARPC1B*
O15144	Actin-related protein 2/3 complex subunit 2	*ARPC2*
O15335	Chondroadherin	*CHAD*
O43490	Prominin-1	*S100A12*
O43707	Alpha-actinin-4	*ACTN4*
O60524	Nuclear export mediator factor NEMF	*NEMF*
O60635	Tetraspanin-1	*TSPAN1*
O60664	Perilipin-3	*PLIN3*

HUMAN EOSINOPHILIC		
PROTEIN	**PROTEIN NAME**	**GEN**
A0A075B6R2	Immunoglobulin heavy variable 4-4	*IGHV4-4*
A0A087WSX0	Immunoglobulin lambda variable 5-45	*IGLV5-45*
A0A0A0MS15	Immunoglobulin heavy variable 3-49	*IGHV3-49*
A0A0C4DH73	Immunoglobulin kappa variable 1-12	*IGKV1-12*
A8K7I4	Calcium-activated chloride channel regulator 1	*CLCA1*
B9A064	Immunoglobulin lambda-like polypeptide 5	*IGLL5*
O00299	Chloride intracellular channel protein 1	*CLIC1*
O00391	Sulfhydryl oxidase 1	*QSOX1*
O00560	Syntenin-1	*SDCBP*
O15143	Actin-related protein 2/3 complex subunit 1B	*ARPC1B*
O15144	Actin-related protein 2/3 complex subunit 2	*ARPC2*
O43490	Prominin-1	*PROM1*
O43707	Alpha-actinin-4	*ACTN4*
O60635	Tetraspanin-1	*TSPAN1*
O60814	Histone H2B type 1-K	*H2BC12*
O75629	Protein CREG1	*CREG1*
P00338	L-lactate dehydrogenase A chain	*LDHA*
P00352	Retinal dehydrogenase 1	*ALDH1A1*
P00450	Ceruloplasmin	*CP*
P00738	Haptoglobin	*HP*
P00739	Haptoglobin-related protein	*HPR*
P00751	Complement factor B	*CFB*

O60814	Histone H2B type 1-K	*H2BC12*	P01008	Antithrombin-III	*SERPINC1*
O75594	Peptidoglycan recognition protein 1	*PGLYRP1*	P01009	Alpha-1-antitrypsin	*SERPINA1*
O75629	Protein CREG1	*CREG1*	P01011	Alpha-1-antichymotrypsin	*SERPINA3*
O95436	Sodium-dependent phosphate transport protein 2B	*SLC34A2*	P01019	Angiotensinogen	*AGT*
O95486	Protein transport protein Sec24A	*SEC24A*	P01023	Alpha-2-macroglobulin	*A2M*
O95837	Guanine nucleotide-binding protein subunit alpha-14	*GNA14*	P01024	Complement C3	*C3*
P00338	L-lactate dehydrogenase A chain	*LDHA*	P01031	Complement C5	*C5*
P00390	Glutathione reductase, mitochondrial	*GSR*	P01033	Metalloproteinase inhibitor 1	*TIMP1*
P00450	Ceruloplasmin	*CP*	P01034	Cystatin-C	*CST3*
P00738	Haptoglobin	*GNS*	P01036	Cystatin-S	*CST4*
P00751	Complement factor B	*CFB*	P01037	Cystatin-SN	*CST1*
P01008	Antithrombin-III	*SERPINC1*	P01042	Kininogen-1	*KNG1*
P01009	Alpha-1-antitrypsin	*SERPINA1*	P01766	Immunoglobulin heavy variable 3-13	*IGHV3-13*
P01011	Alpha-1-antichymotrypsin	*SERPINA3*	P01833	Polymeric immunoglobulin receptor	*PIGR*
P01019	Angiotensinogen	*AGT*	P02533	Keratin, type I cytoskeletal 14	*KRT14*
P01023	Alpha-2-macroglobulin	*CSTB*	P02647	Apolipoprotein A-I	*APOA1*
P01024	Complement C3	*C3*	P02652	Apolipoprotein A-II	*APOA2*
P01033	Metalloproteinase inhibitor 1	*H4-16*	P02671	Fibrinogen alpha chain	*FGA*
P01034	Cystatin-C	*CST3*	P02675	Fibrinogen beta chain	*FGB*
P01036	Cystatin-S	*CST4*	P02679	Fibrinogen gamma chain	*FGG*
P01037	Cystatin-SN	*CST1*	P02746	Complement C1q subcomponent subunit B	*C1QB*
P01602	Immunoglobulin kappa variable 1-5	*IGKV1-5*	P02747	Complement C1q subcomponent subunit C	*C1QC*
P01624	Immunoglobulin kappa variable 3-15	*IGKV3-15*	P02749	Beta-2-glycoprotein 1	*APOH*
P01714	Immunoglobulin lambda variable 3-19	*IGLV3-19*	P02751	Fibronectin	*FN1*
P01717	Immunoglobulin lambda variable 3-25	*IGLV3-25*	P02753	Retinol-binding protein 4	*RBP4*
P01743	Immunoglobulin heavy variable 1-46	*IGHV1-46*	P02763	Alpha-1-acid glycoprotein 1	*ORM1*

P01780	Immunoglobulin heavy variable 3-7	*IGHV3-7*	P02765	Alpha-2-HS-glycoprotein	*AHSG*
P01782	Immunoglobulin heavy variable 3-9	*IGHV3-9*	P02766	Transthyretin	*TTR*
P01825	Immunoglobulin heavy variable 4-59	*IGHV4-59*	P02768	Albumin	*ALB*
P01833	Polymeric immunoglobulin receptor	*TIMP1*	P02774	Vitamin D-binding protein	*GC*
P02647	Apolipoprotein A-I	*APOA1*	P02787	Serotransferrin	*TF*
P02675	Fibrinogen beta chain	*FGB*	P02788	Lactotransferrin	*LTF*
P02679	Fibrinogen gamma chain	*FGG*	P02790	Hemopexin	*HPX*
P02749	Beta-2-glycoprotein 1	*APOH*	P03952	Plasma kallikrein	*KLKB1*
P02750	Leucine-rich alpha-2-glycoprotein	*LRG1*	P03973	Antileukoproteinase	*SLPI*
P02763	Alpha-1-acid glycoprotein 1	*ORM1*	P04003	C4b-binding protein alpha chain	*C4BPA*
P02765	Alpha-2-HS-glycoprotein	*AHSG*	P04004	Vitronectin	*VTN*
P02768	Albumin	*ALB*	P04040	Catalase	*CAT*
P02774	Vitamin D-binding protein	*GC*	P04075	Fructose-bisphosphate aldolase A	*ALDOA*
P02787	Serotransferrin	*TF*	P04080	Cystatin-B	*CSTB*
P02788	Lactotransferrin	*LTF*	P04083	Annexin A1	*ANXA1*
P02790	Hemopexin	*HPX*	P04114	Apolipoprotein B-100	*APOB*
P03950	Angiogenin	*ANG*	P04196	Histidine-rich glycoprotein	*HRG*
P03973	Antileukoproteinase	*SLPI*	P04217	Alpha-1B-glycoprotein	*A1BG*
P04040	Catalase	*CAT*	P04264	Keratin, type II cytoskeletal 1	*KRT1*
P04075	Fructose-bisphosphate aldolase A	*ALDOA*	P04406	Glyceraldehyde-3-phosphate dehydrogenase	*GAPDH*
P04080	Cystatin-B	*CSTB*	P05090	Apolipoprotein D	*APOD*
P04083	Annexin A1	*ANXA1*	P05109	Protein S100-A8	*S100A8*
P04179	Superoxide dismutase [Mn], mitochondrial	*SOD2*	P05155	Plasma protease C1 inhibitor	*SERPING1*
P04217	Alpha-1B-glycoprotein	*A1BG*	P05164	Myeloperoxidase	*MPO*
P04264	Keratin, type II cytoskeletal 1	*KRT1*	P05204	Non-histone chromosomal protein HMG-17	*HMGN2*
P04406	Glyceraldehyde-3-phosphate dehydrogenase	*GAPDH*	P05546	Heparin cofactor 2	*SERPIND1*

P04632	Calpain small subunit 1	*CAPNS1*
P04839	Cytochrome b-245 heavy chain	*CYBB*
P04899	Guanine nucleotide-binding protein G(i) subunit alpha-2	*GNAI2*
P05107	Integrin beta-2	*ITGB2*
P05109	Protein S100-A8	*S100A8*
P05155	Plasma protease C1 inhibitor	*SERPING1*
P05164	Myeloperoxidase	*MPO*
P05204	Non-histone chromosomal protein HMG-17	*HMGN2*
P06310	Immunoglobulin kappa variable 2-30	*IGKV2-30*
P06396	Gelsolin	*GSN*
P06702	Protein S100-A9	*S100A9*
P06703	Protein S100-A6	*S100A6*
P06733	Alpha-enolase	*ENO1*
P06737	Glycogen phosphorylase, liver form	*PYGL*
P06744	Glucose-6-phosphate isomerase	*GPI*
P06865	Beta-hexosaminidase subunit alpha	*HEXA*
P06870	Kallikrein-1	*KLK1*
P07195	L-lactate dehydrogenase B chain	*LDHB*
P07237	Protein disulfide-isomerase	*P4HB*
P07339	Cathepsin D	*CTSD*
P07355	Annexin A2	*ANXA2*
P07384	Calpain-1 catalytic subunit	*CAPN1*
P07437	Tubulin beta chain	*TUBB*
P07602	Prosaposin	*PSAP*
P07686	Beta-hexosaminidase subunit beta	*HEXB*
P07737	Profilin-1	*PFN1*
P06396	Gelsolin	*GSN*
P06702	Protein S100-A9	*S100A9*
P06703	Protein S100-A6	*S100A6*
P06731	Carcinoembryonic antigen-related cell adhesion molecule 5	*CEACAM5*
P06733	Alpha-enolase	*ENO1*
P06744	Glucose-6-phosphate isomerase	*GPI*
P07195	L-lactate dehydrogenase B chain	*LDHB*
P07237	Protein disulfide-isomerase	*P4HB*
P07339	Cathepsin D	*CTSD*
P07355	Annexin A2	*ANXA2*
P07384	Calpain-1 catalytic subunit	*CAPN1*
P07437	Tubulin beta chain	*TUBB*
P07737	Profilin-1	*PFN1*
P07900	Heat shock protein HSP 90-alpha	*HSP90AA1*
P07988	Pulmonary surfactant-associated protein B	*SFTPB*
P08133	Annexin A6	*ANXA6*
P08174	Complement decay-accelerating factor	*CD55*
P08238	Heat shock protein HSP 90-beta	*HSP90AB1*
P08246	Neutrophil elastase	*ELANE*
P08263	Glutathione S-transferase A1	*GSTA1*
P08603	Complement factor H	*CFH*
P08697	Alpha-2-antiplasmin	*SERPINF2*
P08758	Annexin A5	*ANXA5*
P09211	Glutathione S-transferase P	*GSTP1*
P09429	High mobility group protein B1	*HMGB1*
P0C0L5	Complement C4-B	*C4B_2*

P07858	Cathepsin B	*CTSB*	P0CG48	Polyubiquitin-C	*UBC*
P07900	Heat shock protein HSP 90-alpha	*HSP90AA1*	P0DMV9	Heat shock 70 kDa protein 1B	*HSPA1B*
P07988	Pulmonary surfactant-associated protein B	*SFTPB*	P0DUB6	Alpha-amylase 1A	*AMY1A*
P07998	Ribonuclease pancreatic	*RNASE1*	P10153	Non-secretory ribonuclease	*RNASE2*
P08118	Beta-microseminoprotein	*MSMB*	P10599	Thioredoxin	*TXN*
P08174	Complement decay-accelerating factor	*CD55*	P10909	Clusterin	*CLU*
P08236	Beta-glucuronidase	*GUSB*	P11142	Heat shock cognate 71 kDa protein	*HSPA8*
P08238	Heat shock protein HSP 90-beta	*HSP90AB1*	P11217	Glycogen phosphorylase, muscle form	*PYGM*
P08246	Neutrophil elastase	*ELANE*	P11413	Glucose-6-phosphate 1-dehydrogenase	*G6PD*
P08263	Glutathione S-transferase A1	*GSTA1*	P11678	Eosinophil peroxidase	*EPX*
P08311	Cathepsin G	*CTSG*	P11684	Uteroglobin	*SCGB1A1*
P08567	Pleckstrin	*PLEK*	P12273	Prolactin-inducible protein	*PIP*
P08603	Complement factor H	*CFH*	P12429	Annexin A3	*ANXA3*
P08670	Vimentin	*VIM*	P12724	Eosinophil cationic protein	*RNASE3*
P08697	Alpha-2-antiplasmin	*SERPINF2*	P12814	Alpha-actinin-1	*ACTN1*
P08758	Annexin A5	*ANXA5*	P13284	Gamma-interferon-inducible lysosomal thiol reductase	*IFI30*
P08962	CD63 antigen	*CD63*	P13645	Keratin, type I cytoskeletal 10	*KRT10*
P09211	Glutathione S-transferase P	*GSTP1*	P13671	Complement component C6	*C6*
P09429	High mobility group protein B1	*HMGB1*	P13727	Bone marrow proteoglycan	*PRG2*
P09467	Fructose-1,6-bisphosphatase 1	*FBP1*	P13796	Plastin-2	*LCP1*
P09488	Glutathione S-transferase Mu 1	*GSTM1*	P13987	CD59 glycoprotein	*CD59*
P09668	Pro-cathepsin H	*PRG2*	P14780	Matrix metalloproteinase-9	*MMP9*
P09960	Leukotriene A-4 hydrolase	*LTA4H*	P15311	Ezrin	*EZR*
P09972	Fructose-bisphosphate aldolase C	*ALDOC*	P15941	Mucin-1	*MUC1*
P0C0L5	Complement C4-B	*C4B_2*	P16050	Polyunsaturated fatty acid lipoxygenase ALOX15	*ALOX15*
P0CG48	Polyubiquitin-C	*UBC*	P16401	Histone H1.5	*H1-5*

P0DMV9	Heat shock 70 kDa protein 1B	*HSPA1B*	P17213	Bactericidal permeability-increasing protein	*BPI*
P0DOX8	Immunoglobulin lambda-1 light chain	*NA*	P18206	Vinculin	*VCL*
P0DP25	Calmodulin-3	*CALM3*	P18669	Phosphoglycerate mutase 1	*PGAM1*
P0DUB6	Alpha-amylase 1A	*AMY1A*	P19823	Inter-alpha-trypsin inhibitor heavy chain H2	*ITIH2*
P10153	Non-secretory ribonuclease	*RNASE2*	P19827	Inter-alpha-trypsin inhibitor heavy chain H1	*ITIH1*
P10599	Thioredoxin	*TXN*	P20061	Transcobalamin-1	*TCN1*
P10909	Clusterin	*CLU*	P20160	Azurocidin	*AZU1*
P11021	Endoplasmic reticulum chaperone BiP	*HSPA5*	P21333	Filamin-A	*FLNA*
P11142	Heat shock cognate 71 kDa protein	*HSPA8*	P22079	Lactoperoxidase	*LPO*
P11215	Integrin alpha-M	*ITGAM*	P22792	Carboxypeptidase N subunit 2	*CPN2*
P11413	Glucose-6-phosphate 1-dehydrogenase	*G6PD*	P22894	Neutrophil collagenase	*MMP8*
P11678	Eosinophil peroxidase	*EPX*	P23284	Peptidyl-prolyl cis-trans isomerase B	*PPIB*
P11684	Uteroglobin	*SCGB1A1*	P24158	Myeloblastin	*PRTN3*
P12273	Prolactin-inducible protein	*PIP*	P25311	Zinc-alpha-2-glycoprotein	*AZGP1*
P12429	Annexin A3	*ANXA3*	P25815	Protein S100-P	*S100P*
P12724	Eosinophil cationic protein	*RNASE3*	P26038	Moesin	*MSN*
P12814	Alpha-actinin-1	*ACTN1*	P26447	Protein S100-A4	*S100A4*
P12955	Xaa-Pro dipeptidase	*PEPD*	P26583	High mobility group protein B2	*HMGB2*
P13284	Gamma-interferon-inducible lysosomal thiol reductase	*IFI30*	P27797	Calreticulin	*CALR*
P13639	Elongation factor 2	*EEF2*	P29401	Transketolase	*TKT*
P13645	Keratin, type I cytoskeletal 10	*KRT10*	P29508	Serpin B3	*SERPINB3*
P13671	Complement component C6	*C6*	P30740	Leukocyte elastase inhibitor	*SERPINB1*
P13727	Bone marrow proteoglycan	*HP*	P31025	Lipocalin-1	*LCN1*
P13796	Plastin-2	*LCP1*	P31146	Coronin-1A	*CORO1A*
P13987	CD59 glycoprotein	*CD59*	P31946	14-3-3 protein beta/alpha	*YWHAB*
P14780	Matrix metalloproteinase-9	*MMP9*	P31949	Protein S100-A11	*S100A11*

P15090	Fatty acid-binding protein, adipocyte	*FABP4*	P35527	Keratin, type I cytoskeletal 9	*KRT9*
P15121	Aldo-keto reductase family 1 member B1	*AKR1B1*	P35579	Myosin-9	*MYH9*
P15311	Ezrin	*EZR*	P35908	Keratin, type II cytoskeletal 2 epidermal	*KRT2*
P15586	N-acetylglucosamine-6-sulfatase	*A2M*	P36955	Pigment epithelium-derived factor	*SERPINF1*
P15941	Mucin-1	*MUC1*	P37837	Transaldolase	*TALDO1*
P16050	Polyunsaturated fatty acid lipoxygenase ALOX15	*ALOX15*	P40121	Macrophage-capping protein	*CAPG*
P17213	Bactericidal permeability-increasing protein	*BPI*	P41218	Myeloid cell nuclear differentiation antigen	*MNDA*
P17931	Galectin-3	*LGALS3*	P43155	Carnitine O-acetyltransferase	*CRAT*
P18206	Vinculin	*VCL*	P43652	Afamin	*AFM*
P18510	Interleukin-1 receptor antagonist protein	*IL1RN*	P46940	Ras GTPase-activating-like protein IQGAP1	*IQGAP1*
P20061	Transcobalamin-1	*TCN1*	P47756	F-actin-capping protein subunit beta	*CAPZB*
P20160	Azurocidin	*AZU1*	P49913	Cathelicidin antimicrobial peptide	*CAMP*
P20618	Proteasome subunit beta type-1	*PSMB1*	P50395	Rab GDP dissociation inhibitor beta	*GDI2*
P20929	Nebulin	*NEB*	P52209	6-phosphogluconate dehydrogenase, decarboxylating	*PGD*
P21333	Filamin-A	*FLNA*	P52566	Rho GDP-dissociation inhibitor 2	*ARHGDIB*
P21926	CD9 antigen	*CD9*	P52907	F-actin-capping protein subunit alpha-1	*CAPZA1*
P22079	Lactoperoxidase	*LPO*	P53634	Dipeptidyl peptidase 1	*CTSC*
P22314	Ubiquitin-like modifier-activating enzyme 1	*UBA1*	P54108	Cysteine-rich secretory protein 3	*CRISP3*
P22392	Nucleoside diphosphate kinase B	*NME2*	P56199	Integrin alpha-1	*ITGA1*
P22626	Heterogeneous nuclear ribonucleoproteins A2/B1	*HNRNPA2B1*	P59665	Neutrophil defensin 1	*DEFA1*
P22894	Neutrophil collagenase	*MMP8*	P59998	Actin-related protein 2/3 complex subunit 4	*ARPC4*
P23141	Liver carboxylesterase 1	*CES1*	P60174	Triosephosphate isomerase	*TPI1*
P23280	Carbonic anhydrase 6	*CA6*	P60709	Actin, cytoplasmic 1	*ACTB*
P23284	Peptidyl-prolyl cis-trans isomerase B	*PPIB*	P60763	Ras-related C3 botulinum toxin substrate 3	*RAC3*
P23528	Cofilin-1	*CFL1*	P61158	Actin-related protein 3	*ACTR3*
P24158	Myeloblastin	*PRTN3*	P61160	Actin-related protein 2	*ACTR2*

P25311	Zinc-alpha-2-glycoprotein	*AZGP1*	P61204	ADP-ribosylation factor 3	*ARF3*
P25774	Cathepsin S	*CTSS*	P61626	Lysozyme C	*LYZ*
P25786	Proteasome subunit alpha type-1	*PSMA1*	P61769	Beta-2-microglobulin	*B2M*
P25787	Proteasome subunit alpha type-2	*CEACAM8*	P62258	14-3-3 protein epsilon	*YWHAE*
P25789	Proteasome subunit alpha type-4	*PSMA4*	P62805	Histone H4	*H4-16*
P25815	Protein S100-P	*CTSH*	P63104	14-3-3 protein zeta/delta	*YWHAZ*
P26038	Moesin	*MSN*	P68032	Actin, alpha cardiac muscle 1	*ACTC1*
P26447	Protein S100-A4	*S100A4*	P68104	Elongation factor 1-alpha 1	*EEF1A1*
P26583	High mobility group protein B2	*PSMA2*	P68431	Histone H3.1	*H3C12*
P27105	Erythrocyte band 7 integral membrane protein	*STOM*	P80188	Neutrophil gelatinase-associated lipocalin	*LCN2*
P27348	14-3-3 protein theta	*YWHAQ*	P80511	Protein S100-A12	*S100A12*
P27695	DNA-(apurinic or apyrimidinic site) endonuclease	*APEX1*	P80723	Brain acid soluble protein 1	*BASP1*
P27797	Calreticulin	*CALR*	P98088	Mucin-5AC	*MUC5AC*
P28325	Cystatin-D	*CST5*	Q01518	Adenylyl cyclase-associated protein 1	*CAP1*
P29401	Transketolase	*TKT*	Q03591	Complement factor H-related protein 1	*CFHR1*
P29508	Serpin B3	*SERPINB3*	Q05315	Galectin-10	*CLC*
P30086	Phosphatidylethanolamine-binding protein 1	*PEBP1*	Q06323	Proteasome activator complex subunit 1	*PSME1*
P30101	Protein disulfide-isomerase A3	*PDIA3*	Q06830	Peroxiredoxin-1	*PRDX1*
P30740	Leukocyte elastase inhibitor	*SERPINB1*	Q07654	Trefoil factor 3	*TFF3*
P31025	Lipocalin-1	*LCN1*	Q08380	Galectin-3-binding protein	*LGALS3BP*
P31146	Coronin-1A	*CORO1A*	Q14019	Coactosin-like protein	*COTL1*
P31946	14-3-3 protein beta/alpha	*YWHAB*	Q14508	WAP four-disulfide core domain protein 2	*WFDC2*
P31949	Protein S100-A11	*S100A11*	Q14624	Inter-alpha-trypsin inhibitor heavy chain H4	*ITIH4*
P31997	Carcinoembryonic antigen-related cell adhesion molecule 8	*PARK7*	Q16378	Proline-rich protein 4	*PRR4*
P32320	Cytidine deaminase	*CDA*	Q6P5S2	Protein LEG1 homolog	*LEG1*
P34096	Ribonuclease 4	*RNASE4*	Q86YZ3	Hornerin	*HRNR*

P35527	Keratin, type I cytoskeletal 9	*KRT9*
P35579	Myosin-9	*MYH9*
P35609	Alpha-actinin-2	*ACTN2*
P35908	Keratin, type II cytoskeletal 2 epidermal	*KRT2*
P36222	Chitinase-3-like protein 1	*CHI3L1*
P36955	Pigment epithelium-derived factor	*SERPINF1*
P37802	Transgelin-2	*TAGLN2*
P37837	Transaldolase	*TALDO1*
P39687	Acidic leucine-rich nuclear phosphoprotein 32 family member A	*ANP32A*
P40121	Macrophage-capping protein	*CAPG*
P41218	Myeloid cell nuclear differentiation antigen	*PIGR*
P43353	Aldehyde dehydrogenase family 3 member B1	*ALDH3B1*
P43490	Nicotinamide phosphoribosyltransferase	*NAMPT*
P46940	Ras GTPase-activating-like protein IQGAP1	*IQGAP1*
P47756	F-actin-capping protein subunit beta	*CAPZB*
P48595	Serpin B10	*SERPINB10*
P49721	Proteasome subunit beta type-2	*PSMB2*
P49913	Cathelicidin antimicrobial peptide	*CAMP*
P50395	Rab GDP dissociation inhibitor beta	*GDI2*
P52209	6-phosphogluconate dehydrogenase, decarboxylating	*PGD*
P52565	Rho GDP-dissociation inhibitor 1	*ARHGDIA*
P52566	Rho GDP-dissociation inhibitor 2	*ARHGDIB*
P52907	F-actin-capping protein subunit alpha-1	*CAPZA1*
P53634	Dipeptidyl peptidase 1	*CTSC*
P59665	Neutrophil defensin 1	*DEFA1*
P60174	Triosephosphate isomerase	*TPI1*
Q8IWL1	Pulmonary surfactant-associated protein A2	*SFTPA2*
Q8N4C6	Ninein	*NIN*
Q8N4F0	BPI fold-containing family B member 2	*BPIFB2*
Q8TDL5	BPI fold-containing family B member 1	*BPIFB1*
Q96C19	EF-hand domain-containing protein D2	*EFHD2*
Q96DA0	Zymogen granule protein 16 homolog B	*ZG16B*
Q96KK5	Histone H2A type 1-H	*H2AC12*
Q96QB1	Rho GTPase-activating protein 7	*DLC1*
Q96QR1	Secretoglobin family 3A member 1	*SCGB3A1*
Q99102	Mucin-4	*MUC4*
Q9BQE3	Tubulin alpha-1C chain	*TUBA1C*
Q9HC84	Mucin-5B	*MUC5B*
Q9NP55	BPI fold-containing family A member 1	*BPIFA1*
Q9UGM3	Deleted in malignant brain tumors 1 protein	*DMBT1*
Q9UM07	Protein-arginine deiminase type-4	*PADI4*
Q9UPN3	Microtubule-actin cross-linking factor 1, isoforms 1/2/3/5	*MACF1*
Q9Y2Y8	Proteoglycan 3	*PRG3*
Q9Y490	Talin-1	*TLN1*
Q9Y6R7	IgGFc-binding protein	*FCGBP*

P60660	Myosin light polypeptide 6	*MYL6*
P60709	Actin, cytoplasmic 1	*ACTB*
P60953	Cell division control protein 42 homolog	*CDC42*
P61158	Actin-related protein 3	*ACTR3*
P61160	Actin-related protein 2	*ACTR2*
P61204	ADP-ribosylation factor 3	*ARF3*
P61586	Transforming protein RhoA	*RHOA*
P61626	Lysozyme C	*S100P*
P61769	Beta-2-microglobulin	*MNDA*
P61916	NPC intracellular cholesterol transporter 2	*NPC2*
P61981	14-3-3 protein gamma	*YWHAG*
P62258	14-3-3 protein epsilon	*YWHAE*
P62805	Histone H4	*DPP3*
P62879	Guanine nucleotide-binding protein G(I)/G(S)/G(T) subunit beta-2	*GNB2*
P62993	Growth factor receptor-bound protein 2	*GRB2*
P63000	Ras-related C3 botulinum toxin substrate 1	*RAC1*
P63104	14-3-3 protein zeta/delta	*YWHAZ*
P67936	Tropomyosin alpha-4 chain	*TPM4*
P68104	Elongation factor 1-alpha 1	*EEF1A1*
P68133	Actin, alpha skeletal muscle	*ACTA1*
P68871	Hemoglobin subunit beta	*HBB*
P69905	Hemoglobin subunit alpha	*HBA2*
P78417	Glutathione S-transferase omega-1	*GSTO1*
P80188	Neutrophil gelatinase-associated lipocalin	*LCN2*
P80511	Protein S100-A12	*B2M*
P80723	Brain acid soluble protein 1	*BASP1*

P98088	Mucin-5AC	*MUC5AC*
P99999	Cytochrome c	*CYCS*
Q01469	Fatty acid-binding protein 5	*FABP5*
Q01518	Adenylyl cyclase-associated protein 1	*CAP1*
Q04917	14-3-3 protein eta	*YWHAH*
Q05315	Galectin-10	*CLC*
Q06830	Peroxiredoxin-1	*PRDX1*
Q07654	Trefoil factor 3	*TFF3*
Q08380	Galectin-3-binding protein	*LGALS3BP*
Q12923	Tyrosine-protein phosphatase non-receptor type 13	*PTPN13*
Q13228	Methanethiol oxidase	*SELENBP1*
Q13510	Acid ceramidase	*ASAH1*
Q13938	Calcyphosin	*CAPS*
Q14019	Coactosin-like protein	*COTL1*
Q14103	Heterogeneous nuclear ribonucleoprotein D0	*HNRNPD*
Q14508	WAP four-disulfide core domain protein 2	*WFDC2*
Q15404	Ras suppressor protein 1	*RSU1*
Q15631	Translin	*TSN*
Q16270	Insulin-like growth factor-binding protein 7	*IGFBP7*
Q16378	Proline-rich protein 4	*PRR4*
Q16881	Thioredoxin reductase 1, cytoplasmic	*TXNRD1*
Q2VWP7	Protogenin	*PRTG*
Q53GD3	Choline transporter-like protein 4	*SLC44A4*
Q6P5S2	Protein LEG1 homolog	*LEG1*
Q6UX06	Olfactomedin-4	*OLFM4*
Q6UXY8	Transmembrane channel-like protein 5	*TMC5*

Q71DI3	Histone H3.2	*H3C14*
Q7Z404	Transmembrane channel-like protein 4	*TMC4*
Q8N4F0	BPI fold-containing family B member 2	*BPIFB2*
Q8NF91	Nesprin-1	*SYNE1*
Q8TAX7	Mucin-7	*MUC7*
Q8TDL5	BPI fold-containing family B member 1	*BPIFB1*
Q8TEQ0	Sorting nexin-29	*SNX29*
Q8WUM4	Programmed cell death 6-interacting protein	*PDCD6IP*
Q8WXI7	Mucin-16	*MUC16*
Q8WZ42	Titin	*TTN*
Q92820	Gamma-glutamyl hydrolase	*GGH*
Q96C19	EF-hand domain-containing protein D2	*EFHD2*
Q96DA0	Zymogen granule protein 16 homolog B	*ZG16B*
Q96KK5	Histone H2A type 1-H	*H2AC12*
Q96NY7	Chloride intracellular channel protein 6	*CLIC6*
Q96QB1	Rho GTPase-activating protein 7	*DLC1*
Q96QR1	Secretoglobin family 3A member 1	*SCGB3A1*
Q96RL7	Vacuolar protein sorting-associated protein 13A	*VPS13A*
Q99102	Mucin-4	*MUC4*
Q99497	Parkinson disease protein 7	*LYZ*
Q99828	Calcium and integrin-binding protein 1	*CIB1*
Q9BQE3	Tubulin alpha-1C chain	*TUBA1C*
Q9BRF8	Serine/threonine-protein phosphatase CPPED1	*CPPED1*
Q9H299	SH3 domain-binding glutamic acid-rich-like protein 3	*SH3BGRL3*
Q9H3G5	Probable serine carboxypeptidase CPVL	*CPVL*
Q9HAT2	Sialate O-acetylesterase	*SIAE*

Q9HC84	Mucin-5B	*MUC5B*
Q9HD89	Resistin	*RETN*
Q9NP55	BPI fold-containing family A member 1	*BPIFA1*
Q9NY33	Dipeptidyl peptidase 3	*HMGB2*
Q9UGM3	Deleted in malignant brain tumors 1 protein	*DMBT1*
Q9ULZ3	Apoptosis-associated speck-like protein containing a CARD	*PYCARD*
Q9Y376	Calcium-binding protein 39	*CAB39*
Q9Y490	Talin-1	*TLN1*
Q9Y6N6	Laminin subunit gamma-3	*LAMC3*
Q9Y6R7	IgGFc-binding protein	*FCGBP*